The Feasibility of Using Jarosite Waste From the Zinc Industry for Hlsarna Ironmaking

by

Rohan Sivaraj

to obtain the degree of Master of Science
at the Delft University of Technology,
to be defended publicly on August 6, 2020 at 10:00 AM.

Student number:	4822862	
Thesis committee:	Dr. Y. Yang,	TU Delft, supervisor
	Dr. T. Kerry,	TU Delft
	Dr. E. Georgakopoulos,	TU Delft
	Dr. E. Offerman,	TU Delft

TU Delft

Abstract

Jarosites are an Fe-rich waste product from the Zn industry. They contain toxic heavy metals like Pb, Zn, Cu, Ni, and are consequently disposed of in regulated ponds. With Zn demand projected to continually increase in the future, it is anticipated that by 2023, the Fe content in these jarosites will amount to 2.2 million tonnes/year. With the advent of the circular economy and raw materials scarcity it has become imperative that 'wastes', like jarosite, are converted to resources. Since jarosites are Fe-rich, they can be used for ironmaking. HIsarna is a revolutionary ironmaking process that has greater flexibility in the raw materials it uses. It can potentially utilise jarosite, which was unsuitable for a conventional blast furnace, to make hot metal. However, steelmaking, which occurs downstream of HIsarna ironmaking, requires the removal of Cu, Ni, Cr, Sn and Mo (termed CEF metals). Removal of these CEF metals, particularly Cu, from jarosite whilst fixing sulfur is necessary before it is acceptable for HIsarna.

This thesis evaluated several metallurgical approaches in removing the CEF metals from a locally sourced jarosite whilst fixing sulfur. The jarosite was sourced from Nyrstar (Budel, Netherlands) and is commercially known as Budel Leach Product (BLP). The BLP had a CEF concentration of 1.8 wt% which was substantially higher than the HIsarna limit (0.2 wt%); it also had a sulfur content of 9.3 wt%. The metallurgical approaches taken to treat the BLP included: hydrometallurigcal (acid, alkaline. ammoniacal and DES leaching); pyrometallurigcal (thermal decomposition and chloridisation); and a combined pyro- and hydrometallurgical approach (sulfur fixation with Na_2CO_3 with water washing). Ammoniacal leaching was the most effective hydrometallurgical approach in selectively removing Cu from the BLP, however, leaching efficiencies were low. Thermal decomposition resulted in an upconcentration of the CEF metals whilst releasing SO_2. Sulfur could be fixed with the combined approach, however, the presence of Na_2CO_3 converted any soluble CEF metal sulfates to insoluble oxides which increased CEF concentration. The most effective approach was the chloridisation of BLP which reduced the CEF concentration in the treated residue while fixing sulfur. Although the CEF concentration using the chloridisation approach (0.84wt%) was above the HIsarna limits, further refinement of the treatment strategy shows promise for utilising BLP in HIsarna ironmaking.

Acknowledgements

I would like to acknowledge the following people without whose support the completion of this thesis would not have been possible:

- Dr. Yongxiang Yang - Your guidance and mentorship in approaching this challenging research topic helped me structure my approach. Your quick feedback also allowed me to determine when to stop or continue an investigation. Allowing me to conduct experiments during the spread of COVID-19 enabled me to finish on time. This was greatly appreciated.
- Dr. Tim Kerry - As the main point of contact, you've been a stalwart supporter while I completed my thesis. It goes without saying that your feedback and guidance throughout was invaluable. Thank you.
- Dr. Evangelous Georgakopoulos - Thank you for helping me with the TGA. You also provided some guidance on the leaching experiments which was helpful.
- Ruud Hendrikx and Michel van den Brink - I'm very thankful for all the samples that were processed and analysed in a timely fashion.
- Sander Van Asperen - For rapidly processing my orders for consumables and also allowing me to conduct my experiments during the spread of COVID-19.

A big thank you to anyone that was not explicitly mentioned above but provided me with guidance and support while undertaking this research.

Contents

List of Figures

List of Tables

1 Introduction

1.1. Motivation

With the advent of the circular economy, it has become necessary to transform our economies from linear to circular models where waste is utilized as a resource. The metals industry generates substantial quantities of waste containing metals that are ultimately 'lost' to lower value purposes or disposed. As will be detailed in Section 2.4, the Zn industry generates an Fe-rich waste stream (either jarosite, goethite, or hematite). This waste stream also contains a high concentration of toxic heavy metals which requires specialised disposal and subsequent monitoring. Rightfully, it is becoming harder to get the approvals necessary to dispose of these residues. If not disposed of in a landfill, they may be utilised in lower value construction material after treatment. Ideally, this Fe-rich waste stream can be used for higher value ironmaking. Zn also plays an important role in the ironmaking industry as a large portion of steel is galvanised with Zn. Galvanised steel is typically recycled in an Electric Arc Furnace where a Zn-rich dust that is produced can be incorporated into the Zn industry. This highlights how the Zn and Fe industries are coupled and this thesis explores the opportunity to further intertwine the two industries and close the materials loop. Here lies the motivation for this project:

- Utilise a 'waste' stream
- Extract valuable elements (like Fe) that can be consumed in other industries
- Close a materials loop in the Zn industry

The Zn industry will undoubtedly be focusing on minimising the production of these residues as it becomes more costly to dispose of them. This project tackles the issue from a different angle: how do we convert this waste stream to a resource? Due to the high concentration of Fe in the residues, it is appealing to use it in ironmaking. Previously, the residues were considered for use in ironmaking; however, due to the relatively high concentration of heavy metals like Zn and Cu, it was considered not viable for conventional blast furnace ironmaking. Recent progress in steelmaking has brought with it the HIsarna process which allows for greater flexibility in its raw materials. High concentrations of Zn are no longer problematic (although high Cu concentrations remains an issue). The increased flexibility presents an opportunity to use the industrial residues or secondary raw materials in ironmaking which previously was not considered possible.

1.2. Demand and Supply of Zinc

Zn is mainly used as an anti-corrosion coating for steel [24] and is typically applied through processes such as electroplating, thermal spraying of Zn, hot-dip galvanizing (the oldest anti-corrosion process) [25], sheradizing and mechanical plating [26]. The major uses of Zn are indicated in Table 1.1, whereby the galvanizing of steel dominates Zn consumption [19]. Industries that use Zn are also highlighted in Table 1.2 [1]. Table 1.2 indicates that a large portion of Zn demand is driven by the construction and infrastructure industry (66%). This suggests that Zn demand is correlated to global growth and, particularly, growth of emerging economies. Figure 1.1 shows forecasted demand growth from 2017 to 2023 to be 2.2% with the majority of demand coming from developing economies and China [1]. The figure shows the demand is projected to increase to 16,338 kt/year of refined Zn by 2023.

Table 1.1: End uses of Zn [19].

Use	**Percentage**
Galvanizing (corrosion protection of steel)	50%
Zn Alloying (Zn based alloys to supply die casting industry)	17%
Brass and Bronze	17%
Zn Semi-Manufacturers (including roofing, gutters and downpipes)	6%
Chemicals (Zn oxide and Zn sulphate)	6%
Miscellaneous	4%

Table 1.2: Zn use by industry (2018)[1].

Industry	**Usage Percentage**
Construction and Infrastructure	66%
Automotive and Industrial Machinery	28%
Consumer Goods	5.5%
Agribusiness and Others	0.5%

According to the United States Geological Survey, the identified Zn resources of the world amount to 1.9 billion tonnes [20] of which only 230 million tonnes are considered economic reserves. Table 1.3 indicates global production and reserves per country.

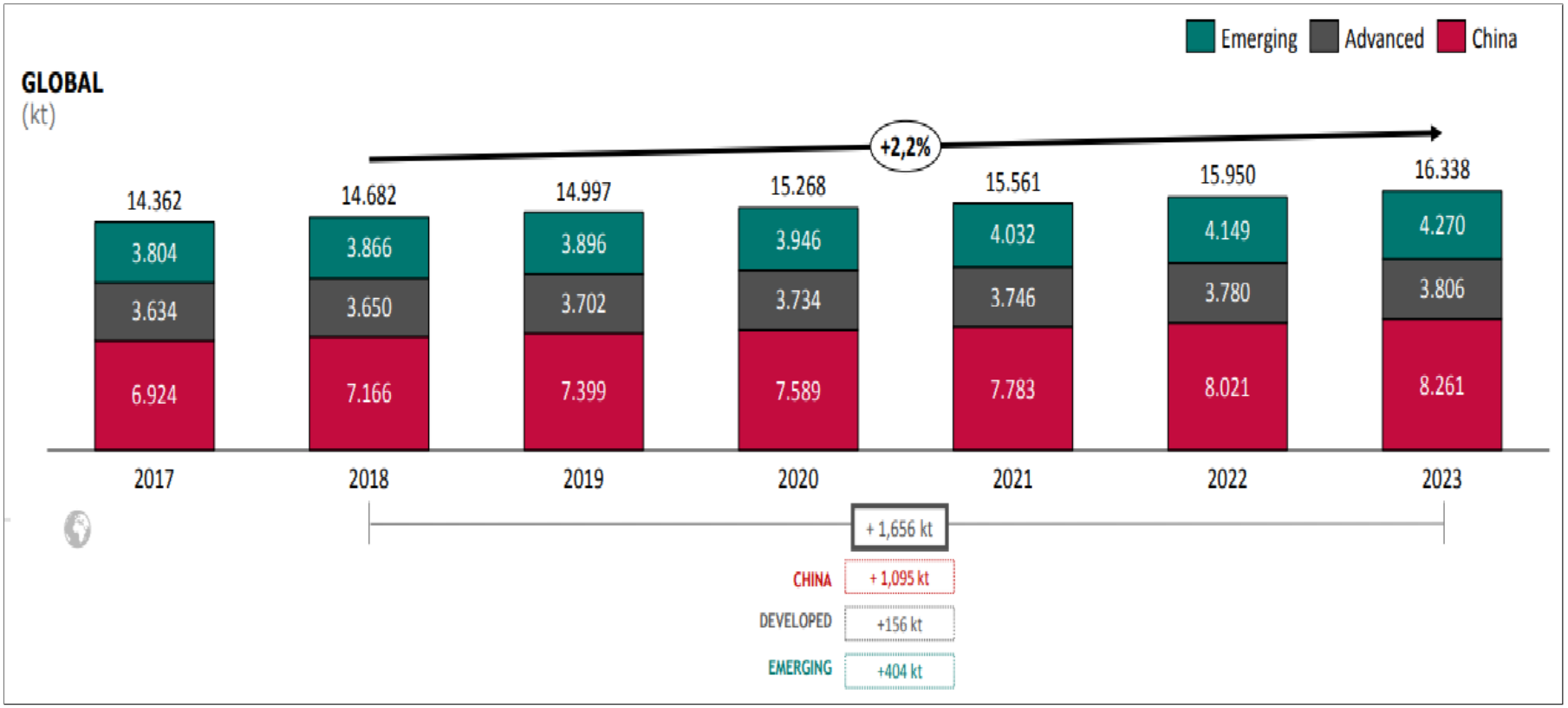

Figure 1.1: Global forecasted demand of refined Zn from 2018 to 2023 with demand expected to reach 16,338 kt/year by 2023. Actual consumption data for 2017[1].

Table 1.3: Global mine production and reserves by country, 2018[20]. Production refers to the amount (ktonnes) produced in 2018 and reserves refers to the amount (ktonnes) available as of 2018.

Country	Mine Production (ktonnes)	Reserves (ktonnes)
United States	790	11,000
Australia	940	64,000
Bolivia	520	4,800
Canada	340	3,000
China	4,300	44,000
India	800	10,000
Kazakhstan	390	13,000
Mexico	650	20,000
Peru	1,600	21,000
Sweden	220	1,400
Other countries	2,300	33,000
World Total	**13,000**	**230,000**

When the data is compared to commercial market information, the production rate and reserves of the various countries do deviate (see Figure 1.2). Regardless, China, Peru and Australia are the top three Zn producers in the world. Zn production is anticipated to rise approximately 3% per year from 2018 to 2023, with production rates reaching approximately 16,500 ktonnes in 2023.

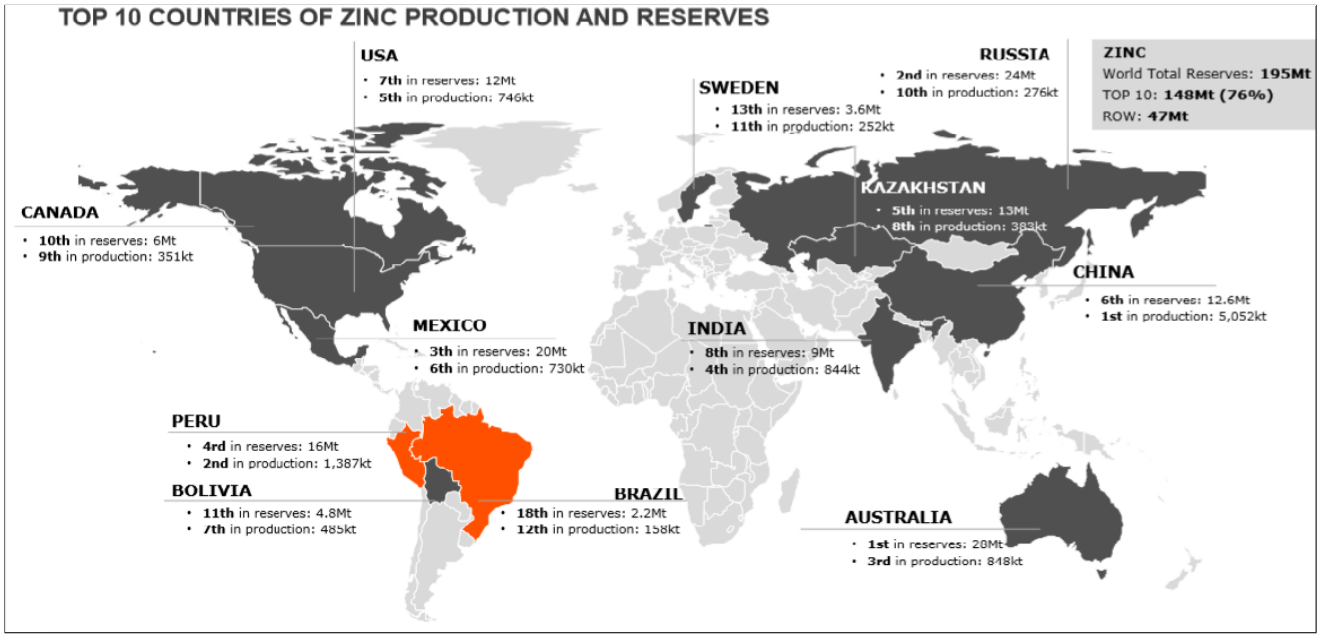

Figure 1.2: Top 10 countries of Zn production and reserves as of Q2, 2018 [1].

The production increase is supported by production expansion in existing mines (47%) and the opening of new mines (40%) [1]. The average Zn and Fe content in Zn concentrates around the world was calculated to be approximately 53.0% Zn and 7.34% Fe. Based on this, by 2023, the amount of Fe generated through primary Zn production amounts to 2.2 million tonnes/year [27].

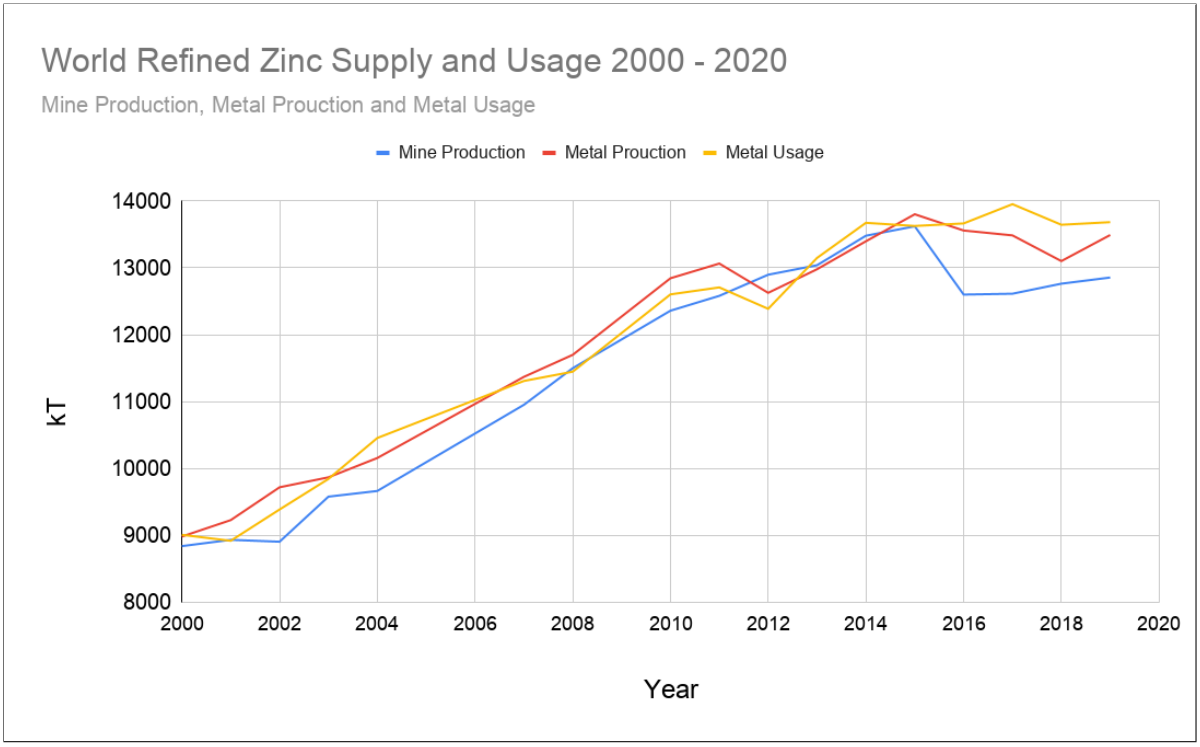

Figure 1.3: Zn Statistics, World Refined Zn Supply and Usage, 2020 [2].

"Metal production" in Figure 1.3 is composed of primary (70%) and secondary production (30%). Primary production includes concentrates and other primary materials (mine tailings and slags, residues, drosses, etc.). Secondary production includes scrap materials and residues from fabricating/processing operations, together with Zn in pellets or other forms recovered from steel plant flue dusts [2]. Figure 1.3 indicates that Zn primary metal production has been insufficient to meet demand which has resulted in a depletion of Zn stocks. This has spurred the expansion of existing production and the development of new Zn mines.

The risks of substitution of Zn in its applications is generally low. In the construction and infrastructure industries the maturity and standardization of Zn application presents a significant barrier for substitution. In addition, the costs of Zn in steel galvanization is low (represents approx 1% of construction costs). In the automotive industry, the Zn substitution risk appears low due to Zn's mechanical properties and low injection costs (die casting of internal parts).

1.3. Zinc and Iron Material Flows

As discussed in Section1.2, Zn is a key industrial element. Consequently, it's worth analysing the material flows of Zn to identify losses of this important industrial element. Figure 1.4 shows the anthropogenic Zn cycle for 2010. The figure highlights that Zn is lost throughout its entire life cycle as industrial waste and landfill. Figure 1.5 assigns values to the material flows (for the year 2010). The important thing to note is that roughly a third of the Zn extracted from the earth is lost to landfill in the form of galvanized steel. This includes the use of galvanized steel scrap in electric-arc furnace steel making (which is incorporated in the W of the diagram).

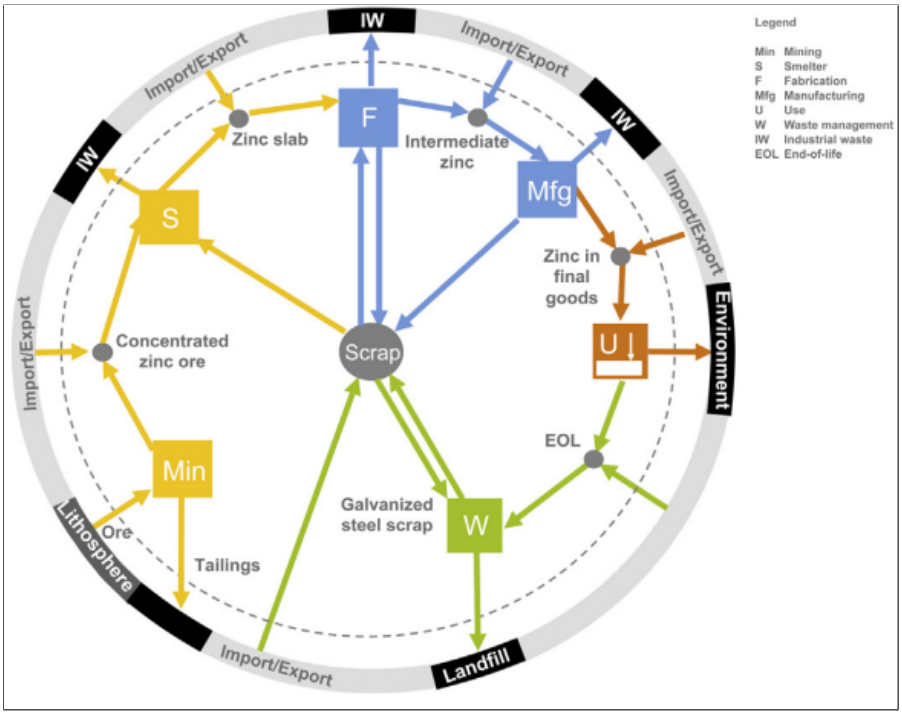

Figure 1.4: Outline of anthropogenic Zn cycle.Min = Mining, S = Smelter, F = Fabrication, Mfg = Manufacturing, U = Use, W= Waste management, IW = Industrial Waste an EOL = End-of-Life.

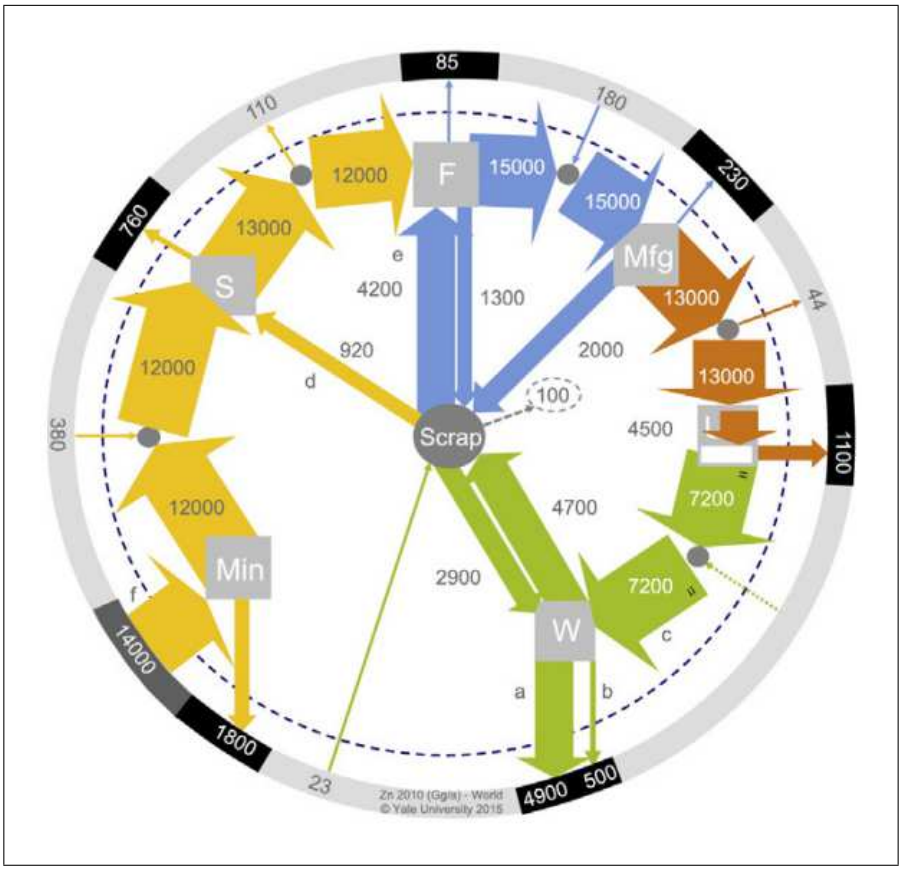

Figure 1.5: Global anthropogenic Zn cycle 2010. Units in Gg/annum.

For iron, 98% of iron ore is used for steelmaking [28]. This is consumed by a blast furnace to produce hot metal (or pig iron) and subsequently steel. Crude steel is also produced via an Electric Arc Furnace, in which steel scrap is the most common charge. The recycling rate of steel is already quite high (80-90%) [29]; however, the residence of steel in the economy is over long time frames (approximately 40 years) depending on its use. This means that demand from primary sources of Fe will continue to rise especially with the industrialisation of developing economies.

The relationship between Fe and Zn is a complicated one. Figures 1.6 show the interaction of a selection of elements. It shows elements are linked in a complex manner in each of the carrier metal's process infrastructure, including their respective refining and alloying capabilities and the inevitable losses to final residues that cannot be processed economically. In the production of hot metal, Zn occurs in BF dust at a concentration of 0.1-0.5 % (w/w) [30]. During the production of galvanized steel Zn and Fe are once again brought together. Galvanised steel is typically recycled via electric arc furnaces (EAF). BOF (Basic Oxygen Furnace) operations can utilise some scrap but there are limitations on how much can be used depending on the Zn concentration. When recycling galvanized steel, EAFs volatilise Zn and produce EAF dust thereby separating Zn from Fe. As was mentioned in Section 1.2 Fe is a major problematic element that exists in Zn concentrates. For reasons discussed in Section 2, Fe needs to be removed from Zn and is a major waste product generated from the Zn industry. This is shown in Figure 1.6 with the existence of FeO_x on the bottom of the Zn and Pb section of the wheel. The wheel essentially indicates that Fe is recovered in Zn hydrometallurgy; however, it is primarily lost to lower-value building material products which also contributes to dissipative loss of the element. By 2023, roughly 2.2 million tonnes/year of Fe will be generated as a waste product [27]. This presents a clear opportunity to address the increasing Fe demand by closing the materials loop in the Zn industry through adding higher value to the Fe residues.

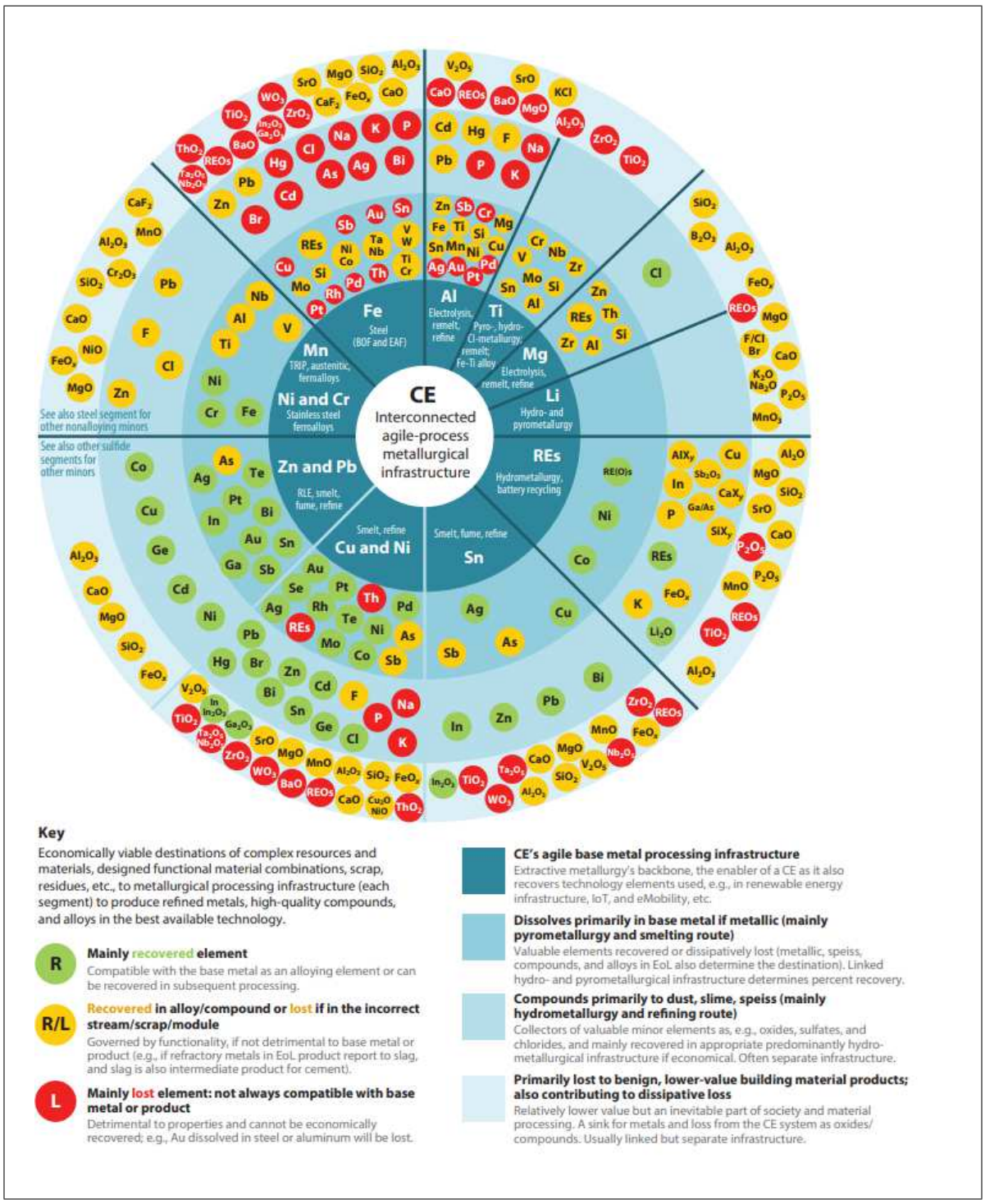

Figure 1.6: The metal wheel shows the interaction of a selection of elements and materials linked in a complex manner in each of the carrier process metallurgical infrastructures [3].

1.4. ReclaMet and Closing the Materials Loop

ReclaMet is a project that is funded by EIT Raw Materials. EIT (European Institute of Innovation and Technology) is the largest consortium in the raw materials sector worldwide whose ambition is to enable sustainable competitiveness of the European minerals, metals and materials sector. ReclaMet aim to reclaim valuable metals from process residues with the HIsarna process. The HIsarna iron-

making technology, which is a breakthrough ironmaking process that has a significantly reduced CO_2 footprint. The CO_2 reduction comes from the fact that HIsarna has very high raw materials flexibility and requires less materials pre-processing than the conventional blast furnace (the technology will be discussed further in Section 3.1). For HIsarna, no coking or agglomeration is required when compared to conventional BF ironmaking; consequently, the carbon produced or energy consumed associated with those activities do not exist for HIsarna.

As discussed in Section 1.2, there has been a deficit in Zn metal production due to the availability of primary Zn ores and concentrates. This is consequently reflected in historic Zn prices (see Figure 1.7). Therefore, there is interest from the Zn industry to find suitable secondary sources of Zn concentrates. The objective of the project is: **to achieve an enrichment level of Zn in the process dust of HIsarna which would make it suitable for direct use in Zn smelting**. Because of the high flexibility in raw materials that is afforded by HIsarna, this is typically achieved by increasing the Zn content of the feedstock which subsequently enriches the Zn content of the off-gas. The materials loop can be closed because Zn-rich galvanized steel scrap and Zn-rich dusts can be incorporated into the feed.

Figure 1.7: Historic Zn prices [4].

A secondary goal of the project is to be able to use Fe-rich wastes from the Zn industry (jarosite, goethite and hematite) for use in HIsarna ironmaking. This could potentially close the materials loop of wastes generated from the Zn industry. Figure 1.8 presents a schematic of the materials flows considered by the ReclaMet project for incorporation into HIsarna steelmaking. Although there is flexibility with the HIsarna feedstock, there are some boundary conditions (concentrations of elements like Cu, Ni, Sn, Mo, and Cr) for feedstock that precludes the use of just any Fe-rich waste stream. This will be discussed in detail in Section 3.2.

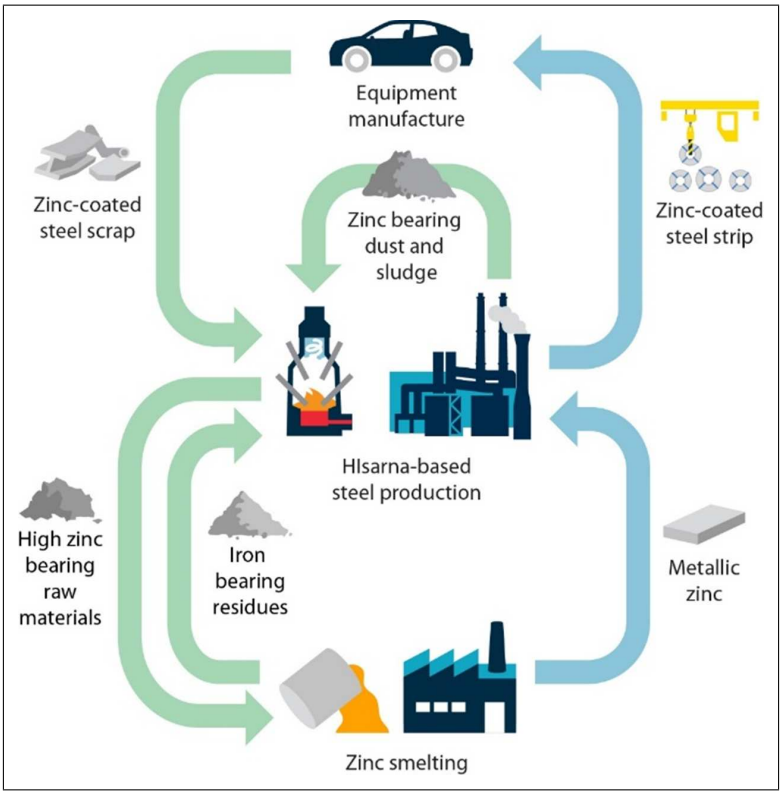

Figure 1.8: Schematic of ReclaMet Project [5].

1.5. Thesis Objective

The following section outlines the objectives of this thesis project. CEF, or Copper Equivalence Factor, refers to a group of metals that are problematic for steelmaking. They include Cu, Ni, Cr, Sn, and Mo and the CEF value is calculated according to the following equation:

$$CEF = Cu + Ni + Cr + 5 * Sn + 10 * Mo \tag{1.1}$$

Sn and Mo are particularly deleterious in steelmaking. It is important that the concentration of these metals in the feed to HIsarna are kept to a minimum. Tata steel, which owns the HIsarna technology, has indicated that their CEF limit should not exceed 0.2 wt%. This is discussed in more detail in Section 3.2. With this in mind this thesis aims to address the following question:

"Can jarosite sourced from a local Zn refinery be treated such that it is acceptable for feedstock for HIsarna ironmaking?"

Specifically, in attempting to address the research question the following strategy is undertaken:

1. Establish CEF value of industrially sourced jarosite and the nature of which CEF elements exist
2. Use hydrometallurgical methods (i.e. leaching) to reduce the CEF value to ≤0.2 wt%
3. Use pyrometallurgical methods to reduce the CEF value to ≤0.2 wt%
4. Use a combination of hydro- and pyrometallurgical methods to reduce the CEF value to ≤0.2 wt%
5. Attempt to retain Zn and remove S hydrometallurgically (reasons for which will be discussed in Section 3.2)

2

Summary of Zinc Extraction and Iron Control

Zinc is the 24th most abundant element in the earth's crust and primarily exists as a sulphide ore sphalerite (ZnS) [25]. The most important impurity, FeS, which exists at concentrations between 0.3-20%, presents a key challenge to the hydrometallurgical Zn industry. Zn metal is produced by processing ZnS concentrates through either hydrometallurgical or pyrometallurgical routes. In 2008, hydrometallurgical processing accounted for 86% of the world Zn production [31]. The main barriers to pyrometallurgical Zn production are the higher costs and reliance on metallurgical coke. With hydrometallurgical processing of Zn, the removal of Fe poses a significant challenge to the industry. This chapter provides a very brief summary of hydrometallurgical extraction of Zn and the Fe removal technologies employed. Hydrometallurgical processing of Zn occurs via the roasting-leaching-electrowinning (RLE) process. An overview of the process is provided in Figure 2.1 [6].

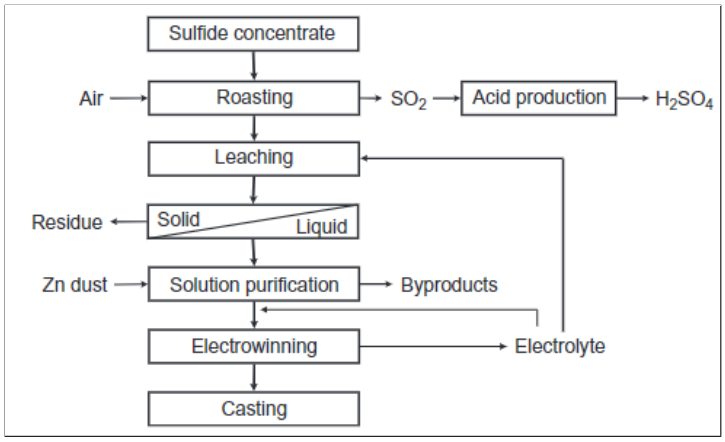

Figure 2.1: Schematic of Zn RLE process [6].

2.1. Roasting-Leaching-Electrowinning

Prior to roasting, Zn sulphide minerals are concentrated and separated from the ore via froth flotation. Roasting is the process of converting the ZnS concentrate into leachable ZnO or $ZnSO_4$ (also known as calcine). Roasting of ZnS also forms zinc ferrite ($ZnO.Fe_2O_3$), also known as franklinite, when the oxygen partial pressure is lower than what is required for ZnO formation. Iron oxides are more stable

than sulphides during sulfuric acid leaching and, therefore, remain in leach residues.

After the ore is roasted it is then leached. The objective of leaching is to extract Zn into solution so that it can be reduced electrolytically. Leaching in Zn production occurs in at least two stages to maximise Zn recovery and minimise Fe contamination. The process involves an initial neutral leach followed by leaching with more hot/concentrated acid.

In the initial neutral leaching step, ZnO in the calcine (consisting of 90% ZnO and 10% zinc ferrites) [6] is dissolved into an impure aqueous solution using sulfuric acid. The following reaction occurs:

$$ZnO(s) + H_2SO_4(aq) -> ZnSO_4(aq) + H_2O(aq) \tag{2.1}$$

Calcine is fed into the neutral leach which increases the pH of the leach solution from pH 3.1 to 3.8. This causes Fe precipitation and reduces the Fe level in the leachate to 10 mg/L [6]. Additional milder leaching stages may be employed to recover more Zn and precipitate more Fe out of solution.

The hot/concentrating leaching step targets the Zn from ferrites present in the neutral leach residue but due to the aggressive conditions (30-80g/L H_2SO_4 at temperatures > 90°C), Fe (and other impurities) is also released into solution [32]:

$$Zn_2Fe_2O_4(s) + 4H_2SO_4(aq) -> ZnSO_4(aq) + Fe_2(SO4)_3(aq) + 4H_2O \tag{2.2}$$

Prior to electrowinning, the leach solution (containing Zn, Fe, and other impurities) will need to be purified. A major step is Fe removal which will be discussed in detail in section 2.4.3. The presence of the impurities interferes with the electrolysis of Zn and reduces the overall Zn recovery. The objective of electrowinning is the recovery of Zn from solution as a solid metal cathode. A direct current is applied to the purified solution to produce Zn metal at the cathode and oxygen gas at the anode:

$$Cathode : Zn^2 + (aq) + 2e^- -> Zn(s) \tag{2.3}$$

$$Anode : H_2O(aq) -> 1/2O_2(g) + 2H^+(aq) + 2e^- \tag{2.4}$$

2.2. Iron Incorporation in Minerals

It is important to get an understanding of the Fe sources in Zn mining. Fe occurs in non-ferrous ores in the following way: ore minerals, gangue minerals, and solid solution [33].

- Ore minerals: Fe is an essential constituent of the targeted mineral containing the metal for mining (that is not Fe). For ZnS ores, Fe is not present in this form in significant quantities [33].
- Gangue minerals: Gangue minerals are undesirable in the ore. The two most common Fe-bearing gangue materials associated with sulphide ores are pyrite (FeS2), the most common, and pyrrhotite (Fe1-xS), containing 46.6 wt% and 59-62 wt% Fe respectively. In the selective flotation of sphalerite, pyrite flotation is usually depressed using lime, a collector chemical (specifically targets ZnS mineral) and Cu [34]. At high pHs, the pyrite surface is more hydrophilic than in low pH ranges due to the formation and adsorption of Fe-hydroxide complexes on the surface [35]. As a consequence, the Fe present in gangue material can be targeted in beneficiation; however, the Fe removal will depend on grain size and texture of Fe-bearing minerals [33].
- Solid solution: Fe substitutes the essential element (Zn) in the crystal structure. The most common form of Fe present in solid solution with ZnS is marmatite (black sphalerite), $(Zn_{1-x},Fe_x)S$. The Fe content varies from 0.1 to 17.4 wt% [33]. Fe present in solid solution cannot be removed by beneficiation.

Fe is present in Zn concentrates typically due to its presence in solid solution with Zn sulphide ores. The average Fe content in Zn concentrates was estimated to be 7.34 wt. % [27].

2.3. Recent Advances in Zinc Hydrometallurgy

This section outlines some recent developments in industrial Zn hydrometallurgy.

Due to the decline of ZnS reserves worldwide and environmental restrictions on SO_2 there has been increasing interest in processing zinc oxide ores. The advantages of zinc oxide ores over sulfide ores include a higher Zn content, lower hardness requiring less detonation, and exploitability in open cast mines. One oxidized ore is zinc silicate (Zn_2SiO_4), which is commercially treated and processed through hydrometallurgy and solvent extraction. The main downside is higher acid consumption rates necessary to increase Zn recoveries to a commercially acceptable standard. Dias [36] implemented a pre-neutralisation step in order to increase Zn recovery whereby 6% of the leached zinc silicate cake is diverted to the end of the process. This increased Zn recoveries by 0.64% without the modification of other process parameters.

A promising study in the literature [7] was cited for removing substantial quantities of Cu from the Zn leach solution. The study uses precipitators to remove Cu and Co from Zn leach solution. First, slow release sulfur agent (precipitator) is added to the leach solution. As S^{2-} is released into solution, it selectively reacts with Cu to form CuS (see Figure 2.2). CuS has the lowest solubility of most of the metal sulphides in solution and hence precipitates. Over a duration of 3 hours, close to 100% of Cu is removed from solution. The precipitator is considered a more economic alternative to using Zn powder for cementation.

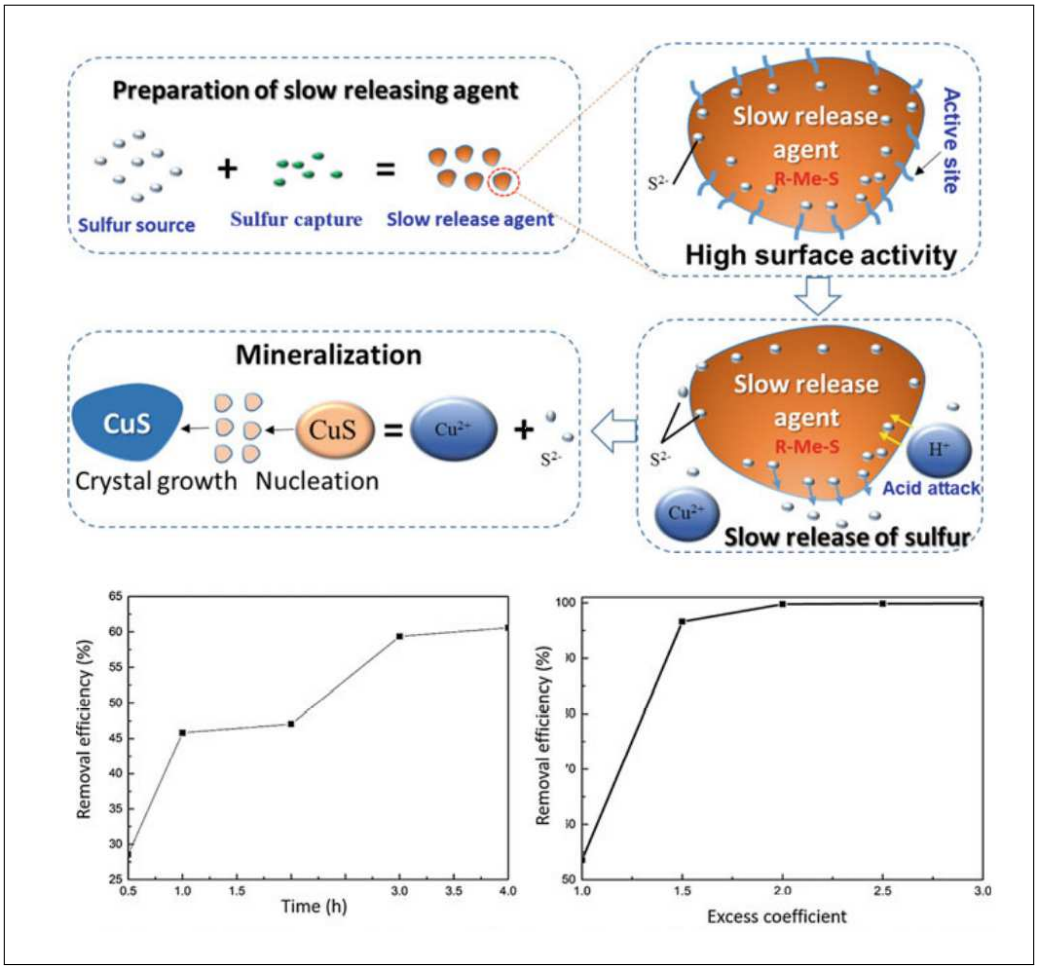

Figure 2.2: Schematic illustration of slow-release mineralization for Cu removal and recovery and observed recovery rates (pH 2-4, T = 70°C, time = 3hrs, precipitant at 2 x required theoretical concentration [7].

2.4. Iron Control in Zinc Hydrometallurgy

2.4.1. Overview of Established Processes

Figure 2.3 incorporates Fe control in Zn hydrometallurgy.

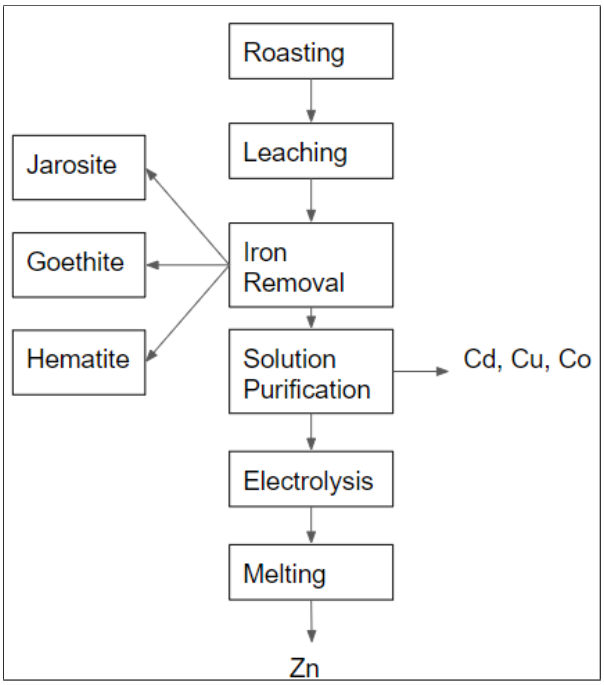

Figure 2.3: Zn extractive metallurgy flow sheet with Fe removal incorporated.

There are three dominant Fe removal processes that are employed in the Zn industry: jarosite, goethite, and hematite. Each of these processes are named after the Fe compound that is precipitated out of the leach solution. Jarosite, goethite and hematite precipitate under specific conditions explained by Figure 2.4.

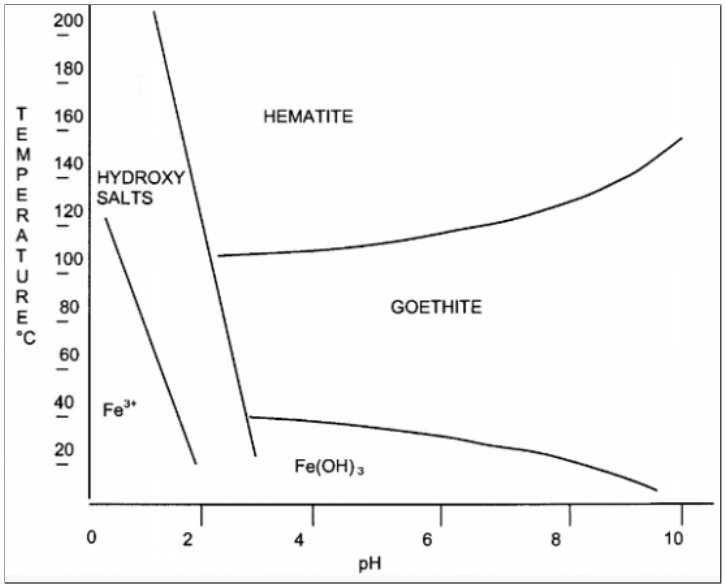

Figure 2.4: Conditions for the precipitation of Fe oxide, oxide, hydroxide and hydroxy salts from 0.5 M Fe(III)SO4[8].

This section provides a high level overview of each of the Fe removal processes. The jarosite process will be explored in more detail as it is of consideration for this thesis. Table 2.1 indicates the concentration of elements like Fe, Zn and Pb in the Fe precipitates. It is important to note that the figure incorporates the paragoethite process which is a variation of the goethite process that is used in industry. It also compares the mass of residues produced per 100 tonnes of Zn concentrate. The figure does not indicate the Cu concentrations in the residue as this was not something that was specifically monitored in the study.

Table 2.1: Comparison of products from Fe removal processes (based on 100 tonne of Zn concentrate feed). The VM Goethite and paragoethite process are variations of the Goethite process [21].

Process	**Jarosite**	**VM-goethite**	**Paragoethite**	**Hematite**
Residue Fe Content	29.0%	40.0%	34.0%	57.0%
Residue Zn Content	3.5%	8.5%	13.0%	1.0%
Residue Pb Content	1.9%	1.9%	2.2%	0.0%
Quantity of Residue	22.5t	16.2t	19.2t	11.2t
Zn Loss in Residue	1.5%	2.7%	4.8%	0.2%
Overall Zn Recovery	97.9%	97.6%	94.6%	99.0%

Table 2.2 provides an overview of the processes based on an economic and environmental perspective. Tables 2.1 and 2.2 demonstrate that the jarosite process is easy to implement with moderate CAPEX and OPEX which is why it is widely adopted; however, it produces an Fe residue with the highest impurity content and also the highest quantity of residue per 100 tonnes of Zn concentrate processed. The hematite process is expensive to operate but produces the least Fe residue with the lowest impurities.

Table 2.2: Comparison of environmental and economic factors of Fe removal processes [22].

Variable	**Item**	**Sub-Item**	**Goethite Process**	**Jarosite Process**	**Hematite**
Environment	**Ponding**	**Management**	Easier	Difficult	Easier
		Rehabilitation	Safer	Difficult	Safer
Economics	**Reagants**	**Oxygen (kg/t Zn)**	32	None	More than goethite
		Ammonia (kg/t Zn)	None	9	None
		Acid (kg/t Zn)	None	+120 vs Goethite	More than Goethite
	Energy	**Steam**	1.2	1.55	More than Goethite
	Cost	**CAPEX**	MED	MED	HIGH
		OPEX	MED	MED	HIGH

2.4.2. Recent Advances

This section describes recent advances is addressing Fe control in Zn hydrometallurgy.

Maghemite (γ-Fe_2O_3) fine particles were used to remove Fe with the goethite process. During goethite precipitation, maghemite and hydrogen peroxide (oxidant) are added to the solution. The maghemite particles are magnetic in nature and form seeds for goethite precipitation. The goethite is removed through a magnetic drum separator. The aim of the study was to produce Fe that can be used for steelmaking; however, the concentrations of impurity metals were not detailed in the study [37].

Akita Zinc Co. is the only Zn refinery that employs the hematite process. This is because it is costly and difficult to operate. Figure 2.5 provides a schematic of the Akita Zinc Process. Increasing Zn production rates and increasing Fe content in concentrates has required Akita to upgrade their plant to accommodate hematite production rates. Leaching autoclaves in use since the 70s were replaced. The reduction in fresh water input and the de-arsenic process filter upgrade was required to stabilise Zn production. The hematite produced by the Akita Process contains 54.1% Fe, 0.6% Zn and no observable quantities of SiO_2, Cu and As. If the economics of the process declines, it may be a promising path forward in reducing the Fe produced from Zn extraction.

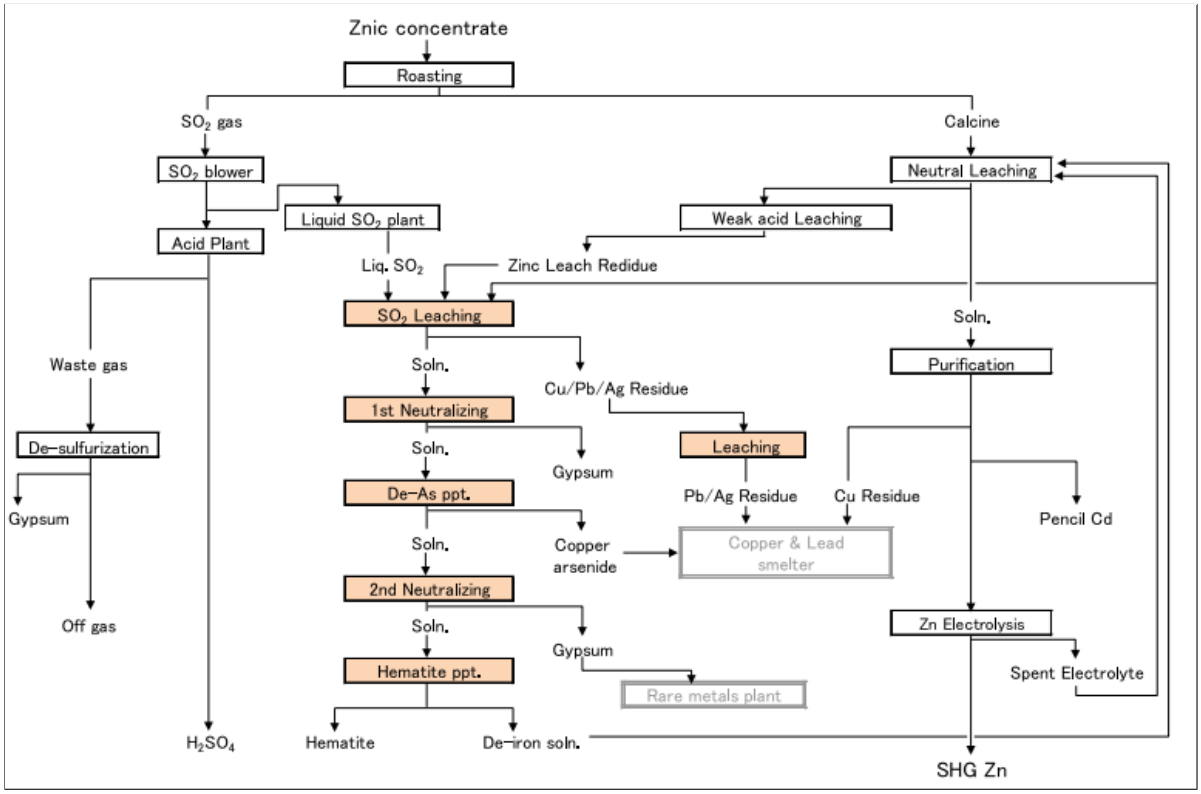

Figure 2.5: Schematic of the Akita Zinc Process[9].

Llamas [38] assessed 10 different Zn production processes to find the most resource efficient method to minimise the amount of Fe precipitates produced. It was a simulation based assessment that was carried out using HSC software. Two major processes were identified and compared: (1) Direct Zinc Smelting (DZS) and (2) Roasting Leaching Electrowinning (RLE) process. Direct Zinc Smelting involves a two stage process where in the first stage the concentrate is smelted to remove SO_2 and some of the volatiles (Zn, Pb, Ag, In, Ge) whilst producing a Zn alloy and slag. The slag is then reduced in the second stage to fume Zn and other metals to form a cleaner Fe-rich slag which can be disposed of or used as construction material. The RLE process, as previously discussed, removes the Fe via jarosite precipitation. From a resource consumption standpoint, using a 100% DSZ process produces the lowest amount of Fe residues whilst consuming the least resources; however, metals like Ni and Co are lost in the slag and the CO_2 emission is high. The paper identifies as the most resource efficient and environmentally friendly alternative the standard RLE process with the addition of pyrometallurgical treatment of jarosite through smelting and reduction stages. This solution has the disadvantage of increased resource consumption and CO_2 production; however, this is offset by the added benefits to society through lower pond volume requirements [38].

2.4.3. Jarosite Process

The jarosite process is the most commonly used Fe removal method used in the Zn industry due to its flexibility and capability of being readily integrated into existing and new Zn leach plants [39]. For jarosite precipitation to occur, low pH values (pH 1.5), elevated temperatures (95°C), and the presence of a monovalent cation (Na+ or NH4+) is required. Neutral residue (from 2.1) is subjected to hot leaching (85-95°C > 100g/L H_2SO_4) to release Zn and also Fe from the zinc ferrite. The hot acid leach solution is still pretty acidic with 40 g/L of free acid, therefore calcine is added to increase and maintain the pH at the level required for jarosite precipitation (pH 1, 10g/L H_2SO_4) [10]. At these higher pH values only the ZnO in the calcine is dissolved and not the ferrite. The residue is returned to the acid leach step. The monovalent cation is then added to precipitate the Fe as a jarosite (iron hydroxysulfate) according to the following reaction:

$$3Fe^{3+} + 2SO_4^{2-} + M^+ + 6H_2O => MFe_3(SO_4)_2(OH)_6 + 6H^+ \tag{2.5}$$

where M = Na^+, NH_4^+, H_3O^+, Ag^+, Pb^{2+}, and K^+. Fe in the structure can be substituted by Cu^{2+}, Zn^{2+}, Cr^{3+}, Al^{3+} [40, 41]

Equation 2.5 indicates that jarosite precipitation results in the formation of more acid. This needs to be neutralised in order to maintain the pH and continue the reaction. The pH of 1.5 is maintained with the addition of more calcine. Jarosite precipitation is carried out at 95°C for a few hours and reduces the overall Fe concentration from 20g/L to 1g/L. Jarosite precipitation incorporates impurities and ferritic Zn which cannot be recovered. Figure 2.6 shows how jarosite precipitation is integrated into Zn production. The processes employed in jarosite precipitation is highlighted by the red rectangle.

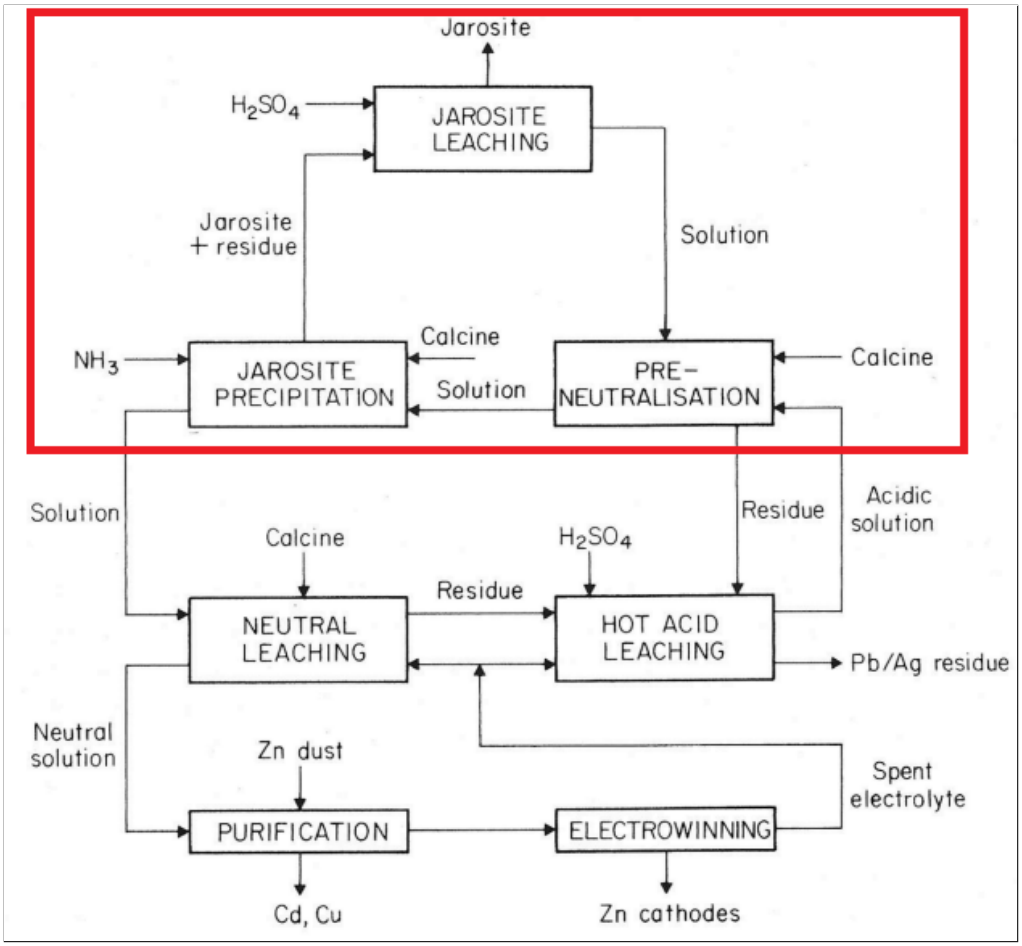

Figure 2.6: Schematic of integrated jarosite precipitation in Zn RLE process[10].

The jarosite is also washed to remove any undissolved calcine. Jarosite residues contains heavy metals (ie. Cd, As, Zn, etc) meaning it is classified as a toxic waste and needs to be landfilled in a controlled environment. For every tonne of Zn metal produced, there is a tonne of jarosite (wet basis) produced with it [42].

2.4.4. Literature Survey - Jarosite Treatment Options

There are three typical approaches to treating the Fe residues that are generated from Zn extraction [43]:

- Stabilisation - blending the waste residue with other materials to make the material less hazardous. The resulting material is either used in construction or stored.
- Hydrometallurgical - leaching the waste residue with aqueous solutions to recover valuable metals. These metals are recovered by subsequent processes (solvent extraction, electrolysis, etc).
- Pyrometallurgical - high temperature process that converts the residue to a metal rich product and a slag. The process generates off-gases and is energy intensive.

2.4.4.1. Stabilisation

Stabilisation involves mixing waste residues with other materials to alter their physical and chemical properties without any metals recovery. The final product is classified as non-hazardous waste [43]. The simplest approach taken by industry is the addition of lime and/or cement to the jarosites to form a compact and inert material that can be stockpiled. Examples are Jarofix and Jarochaux process (see Figure 2.7).

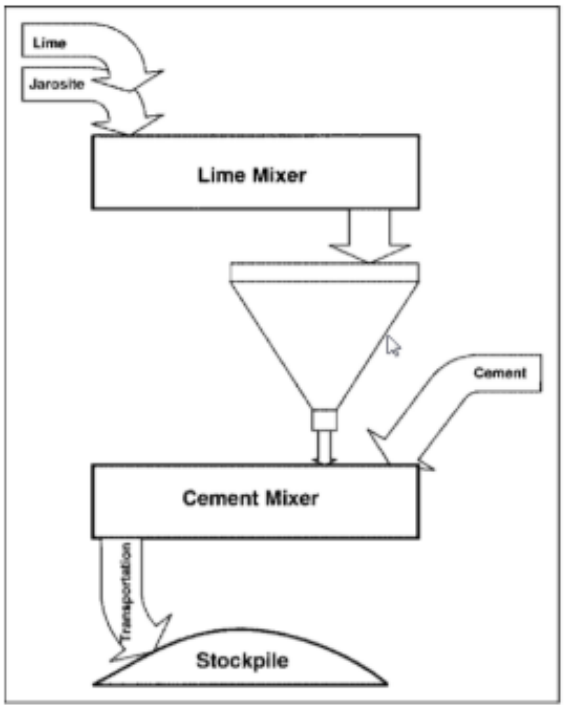

Figure 2.7: Process diagram for the Jarofix [11].

Other methods include the Graveliet process in which goethite residue is mixed with blast furnace and BOS converter slags. Reactions between the slags and the goethite result in an inert material

after curing. The downsides to this stabilisation are that (1) valuable metals are not recovered, (2) it is challenging to find uses for the stabilised product, (3) land is still required for stockpiling, and (4) chemical reagents are required for the process which can be expensive.

Fe residues have also been converted to other inert products. For example, goethite has been mixed with other inexpensive raw material (granite scraps, glass cullet and sand) to produce glass ceramic that has the potential for large-scale commercial application [44]. Mixtures are melted and then quenched to obtain glass. Subsequent nucleation and crystallization produces the glass-ceramic material. Good hardness and mechanical strength provides opportunities for these materials to be used as aggregate or glass concrete.

2.4.4.2. Hydrometallurgy

Hydrometallurgy entails aqueous chemical processes like leaching and re-precipitation [43]. Hydrometallurgical treatments of jarosites to remove impurity metals are largely unproven and there are no current commercial applications; however, some theories and recent attempts at hydrometallurgical treatment of jarosites will be considered in this section. Leaching effectiveness is based off of Pourbaix and predominance diagrams of metal species. These indicate the stability of metal species under specific conditions and can therefore provide guidance on the stability of impurity metal ions during leaching.

Acid Leaching
The general acid dissolution of jarosite occurs as follows [45, 46]:

$$MFe_3(SO_4)_2(OH)_6 + HB -> Me^+ + 3Fe^{3+} + 2SO_4^{2-} + 6H_2O + 6B^- \quad (2.6)$$

Where M represents metals identified in equation 2.5 and impurity metals identified in the same equation (Cu^{2+}, Zn^{2+}, etc) can occupy Fe sites in the jarosite. HB refers to the acidic lixiviant used (B = anion of the acid compound).

This implies that when jarosite is treated with an acid, the leach solution will comprise of species indicated in Equation 2.6. Whether an impurity metal is precipitated out as a solid or remains in aqueous solution will depend on the selectivity of certain metals for B (from HB), SO_4^{2-} and their corresponding solubility in the leach solution. Pourbaix diagrams are indicative of which metals are stable in solution.

Kinetic studies of jarosite dissolution in H_2SO_4 have been carried out by Reyes et. al [47], which demonstrated that dissolution was dependent on temperature. Optimal dissolution rates occurred at temperatures ≥50°C. Metal selectivities, however, were not established. Calla-Choque established high Ag recoveries by decomposing jarosite in an acidic media containing thiourea and sodium oxalate [45]. Nheta [48] leached Ni from jarosite using HCl (0.5-1M), liquid-solid ratio (L/S) = 10, Temp = 25°C and leaching time = 90 minutes. 60% leaching efficiency of Ni was achieved while keeping Fe in the solid (other metals were not monitored). Selectivities of Pb and Zn via acid leaching of jarosite with inorganic acids like HCl, HNO_3 and H_2SO_4 were investigated and compared to the leaching efficiency of methanesulfonic acid (MSA) [49]. Methanesulfonic acid (MSA) is a strong organic solvent that is considered a less toxic alternative to standard inorganic acids. It is non-oxidizing and a highly conductive acid with its metal salts being highly soluble in water. Zn more readily dissolved in all the acids at low concentrations (< 1M) compared to Pb and Zn. At higher concentrations Pb and Fe were released into solution as well. Leaching with pure MSA resulted in all the Pb and some Zn being extracted to the pregnant leach solution (PLS), while the Fe and the remainder of the Zn precipitated. This established that MSA was able to selectivity leach Pb over Fe [49].

Alkaline Leaching
Alkaline decomposition occurs according to the following reaction [40, 41]:

$$MFe_3(SO_4)_2(OH)_{6(s)} + 3OH- > Me_{(a}q_{)}^{+} + 3Fe(OH)_{3(s)} + 2SO_4^{2-} \quad (2.7)$$

An advantage of this approach is the immediate re-precipitation of $3Fe(OH)_{3(S)}$, which allows for separation of the Fe-rich solid via filtration. The optimal dissolution temperature of jarosite in alkaline media was also indicated to be ≥50°C by Reyes [47]. At these elevated temperatures the amorphous and slimy iron hydroxide product converts to more crystalline hematite that can be more easily filtered which is an added advantage [50, 51].

Indium bearing jarosite was decomposed in NaOH [52]. 98% of Jarosite was decomposed in NaOH (Temp = 60°, L/S = 2, time = 2 hrs) with subsequent precipitation of Fe_3O_4. Impurity elements were monitored (Zn, In, Cu, Cd, etc) and remained in the residue after jarosite decomposition. Vu decomposed jarosite in both NaOH (7.5%w) and aqueous ammonia solution(7.5%w) whilst monitoring impurities Cu, Mn, Ni, Co, and S (reaction conditions: L/S = 8, Temp = 40 °C, time = 420 minutes). Although not completely removed, significantly fewer impurities reported to the Fe residue when jarosite was leached with aqueous ammonia solution [51].

Malenga [53] leached Ni bearing ammonium jarosite with KOH, NaOH and NH_4OH. This was compared to the addition of a chelating agent (EDTA) and a reducing agent (Na_2S). Ni was selectively leached from ammonium jarosite with efficiencies of 82.48%, 84.5% and 88.9% in NaOH, KOH and NH_4OH respectively which had 0.1M EDTA-Na_2S. The optimal conditions were 250 rpm, 45°C, pH 9-10, L/S = 20, and leaching time of 4hrs.

Ionic Liquid Leaching
The term ionic liquids refer to salts with low melting points or glass transition temperatures (typically < 100°C). The low melting point is due to at least one of the constituent ions being large and having a low degree of symmetry [54]. Hydrometallurgical routes are considered to be cheaper and cleaner than pyrometallurgical routes but have issues with target metal selectivity over Fe. Replacing the aqueous phase in hydrometallurgy with an organic solvent (which is also the ionic liquid) increases the selectivity of metals as some metals cannot enter into solution without the high solvating power of water [55]. Selective metal recovery from jarosite residue using ionic liquids has been investigated. Jarosite was leached with ionic liquids [A336][Cl] and [C101][Cl] equilibrated with HCl. The metals (Zn, Fe, and Pb) were then stripped from the leachate using ammonia solution. Fe and Zn leaching selectivity was established over Pb when the ionic liquid was equilibrated with very high concentration of HCl (12M) [55].

Deep Eutectic Solvents (DES) are a new class of ionic liquids that are formed from a eutectic mixture of Lewis or Brønsted acids (Hydrogen Bond Donor - HBDs) and bases (Hydrogen Bond Acceptor-HBAs) [56]. The most commonly used HBDs are amides, polyols, and carboxylic acids. Common HBAs are symmetric quaternary ammonium and phosphonium salts. The solubility of several metal oxides in ionic liquids based on choline chloride (HBA) were determined by Abbott [57]. These were compared to aqueous solutions of HCl and NaCl. DESs were also used to selectively recover Zn from electric arc furnace dust [58]. Abbott [57] concluded that the selective extraction of Pb and Zn can be fine tuned through the selection of an appropriate HBD. Purification of the metals can be achieved with subsequent cementation, electrowinning or precipitation using an aqueous based complexing agent. A DES mixture of choline chloride and levulinic acid was used to selectively extract Zn from goethite residues [59]. The presence of choline chloride was shown to increase the leaching efficiency and selectivity of Zn over Fe when compared to just leaching with only levulinic acid; however, the leaching efficiencies of Zn remained below 50% (L/S = 10, Temp = 40°C,time = 48 hrs).

Ammoniacal Leaching

Ammoniacal leaching is typically used in the extraction of nonferrous metals (e.g. Zn and Cu). Metals like Fe and Ca are not soluble in ammoniacal solutions because (1) ammoniacal solutions are typically alkaline and these metals are not stable in high pH solutions, and (2) these metals exhibit poor complexation ability with ammonia [16]. Metals like Zn, Cu, Ni, Cr are, however, capable of forming water soluble complexes with ammonia. Dissolution of Zn, Cu, Ni, Cr in ammoniacal media occurs as follows [60]:

$$M + NH_3 + 0.5O_2 -> [M(NH_3)_4]^{+2} + 2OH^- \quad (2.8)$$

Specific to an ammonium chloride lixiviant, the following reaction occurs to leach Zn (and applies to Cu, Cd, Ni, Pb, Cr and Ag as well) [61]:

$$ZnO + 2NH_4Cl -> Zn(NH_3)_2Cl_2 + H_2O \quad (2.9)$$

Iron oxides, ferrites and silica are not dissolved in ammoniacal leaching. Industrial examples of ammoniacal leaching include the EZINEX process [62]. In this process, Zn rich residues are leached in an ammoniacal solution. The pregnant ammoniacal leach solution is then purified with Zn cementation.

Ammoniacal leaching of jarosite was not observed in the literature. As mentioned in section 2.4.4.2, ammonia water has been used to decompose jarosite with the resulting residue having a lower concentration of elements like Cu and Zn.

2.4.4.3. Pyrometallurgy

Pyrometallurgical treatment of jarosite entails heating the residue (typically with other reactants) to elevated temperatures (>500 °C). Although pyrometallurgical treatments are much more energy intensive than hydrometallurgical treatments, higher throughput and recovery rates can be achieved.

Thermal Decomposition

Thermal decomposition studies of jarosite were primarily carried out to observe the changes in the residue and analyse any gas that was liberated at increasing temperatures. Kerolli [63] observed that complete decomposition of jarosite to hematite occurred at 500°C. The study revealed that water is released at 100-150°C, followed by ammonia at 150-300°C (if it were ammonium jarosite), and finally SO_2 at 420-550°C. Spratt [64] observed dehydration and dehydroxylation occurring at 270-400°C, with desulfurisation occuring at 500-600°C. Spratt proposed the following reactions (at specified temperatures):

$$2Fe_3(SO_4)_2(OH)_5 -> 2Fe_3O_{2.5}(SO_4)_2 + 5H_2O\ (300-400°C) \quad (2.10)$$

$$2Fe_3O_{2.5}(SO_4)_2 -> 3Fe_2O_3 + 4SO_2 + 2O_2\ (500-650°C) \quad (2.11)$$

Alternatively, Steinlechner [65] proposed the following reaction occurring at temperatures > 500°C:

$$2Fe_2(SO_4)_3 -> Fe_2O_3 + Fe_2(SO_4)_3 + 3SO_2 \quad (2.12)$$

Piskunov [66] indicated that jarosite completely decomposed at 750°C. After decomposition, the impurity metal elements remained in the decomposed jarosite.

Chloridisation

Chloridisation involves mixing the waste residue with a chlorine source ($CaCl_2$, NaCl, etc) and then subsequently heating the mixture. Upon heating, impurity metals form volatile chlorides and vaporize while leaving much of the Fe behind. $CaCl_2$ reacts with metal oxides via two methods: (1) direct or (2) indirect [67]. Equations for these reactions are specified below:

$$Direct: MO + CaCl_2 -> MCl_{2(g)} + CaO \quad (2.13)$$

$$Indirect: CaCl_2 + 12O_2 -> CaO + Cl_2$$
$$MO + Cl_2 -> MCl_{2(g)} + 12O_{(2)} \quad (2.14)$$

Where M = metal. The temperatures at which reactions 2.13 and 2.14 occur depend on the metal.

Cu converter slag was chloridised with the intention of using the Fe-rich waste for steelmaking. Cu and Zn were required to be removed as they are problematic elements for conventional steelmaking. Nagasue [68] observed that when the slag was mixed with $CaCl_2$ and roasted at 1000°C the resulting residue was almost completely depleted of Cu and Zn.

Wang applied a similar chloride volatisation process to waste jarosite and observed similarly high impurity removal. Jarosite was mixed with $CaCl_2$ and a small quantity of coal and then roasted at temperatures ranging from 800-1200°C for 2 hours. High volatilisation rates of Zn (98.26%), Pb (99.88%), Cu (97.32%), In (58.73%), and Ag (95.22%) were achieved while the calcium was able to fix the sulfur in the jarosite [69].

Thermal Reduction

Thermal reduction is a more common pyrometallurgical technique used to treat jarosite. A few studies have been conducted with the objective of each varying slightly. Tang [70] mixed jarosite with Ag-Pb residue, coke and other sulfur fixing additives. The solid mix was heated in a box resistance furnace at 1300°C for 2.5 hours to produce a Cu matte (which had high recovery of Cu 98.82%, Zn 98.84%, Pb 90.35%, and Ag 97.17%) and an inert slag which can be used for cement production. In a similar vein, jarosite was first calcined (to remove water, ammonia and sulfur) and subsequently mixed with blast furnace sludge and CaO. This mixture was brought to 1500 °C for 15 minutes in a muffle furnace (in an inert environment) to produce cast iron and a glassy slag [71]. Other thermal reduction approaches focused on recovering volatile valuable elements (Zn, Pb, Cd, Ag, etc) as fume products. In these approaches, jarosite was mixed with a reducing agent (coal) and lime and brought to a temperature range of 1000-1200°C. The volatiles were captured with high recovery rates [72–75]. In addition to the volatiles, the other product was either metallised iron which could be separated with magnets [72, 74, 75] and an inert slag that could be disposed of or used in the construction industry [73, 76].

2.4.4.4. Combined Pyro- and Hydrometallurgy

Ju devised a combined pyro- and hydrometallurgical route to extract Zn, Ag, Pb, Cu, Cd and Fe from jarosite. The approach involved first activating and decomposing the jarosite (650 °C) followed by leaching with NH_4Cl (6M, 105°C). The pregnant leach solution contained Zn, Ag, Cu and Pb with leaching efficiencies of more than 95%. The leach solution required Zn cementation to remove Ag, Pb, Cu and Cd producing a final NH_4Cl solution containing Zn only. The leach residue required further leaching in alkaline conditions to produce a very pure iron oxide [77].

Piskunov [66] attempted to produce commercial grade iron oxide pigment (with very low concentrations of Zn and Cu) from potassium jarosite by calcination and subsequent water washing. Jarosite was mixed with Na_2CO_3 (for sulfur fixation) and heated to 700-800°C. This decomposed the jarosite to a solid consisting of hematite and sulfate salts according to the following equation:

$$2KFe_3(OH)_6(SO_4)_3 + 3Na_2CO_3 -> K_2SO_4 + 3Na_2SO_4 + 3Fe_2O_3 + 3CO_2 + 6H_2O \quad (2.15)$$

The water soluble sulfate salts were then subsequently washed from the solid leaving behind a hematite product that contained 30-40% of the Cu and Zn from the original jarosite.

2.4.4.5. Summary

Overall, this section has highlighted the main metallurgical approaches in treating jarosite. They consist of hydrometallurgical approaches (selective leaching), pyrometallurgical approaches (decomposition,

thermal reduction and chloridisation) and combined pyro- and hydrometallurgical approaches (calcination followed by washing or leaching).

Since multiple approaches have been considered in the literature that show promise, a few approaches will be considered for this thesis. The approaches will be focused on recovering Fe as a valuable product; therefore, stabilisation is not considered as an appropriate treatment strategy. Out of the remaining approaches, effectiveness and simplicity will be highly regarded. Hydrometallurgical approaches such as leaching will be carried out because the treatment effectiveness can be quickly determined. Thermal decomposition is also relatively straightforward. Chloridisation is an approach that has shown great promise in removing Cu from jarosites so it will be attempted in this thesis as well. For combined (hydro- and pyro-) approaches, calcination of jarosite with Na_2CO_3 followed by a subsequent water wash will also be pursued.

3

Jarosite for Ironmaking

This section outlines the purpose of this thesis (i.e. treating jarosite residues so it is acceptable for use in HIsarna ironmaking). It will briefly discuss the main difference between HIsarna ironmaking and conventional blast furnace ironmaking (Section 3.1). This is then followed by an indicating what impurities must be removed prior to HIsarna ironmaking (Section 3.2) and finishes with strategies (given treatment options reviewed in Section 2.4.4) that will be considered to create a product suitable for HIsarna.

3.1. HIsarna Ironmaking Process

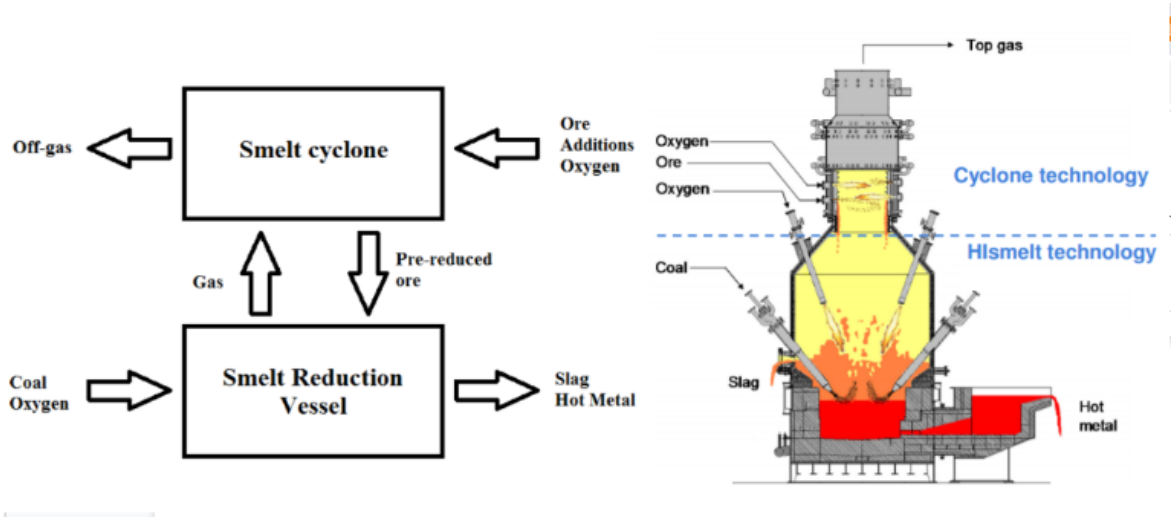

Figure 3.1: HIsarna Process flow diagram (left) [12], and schematic of HIsarna furnace (right) [13]

HIsarna is an Fe production process that was developed between Tata Steel, ULCOS (Ultra-Low Carbon Dioxide Steelmaking - a European Union programme) and Rio Tinto. The HIsarna process aims to reduce CO_2 emissions in steel production by 20%. It aims to achieve this by replacing the coking, sintering, pelletisation and the blast furnace processes of traditional steel operations with a single process. The process is designed to enable efficient CO_2 capture which can reduce CO_2 emissions by up to 75% [78].

The HIsarna process consists of two parts: a pre-reduction (in the Smelt Cyclone) and reduction (in the Smelting Reduction Vessel), see Figure 3.1. In the pre-reduction step, ore and oxygen are injected into the Smelt Cyclone (SC), where partial reduction occurs (10-20%). The ore melts and dissolves into the slag creating an emulsion with high metal-slag interface. CO is also generated which increases both the metal-slag contact and the FeO content in the slag (more so than blast furnace slag). The pre-reduced ore then flows down into the Smelting Reduction Vessel (SRV) where it is further reduced by injected coal. O_2 is also injected to react with the coal to produce CO. The temperature of the SRV is around 1400-1450°C which is lower than a blast furnace. Since pre-reduction occurs in the SC, the environment in the SRV is less reducing than a conventional BF which results in low Si, P and Mn; however, there is higher sulfur content (when compared to BF hot metal) in HIsarna hot metal due to the injected coal (which has higher sulfur content) and the higher oxygen potential in the HIsarna reactor (see Figure 3.1) [12].

Table 3.1: Typical hot metal compositions for BF and HIsarna [12]

Element	BF range [%]	HIsarna range [%]	HIsarna vs BF
C	4.5-5.0	3.7-4.3	lower
S	0.02-0.06	0.1-0.2	higher
Cr	0.009-0.013	0.03-0.10	higher
P	0.06-0.08	0.02-0.06	lower
Mn	0.25-0.4	0.02-0.05	lower
V	0.05-0.07	0.005-0.013	lower
Si	0.3-0.7	0.003-0.013	Close to 0
Ti	0.05-0.11	0-0.002	Close to 0

3.2. Boundary Conditions

Table 3.2 shows the typical elemental composition of some industrial sources of jarosite presented by VTT [23].

In the table, Cu, S and Pb are at concentrations that are considered problematic for the steelmaking industry. In addition, Cr, Sn, Mo and Ni cause problems in steelmaking. These elements do not present issues to the HIsarna ironmaking process but negatively impacts steelmaking that occurs downstream of HIsarna ironmaking. If they are incorporated into the hot metal that is produced by HIsarna ironmaking, these elements are difficult to remove; therefore it is preferential that the concentration of these elements are minimised in the HIsarna feed.

Jarosite has a modestly high sulfur content. It is not high enough to generate a gas stream rich enough in SO_2 for sulfuric acid production but it is sufficiently elevated that it cannot be vented. As a result, off-gas treatments are required adding cost and complexity [79] to any treatment. Therefore, if possible, sulfur removal in solution (i.e. sulfur fixation and subsequent dissolution as a sulfate salt) is a preferred. The presence of sulfur in steel improves machinability in applications where tensile strength and other mechanical properties are not important, as excessive sulfur content leads to a reduction in impact strength, ductility and weldability [80].

Cu is completely soluble in steel and dilution is the only economically feasible way of limiting its concentration. The presence of Cu in hot metal has a very negative effect on the surface of the steel and promotes hot-shortness during hot rolling, forging and casting operations. Cu tends to accumulate in grain boundaries leading to intergranular fractures [80]. Chromium causes a reduction in ductility when tempered or cooled in particular temperature ranges (370°- 600°C). The presence of chromium also causes other issues: (1) chromium oxide is only stable at very high temperatures and therefore more heat and longer processing times are required to remove it in the form of an oxide, and (2) hexavalent chromium can be found in the baghouse which is considered a hazardous waste [80]. Tin

Table 3.2: Composition of different industrial jarosites as provided by VTT [23]

	Boliden, Kokkola	**Nyrstar, Budel**	**Trepça, Kosovo**	**HZL, Debari**	**Gegamines, Kolwezi**
Ag	0.007-0.012	0.052	0.0001		0.008-0.016
Al	0.3-1.0	1.4	0.8	3.6	
As	0.1-0.6		0.5		0.39
Au	0.00005				
Ba			0.06		
Ca	1.5-5.0	4		4.8	
Cd	0.01-0.07	0.05	0.22		0.12-0.16
Cl	<0.005				
Co	0.002-0.010	0.0004	0.003		
Cr			0.04		
Cu	0.1-0.2	0.6	0.92		2.7-2.9
Fe	8.0-32.0	11.5	31.3	23.7	26.6-32.8
Ga					0.045-0.11
Ge	0.003-0.004	0.019			0.047-0.049
Hg	0.0006-0.01				
In	0.006-0.009				
K	0.5	0.9		0.6	
Mg	0.1-0.3			1.1	
Mn	0.01-0.2	0.06	0.63	0.2	
Mo	0.004				
Na	0.3-1.7	0.3		0.7	
NH4			0.6	1.9	
Ni	0.01	0.002	0.009		
Pb	1.0-6.0	13.1	7.5	1.9	2.1-2.4
S	3.0-35.0	10.5	6.6	12.2	4
Sb	0.01-0.08				
Se	0.0003-0.003				
Si	6.8	5	2.9	3.4	
Sr			0.014		
Tl	0.0006-0.0012	0.01			
Zn	2.0-4.0	3.7	10.2	8.2	16.8-19.4

is almost completely soluble in steel and does not oxidise. Upon cooling it segregates into the grain boundaries leading to hot-shortness [81]. Compared to Cu, the presence of tin increases the likelihood of hot-shortness by five times [80]. Molybdenum in solid solution 'stiffens' ferrite and decreases its ductility. In addition, it forms carbides (which impact the hardenability of the steel) and inhibits desirable microstructural changes in the steel. Typically, the presence of nickel has a positive impact on steel properties; however, nickel reduces the ductility of steel if it is present in solid solution [80]. The issues associated with the presence of lead are mainly indirect; however, its presence in hot metal can cause hot shortness. Lead is toxic and has high permeability in refractory bricks. Lead readily volatilises at steelmaking temperatures and ends up in baghouse dust leading the dust to be classified as a hazardous material [80]. Figure 3.2 shows the elemental distribution in a basic oxygen furnace in steelmaking. This is a simulated situation based off the thermodynamics but highlights why the metals are very difficult to remove once they are in the hot metal.

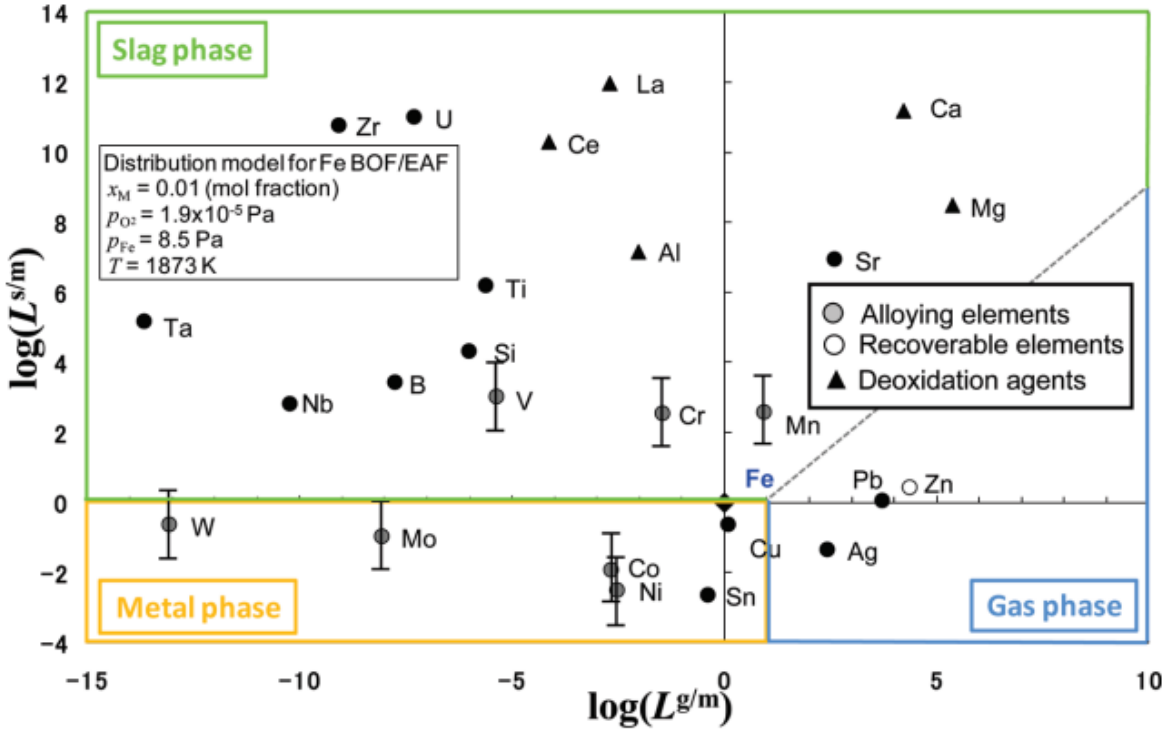

Figure 3.2: Distribution chart of elements among gas, slag, and metal phases for the metal recovery under simulated atmosphere of converter of steelmaking [14]

Cu, Sn, Ni, Mo, Pb and Cr enhance the degree of hot-shortness caused by Cu and are typically grouped together as a "Copper Equivalence Factor" (CEF) to summate their impact [82]. The CEF limit provided by Tata Steel for their applications is shown below:

$$CEF: Cu + Ni + Cr + 5Sn + 10Mo \leq 0.2wt\% \tag{3.1}$$

Zn is typically a problem for blast furnace ironmaking. The build up of Zn causes continuous degradation of blast furnace lining [83]. For HIsarna ironmaking, however, Zn is vaporized and collected as dust without the same refractory issues in conventional ironmaking. If the content of the Zn in the dust is high enough, it can be utilised by the Zn industry. Therefore, it is preferred to maintain the Zn concentration in the BLP whilst removing the CEF metals mentioned in this section. The main challenge is that techniques used to remove Cu from BLP will target Zn and vice-versa, because they have similar chemical properties.

4

Experimental

4.1. Approach

The jarosite residues were provided to the project by Nyrstar, Budel. Strictly speaking, the residue is called ”Budel Leach Product” (BLP) which, as indicated in Section 4.2.1, is a solid mix of plumbojarosite, zinc ferrite and lead sulfate. This thesis aims to treat BLP waste produced from a local Zn smelter (Nyrstar, Budel) by utilising hydro- and pyrometallurgical strategies outlined in Section 2.4.4 such that it is acceptable as feedstock for HIsarna ironmaking. This requires the CEF of the treated BLP to meet the criteria outlined in Equation 3.1 with a special focus on Cu removal. Although sulfur is not mentioned in Equation 3.1, it will also be targeted for removal but ideally not as a gas. As mentioned in Section 3.2, it is preferred to keep Zn in the treated BLP; however, this is challenging to achieve while trying to remove Cu. For the objectives of this thesis, Cu removal is a priority and the corresponding treatment strategies will likely remove Zn as well. In considering which strategies to select, effectiveness, cost and complexity are considered. The following approaches were undertaken as part of this thesis:

1. *Establishing CEF value of BLP*

   Characterisation of the jarosite is required to establish elemental compositions, main phases present, and the morphologies of the phases. XRD, XRF and SEM analyses will be carried out on the BLP sample. TGA analysis will also be performed to support results from the thermal decomposition of BLP.

2. *Hydrometallurgical Treatment of BLP*

   Similar to approaches reviewed in Section 2.4.4.2, BLP leaching will be carried out in an acidic, alkaline, ammoniacal and DES media. With the exception of DES, these reactions can be carried out relatively easily with chemicals that are readily available in the lab. The viability (or requirement) of additional processing steps after leaching can also be determined fairly quickly. Given the wide variety of possible lixiviants it is certain that each lixiviant will have its own optimal leaching parameters. Finding these optimal conditions for each lixiviant would pose a considerable challenge; therefore, it was important to screen the lixiviants to determine which were promising fairly quickly. It was appropriate to fix parameters and apply this consistently across all lixiviants. Selected experimental conditions (temperature, L/S ratio, rpms, and duration) were based on the limits of the experimental setup, potential for upscaling, and optimal conditions established in a handful of leaching experiments carried out in the literature. These conditions were: temperature: 50°C, L/S = 10, RPM = 300, duration = 2 hours, concentration = 0.5M [47, 49, 52, 53, 59]. By

setting these parameters initially, a range of lixiviants screened with only the most promising lixiviants warranting further investigation through a parametric study. The use of DES as a lixiviant is somewhat more of an 'academic' exercise as it is an area not well understood but that provides grounds for interesting exploratory work. The effectiveness of a lixiviant was determined by how the lixiviant could remove Cu (and the other CEF metals) while keeping Fe as a solid. Concentration of Cu and the remaining CEF metals will be confirmed by XRF analysis of the residual solid and ICP analysis of the PLS.

3. *Pyrometallurgical Treatment of BLP*

   Pyrometallurgical approaches are energy intensive and have high associated economic and environment costs. Selecting a pyrometallurgical approach was based on available equipment and its limitations (maximum temperature and gas environment) and the most promising approaches as identified in the literature. This resulted in two strictly pyrometallurgical approaches: thermal decomposition of BLP and chloridisation. Thermal decomposition is not a treatment strategy of BLP but it useful for analytical purposes. It also provides some insight into what results when using untreated BLP as a HIsarna ironmaking feedstock. Chloridisation was selected because it was a relatively simple and effective approach at removing Cu and Pb from BLP whilst fixing sulfur at temperatures ≤1100°C. Concentration of elements in the treated residue will be analysed by XRF. Qualitative off-gas analysis will carried out with a mass-spectrometer for only the thermal decomposition reactions.

4. *Combined Pyro- and Hydrometallurgical Treatment of BLP*

   Out of the two approaches outlined in Section 2.4.4.4, heating BLP with Na_2CO_3 and subsequent water washing [66] was selected. It is a simpler approach and fixes the sulfur in the BLP. A 60% reduction in the Cu content in the final residue (as observed in the paper) is promising and serves the purpose of this thesis. Other metals were not monitored so there is an opportunity to monitor all the CEF metals in this study.

4.2. Jarosite Characterisation

Prior to characterisation, the BLP was dried in a furnace (at 105 °C) overnight and ground into a powder. Approximately 20-22% weight loss (water) was measured when dried overnight.

4.2.1. XRD and XRF

XRD identification of the BLP was carried out as follows:

- Experimental: Bruker D8 Advance diffractometer Bragg-Brentano geometry and Lynxeye position sensitive detector. Cu Kα radiation. Divergence slit V12, scatter screen height 5 mm, 45 kV 40 mA. Sample spinning. Detector settings LL 0.19 W 0.05
- Measurements: Coupled θ -2θ scan 10° - 110°, step size 0.026 ° 2θ, counting time per step 2 s.
- Data Evaluation: Bruker software DiffracSuite.EVA vs 5.2.

The XRD pattern for BLP is indicated by Figure 4.1. The crystalline phases present in the BLP as indicated by XRD measurements are plumbojarosite [$(Pb_{0.34}K_{0.19})Fe_3(SO_4)_2(OH)_6$], zinc ferrite ($ZnFe_2O_4$) and lead sulfate ($PbSO_4$).

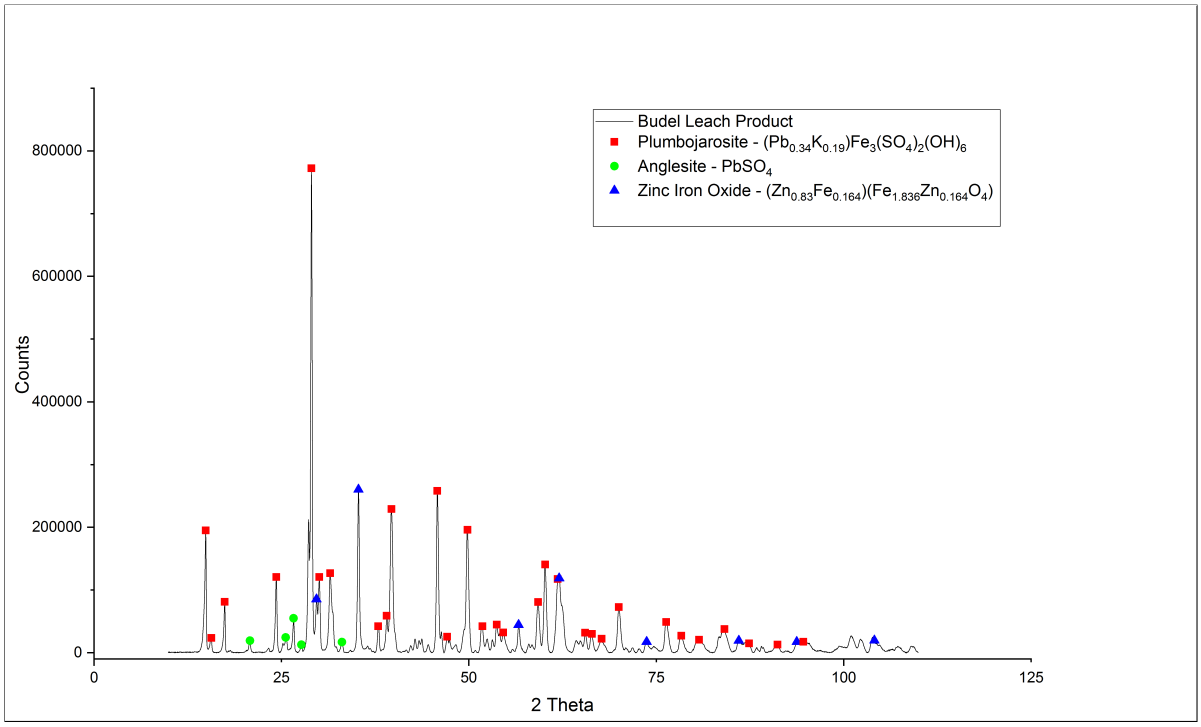

Figure 4.1: XRD Pattern of BLP.

For XRF analysis of the BLP, the measurements were performed with a Panalytical Axios Max WD-XRF spectrometer and data evaluation was done with SuperQ5.0i/Omnian software in oxides mode. Three separate samples were taken of the BLP and an average composition is provided in Table 4.1. In addition, the CEF value, as outlined in Section 3.2, has also been provided in the table. Table 4.1 shows that the CEF value in the BLP residue is approximately 9 times higher than what would be considered acceptable for HIsarna ironmaking feedstock.

Table 4.1: Elemental compositions (wt%) of 3 different samples (and average) of BLP provided by Nyrstar, Budel. This is compared with the the jarosite sample analysis of what is provided by VTT [23]. Elemental concentrations are determined by XRF. CEF = Cu + Cr + Ni + 5*Sn + 10*Mo (wt%).

Leach Residue (element conc wt%)	Sample 1	Sample 2	Sample 3	Average	VTT
Fe	22.965	23.137	22.651	22.918	11.5
Cu	0.754	0.743	0.748	0.748	0.6
Zn	6.125	6.140	6.727	6.331	3.7
Pb	10.679	10.660	13.113	11.484	13.1
Ni	0.000	0.015	0.016	0.010	0.002
Cr	0.060	0.064	0.066	0.063	0
Sn	0.166	0.154	0.190	0.170	0
Mo	0.007	0.011	0.010	0.009	0
Ca	3.583	3.478	3.183	3.415	4
S	9.099	9.096	9.791	9.328	10.5
Si	6.159	6.179	4.877	5.738	5
Al	1.048	1.052	0.728	0.943	1.4
K	0.573	0.504	0.959	0.679	0.9
Ba	0.551	0.598	0.646	0.598	0
Mg	0.334	0.000	0.198	0.177	0
Mn	0.168	0.170	0.187	0.175	0.06
Cd	0.174	0.152	0.193	0.173	0.05
Sr	0.104	0.102	0.130	0.112	0
Ti	0.079	0.119	0.079	0.092	0
P	0.076	0.077	0.055	0.069	0
In	0.012	0.091	0.017	0.040	0
Na	0.591	0.626	0.000	0.406	0.3
As	0.000	0.330	0.000	0.110	0
Sb	0.132	0.122	0.000	0.085	0
Bi	0.073	0.059	0.000	0.044	0
Ag	0.072	0.067	0.000	0.046	0.052
Tl	0.027	0.000	0.000	0.009	0.01
Co	0.000	0.000	0.000	0.000	0.004
Ge					0.019
CEF	1.718	1.696	1.879	1.764	0.602

4.2.2. Analysis of Morphology and Microstructure

BLP was analysed with SEM as shown in Figure 4.2. The image shows many particles of BLP analysed at 1,400x magnification. The sample was then diluted to isolate particles for analysis at 1,000x magnification (see Figure 4.3).

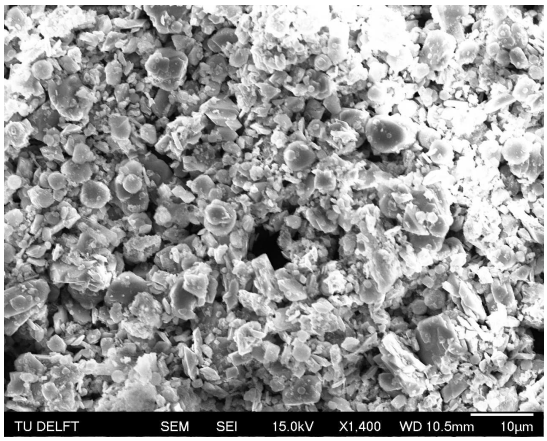

Figure 4.2: SEM SEI of 'bulk' BLP.

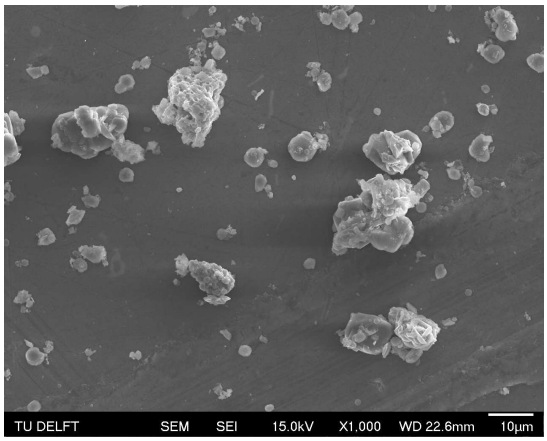

Figure 4.3: SEM SEI of isolated BLP particles.

Elemental mapping with EDS was then carried out on the isolated particles to determine which distinct phases were exist and how the problematic elements, such as Cu, are present (see Figures 4.4 and 4.5). The majority of the elements screened for in Figure 4.4 have extremely low counts and are within the error limits of the instrument; however, it is clear that particles containing Pb, S, O, and Fe are present (most likely plumbojarosite and lead sulfate as indicated by XRF and XRD). Calcium is present in one of these particles which may indicate the presence of $CaSO_4$ In addition, there appears to be a particle containing just silicon and oxygen which is most likely silica (SiO_2). Cu does not appear in a high enough concentration in any particular particle. EDS analysis was carried out to support the elemental mapping (see Figure 4.5). In the figure, Point 1 strongly supports the presence of silica and Point 3 indicates the presence of $CaSO_4$. Points 2, 4, 5 and 6 support the presence of plumbojarosite. Cu appears at its highest concentration at Point 4 coinciding with with presence of plumbojarosite, which suggests that Cu exists within the structure of the jarosite and not as separate particles with high Cu concentrations. Cu likely substitutes Fe in the plumbojarosite (as indicated by Equation 2.5).

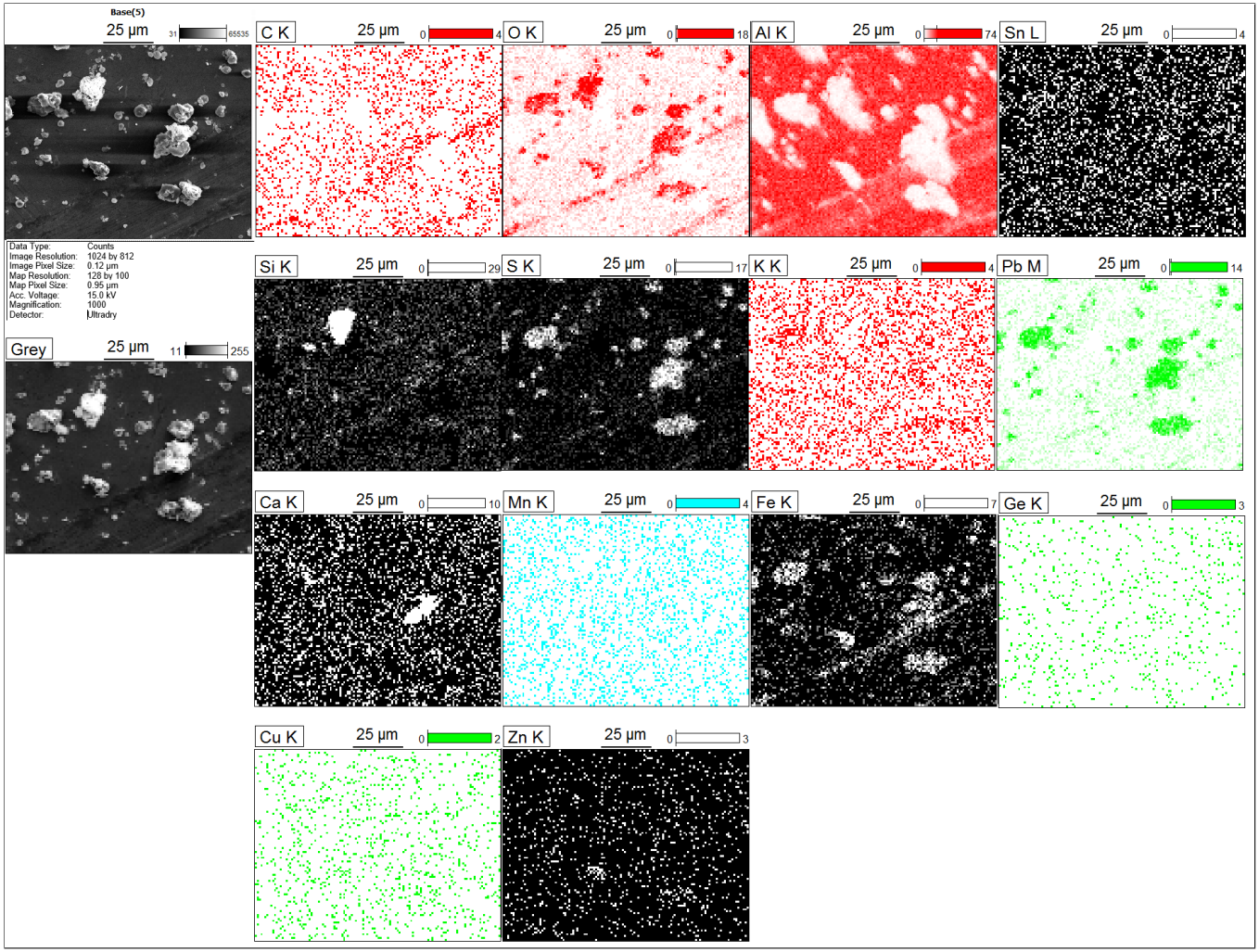

Figure 4.4: Elemental map of BLP based of figure4.3 (EDS).

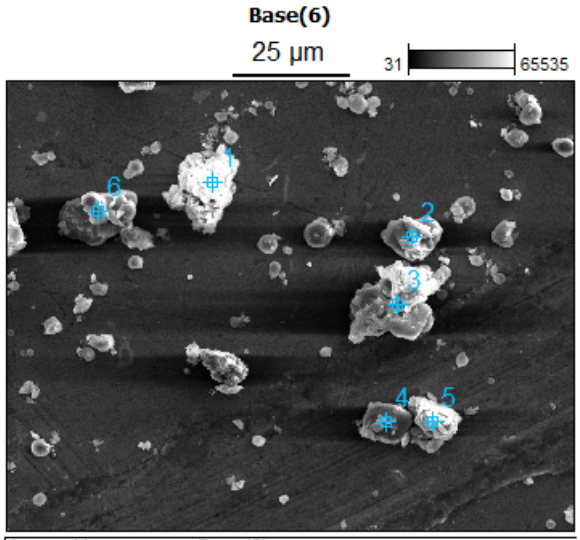

Image Name:	Base(6)
Image Resolution:	1024 by 812
Image Pixel Size:	0.12 µm
Acc. Voltage:	15.0 kV
Magnification:	1000

Weight %

	C-K	O-K	Al-K	Si-K	S-K	K-K	Ca-K	Fe-K	Cu-K	Zn-K	Sn-L	Pb-M
Base(6)_pt1	1.29	57.10	4.17	35.60	0.32	0.08	0.00	0.39	0.06	0.12	0.36	0.50
Base(6)_pt2	2.21	46.55	4.78	0.25	10.43	0.96	0.19	22.19	0.00	3.77	0.16	8.51
Base(6)_pt3	0.87	47.58	2.31	1.66	20.33	0.00	23.54	1.73	0.78	1.20	0.00	0.00
Base(6)_pt4	1.21	35.53	8.07	0.28	10.35	0.66	0.16	22.17	1.38	5.13	0.00	15.05
Base(6)_pt5	2.38	46.03	4.64	0.30	9.12	0.50	0.16	19.34	0.03	4.28	0.12	13.09
Base(6)_pt6	0.94	38.65	3.94	1.35	13.01	1.29	0.03	29.60	0.41	1.63	0.00	9.16

Weight % Error (+/- 1 Sigma)

	C-K	O-K	Al-K	Si-K	S-K	K-K	Ca-K	Fe-K	Cu-K	Zn-K	Sn-L	Pb-M
Base(6)_pt1	±0.20	±0.54	±0.15	±0.30	±0.06	±0.07	±0.00	±0.18	±0.36	±0.40	±0.20	±0.21
Base(6)_pt2	±0.34	±0.72	±0.17	±0.08	±0.44	±0.13	±0.11	±0.92	±0.00	±0.77	±0.40	±0.93
Base(6)_pt3	±0.16	±0.82	±0.14	±0.14	±0.29	±0.00	±0.45	±0.32	±0.48	±0.67	±0.00	±0.00
Base(6)_pt4	±0.20	±0.65	±0.22	±0.10	±0.54	±0.11	±0.11	±1.06	±0.65	±1.06	±0.00	±1.15
Base(6)_pt5	±0.33	±0.71	±0.17	±0.08	±0.49	±0.12	±0.10	±0.87	±0.36	±0.83	±0.37	±1.18
Base(6)_pt6	±0.18	±0.62	±0.18	±0.10	±0.47	±0.12	±0.12	±0.86	±0.74	±0.94	±0.00	±1.04

Figure 4.5: Elemental composition of particles based of point and shoot in Figure 4.5(EDS).

4.2.3. Thermo-gravimetric Analysis

Thermo-gravimetric analysis (TGA) was carried out on the BLP (see Figure 4.6). Approximately 58.3 mg of BLP was heated to 1400°C at 5°C/min in an argon atmosphere. Mass differences were recorded at two points on the curve indicated by point (A) and point (B). Off-gases were not monitored during the TGA. As previously mentioned in Section 2.4.4.3, at point (A), in the temperature range 300-400 °C, it is likely that dehydroxylation of the plumbojarosite within BLP is occurring (Equation 4.1) [64]:

$$2Fe_3(SO_4)_2(OH)_5 -> 2Fe_3O_2.5(SO_4)_2 + 5H_2O(300 - 400°C) \tag{4.1}$$

At point (B), 550-700°C, it is likely that desulfurization according to Equation 4.2 [65] is occurring. This will be discussed further in Section 5.2.1.

$$2Fe_2(SO_4)_3 -> Fe_2O_3 + Fe_2(SO_4)_3 + 3SO_2 \tag{4.2}$$

If we assume that all the mass change occurring at 300-400°C is coming from dehyroxylation then application of a simple stoichiomeric calculation may indicate the percentage of plumbojarosite in BLP:

$$(Pb_{0.34}K_{0.19})Fe_3(SO_4)_2(OH)_6 -> 3H_2O_{(g)} + metalsulfates/oxide) \tag{4.3}$$

Plumbojarosite has a molecular weight of 540g/mol and water weighs 18g/mol. Based on this:

$$\frac{7.50\%}{3 * 18\frac{g}{mol}H_2O} * 540\frac{g}{mol}plumbojarosite = 75\% \tag{4.4}$$

Equation 4.3 is based simply off equating hydrogen atoms. It does not include the complex metal oxides and sulfates that may result from the plumbojarosite decomposition or any other gas species that includes hydrogen or oxygen gas (including O_2) that may evolve from decomposition at that temperature. Equation 4.4 also does not take into account amorphous species of plumbojarosite which may exist but are not detected by XRD (this would reduce the composition of plumbojarosite in the BLP compared to what is calculated in Equation 4.4)

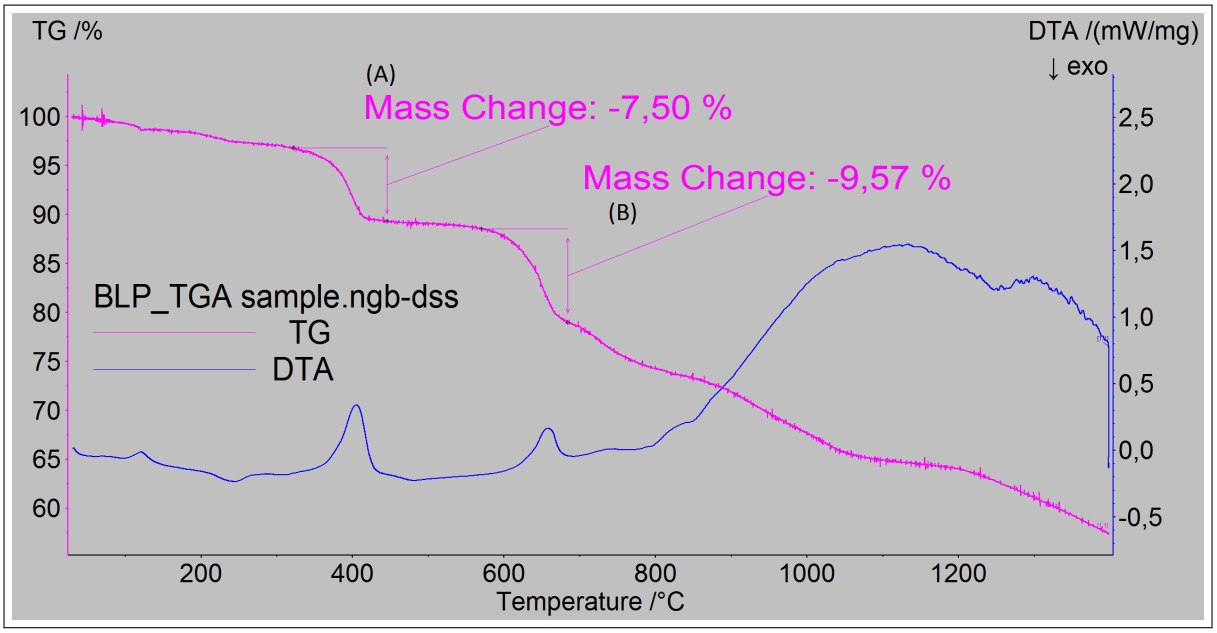

Figure 4.6: DTA/TG Analysis of BLP. Analysis carried out in Ar atmosphere, ramp rate 5°C/min.

4.3. Hydrometallurgical Treatment

This section outlines the hydrometallurgical approaches to treating BLP. As indicated in Section 1.5, leaching parameters (concentration = 0.5M, temperature = 50°C, rpm = 300 rpm, duration = 2hrs, L/S ratio = 10) were set based on optimal conditions in a handful of leaching experiments carried out in the literature. By fixing these parameters, a range of lixiviants could be screened for efficacy prior to carrying out parametric studies.

Aim

The presence of problematic elements (e.g. Cu) are unlikely to exist as isolated particles in high concentrations but instead are within the jarosite structure in the BLP (See Section 4.2.2). Consequently, the following hydrometallurgical approaches were selected based on the described rational:

- Acid leaching - Acids break down jarosite into constituent ions (see Section 2.4.4.2). This would theoretically release problematic elements like Cu into solution. The following acids were selected for their leaching selectivity of Zn and Cu over Fe: HCl (0-1M) [48, 49], H_2SO_4 (0-1M)[49], acetic acid (approximately 0.5M) [84]. Oxalic acid was chosen to selectively target Fe in BLP to produce a PLS rich in only Fe. Optimal leaching conditions for leaching with oxalic acid occurred at a pH of 2.5-3 [85].
- Alkaline leaching - Similarly to acid leaching, alkaline leaching breaks down jarosite but re-precipitates Fe in the form of Fe hydroxide (see Section 2.4.4.2). NaOH was used to leach Ni from jarosite [53]. This approach will be emulated with 0.5M, 1M, and 3M NaOH. EDTA (chelating agent) was also used in the study [53] to hold nickel in solution. EDTA will also be used in these experiments in order to try to hold Cu in solution.
- DES leaching has not been carried out on jarosite. For these experiments choline chloride (HBA - see Section 2.4.4.2) will be mixed with either glycerol or ethylene glycol (both HBDs that are readily available in the lab) at eutectic molar ratios (1:2) [56]. The resulting solution will be used to leach the BLP.
- Ammoniacal leaching was not carried out on jarosite previously but will be attempted here (see Section 2.4.4.2).

Figure 4.7 provides a basic schematic of how the hydrometallurgical experiments will be carried out. BLP (plumbojarosite) will be leached with a lixiviant in the specific conditions mentioned above and the resulting residue and leach solution will be analyzed to determine the efficacy of the experiment (see Section 1.5).

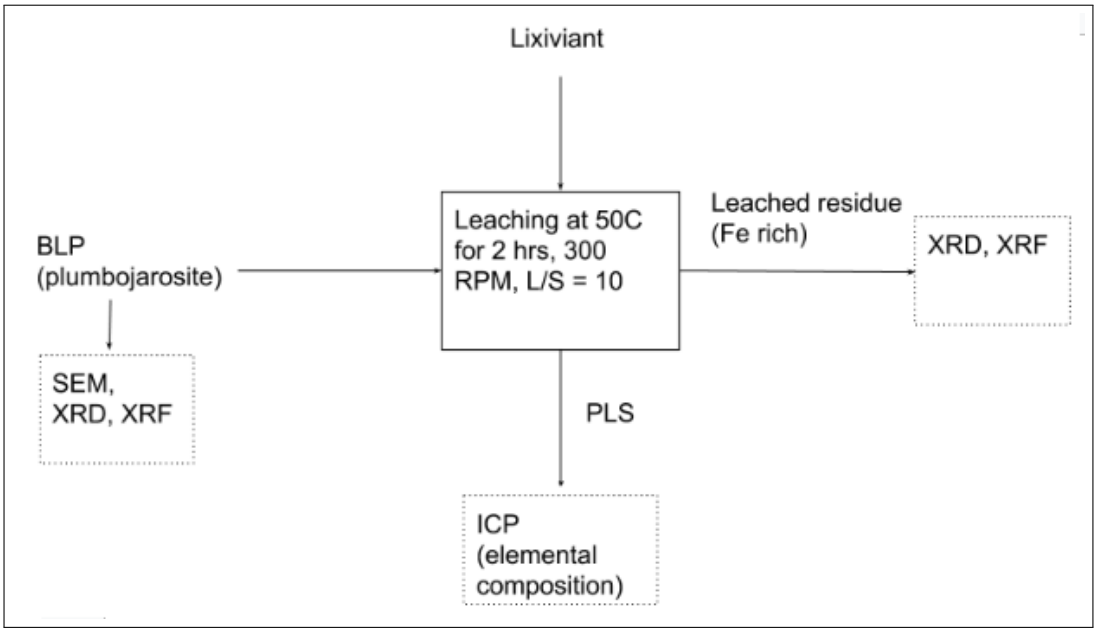

Figure 4.7: Flowsheet of hydrometallurgical experiments.

Experimental

Following steps were performed in the carrying out the hydrometallurgical experiments:

1. BLP from Nyrstar (Budel) was dried in a furnace set to 105°C overnight which resulted in a 20-22% weight loss.
2. The dried BLP sample was ground to a powder.
3. 150mL of lixiviant was added to a borosilicate glass jar with a magnetic stirrer inside. The jar had a cap containing holes for the temperature probe, pH meter and for sampling.
4. The jar was place on a magnetic hotplate with temperature probe.
5. The lixiviant was brought to 50°C.
6. Approximately 15g of the BLP powder was weighed and added to the lixiviant in the jar (L/S = 10).
7. Leaching was carried out over a period of 2 hours with sampling at 2, 5, 10, 15, 30, 60, 90 and 120 minutes.
    - Samples were taken through the top cap with a 5mL syringe
    - 0.5 mL was extracted at each sampling point with a 0.45 μm syringe filter
    - Filtered sample solution was used for ICP analysis to determine elemental composition
    - Temperature and pH was monitored throughout the experiment
8. After 2 hrs the solution was filtered and solid residue was collected and dried in a 105°C furnace overnight.
9. Solutions collected during sampling and the final PLS are sent for ICP analysis.
10. The residue was ground to a powder and sent for XRD and XRF analysis.

Figure 4.8 shows the leaching experiment setup. BLP had been added to the lixiviant, temperature control set to 50°C, pH probe immersed in mixture, and stirrer set to 300 RPM.

Figure 4.8: Setup for leaching experiments: 250mL borosilicate glass jar with holes drilled in caps for the temperature probe, pH meter and for sampling. Jar was placed on a hotplate/magnetic stirrer which was connected to the temperature probe.

4.4. Pyrometallurgical Treatment

This section outlines the pyrometallurgical approaches to treating BLP. Two main approaches will be taken: (1) thermal decomposition, and (2) chloridisation.

Aim

The following pyrometallurgical approaches were selected with their respective rationale:

- Thermal Decomposition - BLP will be subjected to thermal treatments from 500-1000°C. Reasoning for this approach is indicated in Section 1.5. The HIsarna reactor operates at approximately 1600°C at the smelt cyclone and about 1400°C at the metal bath in the smelt reduction vessel (see Figure 3.1). 1600°C was beyond the limits of the available horizontal furnace. The important temperatures to analyse decomposition products are at 500°C and 700°C which is around where substantial mass changes were taking place indicated by the TGA (Section 4.2.3). Treatment temperatures up to 1000 °C will also be carried out as a point of reference for the chloridisation reactions which will occur at 1000-1100°C.
- Chloridisation - Reasoning for picking this approach was stated in Section 1.5. Chloridisation will be carried out at temperatures between 700-1100°C.

Figure 4.9 provides a basic schematic of how the thermal decomposition experiments will be carried out. BLP (plumbojarosite) will be placed in a horizontal furnace at a specified temperature and duration with the resulting solid being analyzed. Off-gases will be monitored with a mass spectrometer. Similarly, Figure 4.10 shows how the chloridisation experiments will be conducted. Off-gases were not monitored.

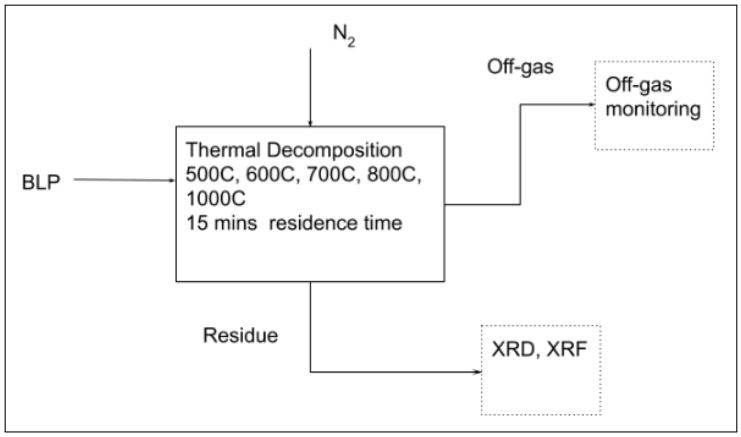

Figure 4.9: Flowsheet of thermal decomposition experiments.

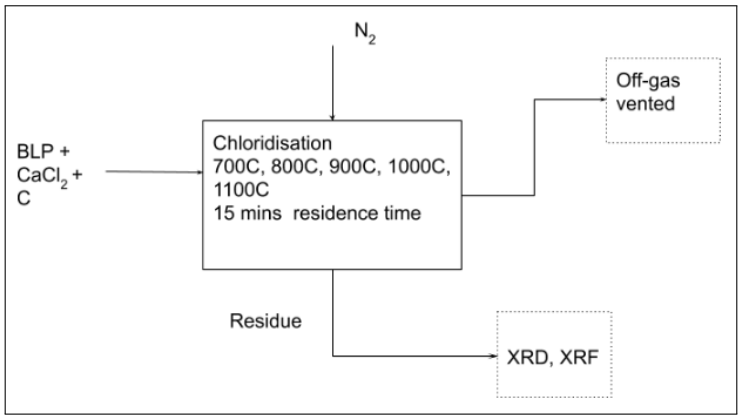

Figure 4.10: Flowsheet of chloridisation experiments.

Experimental

Following steps were performed in carrying out the thermal decomposition and chloridisation experiments:

1. BLP, from Nyrstar (Budel), was dried in a furnace set to 105°C overnight which resulted in a 20-22% weight loss.
2. The dried BLP sample was ground to a powder. For the thermal decomposition experiments only BLP was used. For the chloridisation experiments BLP and $CaCl_2$ (and Na_2CO_3) were mixed due as per the following:
    - BLP (76%) : $CaCl_2$ (24%). This was the optimal ratio indicated in by Wang for removing Cu from jarosite [69]. The same $CaCl_2$ percentages used in the study were used for this experiment (24% $CaCl_2.2H_2O$).
    - BLP (58%) : $CaCl_2$ (19%) : Na_2CO_3 (23%). Na_2CO_3 was added to investigate its impact on sulfur fixation. The amount of Na_2CO_3 added was so that there was 100% excess Na to what was required to fix the sulfur.

3. Approximately 5g of BLP/BLP mix was weighed and introduced into a Carbolite STF 16/50/450 horizontal furnace (image and schematic shown in Figures 4.11 and 4.12) via alumina boat crucibles.
4. The boat sat in the water-cooled flange zone at the start of the experiment. It was then moved to the hot zone at the center of the furnace which was at the desired temperature using a rod.
5. Sample was left in the hot zone for the required duration.
    - As the sample decomposed, off-gasses were monitored using a Hiden Analytical HPR-20 RD mass spectrometer
    - Nitrogen gas was injected into the furnace from the left in Figure 4.11 at 0.5L/min to maintain an inert atmosphere. For the chloridisation experiment, this is a point of difference with the Wang study (where jarosite/$CaCl_2$ mixtures were roasted in air).
6. After the required duration, the samples were quenched by pulling the alumina boats back to the water cooled flange zone.
7. The residue was ground to a powder and sent for XRD and XRF analysis (the same that was conducted on BLP in Section 4.2.1).

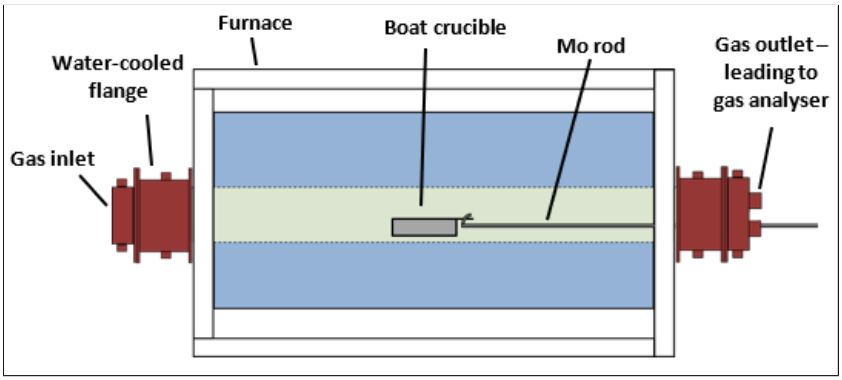

Figure 4.11: Schematic of horizontal furnace experiments.

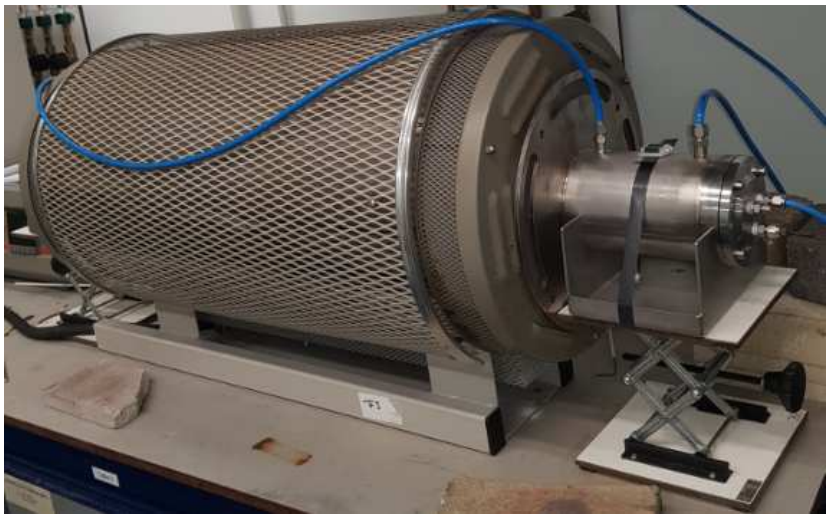

Figure 4.12: Image of horizontal furnace used.

4.5. Combined Hydro- and Pyrometallurgical Treatment

This section outlines a combined pyro- and hydrometallugical treatment of BLP. This experiment essentially follows the approach of the Piskunov study [66].

Aim

The aim of this experiment is to fix the sulfur in the BLP by mixing it with Na_2CO_3 and heating it. This is then followed with water washing to remove the sulfate salts and, in the process, some of the Cu present in the BLP (Piskunov achieved a 60% reduction Cu in the washed residue - see Section 1.5) :

- BLP will be mixed with Na_2CO_3 and heated to two temperatures: 700°C and 800°. At these temperatures, all the jarosite present should be converted to a combination of Fe oxide and sulfate salts (see Section 2.4.4.3 and the Piskunov study [66]).

Figure 4.13 provides a basic schematic of how the sulfur fixation experiments will be carried out. BLP (plumbojarosite) and Na_2CO_3 will be placed in a horizontal furnace at a specified temperature and duration with the resulting solid being analyzed. Off-gases will be monitored with a mass spectrometer. The calcined residue will then be washed (leached) with distilled water at RT and 50°C. Both the washed solid and water will be analysed.

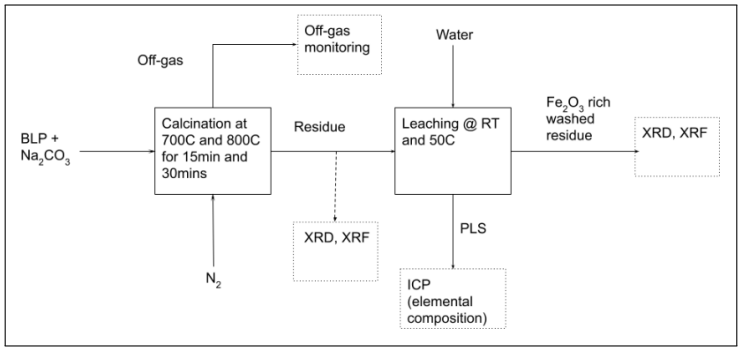

Figure 4.13: Flowsheet of sulfur fixation experiments.

Experimental

The steps followed to perform the sulfur fixation experiment were identical to those described in Section 4.4 with the following exceptions:

- The dried BLP sample was ground to a powder. BLP and Na_2CO_3 were mixed and ground together with the following ratio: BLP (60%) : Na_2CO_3 (40%)
  - This amount of Na_2CO_3 represented 100% excess of the amount required to fix sulfur in BLP. The amount of sulfur in BLP was determined by XRF and a stoichiometric conversion was used to calculate how much Na would be required to fix all the existing sulfur. This was then used to determine how much Na_2CO_3 would be required.
- Since a subsequent washing step would occur, a larger quantity of solid mix (10g) was also subjected to the thermal treatment. Consequently, the duration in the furnace was increased accordingly to 30 minutes to provide sufficient reaction time.
- Washing occurred very similarly to the setup in Section 4.3. The conditions will be indicated on the results charts but are typically: temperature = RT or 50°C, RPM = 300, L/S = 10, duration = 1hr.
  - Due to limited volumes only one sample of the PLS was taken at the end of the washing.

5

Results and Discussion

This section outlines key terms and metrics that will be used in the results and discussion. For Pregnant Leach Solutions (PLS) produced by the hydrometallurgical approaches, leaching efficiency (LE) is calculated as follows:

$$LE\ (\%) = \frac{C_{ms} * V_s}{m_{blp} * G_{mblp}} * 100 \tag{5.1}$$

where LE = Leaching efficiency (%), C_{ms} = concentration of metal in leach solution (g/L), V_s = volume of leach solution (L), m_{blp} = mass of BLP used (g), and G_{mblp} = grade of metal in BLP (%) (the concentration of a particular metal in the BLP).

TTM (total targeted metals) refers to all the problematic metals in Equation 3.1 (Cu, Ni, Cr, Mo, and Sn) and is indicative of their total leaching efficiency:

$$TTM(\%) = \frac{c_{Cu} + c_{Cr} + c_{Ni} + c_{Sn} + c_{Mo}}{C_{Cu} + C_{Cr} + C_{Ni} + C_{Sn} + C_{Mo}} * 100 \tag{5.2}$$

where c_m = concentration of metal in leach solution (g/L) and C_m = Maximum possible concentration of metal in leach solution (g/L), based on quantity of BLP leached.

Since different jarosite (or BLP) treatment strategies will be used (pyrometallurgy, hydrometallurgy and combination of pyro- and hydrometallurgy) it is important to use a metric that compares the effectiveness of each approach. ”Treatment effectiveness” will be used to compare all treatment strategies. This will be calculated as follows:

For residues (all treatments):

$$Treatment\ Effectiveness = \frac{Cu\ or\ CEF\ (wt\%)}{Fe\ (wt\%)} \tag{5.3}$$

For PLS (for hydrometallurgy and combined pyro-hydrometallurgy):

$$Treatment\ Effectiveness = \frac{LE_{Cu}\ or\ LE_{TTM}}{LE_{Fe}} \tag{5.4}$$

Treatment effectiveness is a ratio with no units and provides a point of reference for all the treatment strategies. Based on the equations above, for treated solids, the lower the number the more effective the treatment has been (i.e. it has reduced the level of Cu or CEF relative to Fe). For leach solutions, the opposite is true.

CEF is applied to the leach residue as per in Equation 3.1. When concentrations are too low (as is the case with CEF metals) they are augmented for visibility on the graphs by multiplying by a factor (typically 10). The CEF threshold of 0.2 wt% is also indicated on all the residue graphs (it also multiplied by 10 for visibility) with a dashed line. This provides a reference point for how effective the treatment was in removing CEF metals with respect to the HIsarna limit.

5.1. Hydrometallurgical Treatment

Sections 5.1.1 - 5.1.4 present a summary of results for the hydrometallurgical treatments of BLP. Results were obtained from carrying out leaching reactions with four types of lixiviants: acids, alkali, DES, and ammoniacal. Data from sampling is presented in Appendix A. The following sections provide a direct comparison between the lixiviants (with the exception of DES leaching whereby the leached solids could not be recovered) by comparing the final PLS solutions and leached residues.

5.1.1. Acid Leaching

Figure 5.1 shows the leaching efficiency of some elements of interest when BLP was leached with sulfuric, hydrochloric, oxalic and acetic acid (Figure A.3 in the appendix includes the CEF elements separately).

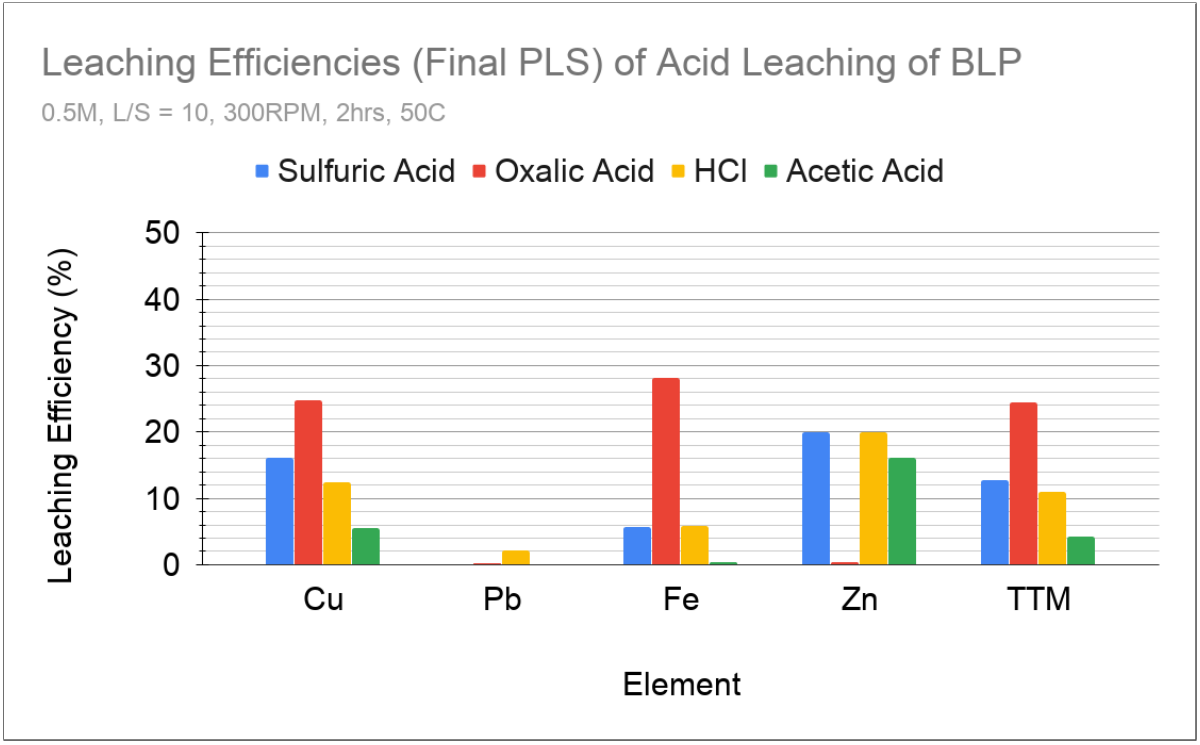

Figure 5.1: Leaching efficiency of elements in PLS. L/S=10, Temp = 50°C, duration = 2hrs, conc = 0.5M, RPM = 300. TTM = Cu + Ni + Cr + Sn + Mo

The results indicate that overall leaching efficiencies of Cu (and the CEF metals) were low. The highest leaching efficiency for Cu (24.8%) was reached using oxalic acid as a lixiviant. In all four cases,

it was expected that the plumbojarosite present in the BLP would be broken down as per equation 5.5 with constituent metal ions released:

$$MFe_3(SO_4)_2(OH)_6 + 6HB- > Me^+ + 3Fe^{3+} + 2SO_4^{2-} + 6H_2O + 6B^- \quad (5.5)$$

The likelihood of that metal staying in solution (and hence the leaching efficiency) will depend on the pH of the solution and the solubility of any metal-lixiviant salts created. Pourbaix diagrams are useful for indicating dominant element species in aqueous media for a given pH. The dominant species is also dependent on whether the environment is oxidative or reductive as indicated by E (the potential difference). The higher the E, the more oxidative the environment. For all the leaching experiments, E was not measured; however, it is a value that is assumed to be within the water stability zone (indicated by the parallel dashed line in Pourbaix diagrams). Multiple species of a metal can exist at a specific pH depending on the E value. Acid leaching of BLP presents a complex system of ions and interactions for which Pourbaix diagram were not developed; however, looking at Pourbaix diagrams of metal-H_2O systems may provide some insight into the leaching behavior observed in the results. Although these diagrams are temperature dependent, the literature indicates that between 25°C and 50°C, the Pourbaix diagrams should not differ materially [86, 87]. Finally, no oxidising or reducing agent was used in the leaching reactions and since E was not measured, if there are multiple metal species stable for a given pH it cannot be assumed one species is more likely to occur. Figures A.1 and A.2 provide Pourbaix diagrams for metal-H_2O systems at 25°C [18]. To capture the relevant information for the leaching reactions, Table 5.1 summarises the dominant metal species within the water stability zone for each of the lixiviants (based off the final pH) and also indicates solubility of the metal lixiviant salts that may exist.

Table 5.1: Dominant species of target metals in each lixiviant based of Pourbaix Diagram in the appendix(Figures A.1andA.2). Also included is the metal lixiviant salt solubility. The A column refers to the stable metal species that exists for a given pH and the B column indicates the solubility of the lixiviant salt. Solubility date is taken from [18]

Pourbaix and Solubility	Oxalic Acid		Sulfuric Acid		Acetic Acid		Hydrochloric	
Final pH		1.419		0.345		3.1		0.226
	A	B	A	B	A	B	A	B
Cu	Cu2+(aq), Cu(s)	Insoluble	Cu2+(aq), Cu(s)	Soluble	Cu2+(aq), Cu(s), Cu2O(s)	Soluble	Cu2+(aq), Cu(s)	Soluble
Fe	Fe3+(aq), Fe2+(aq)	Fe(II) Insoluble Fe(III) Soluble	Fe3+(aq), Fe2+(aq)	Soluble	Fe3+(aq), Fe2+(aq), FeO(OH)(s)	Fe(II) Soluble Fe(III) Insoluble*	Fe3+(aq), Fe2+(aq)	Soluble
Zn	Zn(2+)(aq)	Insoluble	Zn(2+)(aq)	Soluble	Zn(2+)(aq)	Soluble	Zn(2+)(aq)	Soluble
Pb	PbOH(+)(aq)	Insoluble	PbOH(+)(aq)	Insoluble	PbOH(+)(aq), Pb(s)	Soluble	PbOH(+)(aq)	Insoluble
Ni	Ni(2+)(aq)	Insoluble	Ni(2+)(aq)	Soluble	Ni(2+)(aq)	Soluble	Ni(2+)(aq)	Soluble
Cr	Cr(3+)(aq)	Soluble	Cr(3+)(aq)	Soluble	Cr(3+)(aq), HCrO4(-)(aq)	Soluble	Cr(3+)(aq)	Soluble
Sn	SnO2(s), SnO(s), Sn(s)	Insoluble	SnO2(s), Sn(2+), Sn(s)	Soluble	SnO2(s), SnO(s), Sn(s)	Decomposes	SnO2(s), Sn(2+), Sn(s)	Soluble
Mo	Isopolyanions, MoO2(s)	N/A	MoO3.2H2O(s), MoO2(s), Mo(3+)(aq)	Mo(III) Soluble	Isopolyanions, MoO2(s)	N/A	MoO3.2H2O(s), MoO2(s), Mo(3+)(aq)	Mo(III) Soluble

Oxalic acid was used to see if it can selectively target Fe from BLP. It was able to leach Fe with the highest efficiency compared to other acids; however, it also leached the other targeted metals into solution as well. Figure 5.2 provides the sampling results BLP being leached with oxalic acid. Table 5.1 indicates that the final pH of oxalic acid leach solution (pH of 1.419) enables all metals (except Mo) to exist as an aqueous ion. The table also indicates that most of the oxalate salts formed with the metal ions would be insoluble. This being the case however, many insoluble oxalate salts dissolve in excess $C_2O_4^{-2}$ to form complexes [18]. This is most notable with Fe and Cu in Figure 5.1. Fe and Cu are able to form these complexes and stay in solution given the leaching conditions. Metals such as Pb and Zn, however, are unable to do so and reported back to the solid. Sampling results of the leaching reaction show that Zn is initially released into solution but as the reaction proceeded, Zn dropped out of solution as other metals continued to be released into solution . Zinc ferrite leaching with oxalic acid had been carried out in the literature with the results showing that, although there was high Fe leaching efficiency (82.5%), ≥90% of the Zn reported to the solid [88]. Consequently, when compared to untreated BLP, the oxalic acid treatment resulted in an up concentration of Pb and Zn in the leached residue.

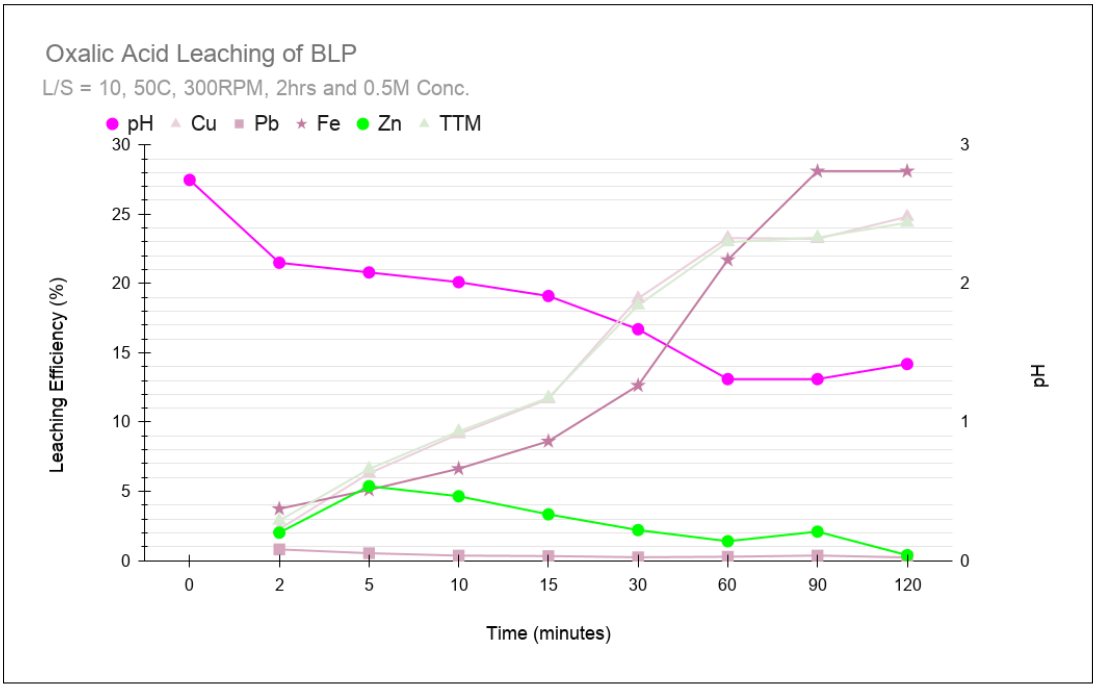

Figure 5.2: Leaching efficiency of elements in BLP with oxalic acid at various time intervals(sulfur removed due to 100% leaching efficiency being achieved). L/S=10, Temp = 50°C, duration = 2hrs, conc = 0.5M, RPM = 300

For HCl leaching, the final pH of the PLS (0.226) results in all metal species also having a stable aqueous species (See Table 5.1). All chloride salts indicated in Table 5.1 are also soluble (except Pb). Figure 5.3 shows all metals being released into and staying in the solution.

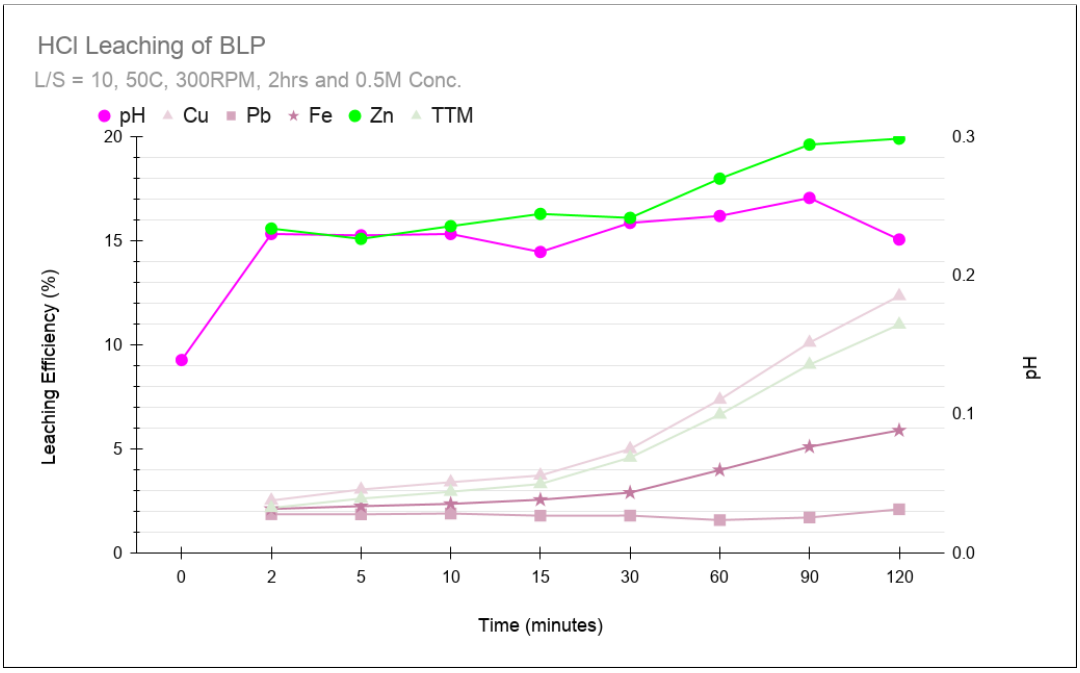

Figure 5.3: Leaching efficiency of elements in BLP with HCl at various time intervals. L/S=10, Temp = 50°C, duration = 2hrs, conc = 0.5M, RPM = 300

Pb is also leached to a degree because it forms a chloride complex [17]:

$$Pb^{2+} + 4Cl^{-} -> PbCl_4^{2-} \tag{5.6}$$

No selectivity was established using HCl as a lixiviant. Marginally better leaching efficiencies were observed using H_2SO_4. With HCl, Pb is able to form complexes that are stable in solution; however, this was not the case with H_2SO_4 as there was barely any Pb leached into solution (See Figure 5.4).

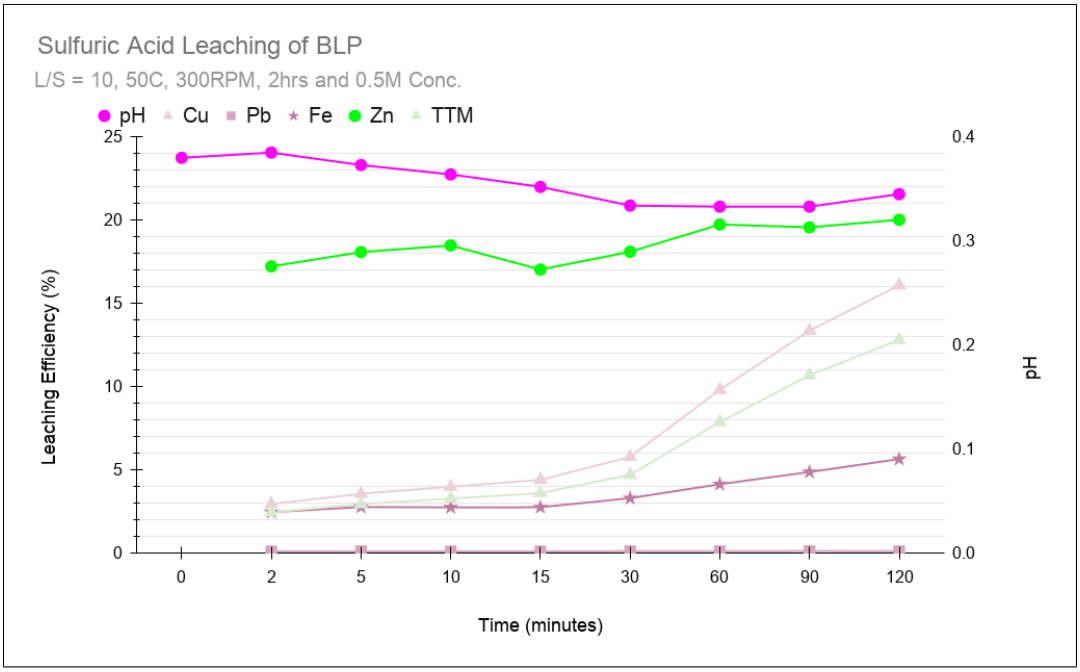

Figure 5.4: Leaching efficiency of elements in BLP with H_2SO_4 at various time intervals. L/S=10, Temp = 50°C, duration = 2hrs, conc = 0.5M, RPM = 300

Figures 5.3 and 5.4 shows that as the leaching proceeded in HCl and H_2SO_4, most monitored metals were released into solution with no selectivity. Leaching efficiencies were lower than that of oxalic acid most likely due to oxalic acid being more effective at targeting Fe in the jarosite (thus being more effective at breaking down the jarosite).

Acetic acid was selective in not dissolving Fe and Pb. Table 5.1 indicates that Fe(III) acetate is not soluble which would explain low Fe leaching efficiencies. The table also indicates that the other metals (Cu, Zn and Pb) should form stable species in solution which is observed for Cu and Zn but not for Pb. One reason could be the presence of SO_4^{2-} ions that combined with Pb to form insoluble $PbSO_4$. There is evidence of this as the leach residue of acetic acid had the highest sulfur content and the PLS has the lowest Pb leaching efficiency. Acetic acid is a weaker acid than HCl and H_2SO_4 which should result in lower leaching efficiencies as is observed. Table 5.2 shows that because acetic acid was able to keep Fe in a solid form, it was the most effective in selectively removing Cu out of BLP.

The XRD spectra of all acid leached residues (see Section A.1.1) show the same phases as the original untreated BLP. Although it is difficult to quantify, the XRD spectra does support the incremental breakdown of jarosite as per equation 5.5. Precipitates that may have formed during leaching were not of a sufficiently high concentration to be detected by XRD.

The kinetics of the leaching reactions is supported by the shrinking core model (see Figure 5.5) as the fraction of reacted BLP (as indicated by the increasing concentration of metal ions in solution) is proportional with time. The model is based on parameters including concentrations of reagents, density of the solid, molecular weight of the reactant, a stoichiometric factor, the initial radius of the particles and the diffusion coefficient in the porous product layer which were not monitored as part of this thesis. The model indicates that the reacted fraction increases with time (multiplied by a kinetic constant which incorporates the many parameters previously mentioned) as per equation(s) 5.7 and 5.8 [41]:

$$1 - (1 - X)^{\frac{1}{3}} = k_{exp}t \tag{5.7}$$

$$1 - 3(1 - X)^{\frac{2}{3}} + 2(1 - X) = k_{exp}t \tag{5.8}$$

Where X = reacted fraction of jarosite, t = time and k_{exp} = rate constant. All four acid leaching reactions were certainly time dependent as shown by the sampling data (see Figures 5.4, 5.3, 5.2 and Figure A.5 in the appendix).

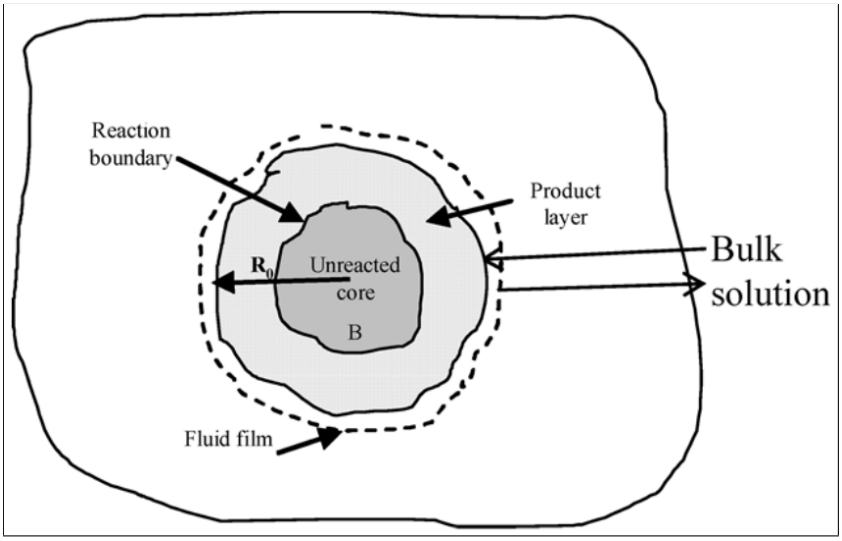

Figure 5.5: Shrinking core model [15]

.

Overall the leaching efficiencies were quite low given the reaction parameters used. In addition, there was also no clear selectivity of Cu over the other elements in most instances. By looking at the treatment effectiveness (see Table 5.2), acetic acid is the most effective lixiviant in selectively removing Cu from BLP; however, it is also had the lowest leaching efficiency out of all the acids.

Table 5.2: Treatment effectiveness of acid leaching. For the PLS: Treatment Effectiveness = LE of [Cu] (or TTM) / LE [Fe], for the residue Treatment Effectiveness = % Cu or CEF/ % Fe

Treatment Effectiveness (Ratio)		**Sulfuric Acid**	**Oxalic Acid**	**HCl**	**Acetic**
PLS	Cu/Fe	2.857	0.883	2.099	14.444
	TTM/Fe	2.275	0.868	1.865	11.025
Residue	Cu/Fe	0.031	0.038	0.024	0.030
	CEF/Fe	0.074	0.100	0.108	0.065

The CEF value in the residual solids (see Figure 5.6) was similar to that of untreated BLP (with the exception of HCl where the CEF value in the residue increased due to a higher concentration of Sn). Due to low selectivity of CEF metals like Cu over Fe, leaching experiments with the acids (HCl, oxalic, acetic and H_2SO_4) were not considered a viable treatment strategy that warranted a parametric study.

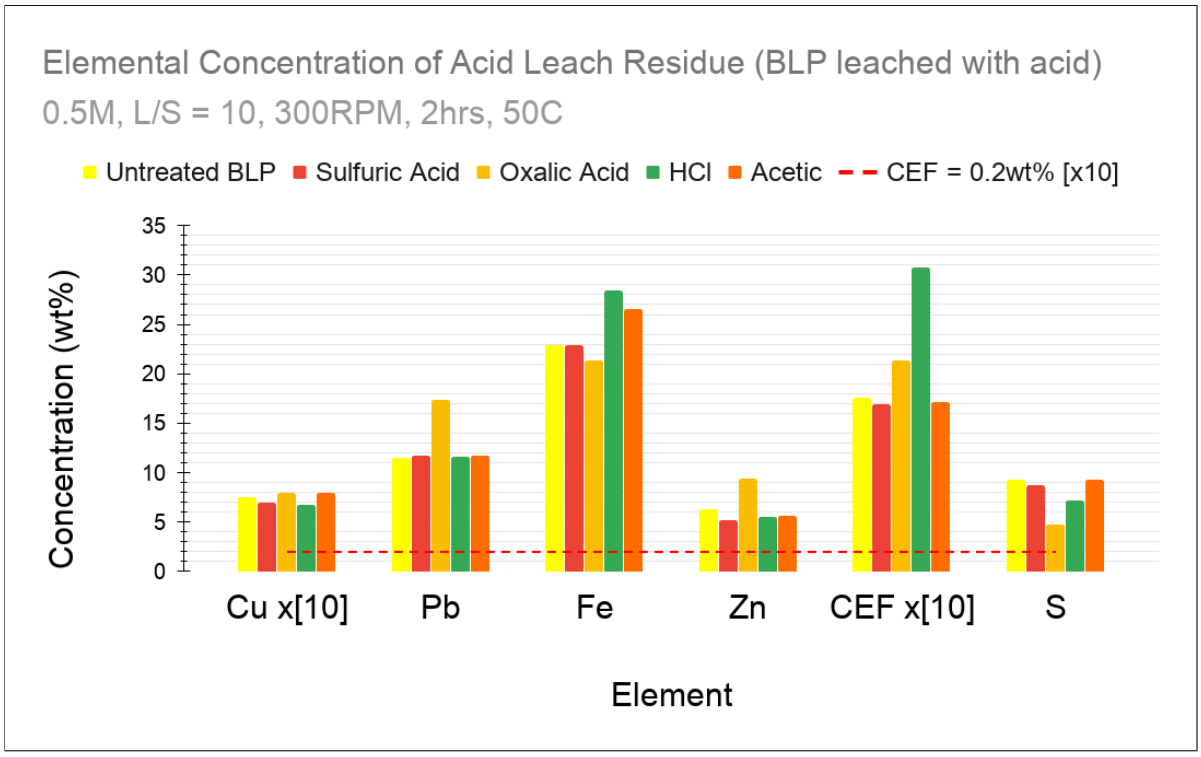

Figure 5.6: Elemental concentration of acid leach residue. L/S=10, Temp = 50°C, duration = 2hrs, conc = 0.5M, RPM = 300. CEF = Cu + Ni + Cr + 5*Sn + 10*Mo

5.1.2. Alkaline Leaching

Figure 5.7 shows the leaching efficiencies in the PLS of the alkaline leaching experiments.

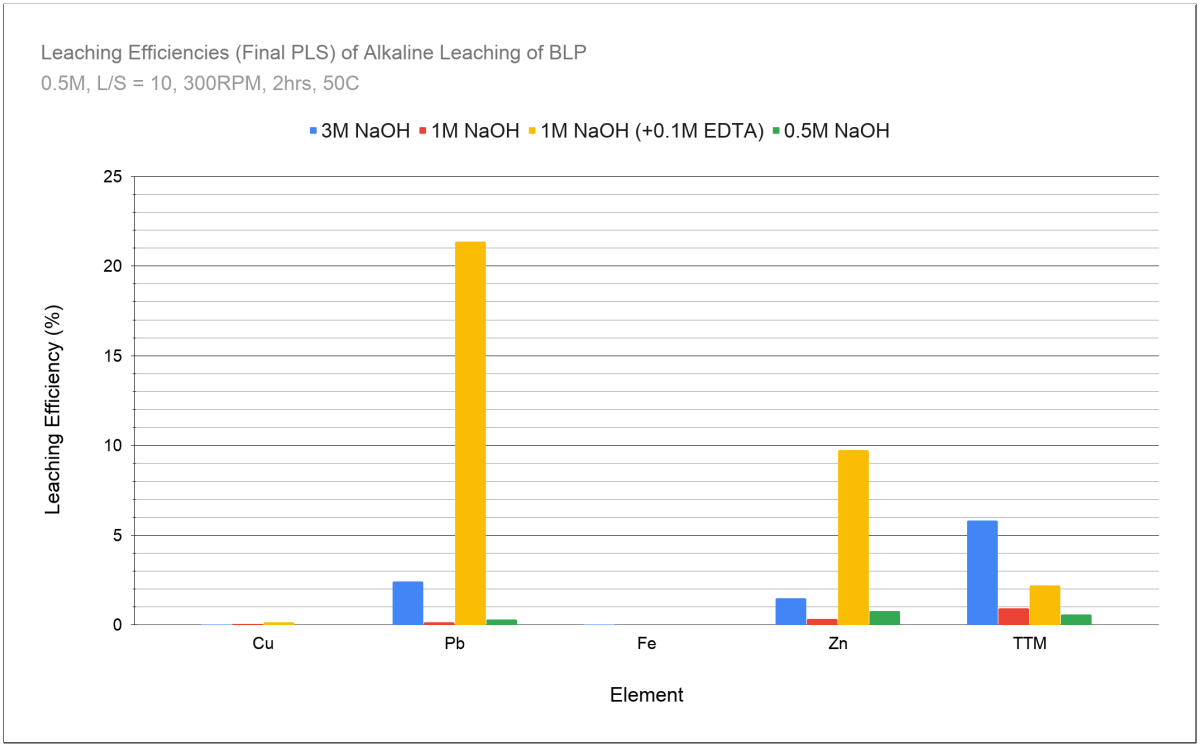

Figure 5.7: Leaching efficiency of elements in PLS. L/S=10, Temp = 50°C, duration = 2hrs, conc = 0.5M, RPM = 300.

Alkaline solutions break down jarosite according to the equation 5.9:

$$MFe_3(SO_4)_2(OH)_{6(s)} + 3OH- > Me^+ + 3Fe(OH)_{3(s)} + 2SO_4^{2-} \tag{5.9}$$

The OH^- ions liberate SO_4^{2-} and the other impurity metal ions. Due to the high pH, once Fe is released into solution it forms $Fe(OH)_3$. $Fe(OH)_3$ is amorphous in nature and this can be demonstrated by Figure 5.8. This shows that 0.5M NaOH was not strong enough to break the jarosite down significantly (plumbojarosite continued to be the one of the main phases present). Increasing the concentration resulted in the broadening of peaks in the region 2Theta = 20-40 and 55-70, suggesting the presence of amorphous $Fe(OH)_3$. This is confirmed in the literature by Majzlan [89] who carried out XRD analysis on Fe hydroxides. Increased alkalinity (3M NaOH) resulted in the conversion of the amorphous hydroxide to a distinctly more crystalline residue containing zinc ferrite and calcium iron silicate hydroxide. One phase present throughout is zinc ferrite. This oxide (present in untreated BLP) is resistant to caustic attack [90] and therefore remains in the final residue after alkaline leaching with 3M NaOH.

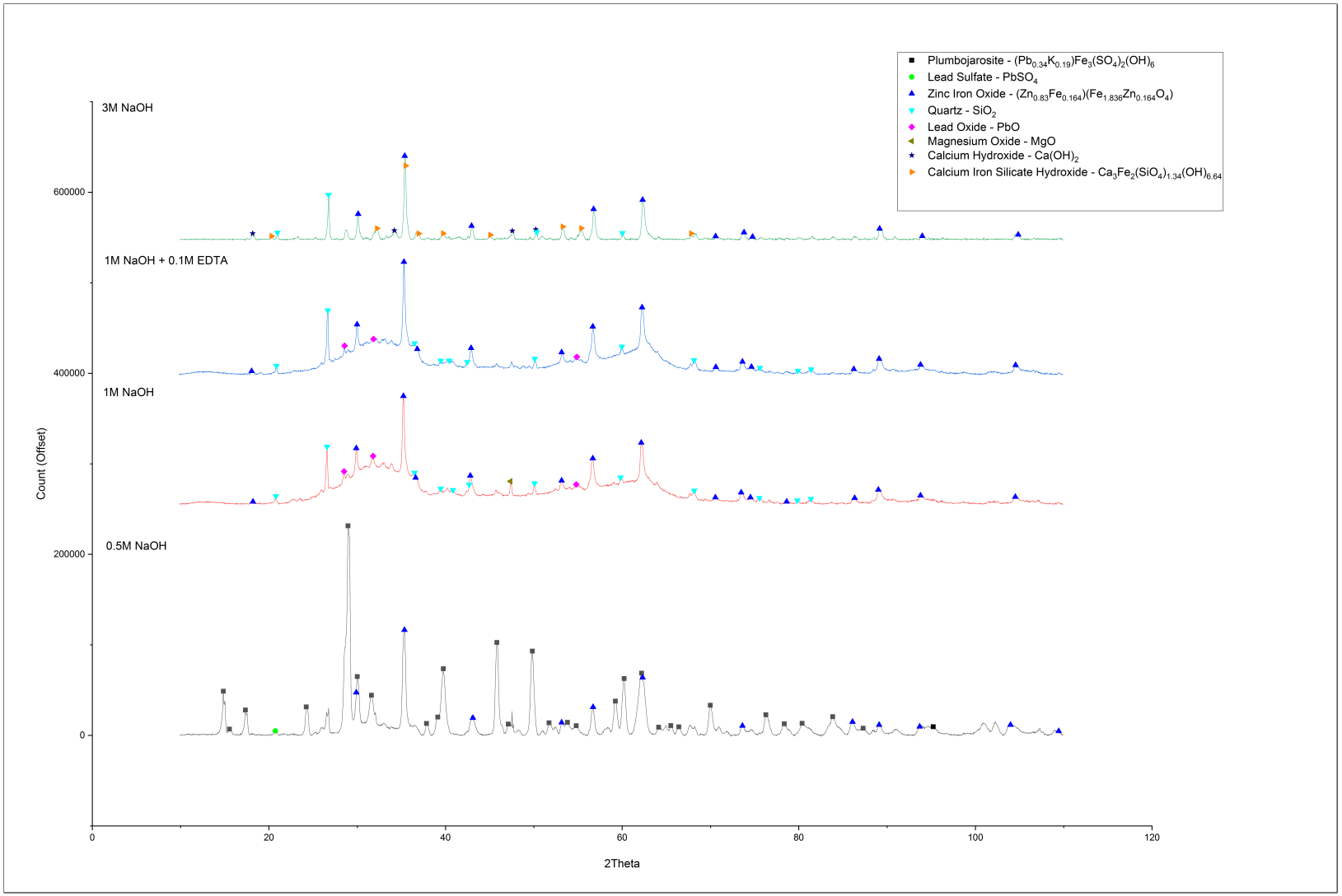

Figure 5.8: XRD spectra of BLP leached in alkaline solutions. Time = 2hrs, L/S=10, 300RPM, Temp = 50°C

Once the plumbojarosite is broken down by NaOH it will release metal ions contained within the structure. Whether the metal ions remain in solution or precipitate out will depend on the most stable phase is, as indicated by the Pourbaix diagrams (see Figures A.1 and A.2 in the appendix). The pH during the alkaline leaching experiments was not measured (due to the sensitivity of the pH meter to strongly alkaline solutions), but one could surmise that the pH of the solutions was sufficiently high. This assumption is based off the measured pH of 11.7 for 0.5M NH_4OH. For a stronger base like NaOH, a pH > 12 was assumed. The Pourbaix diagrams indicate that the only metals that would have stable aqueous species are Zn, Mo, Cr, Sn, and Pb. Pb would have a stable aqueous species at a very high pH (at pH > 14, $HPbO_2^-$ is stable aqueous species). This is partially reflected in the leaching efficiencies in the final PLS (see Figure 5.7) as some Pb is leached into solution when leaching with 3M NaOH. Fe is not reported in the PLS at any concentration and neither is Cu. Pb and Zn are detected in the PLS at very low leaching efficiencies. There is some leaching of the TTM metals with the highest leaching efficiencies occurring at 3M NaOH. This was because of Sn and Mo forming stable aqueous species as shown by the Pourbaix diagrams. Figures 5.9 and 5.10 show the metal concentrations throughout the leaching reaction. Sampling was not carried out with 0.5M NaOH leach. For the 1M NaOH (See Figure 5.9) leach, only Mo seems to be released and stay in solution (and to a much lesser extent Sn). As the reaction proceeds, all leaching efficiencies start dropping. The formation of $Fe(OH)_3$ could be the reason for the decline in leaching efficiency. Amorphous Fe hydroxide is an effective scavenger of impurity metals like Cu [91] due to the large surface area of its gel like structure [10].

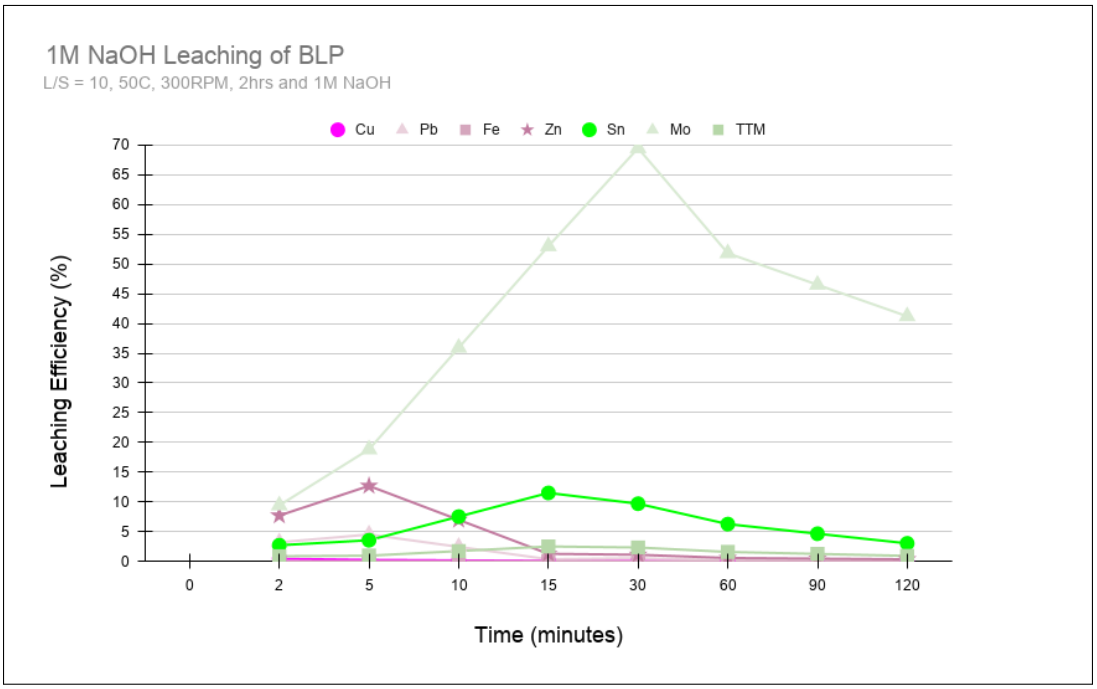

Figure 5.9: Elemental leaching efficiencies of BLP leached with 1M NaOH, 50°C, 300 RPM, Duration = 2hrs, L/S = 10

With 3M NaOH, $Fe(OH)_3$ converts to a more crystalline $Ca_3Fe_2(SiO_4)_{1.34}(OH)_{6.64}$; in addition, the higher pH is likely the reason for the higher leaching efficiencies of Sn and Mo (see Figure 5.10). The resulting decline in leaching efficiencies of Zn and Pb in 3M NaOH is more difficult to explain. According to the Pourbaix diagrams for these metals, stable aqueous species should be formed at high pHs (>11.5 for Zn and >14 for Pb) however this is not observed. $Ca_3Fe_2(SiO_4)_{1.34}(OH)_{6.64}$ could be an effective scavenger of Zn and Pb (similarly to $Fe(OH)_3$ and Fe_2O_3 [92–94]); however this would need to be confirmed with further investigation.

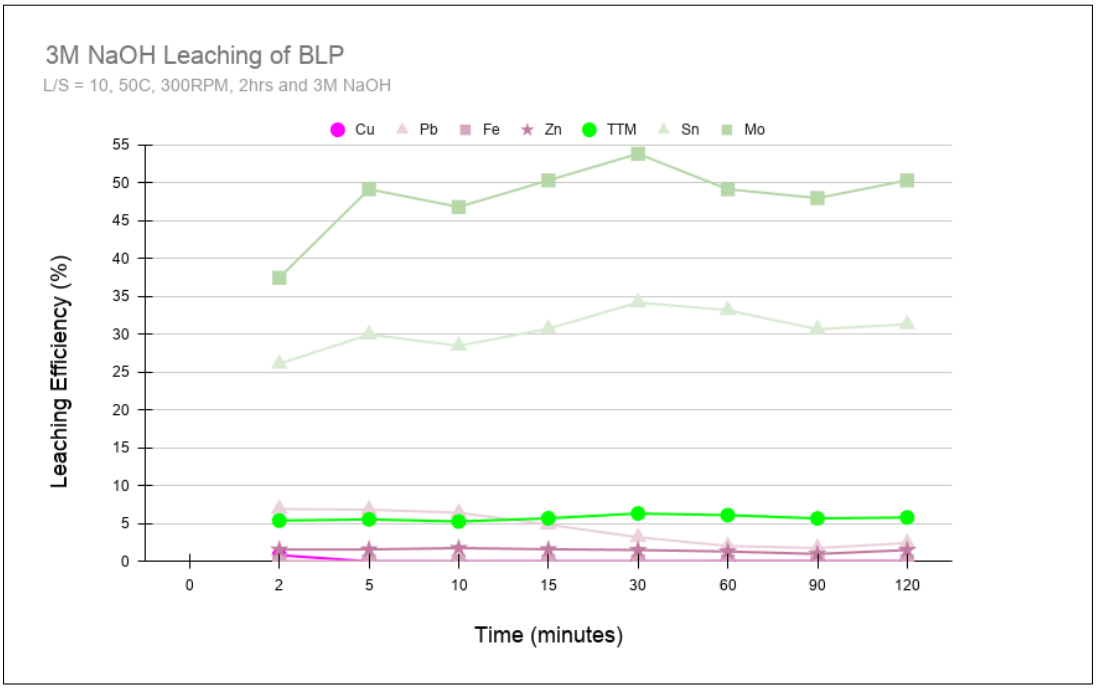

Figure 5.10: Elemental leaching efficiencies of BLP leached with 3M NaOH, 50°C, 300 RPM, Duration = 2hrs, L/S = 10

EDTA is a chelating agent that is used to bind Cu and Zn ions and keep them in solution. This was tested with 1M NaOH solution to see if Cu leaching efficiency could be increased. Figure 5.7 shows that the addition of EDTA increased the leaching efficiencies of Zn and Pb only. Closer inspection of Figure 5.11 shows that initially Cu, Sn, Pb, and Zn are released into solution. As the reaction proceeded Cu, Zn, and Sn dropped out of solution.

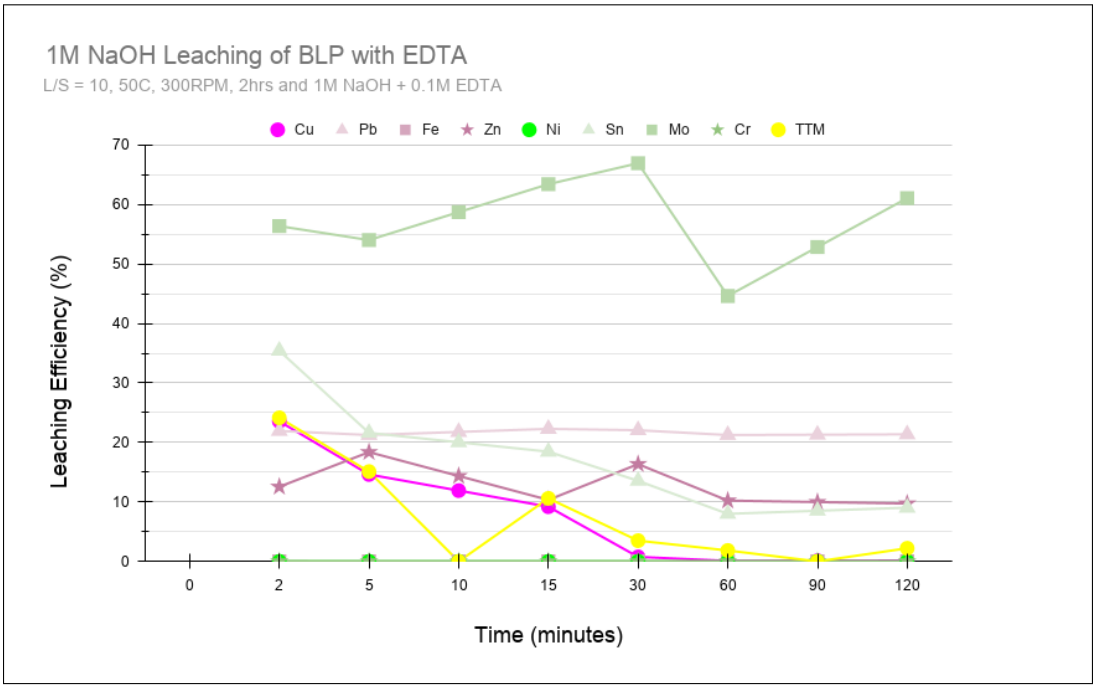

Figure 5.11: Elemental leaching efficiencies of BLP leached with 1M NaOH + 0.1M EDTA, 50°C, 300 RPM, Duration = 2hrs, L/S = 10.

The thermodynamics of a Cu-EDTA-H_2O system support the presence of Cu ions in solution (see Figure 5.12). For alkaline pH within the water stability zone, the presence of $CuOHY^{3-}$ is also supported by the thermodynamics (Y represents the EDTA anion). The presence of amorphous $FeOH_3$ in solution could be a reason for the drop off in leaching efficiencies. As the hydroxide decomposes the jarosite, increasing concentration of $Fe(OH)_3$ is likely to scavenge impurity metals like Cu. Cu is also stable as solid Cu within the water stability zone throughout the pH range 0-16. Cu_2O is also stable in pH 13-16 so it is possible that Cu precipitated out in this form but further investigation of the residue would be required.

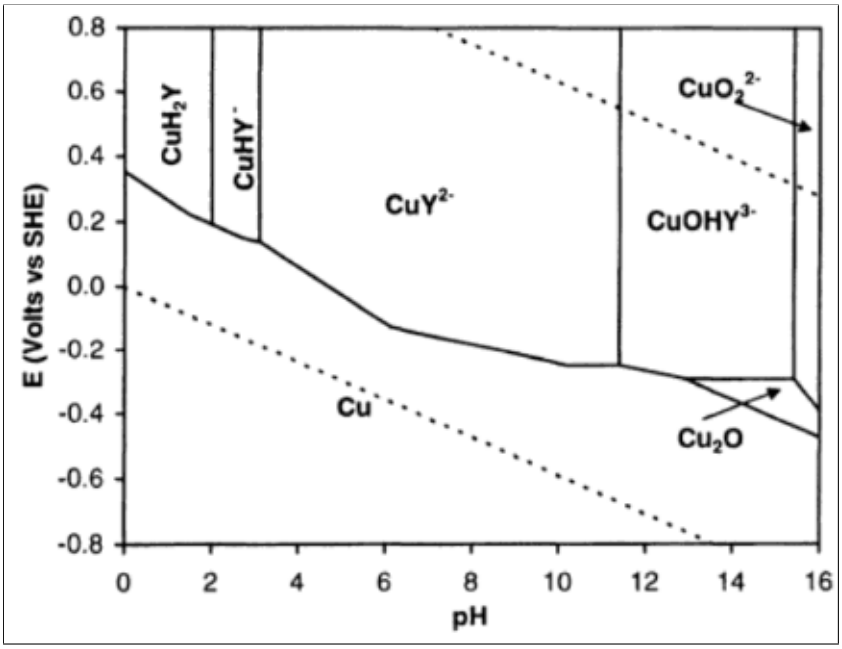

Figure 5.12: Potential-pH diagrams for Cu-water-EDTA system at 25 °C. Total EDTA activity, $[Y_T]$, = 0.1M; total dissolved Cu activity, $[Cu_T=10^{-2}M]$

Figure 5.13 shows an upconcentration of Fe and Cu, supporting what was observed in the PLS. This increase in concentration is due to the removal of sulfur and the lack of Cu leached into solution. When compared to untreated BLP, the sulfur concentration of alkaline leached residues are significantly lower. For 0.5M NaOH leaching, the presence of plumbojarosite in the XRD and the significantly higher concentration of sulfur in the treated residue supports the claim that only some of the plumbojarosite had reacted. Increasing the concentration to 1M and 3M resulted in a more complete reaction with plumbojarosite. The CEF values of the treated residues also remain similar to the untreated BLP. This is because although Cu was not removed into the solution, some Sn and Mo is leached into solution at high pH.

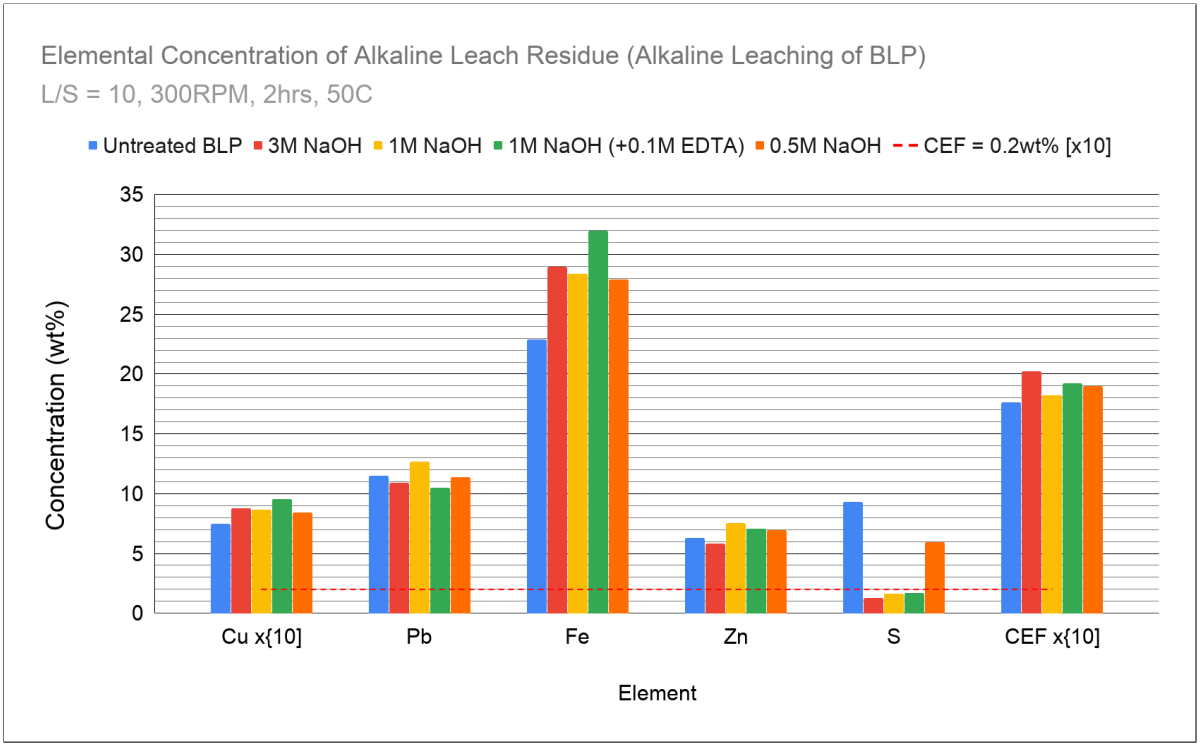

Figure 5.13: Elemental composition of alkaline leached residue. L/S=10, Temp = 50°C, duration = 2hrs, conc = 0.5M, RPM = 300. The dashed CEF refers to the CEF < 0.2wt% limit for HIsarna Ironmaking.

The treatment effectiveness for the CEF metals has improved (see Table 5.3) when compared to acid leaching treatment. This is due to the higher Fe content in the solid whilst removing Sn and Mo. The very low leaching efficiencies of Cu suggested that alkaline leaching of BLP did not warrant further investigation.

Table 5.3: Treatment effectiveness of alkaline leaching. For the PLS: Treatment Effectiveness = LE of [Cu] (or TTM) / LE [Fe], for the residue Treatment Effectiveness = % Cu or CEF/ % Fe

Treatment Effectiveness (Ratio)		3M NaOH	1M NaOH	1M NaOH (+0.1M EDTA)	0.5M NaOH
PLS	Cu/Fe	1.021	45.942	34.031	0.000
	TTM/Fe	203.030	973.172	513.936	303.401
Residue	Cu/Fe	0.030	0.030	0.030	0.030
	CEF/Fe	0.070	0.064	0.060	0.068

5.1.3. DES Leaching

The viscosity of the DES solution was very high and it was difficult to carry out sampling under the setup (see Section 4.3). The final leach solids were not recovered because the lixviant could not be filtered. Consequently, analysis was only carried out with the PLS that was obtained during sampling (see Figures 5.15 and 5.14). DES leaching showed the lowest leaching efficiencies overall for Cu and the CEF metals. Some selectivity was established for Zn and S over the other elements. Choline chloride and glycerol had a higher treatment effectiveness (see Table 5.4) than choline chloride and ethylene glycol. It is difficult to comment on the mechanisms involved in leaching with DES as this was a scoping exercise and a more thorough investigation into the choice of HBDs, experimental conditions, and experimental setup may have yielded more insight. What is clear is that glycerol, as a HBD, is more effective at selectively extracting Zn and sulfur than ethylene glycol when couple with choline chloride. It was quickly determined that because of the difficulty in handling and very low leaching efficiencies,

DES leaching of BLP was not a viable path forward.

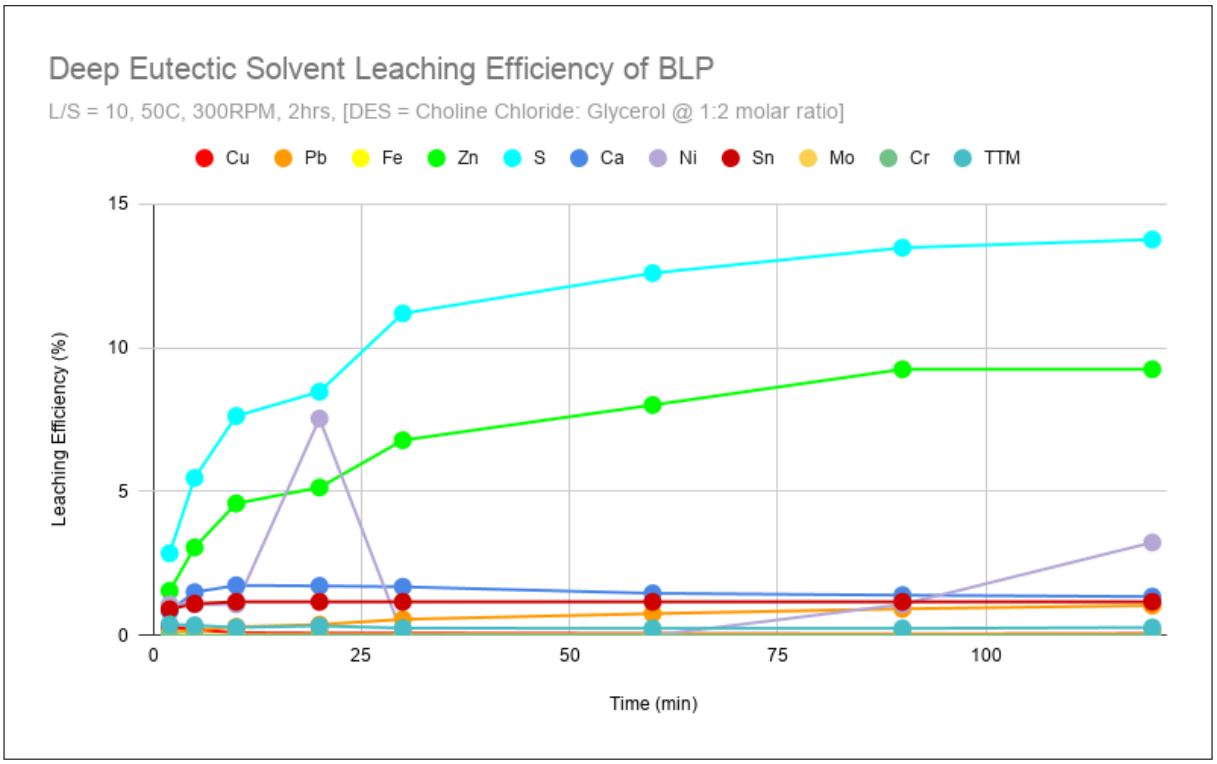

Figure 5.14: DES Leaching (choline chloride and glycerol) of BLP - PLS leaching efficiencies. Time = 2hrs, L/S=10, 300RPM, Temp = 50°C

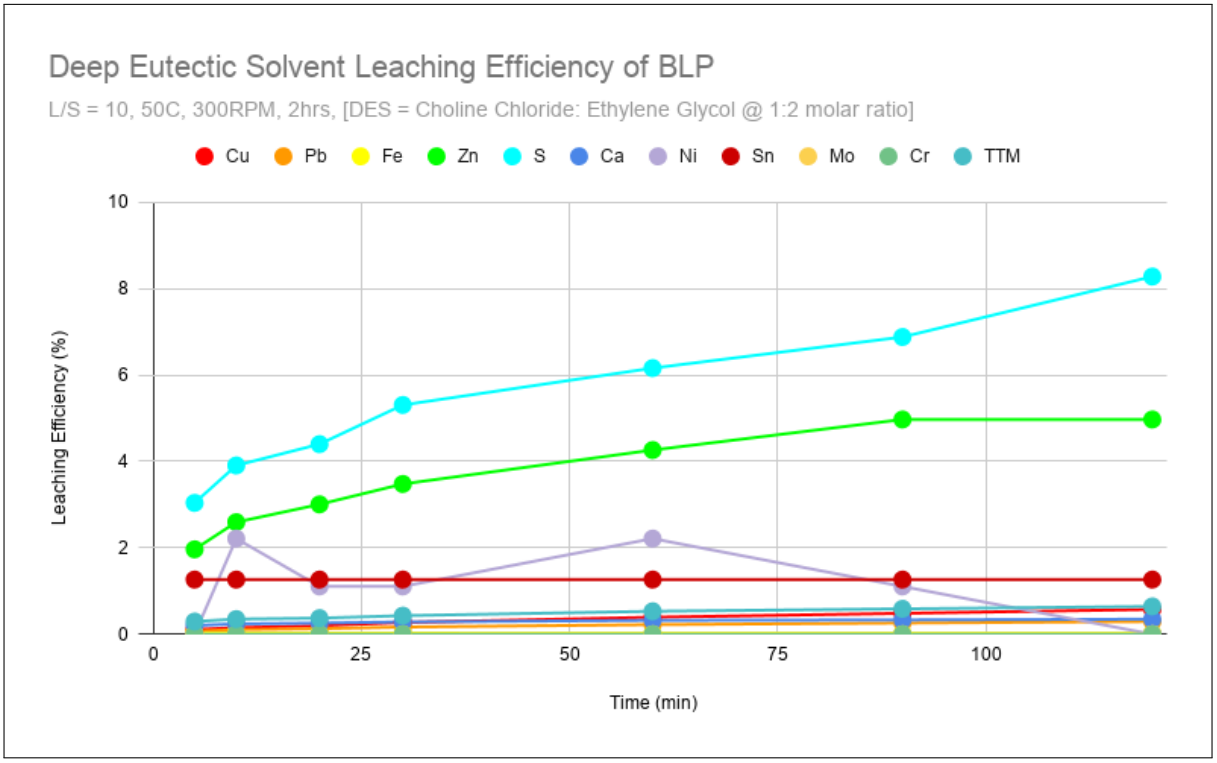

Figure 5.15: DES Leaching (choline chloride and ethylene glycol) of BLP - PLS leaching efficiencies. Time = 2hrs, L/S=10, 300RPM, Temp = 50°C

Table 5.4: Treatment effectiveness of DES leaching. For the PLS: Treatment Effectiveness = LE of [Cu] (or TTM) / LE [Fe], for the residue Treatment Effectiveness = % Cu or TTM/ % Fe

Treatment Effectiveness (Ratio)		Choline Chloride and Glycerol	Choline Chloride and Ethylene Glycol
PLS	Cu/Fe	3.952	23.277
	TTM/Fe	18.466	26.104

5.1.4. Ammoniacal Leaching

BLP was leached in ammoniacal solutions with the results indicated by Figures 5.16 and 5.17. These results refer to the initial screening experiments where only the [OH^-] and [Cl^-] ratios and concentrations were varied.

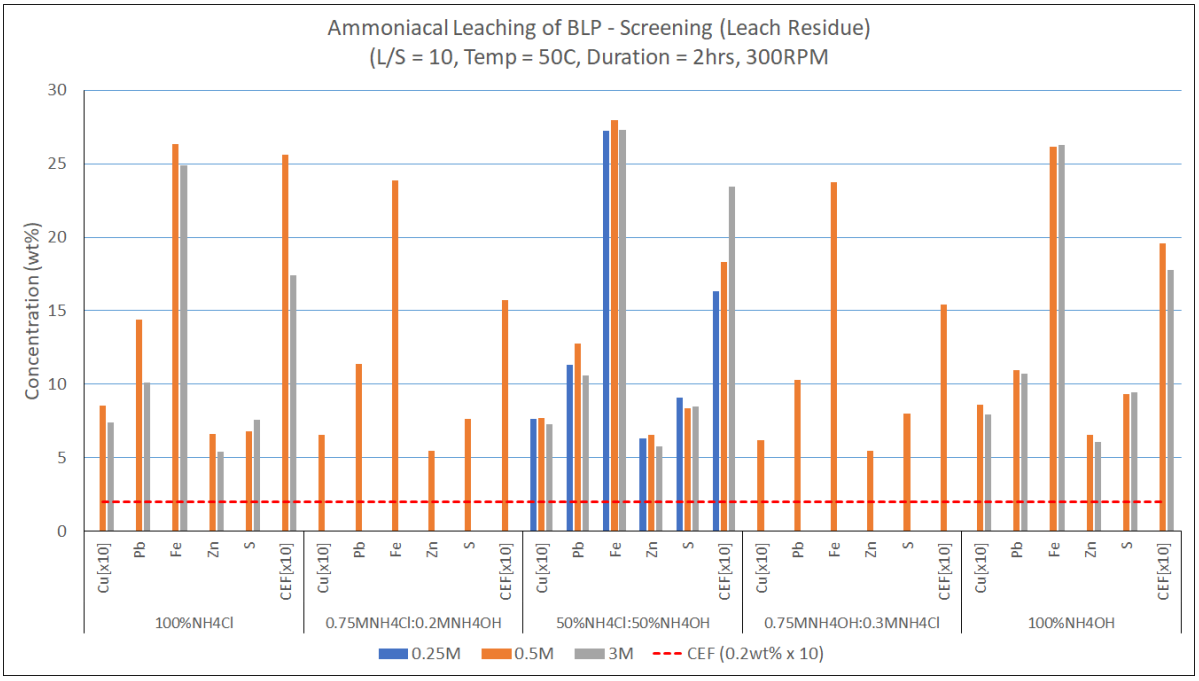

Figure 5.16: Ammonical Leaching of BLP (initial screening)- Leach residues. Time = 2hrs, L/S=10, 300RPM, Temp = 50°C

.

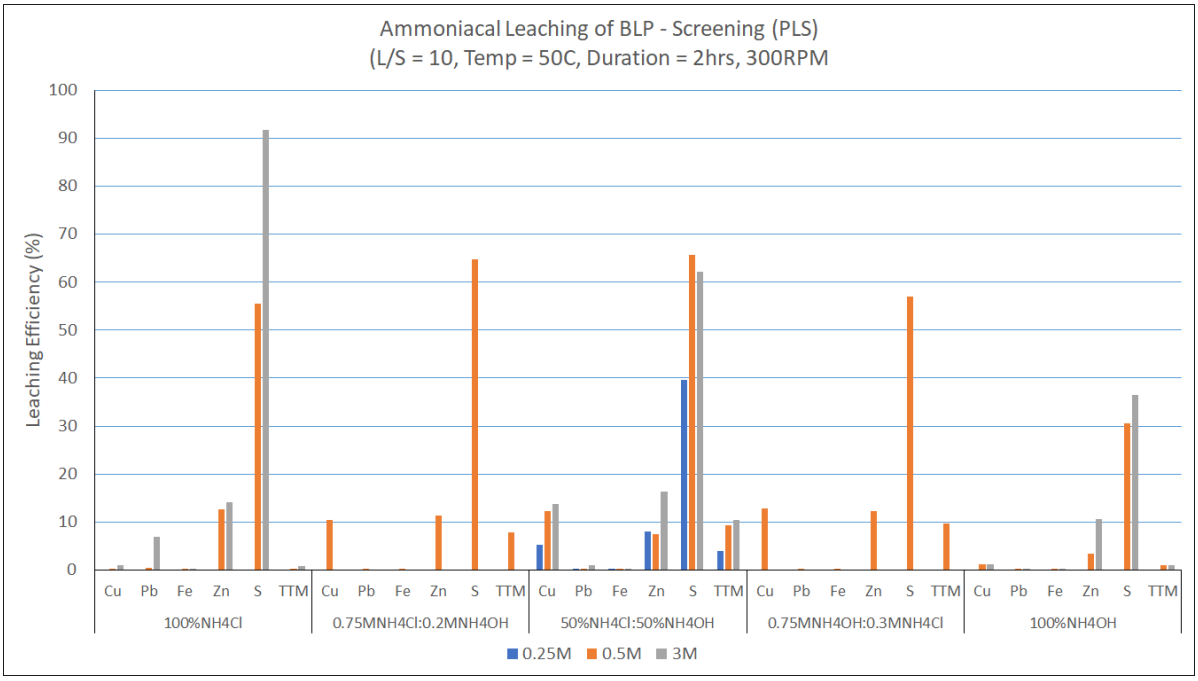

Figure 5.17: Ammonical Leaching of BLP (initial screening)- PLS leaching efficiencies. Time = 2hrs, L/S=10, 300RPM, Temp = 50°C

.

Zn and Cu form complexes in ammoniacal leach solutions as per the following equation:

$$M + NH_3 + 0.5O_2 -> [M(NH_3)_4]^{+2} + 2OH^- \tag{5.10}$$

Where M = Zn or Cu. This is observed in Figure 5.17 with the presence of Cu and Zn in all of the leach solutions that contain both $[OH]^-$ and $[Cl]^-$. It is important to note the presence of oxygen in Equation 5.10 which is a reactant that was not controlled for in the leaching reactions. Industrial ammoniacal leaching processes usually provide O_2 (or air) in addition to the ammonia source(s). Considering the leaching setup that was employed for these leaching experiments, O_2 (air) was not controlled to minimise the complexity of the setup. The following observations can be made about the initial screening results:

- Fe - The initial screening showed that Fe was not leached into the solution in all reactions. For all ammoniacal solutions except NH_4Cl the final pH of all the solutions were greater than 8.5. The Pourbaix diagram for Fe (see Figure A.1) shows that Fe is stable as a solid hydroxide at this pH which supports the leaching results. For NH_4Cl solutions, the final pH of the solution was <6 which allows Fe to be stable in solution as Fe^{2+}. Fe is present in jarosite as Fe(III) and would need to be reduced to Fe^{2+} and form a complex with NH_4^+, which does not occur.
- Pb - Similarly to Fe, the high pH of ammoniacal solutions results in Pb only being stable as a solid oxide. For the case of NH_4Cl, Pb could form a chloride complex to stay in solution which is potentially what is being observed with 3M NH_4Cl.
- Zn - According to the Pourbaix of a Zn-H_2O system (see Figure A.2), at pH < 8, Zn is stable as Zn^{2+} which is supported by some leaching of Zn into solution when using NH_4Cl. From pH 8-11, Zn forms $Zn(OH)_2$; however, in a Zn-NH_3-H_2O system, Zn forms $Zn(NH_3)_4^{2+}$ in a pH range of 8-11 (see Figure 5.18). This is supported by the results as lixiviants containing both NH_4OH and NH_4Cl (pH > 8.5) leached Zn into solution. It is uncertain what occurs at pH > 11. In a Zn-H_2O system, pH > 11 allows for the $Zn(OH)_4^{2-}$ to exist which supports what is being observed with the

0.5M and 3M NH_4OH solutions; however, the Pourbaix diagram of a Zn-NH_3-H_2O system (Figure 5.18) indicates that Zn would exist as $Zn(OH)_2$ from pH 11-14.

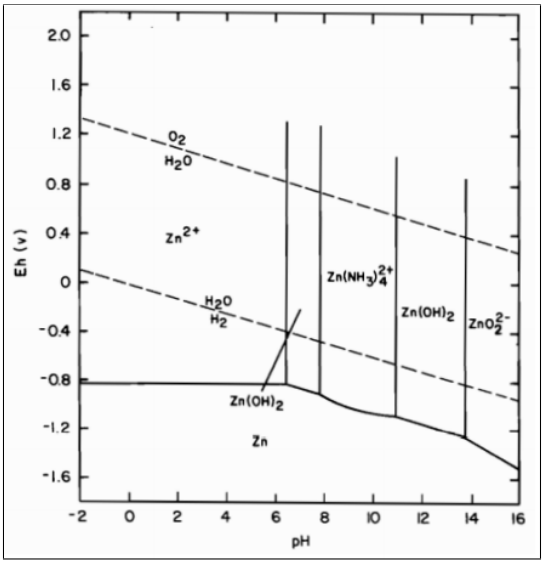

Figure 5.18: Pourbaix of Zn-NH_3-H_2O system at 25 °C [16].

- Cu - Similarly to Zn, Cu forms $Cu(NH_3)_4^{2+}$ in the Cu-NH_3-H_2O system in the same pH range (pH = 8-11). Hence Cu is observed in the PLS for all ammoniacal solutions containing both NH_4Cl and NH_4OH. Cu is not leached into solution with NH_4Cl because both the Cu-H_2O and Cu-NH_3-H_2O (See Figure 5.19) Pourbaix diagrams indicate that at pH 4-6, Cu is stable as Cu_2O or CuO (pH of 5-7). Neither is Cu leached in 0.5M and 3M NH_4OH as the pH is probably too high, resulting in Cu_2O or CuO formation.

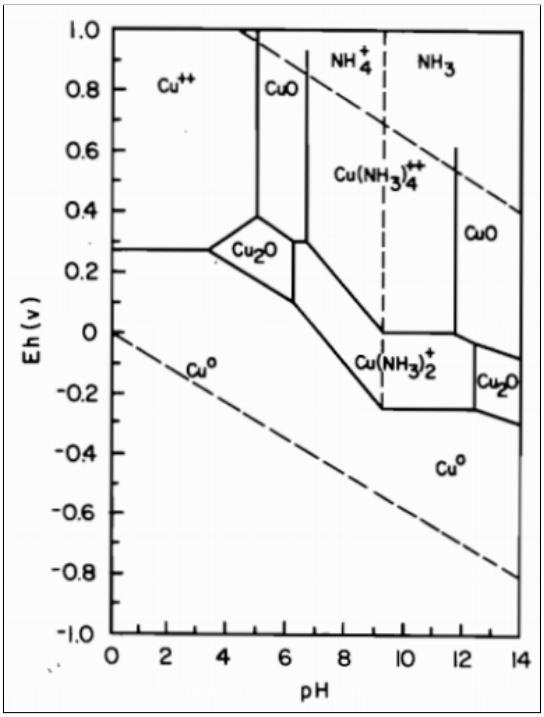

Figure 5.19: Pourbaix of Cu-NH_3-H_2O system at 25 °C [16].

- TTM - Leaching of TTM (Cu, Ni, Cr, Sn, Mo) largely follows the leaching of Cu. appendix A.3 shows that the leaching efficiency tracks the leaching efficiency of Cu for the screening reactions. No notable presence of the other metals was observed in the PLS.

Leaching Cu is grounded in ensuring the leaching conditions favour the presence of the $[Cu(NH_3)_4]^{+2}$. When solution conditions are favourable for the presence of $[Cu(NH_3)_4]^{+2}$, Cu ions will stay in solution rather than report to any solids. The stability of $[Cu(NH_3)_4]^{+2}$ depends on factors such as temperature, pH, and $[NH_3]/[NH_4^+]$ ratio (see Figure 5.20) [17].

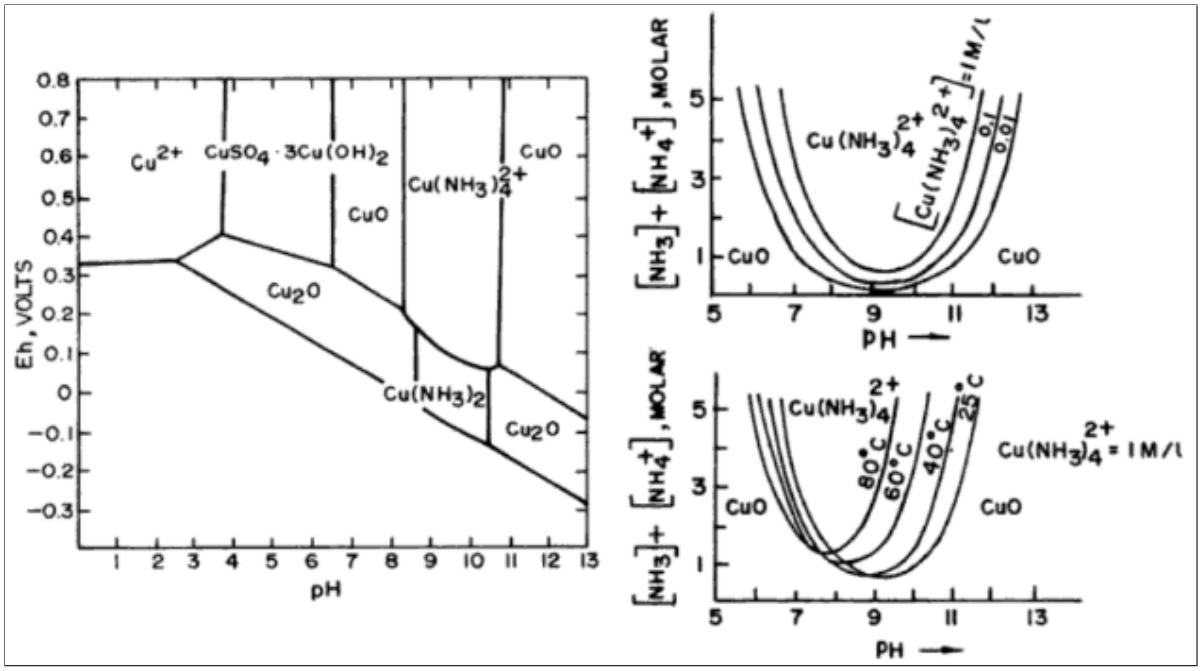

Figure 5.20: Left: portion of Eh-pH diagram of Cu-Fe-S-H_2O system at 25°C incorporated with NH_3 (pH 9.25) or NH_4^+ (pH9.25) at 1M activity. Right:Variation of $[Cu(NH_3)_4]^{+2}$ - stable region with its concentration and temperature [17]

Although Figure 5.20 is not a completely accurate representation of the BLP leaching experiments in this study, it provides some insight and may highlight what is required to improve leaching efficiencies. It may also indicate what the limits are of the leaching efficiency (if any). If we adopt a similar graphical approach (pH vs $[NH_4^+]$ + $[NH_3]$ concentration vs Cu leaching efficiency) Figure 5.21 is generated. It resembles Figure 5.20, which implies that, indeed, there is a 'sweet spot' of a fixed pH and $[NH_4^+]$ + NH_3 concentration where the Cu leaching efficiency reaches its highest. This is somewhat confirmed by a similar heat map generated for the Cu (wt%) in the leached residue (see Figure 5.22). These graphs needs to be incorporated with Table 5.6 for a more complete picture.

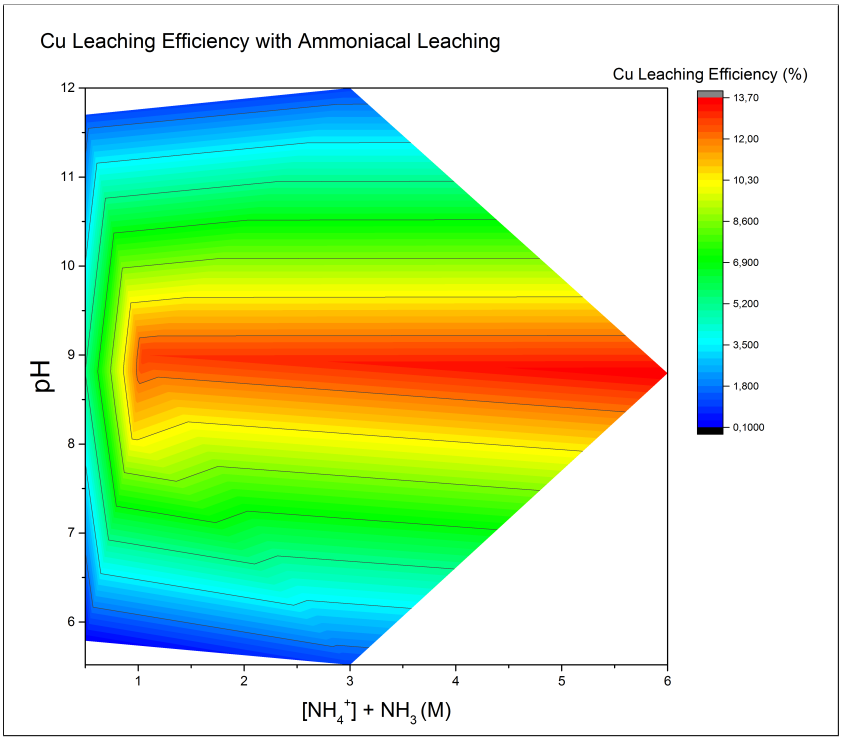

Figure 5.21: Heat map - Cu leaching efficiencies(%) in PLS with ammoniacal leaching (screening) at 50°C. X and Y axis refer to PLS conditions

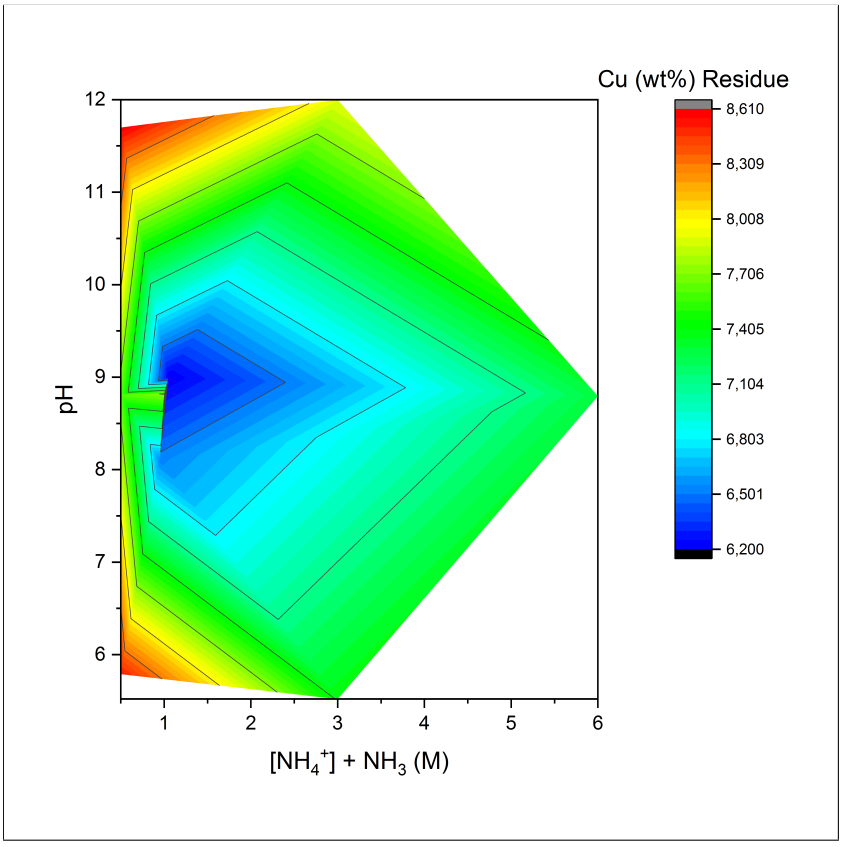

Figure 5.22: Heat map - Cu (wt%) in residue with ammoniacal leaching (screening) at 50°C. X and Y axis refer to PLS conditions

In Table 5.6, the pH of the NH_4OH and 0.3M NH_4Cl: 0.75M NH_4OH solutions was not measured as the pH meter available was sensitive to alkaline conditions. The pH value for the 0.3M NH_4Cl: 0.75M NH_4OH solution was assumes to be higher than 0.5M NH_4Cl: 0.5M NH_4OH. For the 0.5M NH_4OH solution, the initial pH was measured and used; based on this it was assumed for 3M NH_4OH that the pH would be higher than 0.5M NH_4OH. Figure 5.21 and Table 5.6 show that the optimal pH was around 8.5-9.5. In addition, having a $[NH_4^+]$ + $[NH_3]$ concentration = 1 achieved a similar Cu leaching efficiency of a leach solution with $[NH_4^+]$ + $[NH_3]$ concentration = 6 (3M NH_4Cl: 3M NH_4OH). This suggested that increasing the concentration of NH_3 sources doesn't necessary translate to increased leaching efficiency of Cu which Figure 5.20 indicates. Further investigation into the kinetics (e.g. particle size, temperature, etc) may highlight what the limiting parameter may be.

The XRDs of ammoniacal leached residues all show the same phases as the initial untreated BLP. Figure 5.23 indicates that the same 3 phases of BLP (plumbojarosite, lead sulfate, and Zn ferrite) are present in one of the ammoniacal leached residues. Ammoniacal leaching is not anticipated to breakdown the jarosite in the BLP. The XRD does not necessarily confirm this as jarosite was still present in acid leached residues of BLP and acid breaks down jarosite. For both ammoniacal and acid leaching, any broken down products were not in high enough concentration to be detected by XRD. If one considers that ammoniacal leaching does not break down the jarosite then Cu may be extracted into solution either because it is on the surface of a jarosite particle or by diffusion. If Cu is released into solution because it is on the surface of jarosite particles then smaller particles will yield high leaching efficiencies (not untypical of leaching reactions); however, there would be a limit to how much Cu could be extracted (Cu located in the core of the particles would not react). If Cu is released into solution by diffusion, which is supported by the shrinking core model, then theoretically 100% of the Cu could be extracted given sufficient time. Both these claims can only be supported by a more thorough investigation into the kinetics of the leaching reaction in future studies.

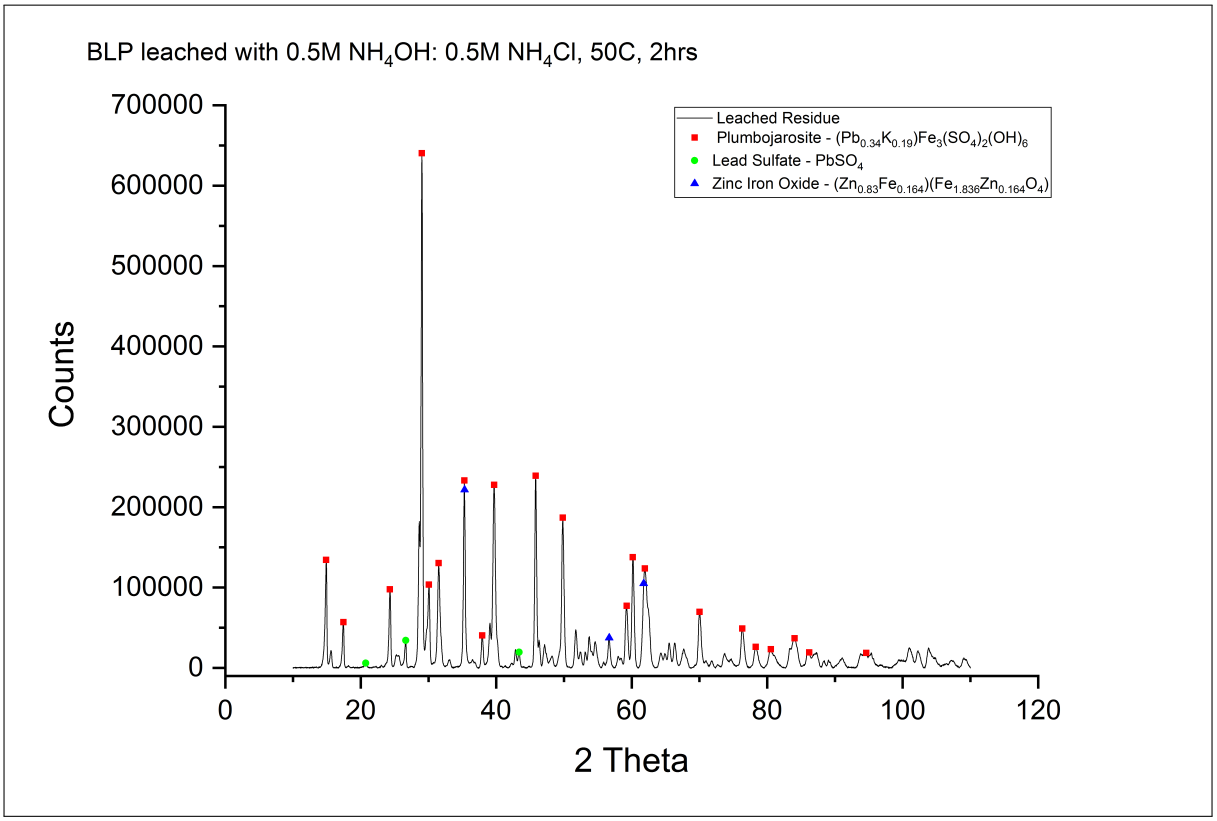

Figure 5.23: XRD of BLP leached with 0.5M NH_4OH: 0.5M NH_4Cl. Time = 2hrs, L/S=10, 300RPM, Temp = 50°C

.

A parametric study was then conducted on ammoniacal solutions based of 0.5M NH_4Cl and 0.5M NH_4OH leach solutions. This solution will be considered as (A) going forward. Results are indicated in Figure 5.24 and Figure 5.25. It is difficult to say why leaching (A) at 25°C resulted in poorer treatment effectiveness. By considering Figure 5.20, a lower temperature and corresponding shift in optimal pH should not affect the solutions position in the $[Cu(NH_3)_4]^{+2}$ stability zone. One possible reason may be kinetics of the solution. The rate constant term (k_{exp}) in Equations 5.7 and 5.8 incorporates a diffusion coefficient which has a positive correlation with temperature. Consequently, lower temperatures would result in lower reaction rates. There are limits as to how high the temperature can be increased to improve leaching rates. For (A) at 75°C, for $[Cu(NH_3)_4]^{+2}$ to remain stable at elevated temperatures, additional $[NH_3]$ + $[NH_4]^+$ is required along with a corresponding reduction in pH. The reaction at 75°C did have a reduction in pH; however, given that the setup (see Figure 4.8) was not hermetic, ammonia gas would have left the solution. This was confirmed by an ammonia odour released from the leaching container (which was not the case at 50°C), resulting in a reduction of the $[NH_3]$ + $[NH_4]^+$] concentration and likely placing the leaching solution outside the stability zone.

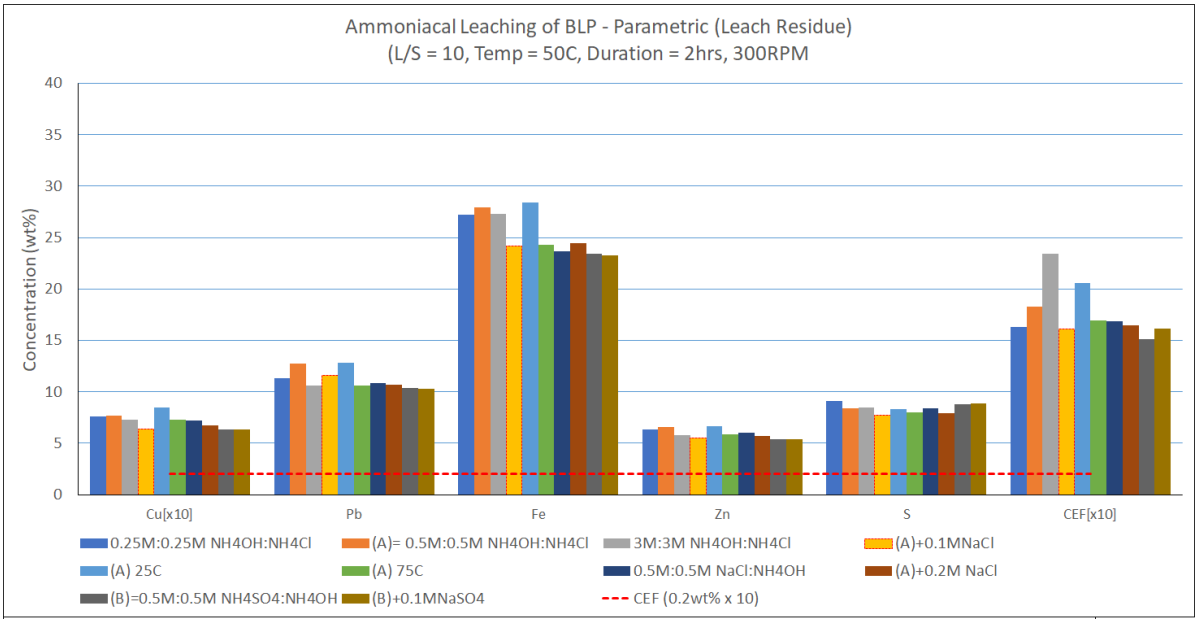

Figure 5.24: Ammoniacal Leaching of BLP (parametric study)- Leach residues. Time = 2hrs, L/S=10, 300RPM, Temp = 50°C

.

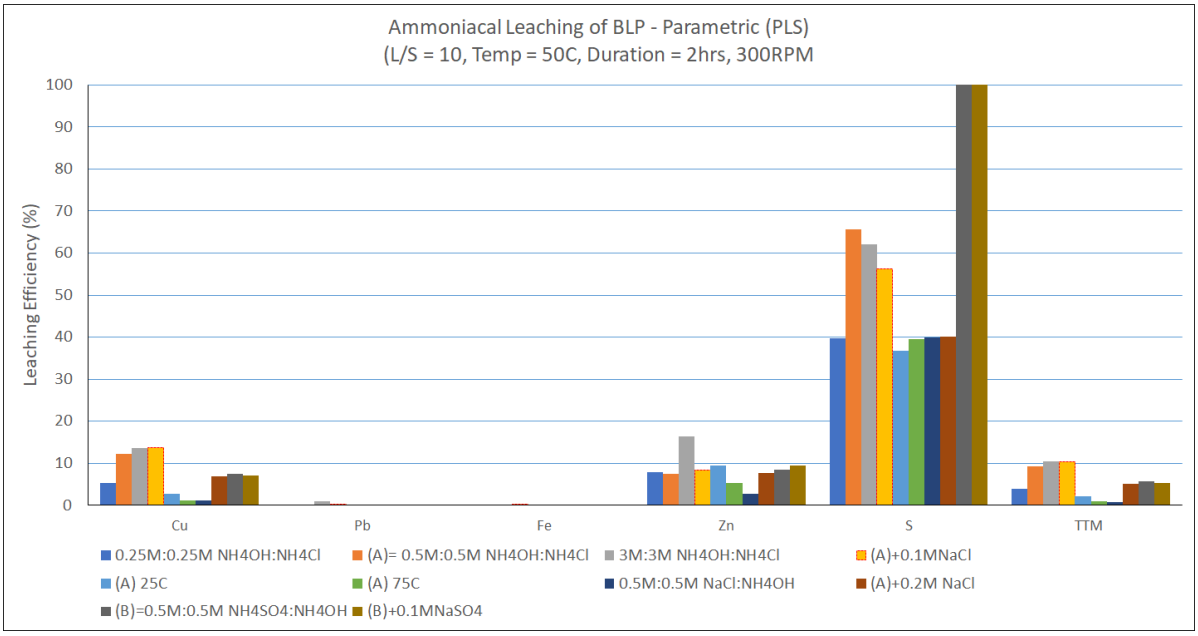

Figure 5.25: Ammoniacal Leaching of BLP (parametric study)- PLS leaching efficiencies. Time = 2hrs, L/S=10, 300RPM, Temp = 50°C

The requirement of a $[NH_4]^+$ source for Cu leaching was confirmed when BLP was leached with 0.5M NaCl and 0.5M NH_4OH. NaCl was used instead of the standard NH_4Cl. This resulted in significantly lower leaching efficiencies of Cu and a lower treatment effectiveness. The reduced $[NH_3]$ + $[NH_4]^+$] in addition to the higher pH (approximately 9.5), which would have put the solution outside the $[Cu(NH_3)_4]^{+2}$ stability zone.

The most effective treatment occurred when 0.1M NaCl was added to (A). It is hard to speculate as to why the presence of NaCl increased leaching efficiency. The presence of NaCl in ammoniacal leaching of BLP was initially investigated based on the success of the EZINEX Process. The EZINEX process is an industrial ammoniacal leaching process for Zn recovery which uses the presence of alkali salts to increase the leaching efficiency of Zn. Since both Cu and Zn form ammonia complexes in a similar fashion, the addition of alkali salts was considered for this thesis. Adding NaCl lowered the pH of the solution of (A) from 8.82 to 8.54 making it more neutral (potentially a more favourable pH). Figure 5.26 is a Pourbaix diagram of a Cu-NH_3-H_2O system showing that the presence of Na in the Cu-NH_3-H_2O has no appreciable impact on the $[Cu(NH_3)_4]^{+2}$ stability zone. Consequently, the combined impact of Na and Cl must increase the Cu leaching efficiency. Increasing the concentration of NaCl to 0.2M reduced the pH further to 8.5; however, this resulted in lower leaching efficiencies and higher Cu concentrations in the residual solid. This suggests that excessive NaCl had a negative effect. A deeper investigation into the presence of NaCl in ammoniacal leaching would provide greater insight as to why 0.2M NaCl reduced the leaching efficiency when compared to 0.1M NaCl.

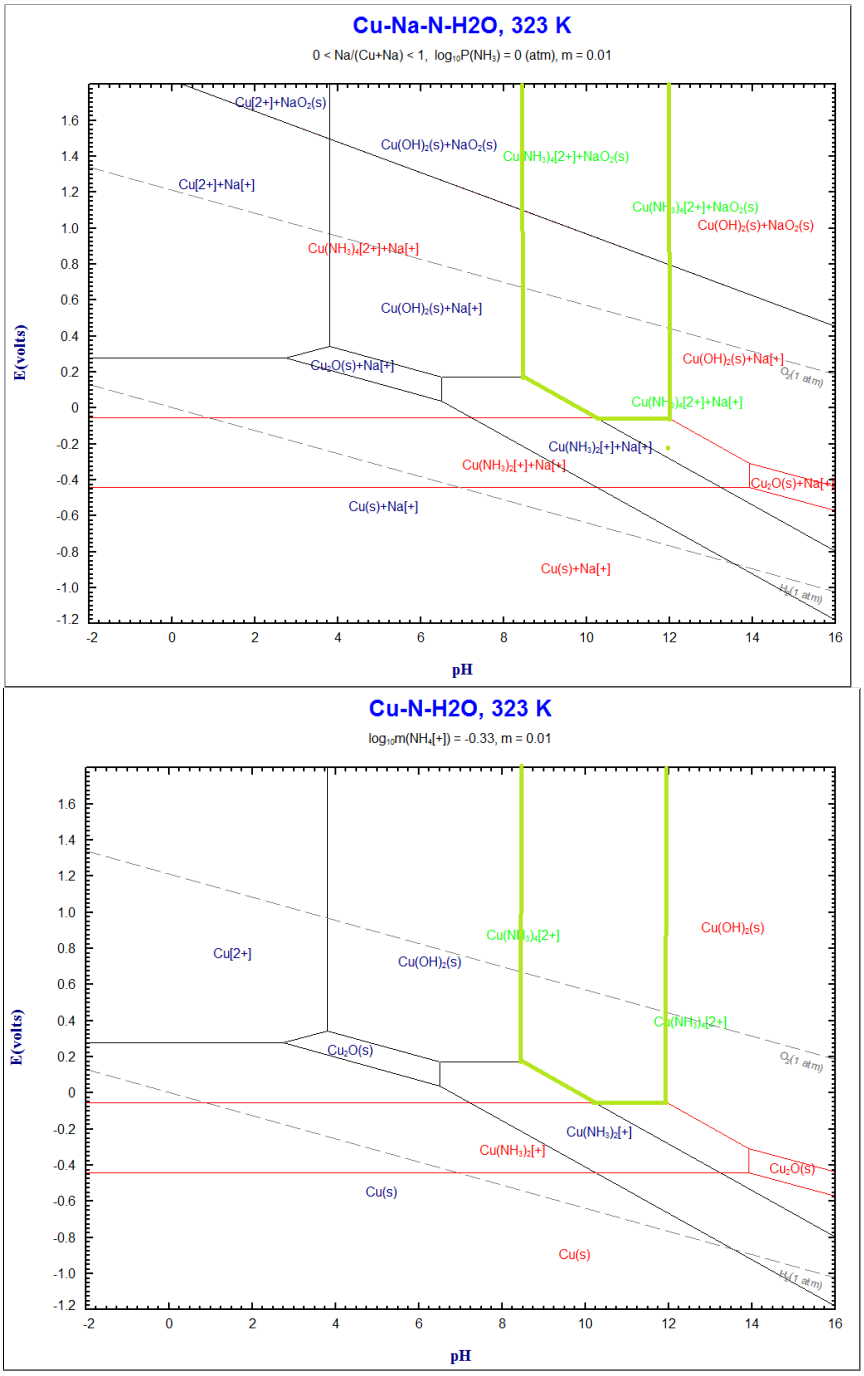

Figure 5.26: (Top) Pourbaix of Cu-Na-NH3-H2O system at 50°C (0.5M NH_4Cl, P = 1 atm NH_3, Cu a = 0.01 (Bottom) Pourbaix of Cu-NH3-H2O system at 50°C (0.5M NH_4Cl, P = 1 atm NH_3, Cu a = 0.01. Green highlighed section represents $[Cu(NH_3)_4]^{+2}$ stability zone. Produced with FactSage Software

It is important to consider ammoniacal leaching in a sulfate system because the hydrometallurgy used in Zn mining is sulfate based. If the leaching efficiency of a sulfate based ammoniacal leach was sufficiently high, it is something that can be incorporated into a Zn hydrometallurgical circuit more readily. Changing the system from a chloride to a sulfate based system also had similar residue treatment effectiveness to a chloride based system. In fact, the leach residue from a sulfate based ammoniacal leach system had the lowest Cu concentration (see Figure 5.24). The residue with the lowest Cu (wt%) resulted from BLP being leached with 0.5M:0.5M:0.1M $9NH_4)_2SO_4$: NH_4OH: Na_2SO_4. This is not reflected in the leaching efficiency however. The PLS analysis of the sulfate systems (see Figures

A.23 and A.24) indicates lower Cu leaching efficiencies when compared to ammoniacal leaching in a chloride system. The treatment effectiveness of a sulfate based system was reduced compared to a chloride based system because the Cu/Fe and CEF/Fe ratio was impacted by lower Fe content. This can be attributed to higher Ca (not shown) and S presence in the residue for the sulfate based system (see Figures 5.24).

Since the overall leaching efficiencies of Cu in the PLS were low, and the concentration of Cu (and CEF) in the treated residues was well in excess of what was required for HIsarna ironmaking, further investigation into ammoniacal leaching was not conducted. Further investigation may be warranted for a more conclusive understanding of the complex interactions of pH, temperature and $[NH_3]$ + $[NH_4]^+$ concentration on the leaching of Cu from BLP. In the most 'aggressive' conditions (i.e. 3M:3M NH_4Cl:NH_4OH), the leaching efficiency was only 13.6%. It is unlikely that ammoniacal leaching is an effective strategy in removing Cu and CEF metals from BLP.

Table 5.5: Treatment effectiveness of ammoniacal leaching. For the PLS: Treatment Effectiveness = LE of [Cu] (or TTM) / LE [Fe], for the residue Treatment Effectiveness = % Cu or CEF/ % Fe

Treatment Effectiveness	**PLS**		**Leach Residue**	
Lixiviant	**Cu/Fe**	**TTM/Fe**	**Cu/Fe**	**CEF/Fe**
0.5M NH4Cl	4.562	8.282	0.032	0.097
3M NH4Cl	88.209	73.274	0.030	0.070
0.75MNH4Cl:0.2MNH4OH	2733.555	2047.824	0.027	0.066
0.25M:0.25M NH4OH:NH4Cl	520.677	395.811	0.028	0.060
(A)= 0.5M NH4OH: 0.5M NH4Cl	12817.845	9640.125	0.028	0.066
3M NH4OH: 3M NH4Cl	1373.887	1042.411	0.027	0.086
(A)+0.1M NaCl	14379.876	10750.685	0.026	0.067
(A) 25C	5666.192	4236.159	0.030	0.072
(A) 75C	589.590	440.790	0.030	0.070
0.5M NaCl: 0.5M NH4OH	2327.733	1740.260	0.031	0.071
(A)+0.2M NaCl	7243.537	5415.414	0.028	0.067
(B)=0.5M NH4SO4: 0.5M NH4OH	5237.399	3915.585	0.027	0.065
(B)+0.1MNaSO4	4920.909	3678.971	0.027	0.070
0.75M NH4OH:0.3M NH4Cl	13445.720	10109.537	0.026	0.065
0.5M NH4OH	796.330	641.148	0.033	0.075
3M NH4OH	453.295	375.530	0.030	0.068

Table 5.6: Leaching efficiencies of Cu in ammoniacal leach solution

Screening									
Solution	**05MNH4Cl**	**0.25MNH4Cl: 0.25MNH4OH**	**3MNH4OH: 3MNH4Cl**	**3MNH4Cl**	**0.5MNH4Cl: 0.5MNH4OH**	**0.75MNH4Cl: 0.2MNH4OH**	**0.3MNH4Cl: 0.75MNH4OH**	**0.5M NH4OH**	**3M NH4OH**
NH3 + [NH4+]	0.5	0.5	6	3	1	0.95	1.05	0.5	3
Final pH	5.79	8.807	8.795	5.52	8.821	8.099	>8.82	11.7*	>11.7
Cu Leaching Efficiency	0.103	5.277	13.675	1.056	12.247	10.489	12.839	1.140	1.089
Cu [x10] (wt%) in Residue	8.52	7.62	7.29	7.39	7.717	6.53	6.21	8.6	7.92
Parametric									
Solution	**0.5MNH4Cl: 0.5MNH4OH: 0.1MNaCl**	**0.5MNH4Cl: 0.5MNH4OH 25C**	**0.5MNH4Cl: 0.5MNH4OH 75C**	**0.5MNaCl: 0.5MNH4OH**	**0.2MNaCl: 0.5MNH4OH: 0.5MNH4Cl**	**0.5MNH4OH: 0.5MNH4SO4**	**0.5MNH4OH: 0.5MNH4SO4: 0.1MNa2SO4**		
NH3 + [NH4+]	1	1	1	0.5	1	1	1		
Final pH	8.543	9.345	7.941	9.41	8.506	8.31	8.44		
Cu Leaching Efficiency	13.750	2.711	1.130	1.116	6.94	7.523	7.067		
Cu [x10] (wt%) in Residue	6.35	8.45	7.26	7.24	6.74	6.36	6.30		

5.2. Pyrometallurgical

In this section, the results of the pyrometallurgical treatments of BLP will be discussed and analysed. BLP was treated pyrometallurgically using two approaches: thermal decomposition and chloridisation. In the thermal decomposition treatment, approximately 5g of BLP was introduced into a horizontal furnace at various temperatures. The aim of thermal decomposition was to explore what was observed with the TGA and to determine what compounds would be produced at various temperature treatments. It was also a strategy to determine if thermal decomposition would volatilise some elements and produce a solid that would be an acceptable feed into HIsarna. After the treatment, the solid residues were analysed with XRD and XRF. Similarly, for the chloridisation strategy, BLP and $CaCl_2$ were mixed in a predetermined ratio based of promising results from the literature [69]. The aim of this strategy was to volatilise the CEF metals as chlorides. Wang [69] was able to remove 97% of the Cu from a jarosite waste stream by roasting it with $CaCl_2$. This approach aims to investigate the behaviour of these volatile metals in an inert atmosphere. Again, approximately 5g of this solid mix was placed in a furnace at various temperatures and the residue analysed.

For the pyrometallurgical treatments, elemental changes needed to be calculated to determine which elements were being lost. They were calculated according to the following equation:

$$Elemental\ Mass\ Change(\%) = \frac{(m_{blp} - m_{rs}) * G_E}{m_{blp} * G_E} * 100 \tag{5.11}$$

where m_{blp} = mass of BLP (g), m_{rs} = mass of residual solid (g), G_E = grade of element (%).

5.2.1. Thermal Decomposition

The thermal decomposition treatment is a continued investigation of what was observed with the TGA of BLP (see Section 4.2.3 and Figure 4.6). The TGA revealed substantial mass changes occurring at approximately 400°C and 650°C, indicating that decomposition reactions had occurred. Based on this, conducting thermal treatments at 500°C and 700°C would be appropriate to decide the necessary treatment duration.

To determine the appropriate treatment duration in the horizontal furnace, 5g of BLP was placed in the furnace for two durations (15 minutes and 30 minutes) and at the two temperatures (500°C and 700 °C) previously mentioned. From Table 5.7, increasing the duration from 15 to 30 minutes had limited impact on the mass change. Based on this, it was determined that 15 minutes was sufficient time for the completion of any reactions occurring at these temperatures and all other temperatures.

Table 5.7: Mass change of decomposed BLP at 15 and 30min, and 500 and 700°C

Temperature (C)	**Time (mins)**					
	15			**30**		
	Initial (g)	**Final (g)**	**Change (%)**	**Initial (g)**	**Final (g)**	**Change (%)**
500	5.02	4.55	-9.36	5.05	4.55	-9.90
700	5	3.94	-21.20	5.00	3.99	-20.20

Approximately 5g of BLP was introduced into the furnace at 500, 600, 700, 800 and 1000°C and left for a duration of 15 minutes. A thermal decomposition reaction was not carried out at 900°C because it was not a point of interest based on the TGA. Figure 5.27 shows the mass change of the sample after decomposition had occurred at the various temperatures. The figure indicates the relative mass change and the portion of the mass change that is attributed to the loss of sulfur.

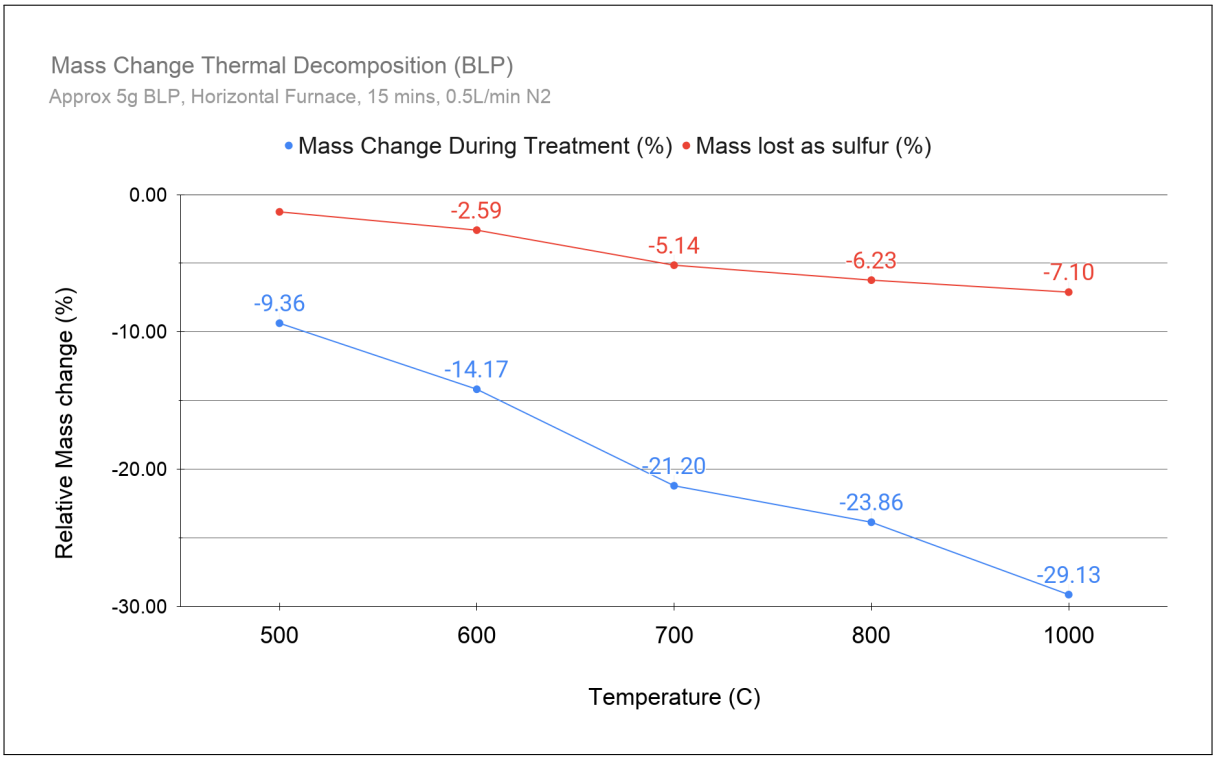

Figure 5.27: Mass change of decomposed BLP at various temperatures.

Equation 5.11 was applied to the treated residue. Elemental compositions were determined with XRF analysis to produce Figure 5.28.

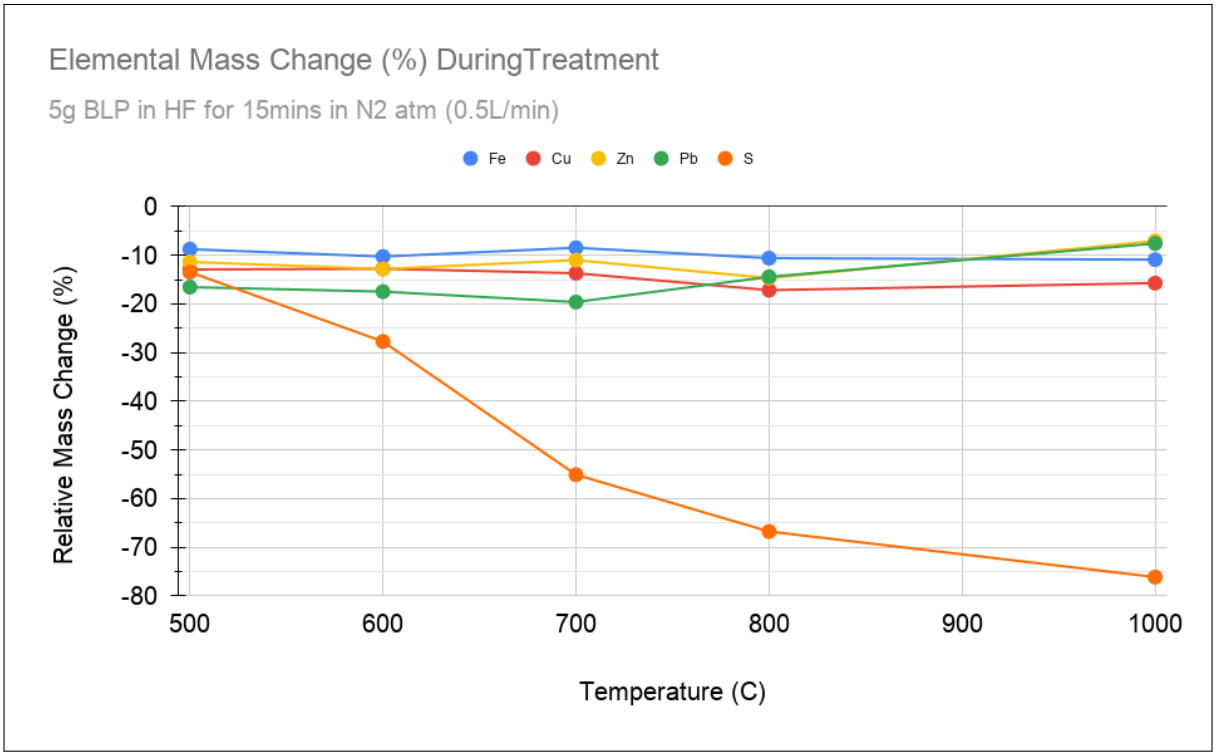

Figure 5.28: Elemental mass change(%) during BLP decomposition at various temperature. This indicates the elements leaving the sample.

Figure 5.28 shows sulfur leaving throughout the thermal decomposition of BLP. Sulfur leaves the sample according to Equations 5.12 and 5.13 from 500°C onwards. Prior to this temperature, dehydroxylation occurs (see Section 2.4.4.3). Figure 5.27 reveals that sulfur only comprises of roughly 20% of the total mass leaving the BLP. The loss of O_2 and water accounts for some of the remaining mass. Water leaves as per Equation 4.1; however, this was impossible to detect with the mass spectrometer. Equation 5.12 is likely to be occurring at lower temperatures (500-700°C), as suggested by Steinlechner[65], because Δ G of Equation 5.13 is not negative until T > 775 °C (see Table 5.8).

$$2Fe_2(SO_4)_3 -> Fe_2O_3 + Fe_2(SO_4)_3 + 3SO_2 \tag{5.12}$$

$$Fe_2(SO_4)_3 -> Fe_2O_3 + 3SO_2 + 1.5O_2(\Delta G < 0, T = 775^{\circ}C) \tag{5.13}$$

Table 5.8: ΔG^o calculations for Equation 5.13.

G^o for Equation 5.13	
T(K)	**ΔG*(kJ)**
673	308.3527
773	226.6047
873	145.2231
973	64.045
1073	-16.8345
1173	-97.2404
1273	-177.1527

The TGA clearly indicated that two distinct mass transitions were occurring at 400°C and 650 °C. When the residue of the 500°C treatment is compared to untreated BLP, the main change is presence of plumbojarosite. The XRD (see Figure 5.29) of the 500°C residue no longer shows plumbojarosite indicating that this had decomposed. There is no crystalline Fe structure in the treated residue either. Although mass spectrometry of the 500°C treatment shows SO_2 (See Figure 5.30) leaving the solid, the amount of sulfur leaving the sample is low and is comparable with the other elements in Figure 5.28. This suggests that an amorphous iron oxysulfate had formed as previously identified in the literature [64].

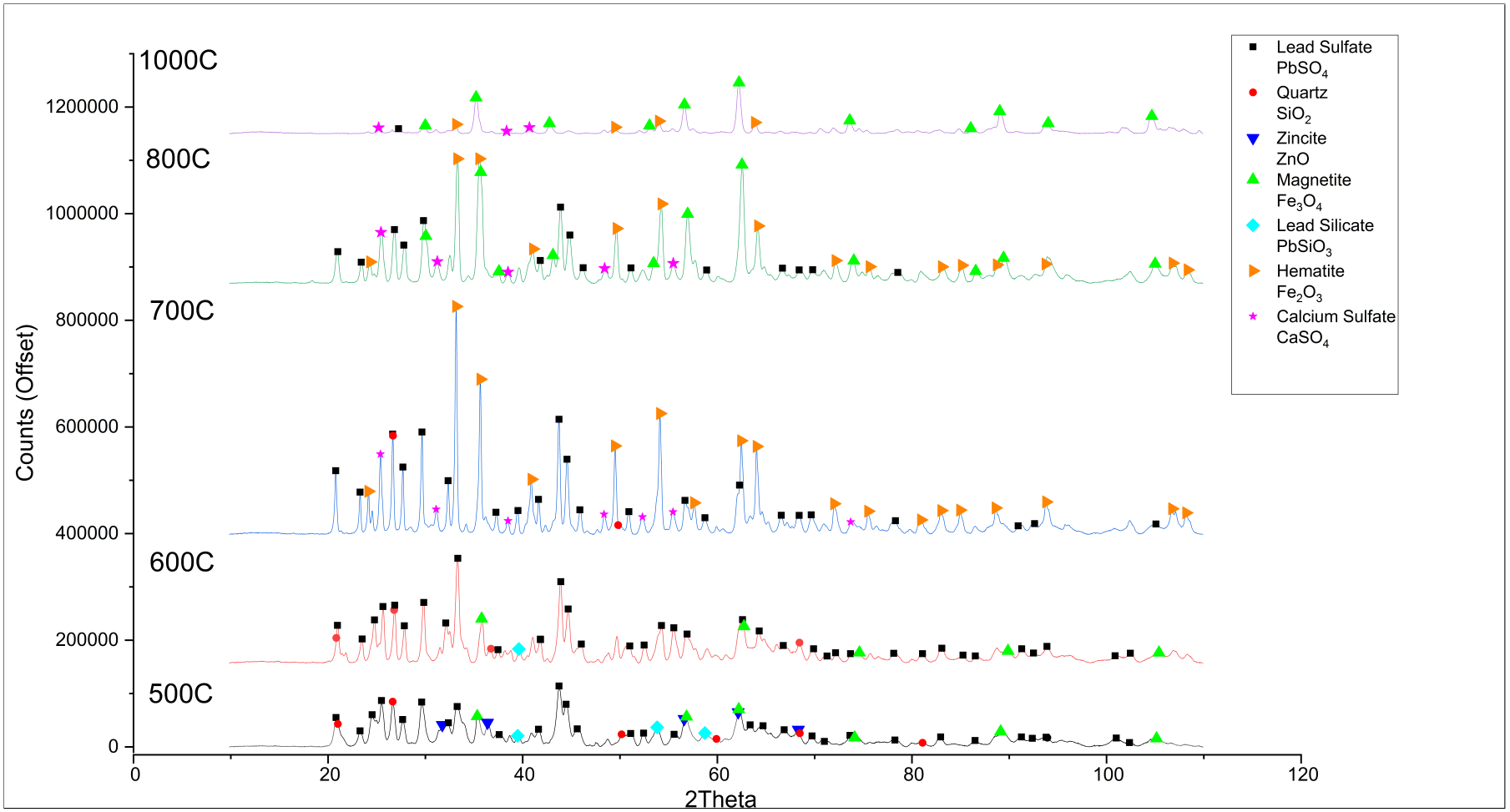

Figure 5.29: XRD spectra of thermally decomposed BLP at various temperatures. 5g of BLP in horizontal furnace. N_2 atmosphere 0.5L/min.

When comparing the 500°C and 700°C residue there are two distinct changes. The first is the substantial loss in sulfur. XRF reveals that the sulfur loss increases from 13% (500°C) to 55% (700 °C). Mass spectrometry of the reactions show a significant increase in the SO_2 emitted in the 700°C treatment when compared to the 500°C treatment (see Figure 5.30). This combined with XRD shows the second change which is the decomposition of any iron sulphates to form hematite and SO_2. The XRD detects the presence of hematite at 700°C treatment confirming that decomposition occurred. The complete conversion of iron sulphate to hematite does not seem to occur at a particular temperature as the sulfur content in the treated residues is gradually reduced throughout 500-1000°C. The percentage of sulfur loss increases with increasing treatment temperature. 77% of the sulfur leaves the sample at the 1000°C treatment. At 1000°C, sulfur still remains in the residue in the form of calcium sulphate and lead oxide sulphate (see Figure 5.29 and Figures B.7 and B.8 in the appendix). Also, at higher temperatures (800°C) hematite (Fe_2O_3) is converted to magnetite (Fe_3O_4).

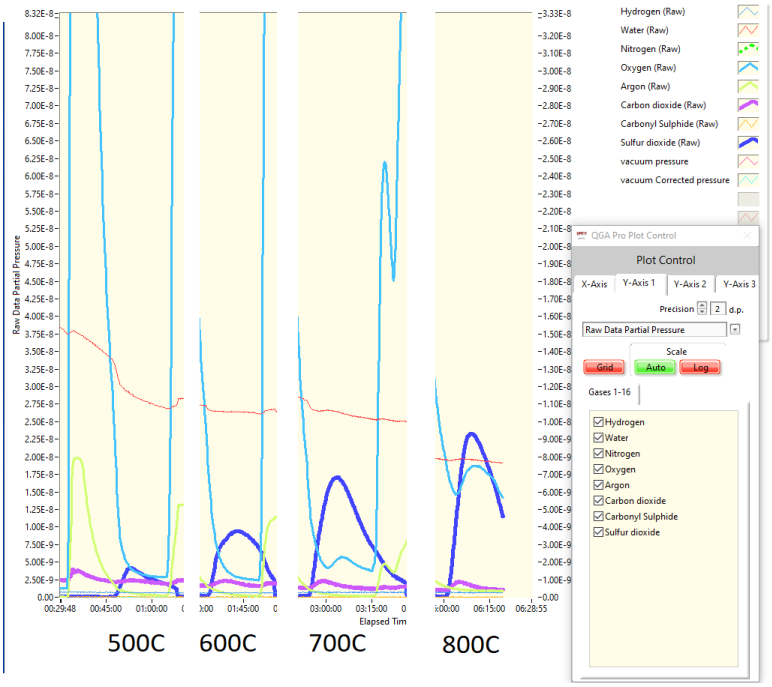

Figure 5.30: Mass spec of BLP thermal decomposition reactions occurring at 500, 600, 700, and 800°C showing evolution of SO_2 (dark blue line) and O_2 (light blue).

.

The presence of O_2 is detected at 700°C onwards by the mass spectrometer indicated by a light blue line (see Figure 5.31). This is further confirmation that reaction 5.13 is taking place. The mass spectrometer results for the thermal decomposition of jarosite at other temperatures can be found in the appendix (see Figures 5.30 and B.9).

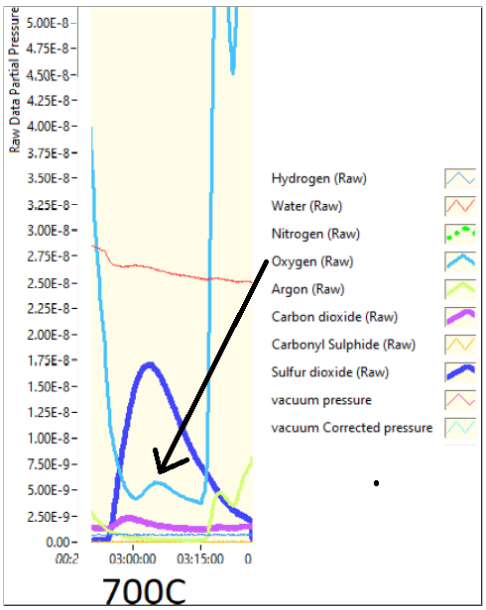

Figure 5.31: Mass spectrometer results (qualitative) of 5g of BLP in horizontal furnace at 700C. N_2 atmosphere 0.5L/min.

Since none of the CEF metals were shown to be leaving the sample, this suggests there should be an up concentration of these elements in the residue. Figure 5.32 shows that as the temperature of the treatments rise, the concentration of most metals in the residual solid increases including Cu and the other CEF metals. At 1000°C, the presence Sn and Mo is most noticeable in the CEF value.

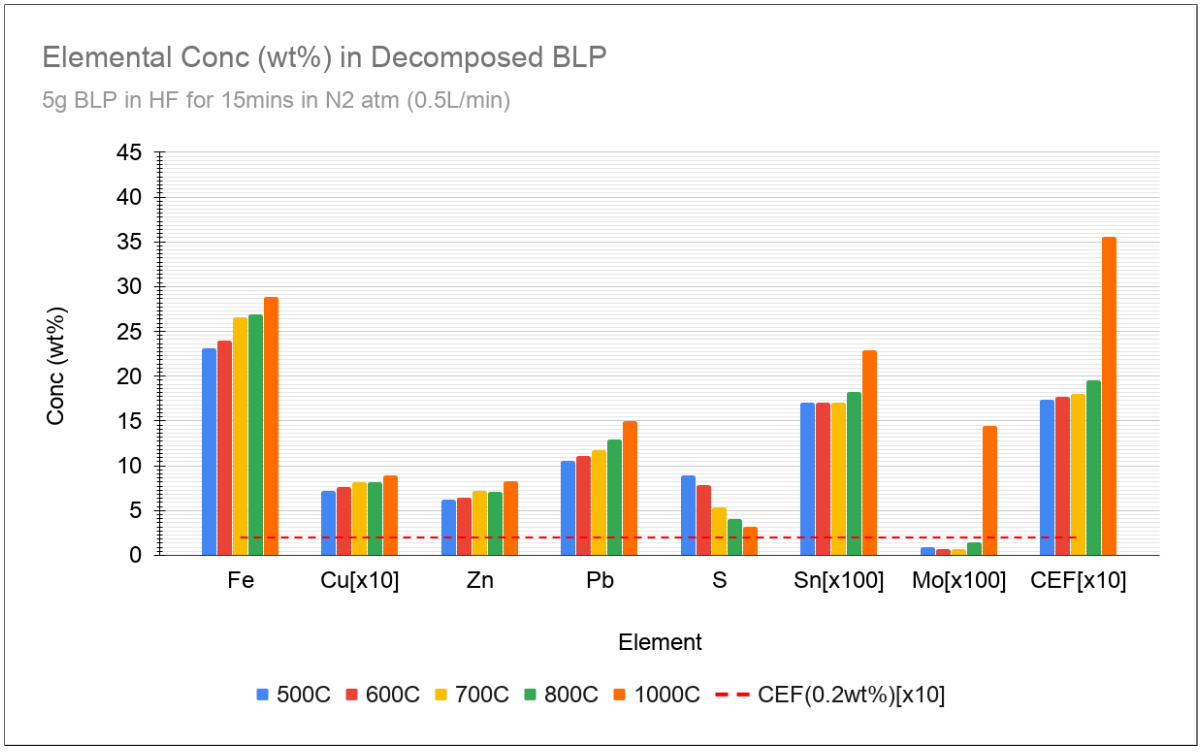

Figure 5.32: Elemental conc(wt%) of decomposed BLP at various temperatures.

Thermodynamic modelling (with HSC chemistry v6) was conducted to see if the volatiles should be leaving the sample or, if not, how they would remain in the residue. Analysis was carried out on

a typical sample of jarosite (identified in Table 3.2) heated from RT to 1000°C in a N_2 environment. Figure 5.33 shows the results and indicates that H_2O and SO_2 should be leaving the sample at the temperatures outlined in Section 2.4.4.3. Volatile metals are not shown to be leaving the sample at elevated temperatures. What compounds remain are shown to be a mix of Fe oxides, metal silicates, and metal sulfates which are thermodynamically more stable than the volatilisation of metals like Pb and Zn. This is what is identified with XRD spectra of the thermally decomposed BLP (see Figure 5.29 and the more detailed XRDs in Section B.1.1 in the appendix). Figure 5.29 shows the presence of $CaSO_4$, $PbSO_4$, SiO_2, Fe_2O_3 and Fe_3O_4 at elevated temperatures (> 700 °C).

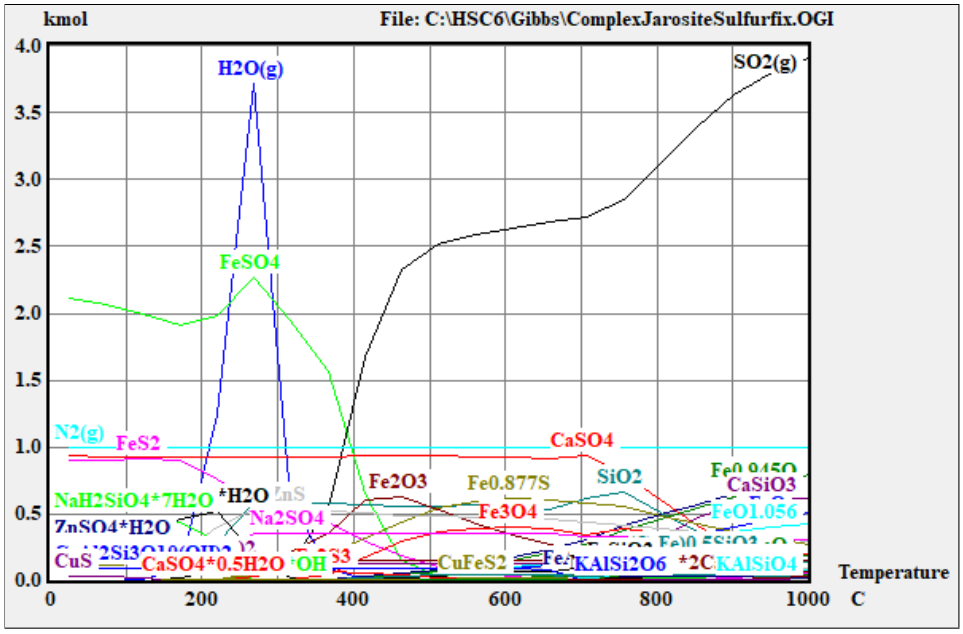

Figure 5.33: Equilibrium chemical compositions of jarosite mix when heated to 1000°C in N_2 atm. Using HSC Chemistry v6.

For all the thermal decomposition experiments, sulfur was the only element that left. There were no losses observed with the other metals present in BLP. This consequently resulted in an upconcentration of metals which indicates that thermal decomposition was not an effective treatment in removing the Cu and the other CEF metals. Table 5.9 shows the treatment effectiveness of thermal decomposition. The values are similar to all the hydrometallurgical treatments.

Table 5.9: Treatment effectiveness of the thermal decomposition of BLP at various temperatures (duration is 15 minutes unless specified in the brackets). Experiment was carried out twice at 1000 °C.

Treatment Effectiveness (Residue)	**500°C**	**500°C(30 mins)**	**600**	**700°C**	**700°C(30 mins)**	**800**	**1000°C**	**1000°C**
Cu/Fe	0.0312	0.0327	0.0317	0.0308	0.0302	0.0302	0.0309	0.0319
CEF/Fe	0.0751	0.0746	0.0737	0.0677	0.0733	0.0726	0.1235	0.1235

5.2.2. Chloridisation

Chloridisation of jarosite was selected as an approach in treating the BLP residue because it was a relatively simple one-step process that showed great promise in removing Cu from BLP. Wang [69] was able to remove approximately 97% of the Cu from an industrially sourced jarosite by simply roasting the jarosite with $CaCl_2$ at 1100°C. This approach requires a simpler flowsheet for Cu removal compared to the hydrometallurgical or the combined pyro- and hydrometallurgical treatments. The key difference to

the Wang study is that this thesis investigates chloridisation in an inert atmosphere rather than roasting in air. 5g of solid mix consisting of BLP (76%) and $CaCl_2$ (24%), as per the optimal ratio highlighted in the study, was placed in a horizontal furnace at various temperatures in an N_2 environment.

To determine the appropriate reaction time in the furnace, 5g of the solid mix (BLP and $CaCl_2$) was placed in the furnace for the following durations: 5, 10, 15, 30 and 60 minutes. Figure 5.34 shows that after 15 minutes the sample had lost approximately the same amount as the 60 minute sample (where the final mass change seemed to have stabilised). Consequently, 15 minutes was determined to be sufficient to carry out further experiments based on temperature.

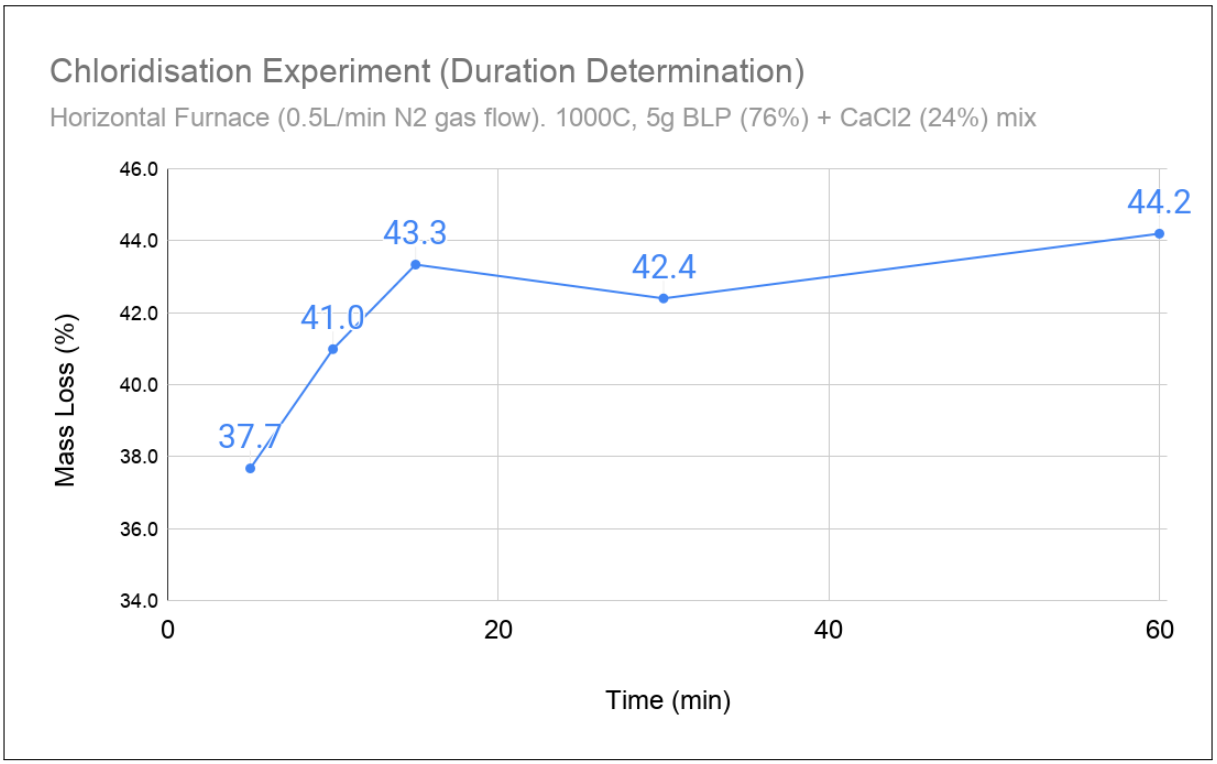

Figure 5.34: Mass loss of heating BLP + $CaCl_2$ at 1000°C at various durations.

Figure 5.35 shows the elemental losses that occurred for the chloridisation reactions. It shows how much of each element is leaving the sample. At lower temperatures (600°C), elements such as Cu do not volatilise. Sn loses its largest fraction at 600°C. Zn and Pb start leaving the solid at 600°C and continue to do so at a greater proportion with increasing temperature. Cu is lost only to a significant degree at 1000-1100°C which is supported by the thermodynamics and the literature [68, 69].

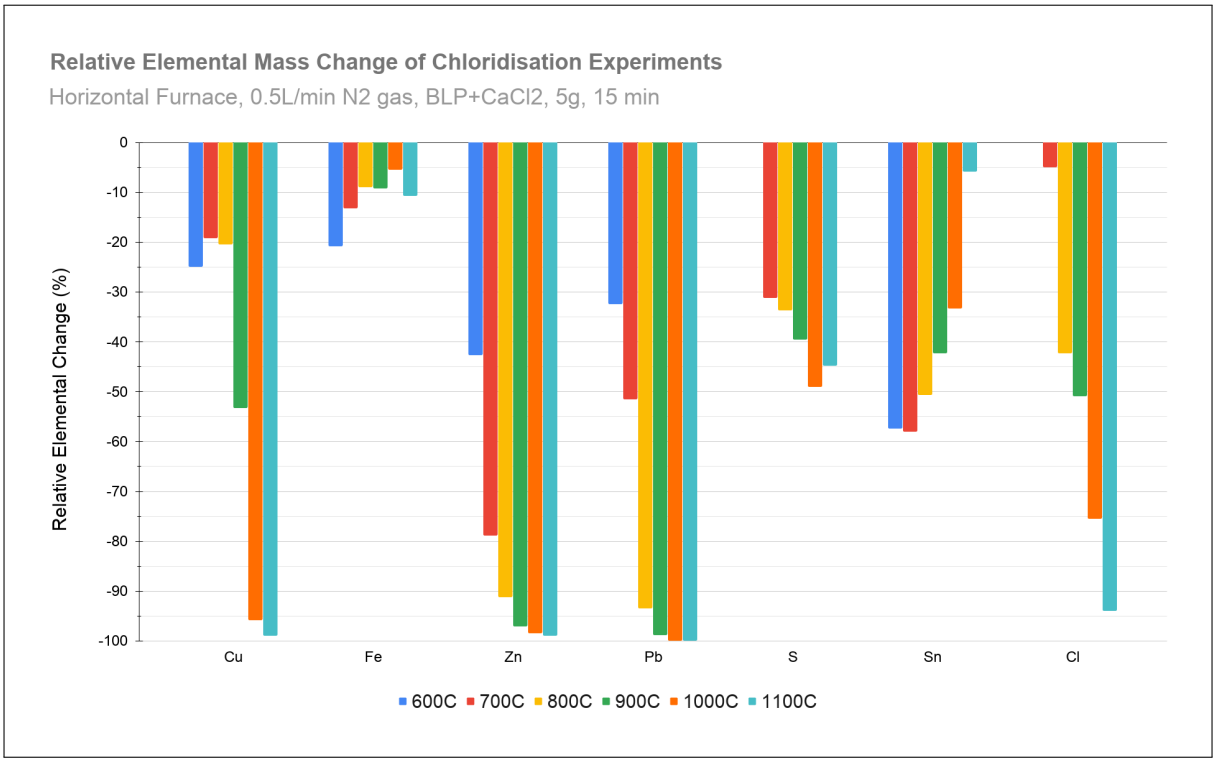

Figure 5.35: Relative elemental change of BLP + $CaCl_2$ mix when heated at various temperatures for 15 minutes.

The sequence in which the metals volatilise can be supported by simple thermodynamic calculations. As presented in the Section 2.4.4.3, chloridisation occurs via the direct or indirect method. Because these reactions were occurring in an inert environment, it is unlikely for the reaction to follow the indirect path. Consequently, the following general reaction was anticipated (via the direct method):

$$Direct: MO + CaCl_2 -> MCl_{2(g)} + CaO \tag{5.14}$$

For the metals in question, the following reactions were inputted into the thermodynamic software (HSC Chemistry v6):

$$CuO + CaCl_2 -> CuCl_{2(g)} + CaO \tag{5.15}$$

$$ZnO + CaCl_2 -> ZnCl_{2(g)} + CaO \tag{5.16}$$

$$PbO + CaCl_2 -> PbCl_{2(g)} + CaO \tag{5.17}$$

$$Fe_2O_3 + 3CaCl_2 -> FeCl_{3(g)} + 3CaO \tag{5.18}$$

$$SnO_2 + 2CaCl_2 -> SnCl_{4(g)} + 2CaO \tag{5.19}$$

The reactions above are not a completely accurate representation of the reactions that are occurring during the experiment; however, they do provide some insight into metal volatilisation behavior. The selection of chloride species was based on the most stable metal chlorides (i.e. $PbCl_2$ is more stable than $PbCl_4$). Gibbs free energy reactions were determined based off temperatures ranging from 0-1100°C, with the results shown in Figure 5.36. $ZnCl_2$, $PbCl_2$ and $SnCl_4$ are the most stable gaseous chlorides at 700C and below. As the temperature increases to > 750°C, $CuCl_2$ formation becomes one of the more stable gaseous chlorides and hence starts leaving the sample.

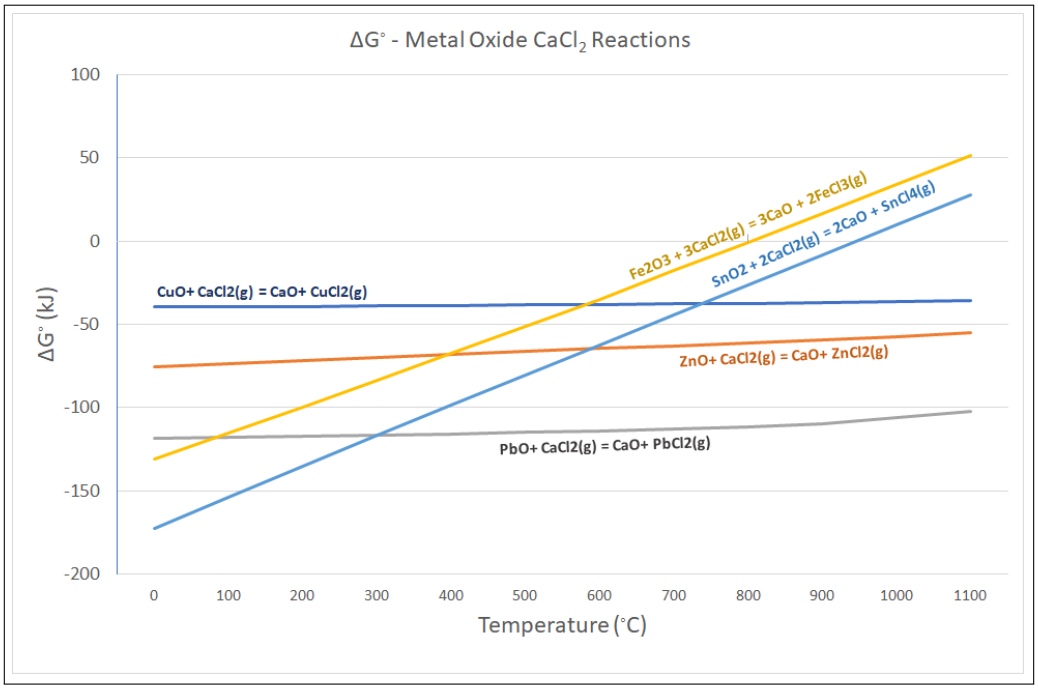

Figure 5.36: Gibbs free energy of metal oxide-chlorine reactions of some key metals

Figure 5.37 indicates the chloridisation of any metal sulfates present. When jarosite decomposes, it produces $Fe_2(SO_4)_3$ and in the process, potentially other metal sulfates. From the graph, it can be seen that $PbSO_4$ and $Sn(SO_4)_2$ readily converts to $PbCl_{2(g)}$ and $SnCl_{4(g)}$ throughout the entire temperature range. Conversion of $ZnSO_4$ and $Fe_2(SO_4)$ to $ZnCl_2$ and $FeCl_3$ is not thermodynamically possible until approximately 150°C. For Cu this occurs at temperatures > 250 °C. The observed results are more aligned with Figure 5.36 than Figure 5.37 suggesting that metals such as Zn, Cu, and Sn are more likely to be present in BLP during the treatment in an oxide form.

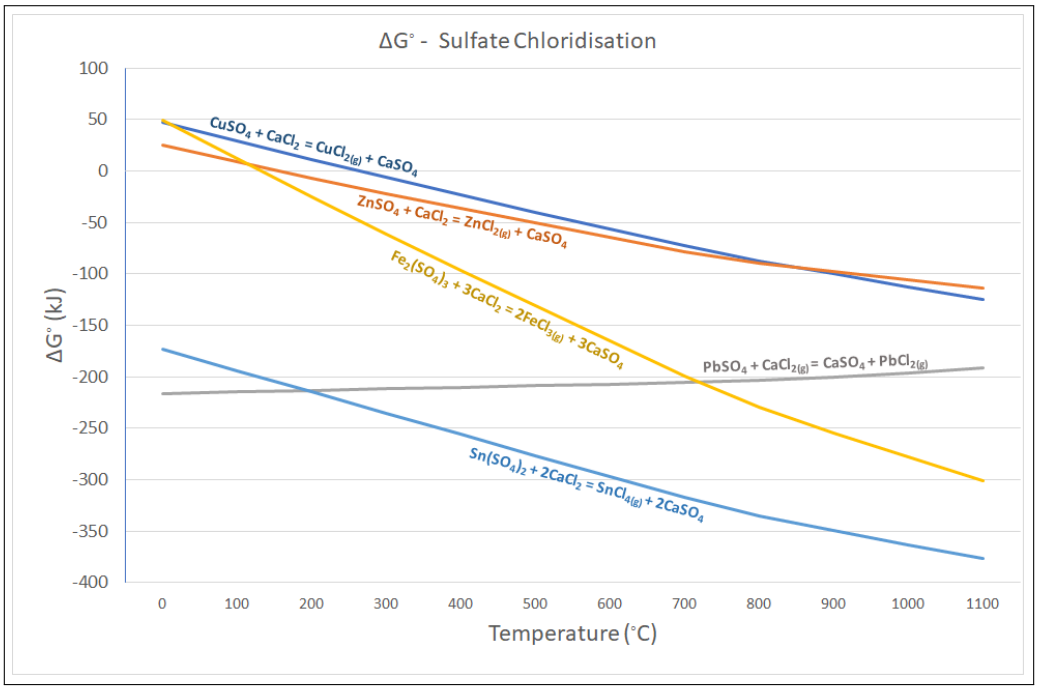

Figure 5.37: Gibbs free energy of metal sulfate-calcium chloride reactions of some key metals.

Since it has been established that PbSO4, $ZnFe_2O_4$ and some potassium jarosite exists in the BLP, it was worth understanding the chloridisation of these phases:

$$PbSO4 + CaCl_2 -> PbCl_{2(g)} + CaSO4 \tag{5.20}$$

$$ZnFe_2O_4 + 3CaCl_2 -> ZnCl_{2(g)} + 3CaO + Fe_2O_3 \tag{5.21}$$

$$KFe_3(SO_4)_2(OH)_6 + 2CaCl_2 -> 2CaSO_4 + 1.5H_2O_{(g)} + KCl + 3HCl_{(g)} + 1.5Fe_2O_3 \tag{5.22}$$

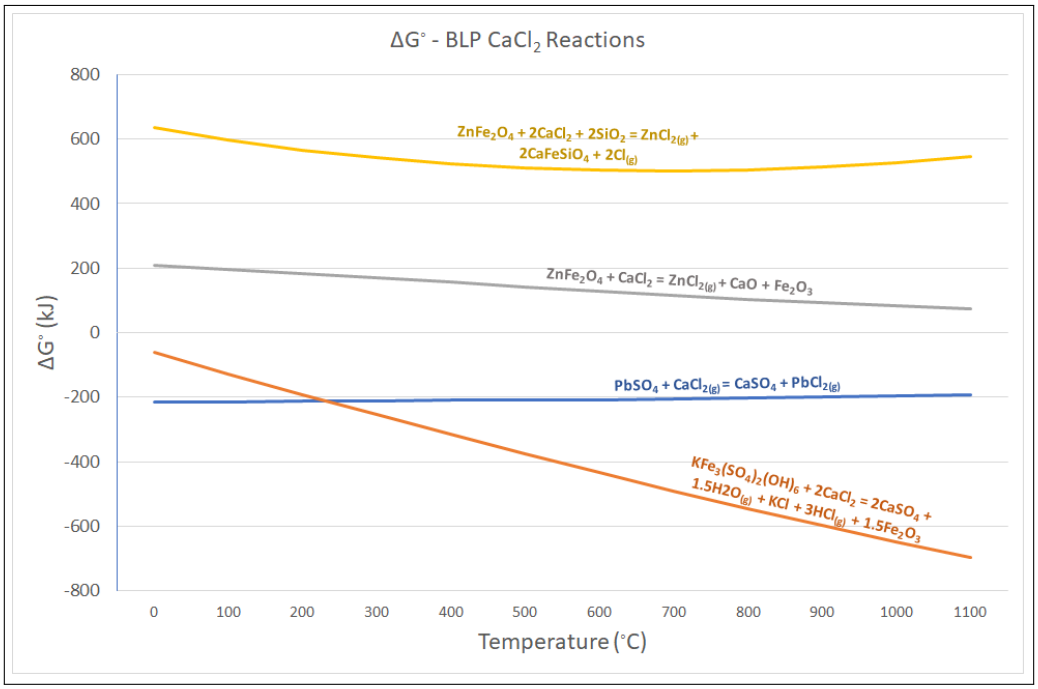

Figure 5.38: Gibbs free energy of some BLP phases-$CaCl_2$ reactions.

Figure 5.38 indicates that only chloridisation of potassium jarosite and $PbSO_4$ in the BLP is thermodynamically possible. Zn in $ZnFe_2O_4$ does not volatilise in the presence of $CaCl_2$. An additional reaction was included in the figure involving SiO_2 since the BLP contains Si, however, the formation of $CaFeSiO_4$ was not favourable either. The decomposition of $ZnFe_2O_4$ to ZnO and hematite is also not possible according to the thermodynamics (see Equation 5.23). This suggests that either a large portion of Zn present in BLP is not in a ferrite form or that there is a different reaction mechanism occurring to volatilise Zn (i.e. Zn is not first converted to ZnO and then chloridised).

$$ZnFe_2O_4 -> ZnO + Fe_2O_3 \ (\Delta G \ > 0, \ T = 0 - 1100°C) \tag{5.23}$$

Figure 5.39, presents the elemental losses in proportion to each other. At lower temperatures Sn leaves the sample at a larger fraction and this reduces as the temperature increases; this agrees with the thermodynamics in Figure 5.36. Similarly there are large Pb and Zn loses at moderate to high temperatures as the formation of these chlorides remains thermodynamically possible throughout the entire temperature range. Significant Cu losses start occurring at higher temperature when the ΔG of Cu chloridisation is below Fe and Sn. Some Fe losses are also incurred at lower temperatures; the Fe losses are not as high as the Sn losses which is supported by the thermodynamics. The removal of Zn is also a point of discussion as Zn is present in the BLP in the zinc ferrite form. The Zn specific reactions in Figure 5.38 must not be occurring, suggesting that other reactions are occurring before Zn is volatilised. The chloridisation of Pb is supported by both Figures 5.36 and 5.38.

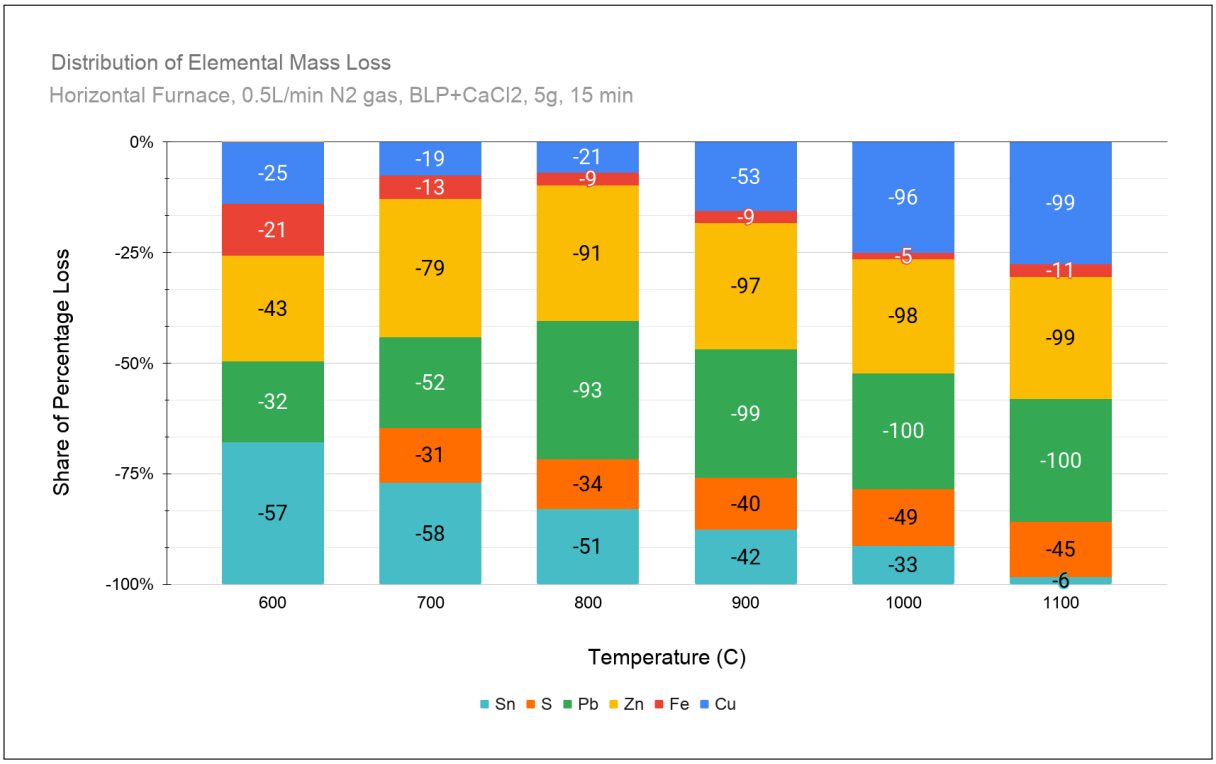

Figure 5.39: Distribution of elemental mass loss when BLP + $CaCl_2$ is heated at various temperatures.

Figure 5.44, shows the elemental concentration in the treated residues. This is compared with untreated BLP. As previously mentioned, lower temperature treatments have higher CEF values. This can be attributed to Cu not volatilising until temperatures ≥1000°C which more than compensates for any reduction in Sn that occurs. Sn becomes an issue at higher temperatures. Almost all the Cu (99%) is removed at temperatures ≥1000°C; however, Sn remains and has an observable impact on the CEF value.

The presence of sulfur is worth discussing as sulfur fixation was also desired. The reaction at 1000°C resulted in 49% sulfur loss. Less sulfur is lost when compared to thermal decomposition reaction at 1000°C (77% of sulfur was lost during thermal decomposition of BLP at 1000°C) indicating that some sulfur fixation had taken place. At 600°C, roughly 28% of the sulfur is lost in the thermal decomposition experiments whereas virtually no sulfur is lost with the chloridisation experiment. At higher temperatures, Ca is unable to completely fix the sulfur. This is probably due to decomposition reactions before $CaCl_2$ is able to fix the sulfur. Thermodynamically, the ΔG of the $CaCl_2$ reacting with potassium jarosite is negative from 0-1100 °C (see Figure 5.38):

$$2CaCl_2 + KFe_3(SO_4)_2(OH)_6 = 2CaSO_4 + 1.5Fe_2O_3 + KCl + 3HCl(g) + 1.5H_2O(g) \quad (5.24)$$

The lower temperatures (600°C) slowed any parallel decomposition reactions and enabled the $CaCl_2$ to fix the sulfur. Equation 5.24 is a relevant equation to use because the jarosite present in BLP contains a fraction of potassium jarosite. Plumbojarosite was not available in the HSC (v6) database.

5.2.2.1. Staging Reaction

A staged treatment was followed in order to remove Sn at lower temperatures and remove Cu at higher temperatures. The BLP + $CaCl_2$ mix was placed in the furnace at 600°C where it was left for 15 minutes. The temperature was then increased by increments of 100 where it was left for another 15 minutes.

This was repeated until 1,000°C. The results are shown in Figure 5.40 as a direct comparison with the other treatments.

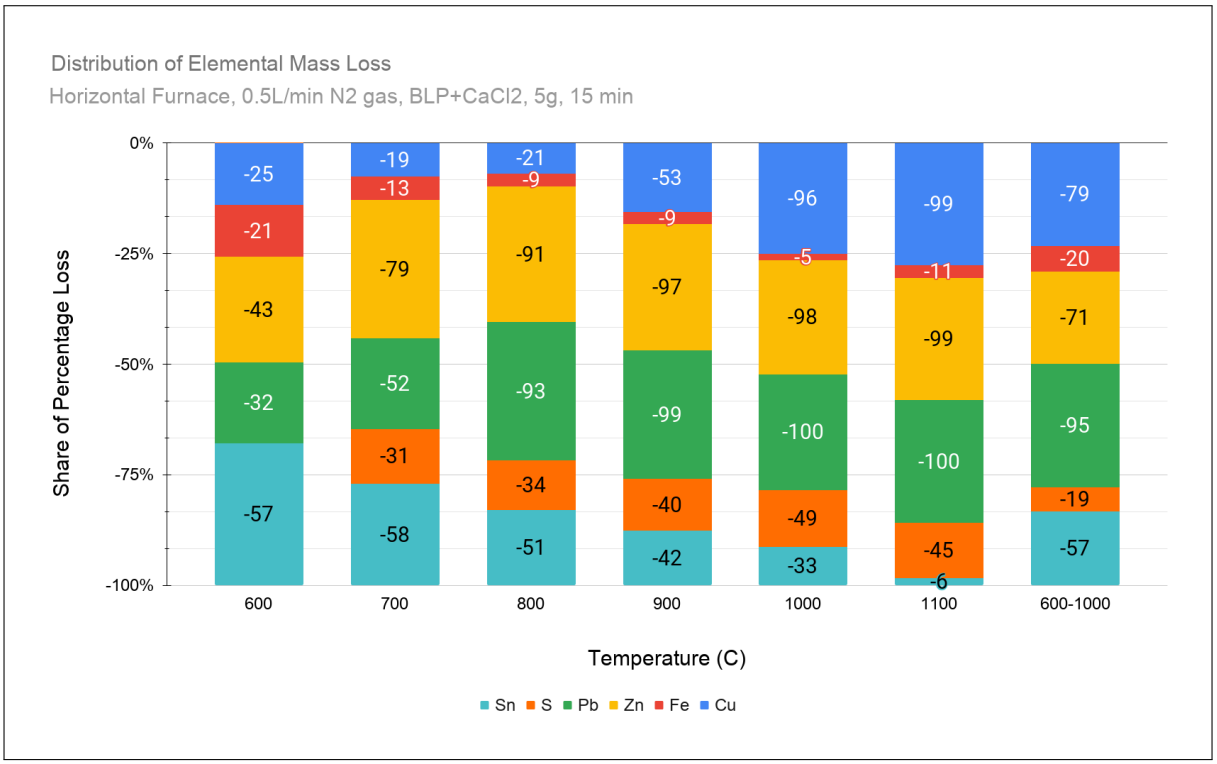

Figure 5.40: Distribution of elemental mass loss when BLP + $CaCl_2$ heated at various temperatures with the staging reaction included.

The staged treatment was able for fix 81% of the sulfur. Aside from the greater sulfur fixation, the amount of Sn removed was similar as the for the 600°C treatment. The amount of Fe lost also increased due to the lower starting temperature of the treatment at 600°C. There was less Zn, Pb and Cu lost, however. This implied that perhaps there was insufficient chlorine provided by the calcium chloride.

Figure 5.41 presents the chloride requirements for metal volatilisation based of the reactions in Equations 5.15, 5.17, 5.16, and 5.19. There are four lines on the graph: the blue line which indicates the amount of chloride required to volatilise all the Cu, Zn, Pb, and Sn in BLP; the grey line which indicates the amount of chloride required to volatilise the amount of metal (previously indicated) that was a actually lost; the orange line which indicates the amount of chloride provided by $CaCl_2$; and the yellow line indicates how much chloride that has left the sample. The chloride requirements for the blue and grey lines are based off equations 5.15 - 5.19. In general, the theoretical amount of Cl required to volatilise all the Cu, Zn, Pb, and Sn exceeded what is provided by $CaCl_2$. This suggests that if Equations 5.15 - 5.19 were to occur than there is insufficient chloride present in the solid mix. Metals were lost throughout the chloridisation experiments and the grey line suggests how much chloride would have been required to account for this metal loss. From 700°C on wards, the grey line exceeds the orange line which indicates that Equations 5.15 - 5.19 may not be occurring, otherwise the grey line would never exceed the orange line. This suggests that other metal-chlorine compounds are formed with the metals in question. Further, the yellow line shows how much chloride has left the residue. At 600°C virtually all the chloride remains in the residue. The amount reduces until the staging reaction whereby all the chloride provided by the $CaCl_2$ has left the residue.

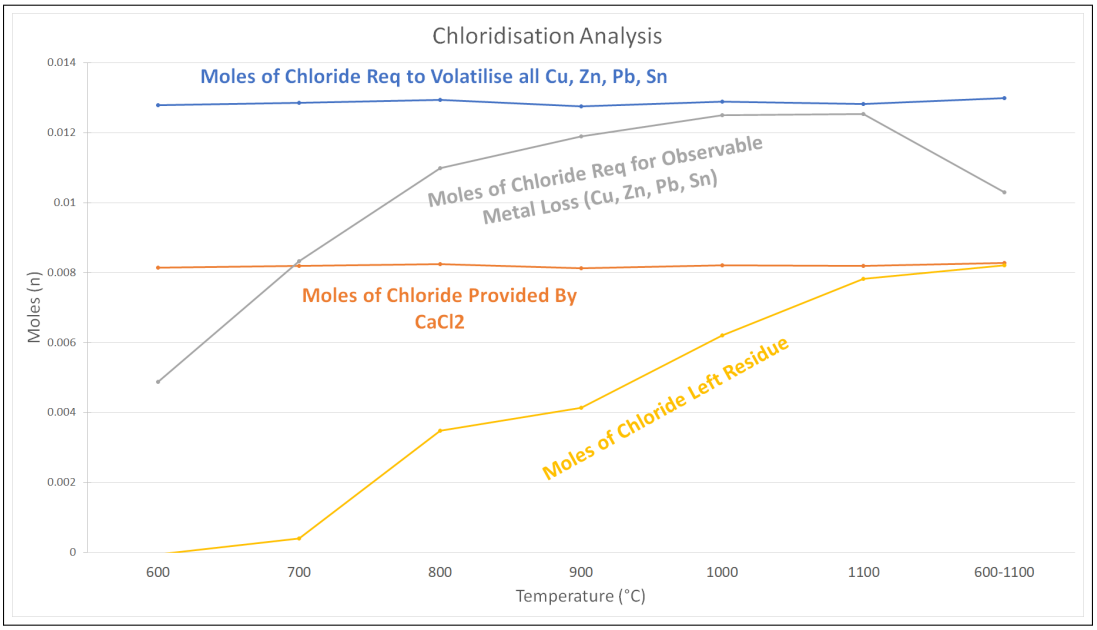

Figure 5.41: Analysis of chlorine requirements and losses if direct chloridisation occurs with Fe, Zn, Pb, Zn and Sn. BLP is mixed with $CaCl_2$ and heated to at various temps (600-1000°C) for 15 minutes.

The formation of different metal chlorides other than what is suggested by Equations 5.15 - 5.19 is confirmed by a review of the literature. This revealed that metals such as Cu and Zn form Cu_2Cl_2 and Zn_2Cl_2 at elevated temperatures. According to the literature [95], Cu forms two chlorine salts: $CuCl_2$ and Cu_2Cl_2. Cu_2Cl_2 is the most stable at higher temperatures. Cu_2Cl_2 was not an element available for analysis in HSC chemistry and hence was not considered for the ΔG calculations. Any $CuCl_2$ that may be present converts to Cu_2Cl_2 and volatilises. Oxychlorides are also a possibility but do not constitute a large fraction of Cu chlorides based on analyses of fume products generated when Cu ores are roasted with $CaCl_2$. In addition, the experiments conducted for this project were carried out in an inert environment so oxychlorides are even less likely. Similarly, the volatilisation of Zn occurs when Zn reacts with $ZnCl_2$ to form Zn_2Cl_2 at temperatures greater than 285°C[96]. Indeed, when these two compounds (Zn_2Cl_2 and Cu_2Cl_2) and are taken into consideration and the molar requirements are adjusted in Figure 5.41, the chloride provided by $CaCl_2$ more closely aligns with theoretical values (see Figure 5.42). Namely the blue and orange lines are brought closer together converge, indicating the theoretical moles required to volatilise the key metals is similar to what is provided by the $CaCl_2$. The grey line only just exceeds the orange line at 1000-1100°C which suggests the formation of Zn_2Cl_2 and Cu_2Cl_2 is more in line with the observations. Further investigation of other volatile chloride species of Pb and Zn may even lessen the discrepancy between the theoretical and observed calculations.

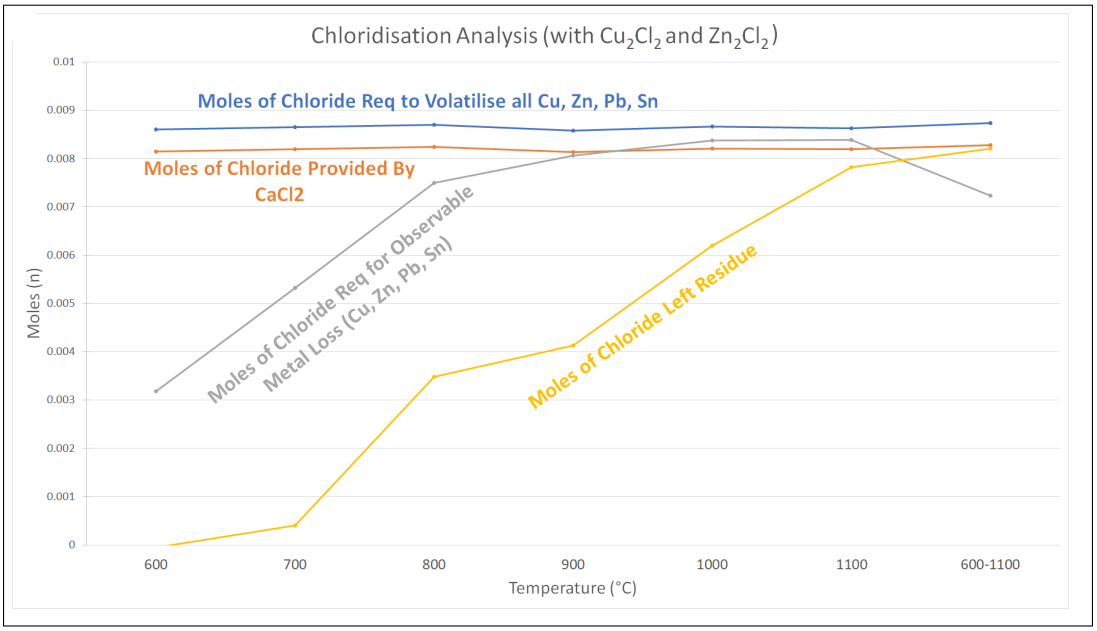

Figure 5.42: Analysis of chlorine requirements and losses if direct chloridisation occurs with Fe, Zn, Pb, Zn and Sn. BLP is mixed with $CaCl_2$ and heated to at various temps (600-1000°C) for 15 minutes. This is an update from Figure 5.41 to incorporate Zn_2Cl_2 and Cu_2Cl_2.

XRDs of the residues (see figure 5.43) primarily shows the presence of $CaSO_4$, Fe_2O_3 and SiO_2. The presence of $CaSO_4$, is supported by Equation 5.24 as Ca fixes the sulfur to form $CaSO_4$ which is observed on the XRDs. The presence of chloride is more puzzling as a fair portion of the chlorine remains in the residue and remains unaccounted for by the XRDs.

As previously mentioned, at temperatures < 1100 °C, Figures 5.42 and 5.41 indicate that not all the chlorides have left the residue suggesting that either:

- (1) Not all the chloride goes into volatilising the metals. This is difficult to establish as the only crystalline phases detected by XRD are SiO_2, $CaSO_4$, and Fe_2O_3 (see Figure 5.43).
- (2) Chloridisation occurs but the metal product is not a volatile gas but a solid. Indeed, this is observed in the XRD for the reaction at 600°C. The XRD shows the presence of $PbCl_2$ in the solid (see Figure 5.43).

Since significant amounts of chlorides are present in the residues that were treated at temperatures < 1000°C, it presents an opportunity for further investigation. Aside for the 600°C residue which shows the presence of $PbCl_2$, XRDs of the remaining residues that were subjected to higher temperature treatments do not indicate the presence of chlorides. The XRDs of the residues for the treatments temperatures at 900 °C, 1100°C and the staging treatment can be found in the appendix. They show the presence of the $CaSO_4$, Fe_2O_3 and SiO_2, except for the 1000°C and the staging treatment, where there is the presence of calcium magnesium silicate. The presence of chloride in the residue an opportunity for further investigation. Subsequent washing of the residues may yield greater insight into whether there is a presence of metal chloride salts formed during the heat treatment which have not been volatilised yet. Subsequent washing would release any soluble chlorides that are present in the residue and XRF analysis of the washed residue would indicate if which metals formed solid chlorides.

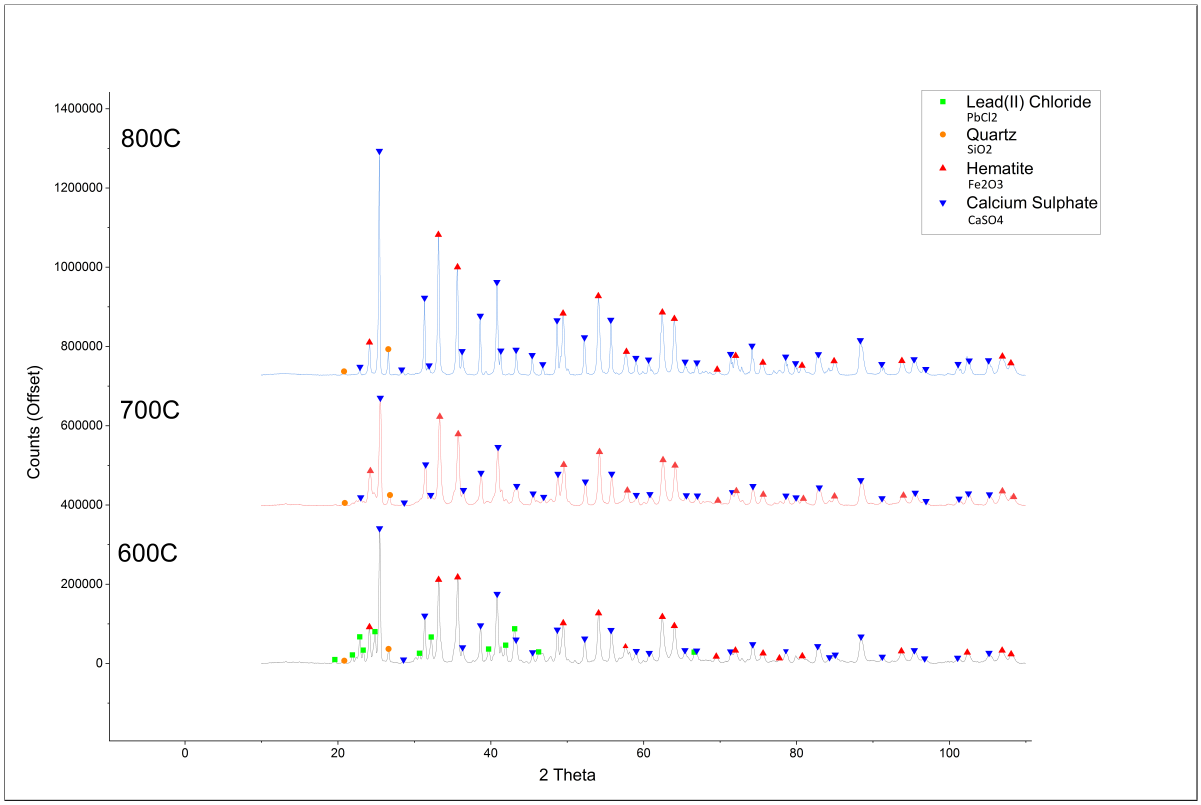

Figure 5.43: XRDs of solid residues when BLP is mixed with $CaCl_2$ and heated to at various temps (600-800°C) for 15 minutes.

Finally, Figure 5.44 shows the elemental concentrations of the treated residues. When combining the figure with Table 5.10, it can be shown that BLP with $CaCl_2$ heated to 1100°C was the most effective treatment method for removing Cu. The treatment that removed the most CEF relative to Fe was the staging treatment. With the staging treatment CEF = 0.84 wt% was achieved. Sn which was present in the higher temperature treatments was removed at lower temperatures giving lowest CEF concentration in the residue. Overall chloridisation was effective in removing Cu and the other CEF metals from the BLP; however, there seems to be a balance between the appropriate temperature and the amount of $CaCl_2$ provided. At lower temperatures, problem elements like Sn are able to leave the sample but at these temperatures Fe is more likely to leave. As the temperature treatments are increased, more Zn, Pb and eventually Cu leave the sample. High temperature treatments are effective at removing Cu, Pb, and Zn whilst limiting the Fe removal; however, higher temperatures keep Sn in the residue which has a major impact with the overall CEF value. $CaCl_2$ was somewhat effective is fixing the sulfur. At lower temperatures, most of the sulfur was fixed but at higher temperatures, competing decomposition reactions likely prevented Ca from fixing the sulfur. Varying the concentrations of $CaCl_2$ is worth investigating to determine the optimal concentrations for Cu and CEF removal whereas sulfur fixation will likely depend on the temperature of the treatment. In addition, washing of treated residues is worth investigating to determine the extend to which metal chlorides are formed (not detected by XRD) at lower temperatures.

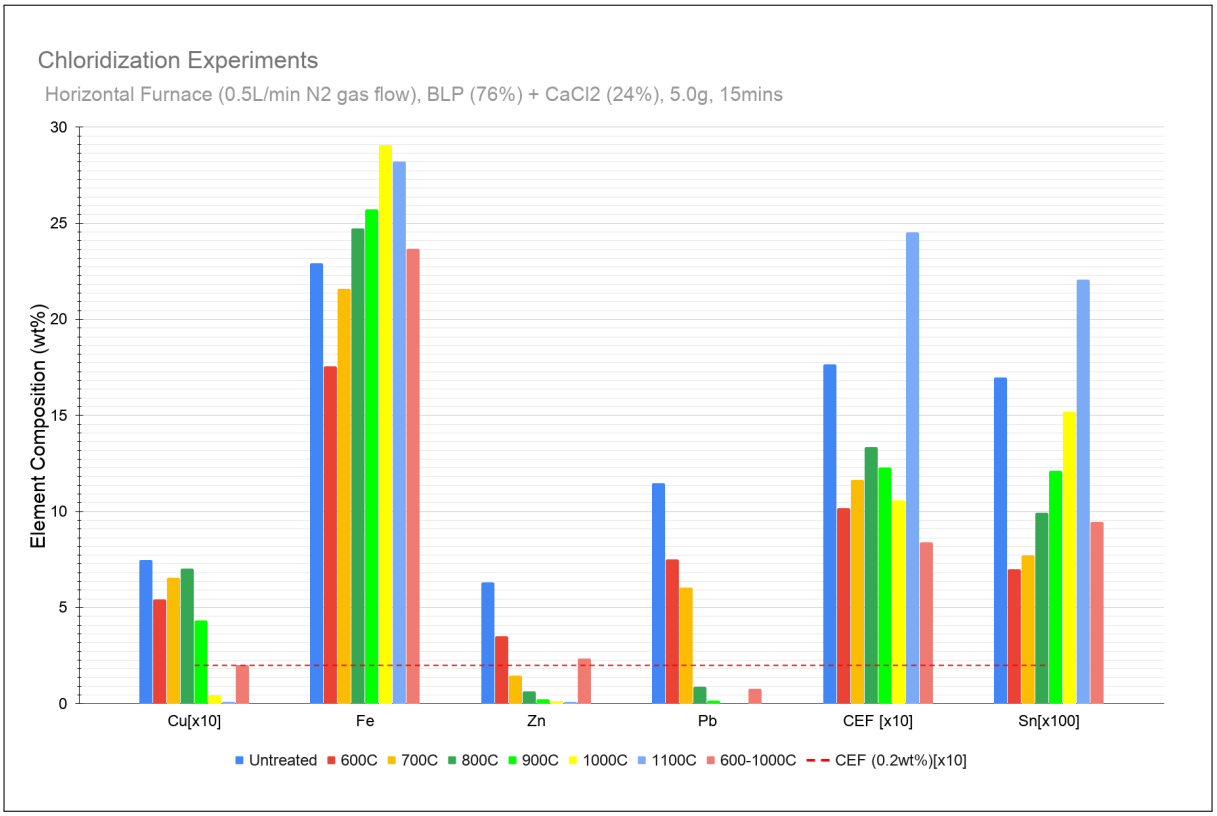

Figure 5.44: Elemental of residue when BLP + $CaCl_2$ heated at various temperatures.

Table 5.10: Treatment effectiveness of the chloridisation of BLP at various temperatures.

	Chloridisation Reactions	
Temperature	**Cu/Fe**	**CEF/Fe**
600	0.031	0.058
700	0.030	0.054
800	0.028	0.054
900	0.017	0.048
1000	0.0015	0.036
1100	0.0004	0.087
600-1000	0.0085	0.035

5.2.2.2. Addition of Na_2CO_3

This section looks at the addition of Na_2CO_3 to the BLP + $CaCl_2$ mix. This was not specifically mentioned in the experimental section but it was carried out. The motivation for this was due to the sulfur loss that was occurring at 1000°C with the BLP + $CaCl_2$ mix. Although $CaCl_2$ was able to fix some of the sulfur (49% sulfur loss compared to 77% which occurred with sulfur fixation) it worth investigating if the presence of Na_2CO_3 would enhance sulfur fixation. As will be discussed in detail in Section 5.3, Na_2CO_3 is able to fix sulfur in BLP. The solid mix that was place in the horizontal furnace consisted of 58% BLP, 19% $CaCl_2$, and 23% Na_2CO_3. This mix was to maintain the 24% $CaCl_2$: 76% BLP ratio that was used for the other chloridisation experiments whilst adding 100% excess of Na to the sulfur present in the BLP. Figure 5.45 shows the elemental mass change that resulted from adding Na_2CO_3.

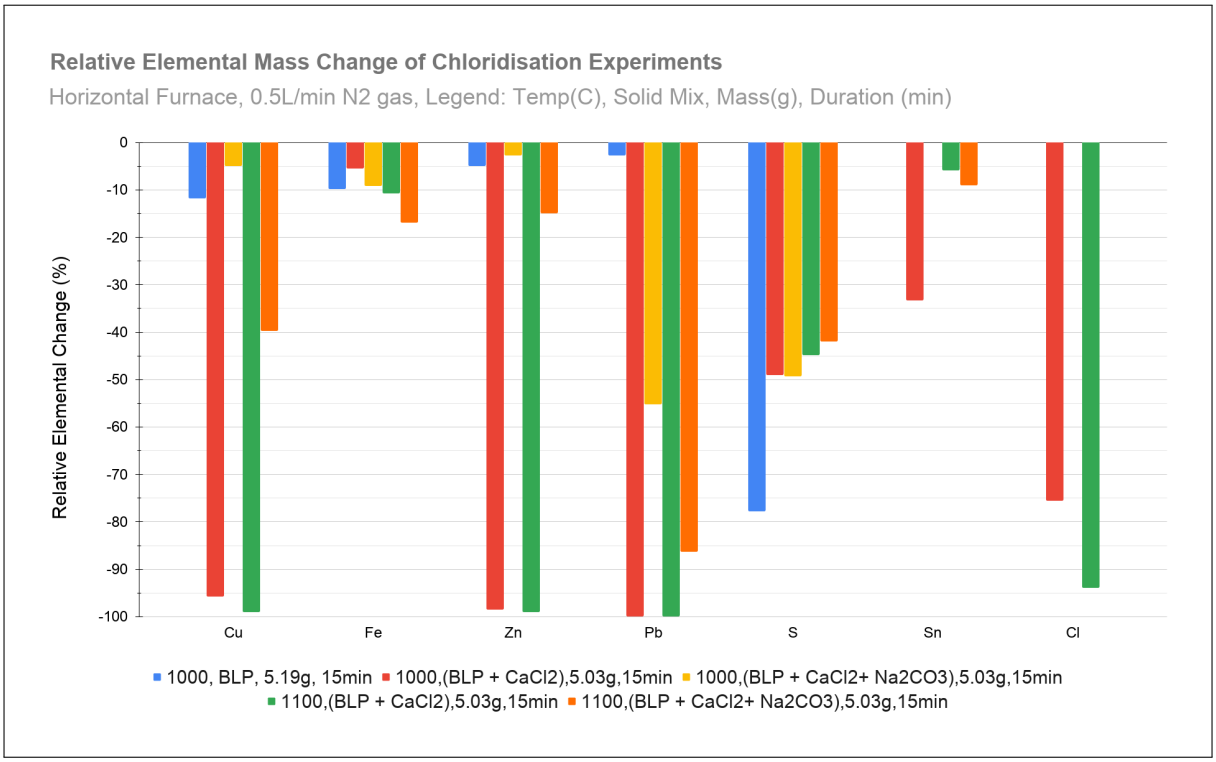

Figure 5.45: Elemental change of BLP + $CaCl_2$ + Na_2CO_3 heated at 1000°C and 1100°C. This is compared to thermally decomposed BLP at 1000°C and BLP + $CaCl_2$ solid mix.

The presence of Na_2CO_3 did not materially improve the sulfur fixation of the BLP + $CaCl_2$ mix. In addition, the presence of Na_2CO_3 hampered the removal of Cu, Zn, Pb, and Sn at 1000°C and 1100°C (with the exception of Sn at 1100 °C). What is interesting to observe is that the presence of Na_2CO_3 stopped chloride from leaving the sample. This suggests that the chloride could potentially remain in the residue in the form of metal chlorides. Figure 5.46 shows the XRDs of the residues when BLP, $CaCl_2$ and Na_2CO_3 is heated in the horizontal furnace at 1000°C and 1100 °C. The figure indicates that the only chloride containing phase detected is NaCl. This suggests that Na_2CO_3 reacted directly with $CaCl_2$. The presence of any other metal chlorides were not detected by XRD. Subsequent washing of the residue would confirm if this strategy is effective in removing Cu and the other CEF metals. Any $CuCl_2$ formed in the furnace, for example, should be readily removed by washing.

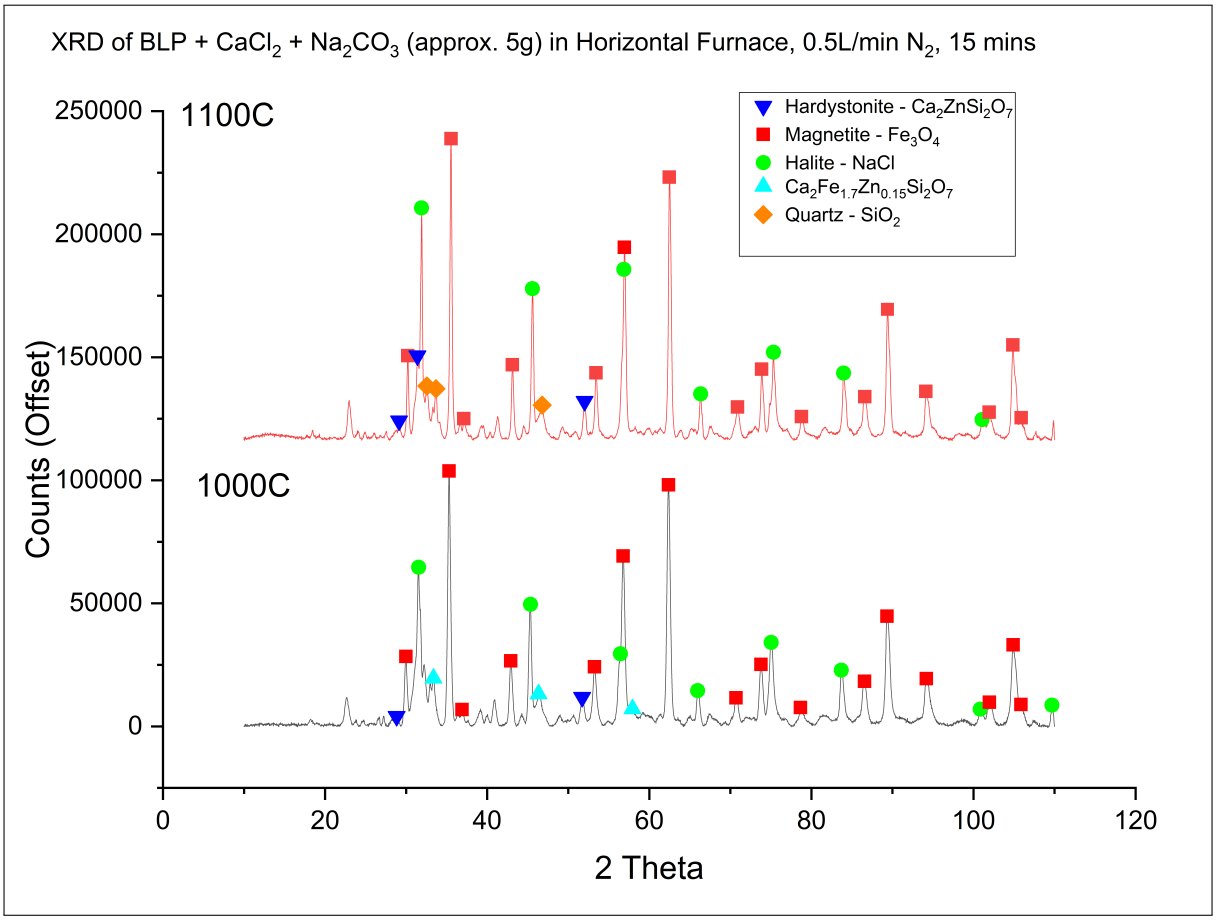

Figure 5.46: XRD of BLP + $CaCl_2$ + Na_2CO_3 heated at 1000°C and 1100°C.

5.3. Combined Pyro- and Hydrometallurgical Treatment

This section focuses on the sulfur fixation of BLP with Na_2CO_3 followed by subsequent washing. Similar to the chloridisation treatment, this is a relatively simple approach to fix sulfur. This approach also had the added benefit of Cu removal based of what was observed in the literature [66].

As per the chloridisation reactions, it was necessary to identify the shortest time frame at which the sulfur fixations occurred. It was assumed that 15 minutes would be sufficient for a 5g sample to react. This was based on what was observed with the chloridisation reactions. To support this, 5g was reacted for 15min at 700°C and 800°C. For comparison, a 10 g sample was reacted for 15 and 30 minutes at 700C and 800°C. 10g was selected because it was the maximum amount of solids that could fit in the alumina boats. As much sample as possible was required to be treated in order to recover solids after the subsequent washing step. Table 5.11 shows the results of the mass changes that occurred during the heat treatment. The relative mass change between all three of the 700°C samples was 2%; it was 3% for the 800°C samples. The mass changes for the 10g samples at 15 and 30 minutes confirms that 15 minutes was sufficient time for the reaction occur.

Table 5.11: Mass change of BLP mixed with Na_2SO_4, heated at 700°C and 800°C with different quantities and durations.

Mass Loss (%)	Temperature (C)/ mass (g)			
Time (min)	700/5g	700/10g	800/5g	800/10g
15	14.40	14.91	17.17	17.77
30	-	15.58	-	19.50

Sulfur fixation occurs via the following reaction with potassium jarosite:

$$2Na_2CO_3 + 4KFe_3(SO_4)_2(OH)_6 -> 4Na_2SO_4 + 3Fe_2O_3 + KO + 4CO_{2(g} + 6H_2O(g) (\Delta G < 0, T > 100°C) \quad (5.25)$$

As previously mentioned, plumbojarosite was not available in the HSC database, however, BLP does consist of a fraction of potassium jarosite therefore equation 5.25 is still relevant. According to HSC chemistry software, the ΔG of equation 5.25 is < 0 for temperatures > 100°C.

Figure 5.47 shows the elemental changes that occurs when BLP is mixed with Na_2CO_3, heated at 700°C for 15 and 30 minutes, and subsequently washed with water. Coloured columns refer to elemental changes that occur during the calcination step and the faded colour columns refer to changes that occur with the subsequent washing. For the elements Fe, Cu, Zn, Pb, and Sn, the calcination step resulted in an increase in the element. This is impossible as no additional sources of these metals were present in Na_2CO_3 that was added. This increase is difficult to explain as the calculations were based of XRF data. With this is mind, the calcination step is likely to have resulted in no observable elemental losses for Fe, Cu, Zn, Pb and Sn. Some sulfur is lost in the sulfur fixation experiments. This is likely due to parallel reactions involving the decomposition of the jarosite where sulfur could not be fixed. At 700°C, roughly 55% of sulfur is lost in the thermal decomposition reactions at 700°C in comparison to 17% for the reactions with Na_2CO_3 (highest sulfur loss occurring with 10g, 30 minutes).

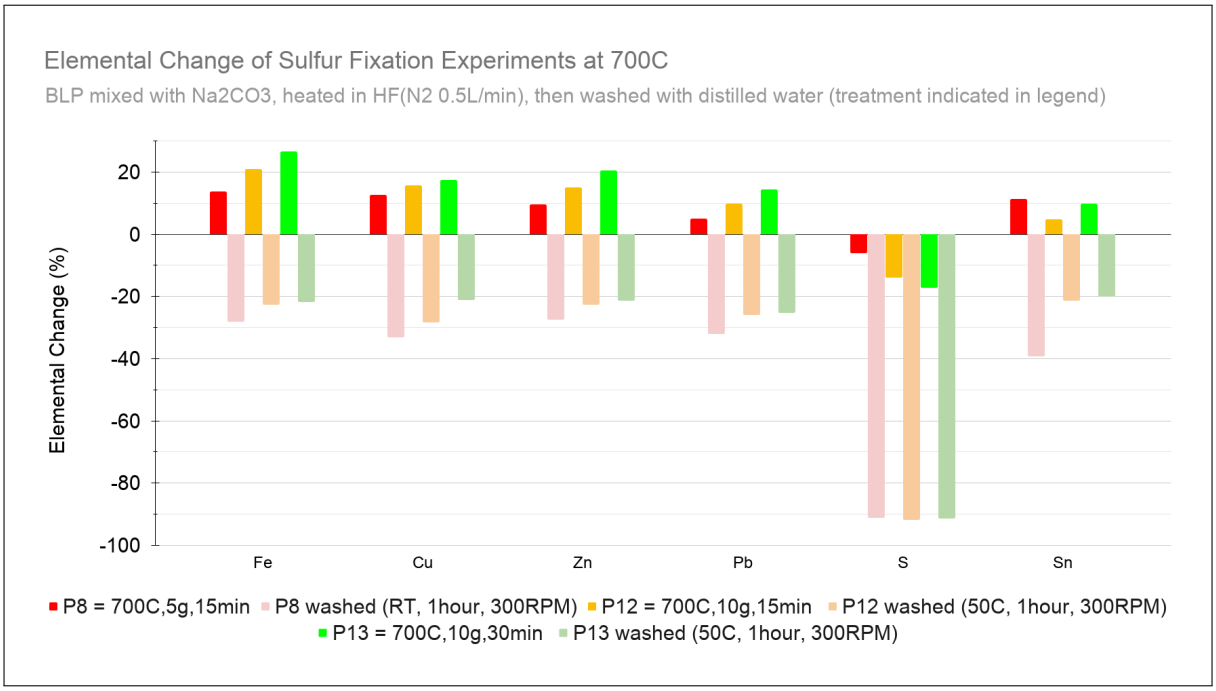

Figure 5.47: Elemental change of BLP mixed with Na_2CO_3, heated at 700°C for various durations. This is then subsequently washed with water at RT and 50°C. Coloured columns refer to elemental changes that occur during the calcination step and the blue columns refer to changes that occur with the subsequent washing.

The mass spectrometry results of the sulfur fixation experiment (see Figure 5.48) show a reduction in SO_2 (dark blue line) emission during the sulfur fixation experiment when compared to thermally decomposed BLP. Indeed, some jarosite decomposition was still occurring. Also present is CO_2 (purple line) which is an anticipated product as per equation 5.24.

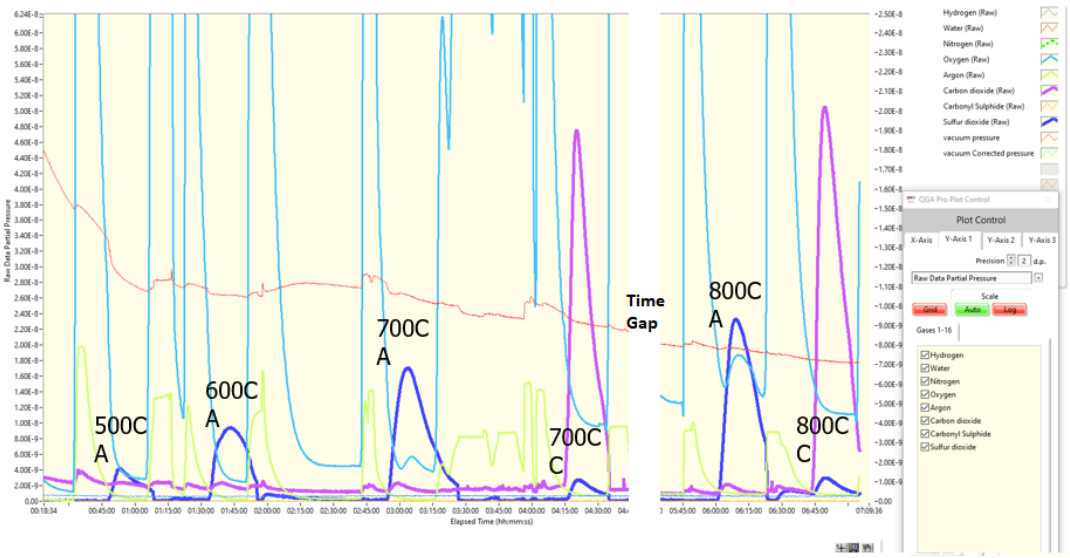

Figure 5.48: Mass spec indicating sulf fixation occurring. In the image A = 5g of BLP, C= 5g Na2CO3 powder mixed with BLP. All reactions occurred for 15 minutes. Dark blue line indicated SO_2, light blue is O_2 and purple is CO_2.

The XRDs of the sulfur fixation experiments at 700°C and 800°C (see Figure 5.49) show the presence of the main intended products as predicted by Equation 5.25, namely the presence of hematite and sodium sulfate. The XRDs do show additional products (as the BLP was a mix of plumbojarosite,

$PbSO_4$ and SiO_2) such as $CaSO_4$ (Ca present in the BLP would have fixed any sulfur as well).

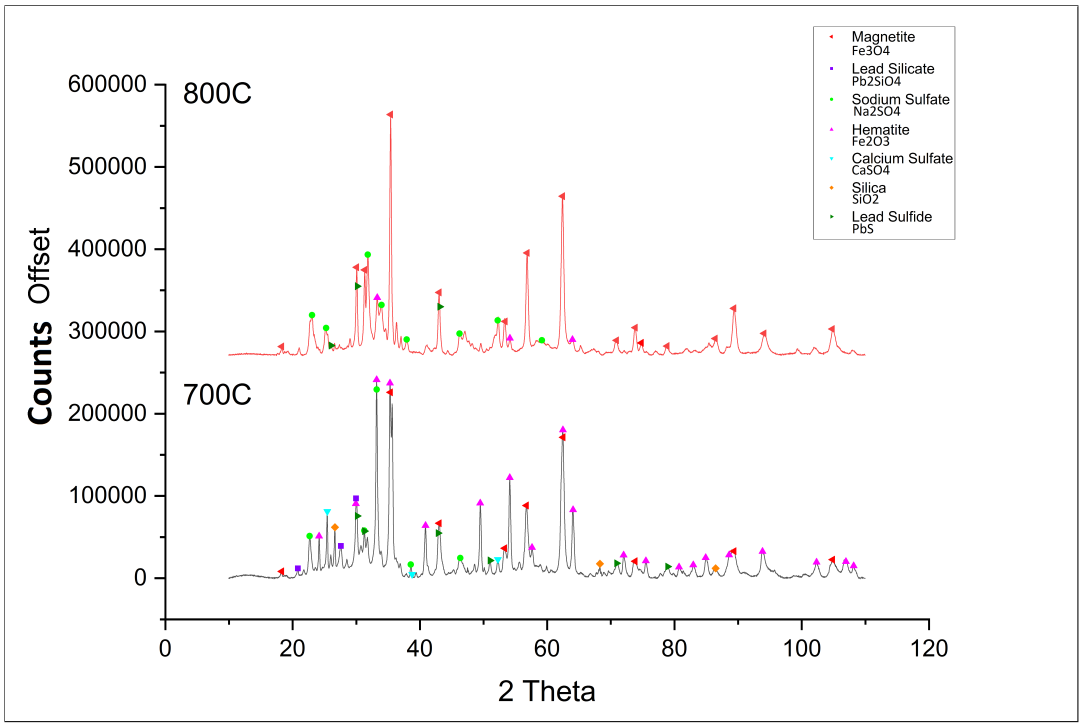

Figure 5.49: XRDs of sulfur fixation experiments. 10g of BLP + Na_2CO_3 mix was placed in a horizontal furnace at 700°C and 800°C for 30 minutes.

PbS is also detected by the XRD as a product of the reaction. PbS is produced by reduction of $PbSO_4$ with CO:

$$PbSO_4 + 4CO_{(g)} -> PbS + 4CO_{2(g} \tag{5.26}$$

Based on this, it is very likely that CO was present during the reaction. CO is likely produced from incomplete decomposition of Na_2CO_3 in the solid mix. Other metal sulfates present in the solid would also react with CO in a similar manner. The N_2 and CO peaks in the mass spectrometer overlapped which prevented the detection of CO separately. Depending on the quantity of CO that was present in the furnace it could have reduced any other metal sulfates to sulfides. Reduction of Cu, Zn, Pb, and Sn sulfates to their respective metal sulfides occurs much more readily than Na_2SO_4 at temperatures 0-1100°C. This is based of ΔG calculations for equations similar to Equation 5.26 (see Figure 5.50). For metals other than Pb, it seems unlikely that this reaction would have occurred since Zn and Cu were not present in BLP in a sulfate form. The other metals would need to be converted to a sulphate and then subsequently reduced for them to exist as a sulphide. It is very likely to occur for Pb since it already existed as a sulphate in the BLP residue.

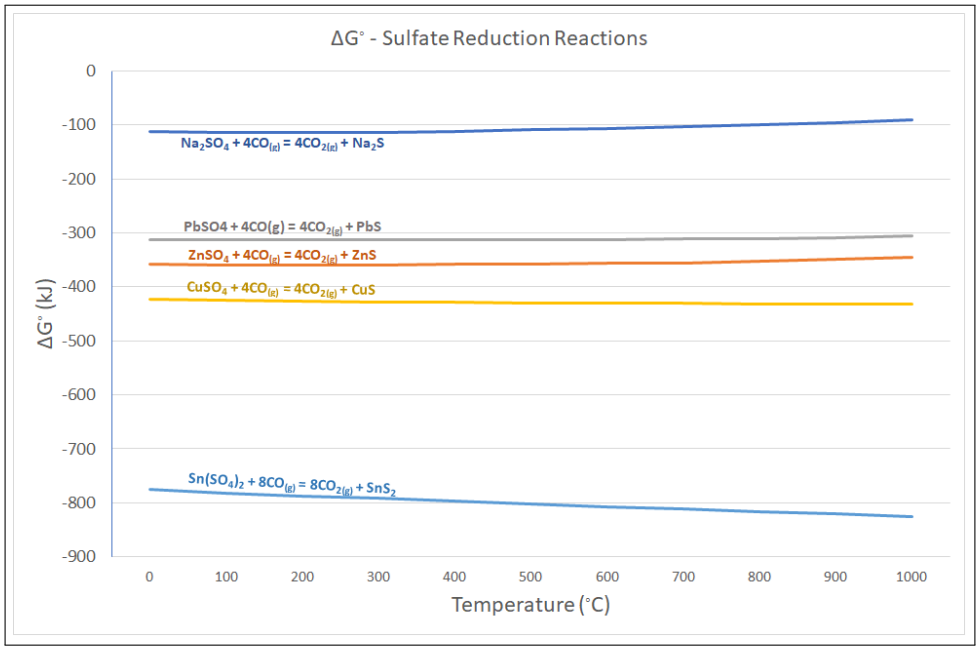

Figure 5.50: ΔG of metal sulphate reduction reactions. Temperature is in °C. Values generated by HSC Chemistry (v6) software.

If compounds like CuS and ZnS did exist then they are not water soluble; consequently, if the reduction did occur this would have impeded its removal in the subsequent washing step. This is shown by the XRDs of a washed residue (see Figure 5.51). The PbS present from the calcination step at 700°C (see Figure 5.49) remained in the solid after the subsequent wash step. The concentration of Pb and $PbSO_4$ is high enough to be detected by XRD analysis; however, for the other metals the concentrations are too low to confirm that reduction is happening.

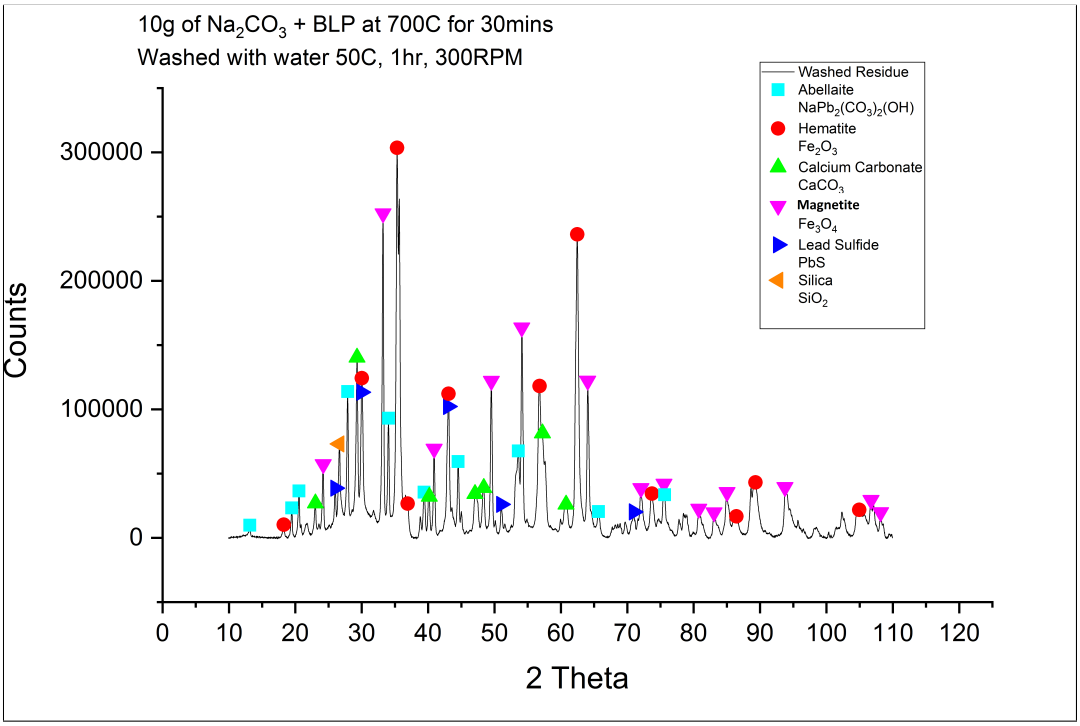

Figure 5.51: XRD of washed residue of sulfur fixation experiment. 10g of Na_2CO_3 + BLP placed in furnace at 700°C for 30 minutes. The calcined solid was washed with water (50°C, 1 hr, 300RPM).

Figure 5.47 shows that the subsequent washing step reduced the concentration of some metals. This can be considered unlikely because of the elemental gains observed in the calcination step. It is more likely that the reduction of the metals relates to the gains in the calcination step, so in reality there was no net gains or losses of metals. This claim is supported by none of the metals being present in the wash solution (see Figure 5.52). There is some minor reduction in S during the calcination step. During the washing step most of the sulfate is removed into the wash solution. This is show by the elemental mass change during the washing step and the presence of S in the leach solution.

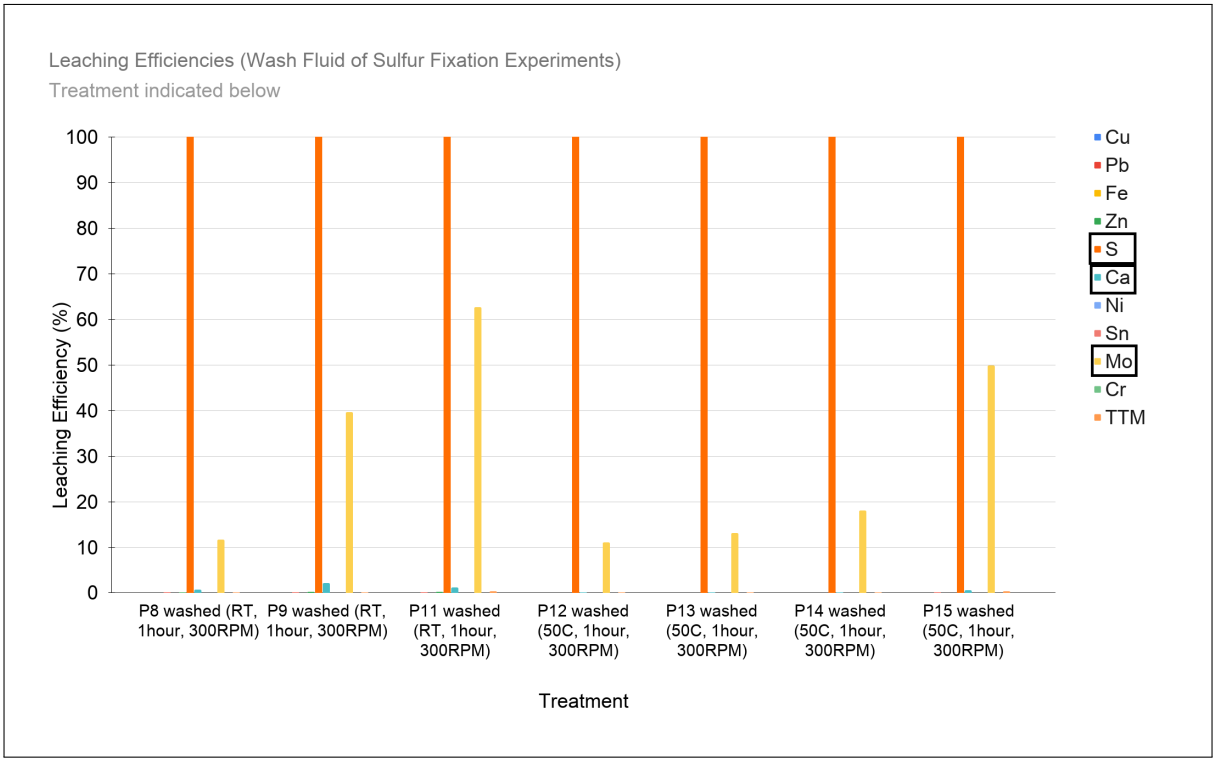

Figure 5.52: Leaching efficiencies when water washing the calcined BLP + Na_2CO_3. S (orange), Mo (yellow) and Ca (light blue) are the only elements visibly leached. These metals have been identified by a black box.

As previously suggested by Section 4.2.2 and Equation 2.5, Cu does not exist as a distinct phase but is likely to occupy the Fe position in jarosite. According to Equation 5.25, Na from Na_2CO_3 fixes the sulfur and converts the Fe to an insoluble hematite product. It was theorised that metals such as Cu may have remained as a sulfate salt during the calcination and could be removed by washing [66]. This was not observed with the results at 700°C. What was observed was an increase in concentrations of metals like Cu, Zn, Pb and Sn (see Figure 5.53). This suggests that metals like Cu did not exist as a water soluble sulfate salt after calcination.

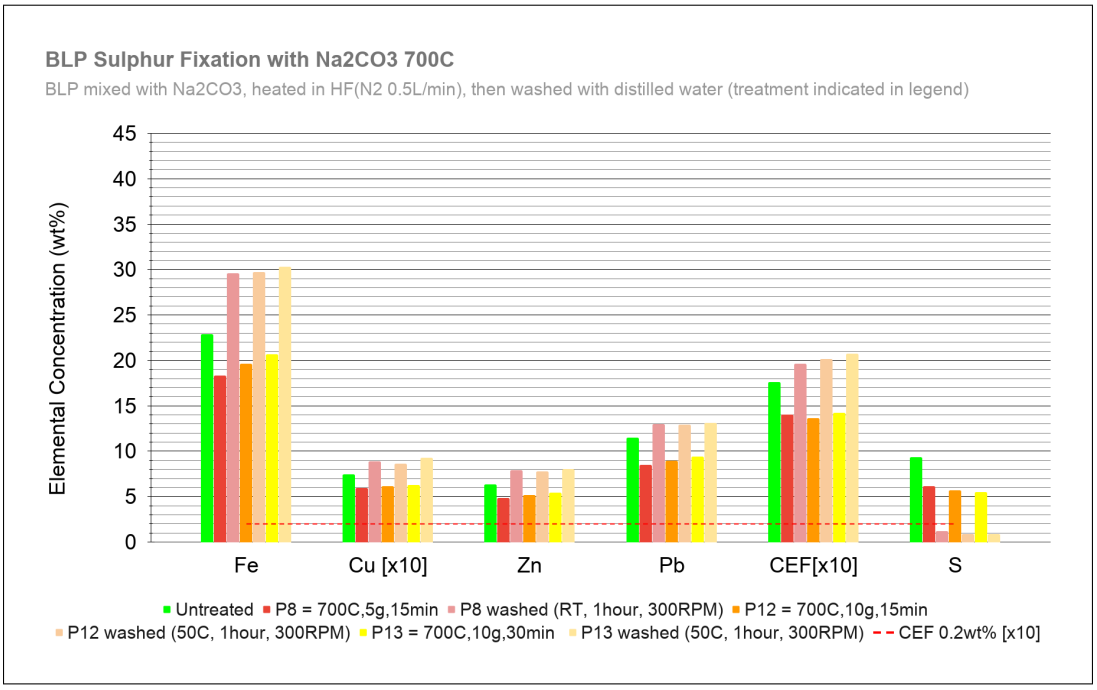

Figure 5.53: Residual elemental concentrations of BLP mixed with Na_2CO_3, heated at 700°C for various durations. This is then subsequently washed with water at RT and 50°C.

It is possible that Na_2CO_3 converts any metal sulphates to oxides:

$$MSO_4 + Na_2CO_3 -> MO_2 + Na_2SO_4 + CO_{2(g)} \tag{5.27}$$

Where M represents Fe, Cu, Pb, Zn, and Sn. Figure 5.54 shows that Equation 5.27 has a negative ΔG value from 0-1000°C for Fe, Cu, Pb, Zn, and Sn. This suggests that it is thermodynamically possible for these reactions to occur.

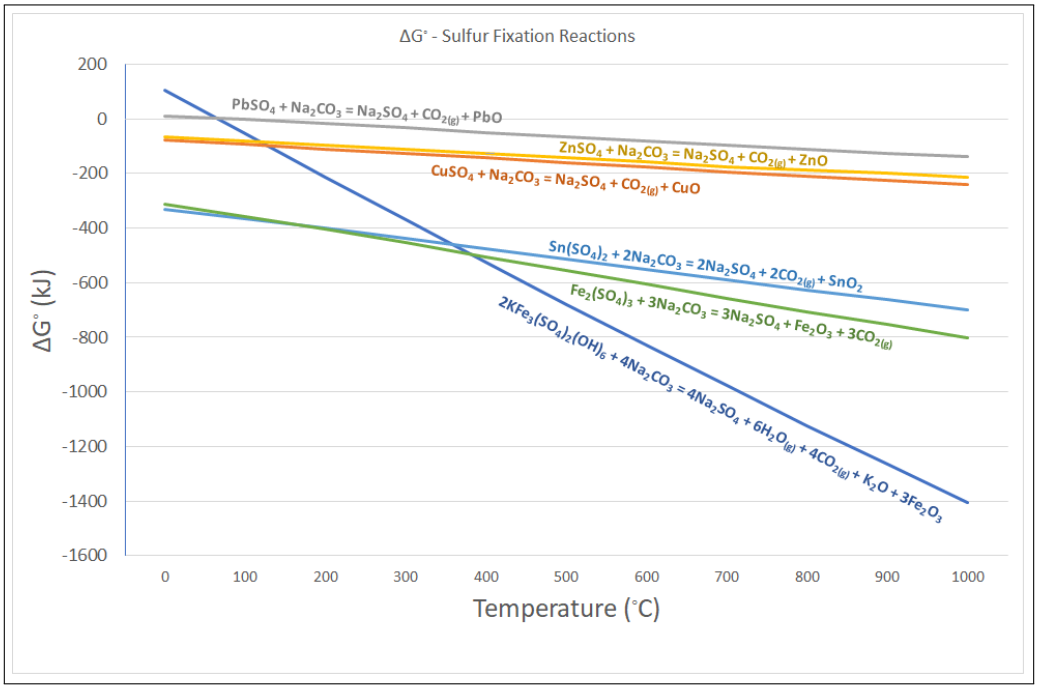

Figure 5.54: ΔG of sulfur fixation of metal sulphates with Na_2CO_3 at various temperatures. Values calculated using HSC (v6) software.

It is worth mentioning that this is difficult to observe experimentally due to the low concentration of metals like Cu and Zn; however, the presence of PbO was detected in the calcined residue (see Figure 5.55). This supports the notion that Na_2CO_3 converted any water soluble metal sulphates to oxides. Also worth mentioning is that the XRDs in Figure 5.55 also indicates the presence of Pb which bolsters the previous assertion that CO was present. Pb can be formed by first the conversion of $PbSO_4$ to PbO (also observed in the XRD). The PbO subsequently reacts with CO present to form elemental Pb.

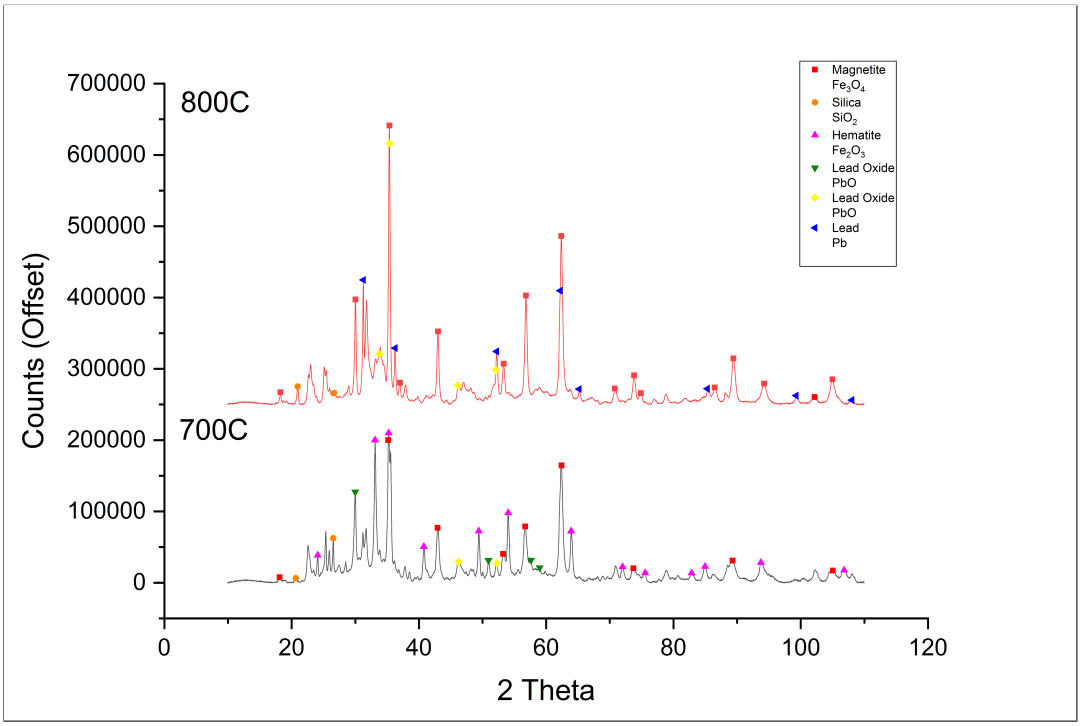

Figure 5.55: XRDs of sulfur fixation experiments. 5g of BLP + Na_2CO_3 mix was placed in a horizontal furnace at 700°C and 800°C for 15 minutes.

The conversion of any $CuSO_4$ to CuO (similarly with the other CEF metals) would also explain the increase in concentration of the CEF metals in the residue and their lack of presence in wash solution. Essentially all the sulphates were fixed as sodium sulphate and any of the Cu (or CEF metals) is converted to an insoluble oxide. Figure 5.54 also includes the ΔG of equation 5.25 which shows it is the most stable reaction relative to the other sulfur fixation experiments.

The explanations for what is observed during calcination at 700°C also applies to the 800°C treatment (see Figures 5.56 and 5.57). One point of difference is the significant increase in Cu concentration in the washed residues after the 800°C calcination. It's difficult to ascertain why this is the case because, as previously discussed, if no Cu is being washed out (because of it's presence as an oxide or sulfide) then the elemental changes should be similar. Figure 5.52 shows that essentially no Cu is washed into solution for both the 700°C and 800°C treatments. This suggests that the elemental changes should be essentially the same for the two temperature treatments. One difference between the residues at the two temperature treatments is the relative concentrations of hematite to magnetite. Section C.2 and Figure 5.49 shows that the 800°C treatment has more intense peaks of magnetite compared to hematite. There is a higher proportion of hematite for the 700°C treatment. It is uncertain if these phases impact the XRF values for the other elements.

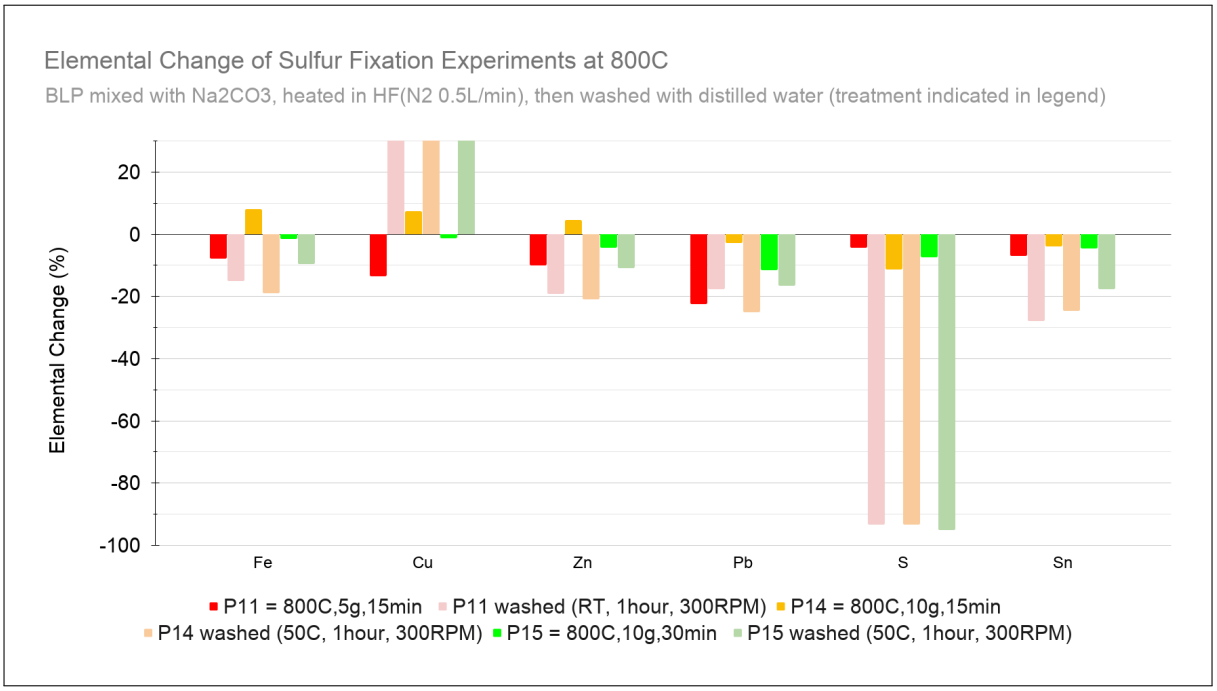

Figure 5.56: Elemental change of BLP mixed with Na_2CO_3, heated at 800°C for various durations. This is then subsequently washed with water as RT and 50°C.

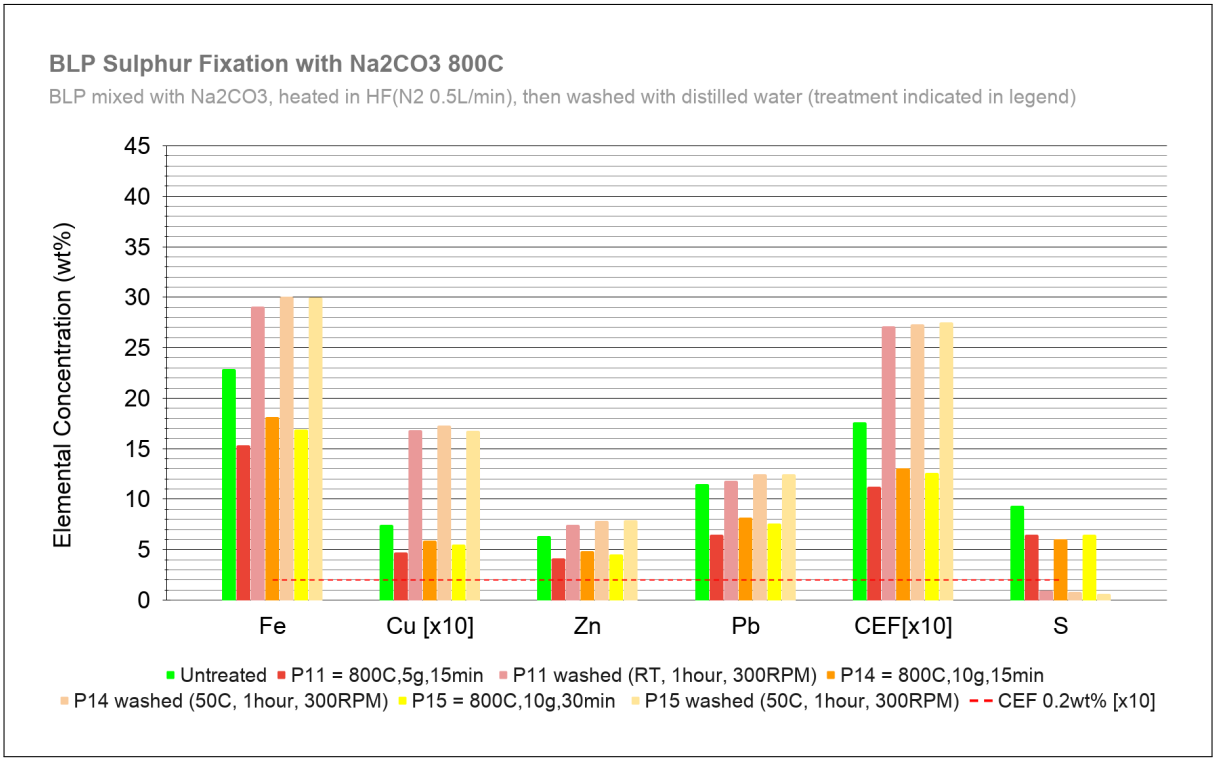

Figure 5.57: Residual elemental concentrations of BLP mixed with Na_2CO_3, heated at 800°C for various durations. This is then subsequently washed with water as RT and 50°C.

Overall, if the residual concentrations of both temperature treatments are compared with untreated BLP we see an increase in concentration of of Fe, Cu, Zn, Pb and Sn (see Figures 5.53 and 5.57).

This is primarily due to only sulfur being removed. The washing solutions confirm this with the high leaching efficiencies of sulfur. It should be noted that at lower washing temperatures the presence of Ca is detected. $CaSO_4$ solubility decreases with increasing temperature as is observed in the wash solutions. If the CEF values of both temperature treatments are compared (see Figure 5.58), the 800°C treatment resulted in a higher CEF concentration after washing. During the calcination step, the CEF concentration in the 800°C treatment was lower than the 700 °C treatment. XRF data showed a higher concentration of Na and S for the 800°C treatment suggesting that sulfur fixation had occurred to a greater extent. With greater sulfur fixation, more metal sulfates (including CEF metal sulfates) would have been converted to metal oxides by the Na_2CO_3 and subsequently reported to the washed residue; this is what is observed in Figure 5.58.

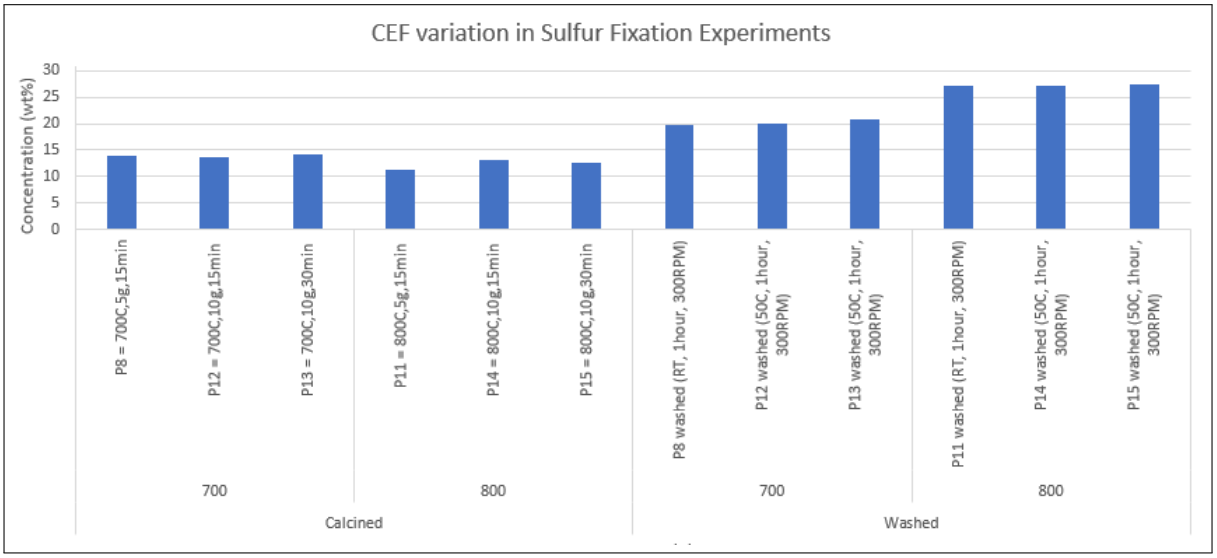

Figure 5.58: Comparison of CEF values for BLP + Na_2CO_3 calcined at 700°C and 800C and subsequently washes.

Sulfur was certainly fixed using this approach. Significantly less sulfur remained in the residual solid during calcination when compared with thermal decomposition. The subsequent washing removed all of the remaining sulfur. With respect to CEF metal removal, the treatment effectiveness (see Table C.1) of this strategy shows that this approach was not effective. Concentrations of the CEF metals are these metals are higher than untreated BLP. This highlights that this approach (sulfur fixation and washing) is not a viable approach for removing Cu from BLP. The lowest CEF value was achieved by calcining BLP and Na_2CO_3 at 700°C with subsequent washing at room temperature (Figure C.1). In addition, the washing method might be worth investigating too. The washing in the experiment was carried out with the setup used for leaching. In those conditions, Fe oxide particles that are present may scavenge metals like Cu in solution which may have prevented the metals like Cu from staying in solution.

5.4. Error Analysis

What was not discussed in the results was the sources of error and their magnitudes. Only one experiment was carried out with each treatment, therefore, errors will only be considered from analytical equipment (i.e. XRF for residues and ICP for PLS).

5.4.1. Residues

For treated residues, analysis were carried out by XRF to determine elemental concentrations. Consequently, all elemental concentrations in residues do have errors that stem from XRF analysis. Typically

for XRF, the relative error associated with the concentration of a particular element is proportional to the concentration of that element. For this project, XRF analysis provided the elemental concentrations in oxide form. The following calculations are performed to obtain the relative errors:

Firstly, XRF data is provided in oxide percentages (and errors) which needs to be converted to elemental percentages (and errors):

$$E(\%) = \frac{EO(\%)}{CF} \tag{5.28}$$

$$AbEE(\%) = \frac{AbEEO}{CF} \tag{5.29}$$

Where E(%) = element percentage, EO(%) = element oxide percentage provided by XRF, CF = conversion factor specific to each oxide, AbEE (%) = absolute error of element, AbEEO (%) = absolute error of element.

The Relative Error (RE) is then calculated by:

$$RE(\%) = \frac{AbEE(\%)}{E(\%)} * 100 \tag{5.30}$$

The equations above are applied to the XRF results of the residue when BLP and $CaCl_2$ is heated from 600 - 1000°C for 15 minutes (this yielded the lowest CEF value out of all the treatments carried out for this thesis). Table 5.12 shows the condensed XRF results and the associated errors. The table shows that elements that are high in concentration (e.g. Fe and S) have low relative errors whereas low concentration elements (e.g. Mo and Ni) have high relative errors. For this particular residue, the relative error of CEF metals was 10.5%. Since the concentration of the CEF metals was the lowest for this residue, the relative errors were also the highest; therefore, the maximum error associated with the CEF values of all residues should be 10.5%. As the concentration of CEF metals were higher with all other treatments their relative errors should be lower than 10.5%.

Table 5.12: Absolute and relative errors of elements based of XRF results of treated residue. BLP + $CaCl_2$ heated in horizontal furnace from 600-1000°C.

Compound	**Conc. (wt%)**	**Absolute Error (wt%)**	**Conversion**	**Elemental Conc. (%)**	**Element Absolute Error (wt%)**	**Element Relative Error (%)**
Fe2O3	33.836	0.1	1.430	23.667	0.070	0.296
SO3	24.247	0.1	2.497	9.710	0.040	0.412
SnO2	0.12	0.01	1.270	0.095	0.008	8.464
ZnO	2.909	0.01	1.245	2.337	0.008	0.344
CuO	0.251	0.007	1.252	0.201	0.006	2.789
Cr2O3	0.101	0.009	1.462	0.069	0.006	8.911
MoO3	0.012	0.005	1.500	0.008	0.003	41.667
NiO	0.022	0.004	1.273	0.017	0.003	18.182
			CEF	0.839	0.088	10.509

5.4.2. Pregnant Leach Solutions

For calculating errors associated with leaching efficiencies, two sources of error are focused on: dilution factor and ICP-OES.

Approximately 0.5mL of fluid was collected during sampling for PLS analysis. The pipette used had 0.01mL precision, consequently the error associated with the pipette is 0.005mL (half the precision value). The minimum volume of fluid required for ICP analysis was 5mL. Consequently, a 5mL pipettor with 0.5mL precision was used for dilution. The volume error associated with this was 0.25mL. For procedural reasons, 11x, 121x and 1,331x dilutions were prepared for ICP analysis. The variations in dilutions associated with pipetting the 0.5mL sample and the subsequent dilutions (with 5mL) are summarised in Table5.13:

Table 5.13: Variation in dilutions associated with pipetting errors.

Dilutions		**11x**		**121x**		**1331x**	
Volume Pipetted(mL)		Min	Max	Min	Max	Min	Max
		4.75	5.25	4.75	5.25	4.75	5.25
Min	0.495	**10.6**	**11.6**	**112**	**135**	**1190**	**1563**
Max	0.505	**10.4**	**11.4**	**108**	**130**	**1127**	**1480**

Table 5.13 shows that if the pipetting errors are taken into consideration, the actual dilution varies by 10.4-11.6x for the 11x dilution, 108-135 for the 121x dilution, and 1127-1563x for the 1331x dilution. For ICP-OES, the precision of analysis is anticipated to be 1% or less RSD (relative standard deviation) at sufficient concentrations of the measured element [97]. Although, higher RSD values have been considered acceptable in the literature (10%)[98]. To be conservative, a RSD value of 10% will be considered appropriate. As the leaching efficiency error is dependent on the product of the dilution and ICP errors, the following equation is used for the propagation of errors:

$$RE_{LE} = RE_{Dil} + RE_{ICP-OES} \tag{5.31}$$

Where RE_{LE} = relative error of leaching efficiency, RE_{Dil} = relative error associated with dilutions, and $RE_{ICP\text{-}OES}$ = relative error associated with ICP-OES (the RSD value). Table 5.14 shows the leaching efficiency errors for a given dilution. Measuring the concentration for a particular element using ICP-OES is dependent on the detection limit for a particular element and the corresponding dilutions necessary to obtain a measurement. The dilutions that are necessary to detect a particular element will also change depending on the concentration of that element in the PLS. Therefore, it is necessary to understand the leaching efficiency errors for each dilution. Table 5.14 shows that, depending on the element being measured, the relative error can range from -15.4% to 27.5%. For example, for a 1,331x diluted sample, where the dilutions have occurred with less volume (i.e. 4.75mL x 3), the measured concentration for an element could be 25.3% higher than the actual value. Similarly, dilutions with higher volumes may produce measured concentrations that are 27.5% less than the actual value.

Table 5.14: Leaching efficiency errors incorporating errors associated with dilution and ICP-OES analysis.

Relative Error (%)				
Pipetting	Dilution	11	121	1331
	Min Dilution	10.4	108	1127
	Max Dilution	11.6	135	1563
	Low Dilution RE_{Dil} (%)	5.4	10.5	15.3
	High Dilution RE_{Dil} (%)	-5.51	-11.3	-17.5
$RE_{ICP\text{-}OES}$ (%)		±10	±10	±10
RE_{LE} (%)	Low Dilution	**15.4**	**20.5**	**25.3**
	High Dilution	**-15.5**	**-21.3**	**-27.5**

5.5. Incorporation of Treated Jarosite in HIsarna Ironmaking

Out of all the treatments employed to remove CEF metals from BLP, the staged chloridisation reaction was the most effective (the treated residue had the lowest treatment effectiveness with respect to CEF/Fe). This involved mixing BLP (26%) with $CaCl_2$ (24%) and heating the mixture from 600°C to 1000°C. With this treatment, the CEF value was 0.84% which was still higher than what is required for HIsarna feedstock (0.2 wt%). Consequently, the treated residues cannot be used directly as a feedstock for HIsarna ironmaking. The treated residue, however, can be combined with the conventional feedstock in HIsarna ironmaking at proportions that ensure that CEF criteria are met. Figure 5.59 is a simple schematic of the HIsarna reactor which only considers Fe containing inputs and outputs of the process.The figure is based of HIsarna Pilot Plant operations that use a feed rate of 8263kgs/hr of iron ore to produce 4923kg/hr of hot metal.

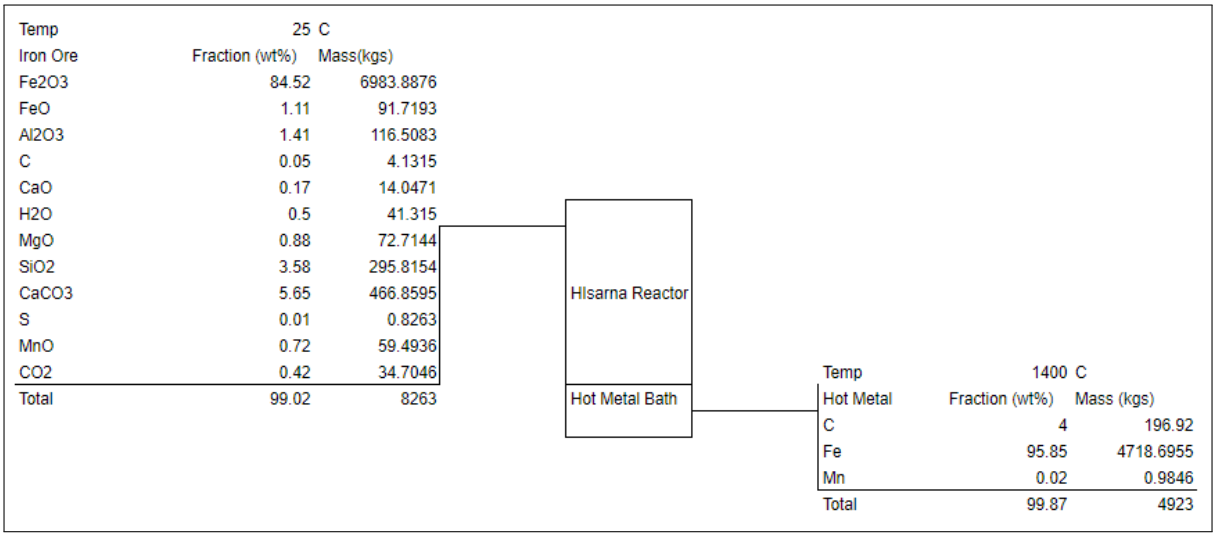

Figure 5.59: Simple schematic of the HIsarna reactor showing mass flow and elemental composition of Fe containing inputs and outputs only.

Figure 5.60 indicates the feed stream but converting all inputs into elemental percentages (i.e. removing the oxygen). This was then compared to a feed with the inclusion of treated BLP (the residue that resulted from the staged chloridisation treatment). Table 5.15 shows the elemental composition of the resulting residue.

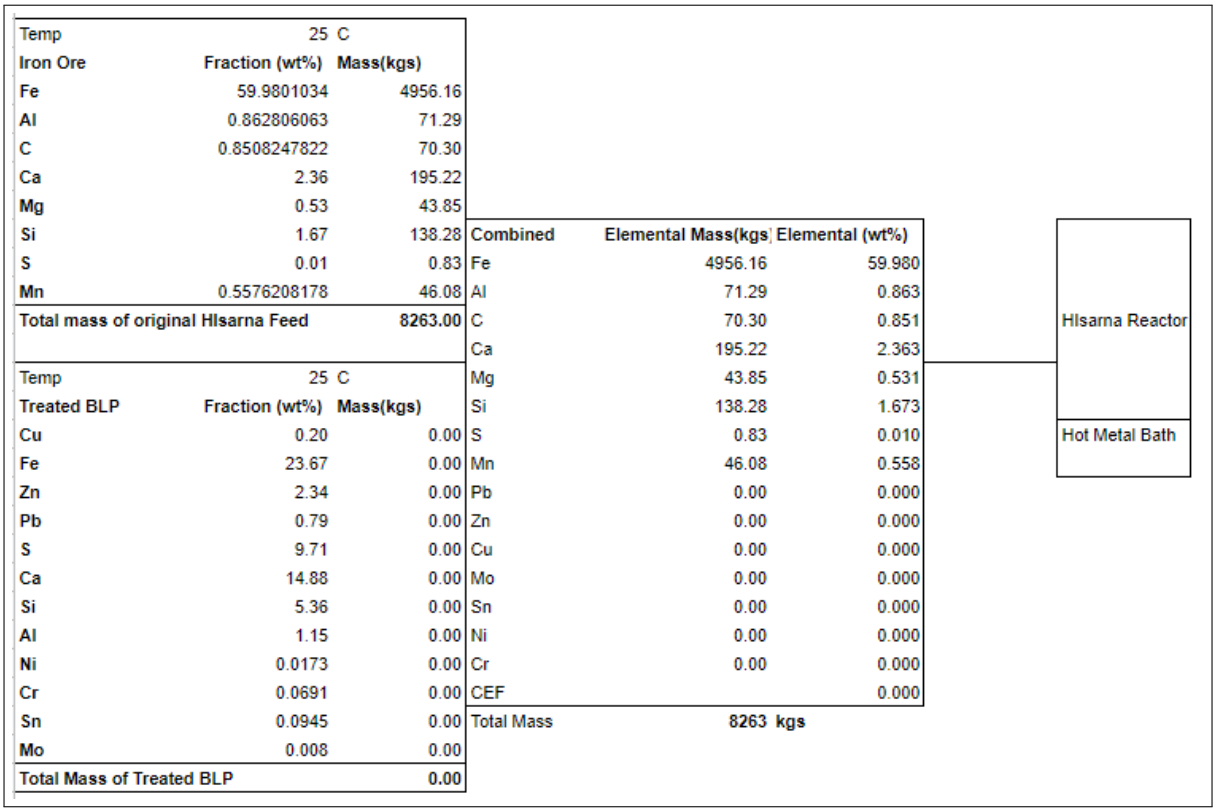

Figure 5.60: Elemental composition of the feed stream entering HIsarna reactor.

Table 5.15: BLP mixed with $CaCl_2$, heated to 600°C and treatment temperature increased to 1000°C with 18min staging occurring at 700, 800, 900 and 1000 °C in a horizontal furnace (inert atmosphere).

	Conc (wt%)
Cu[x10]	2.01
Fe	23.67
Zn	2.34
Pb	0.79
S	9.71
Ni[x100]	1.73
Ca	14.88
Si	5.36
Al	1.15
CEF [x10]	8.39
Sn[x100]	9.45
Cr[x100]	6.91
Mo[x100]	0.80
Cl	0.09

Figure 5.61, shows the inclusion of residue into the HIsarna feed stream. Up to 1970kgs can be added to about 6293kgs of conventional feed while ensuring that the CEF concentration does not exceed 0.2 wt% and the original feed rate is maintained.

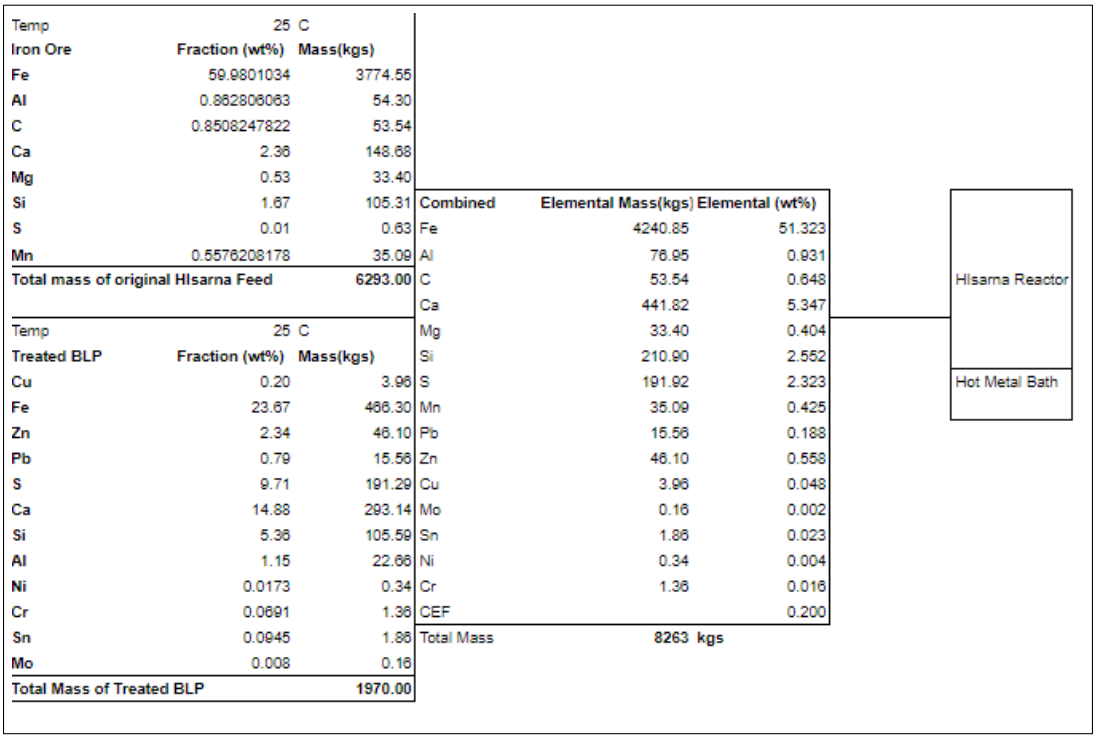

Figure 5.61: Elemental composition of the feed stream entering HIsarna reactor if considering treated BLP as well.

From Figure 5.61 the following points are worth discussing:

- The residue in the treated BLP contains a small amount of chlorine. The $CaCl_2$ used to treat the BLP will be optimised such that there is no chlorine in the treated residue. For the purposes of this exercise, 0.09wt% chlorine concentration is considered acceptable and is neglected in the analysis.
- Lead is problematic because it can get absorbed into the refractory lining. The assumption is that at levels indicated in Table 5.15, this will not be problematic. Any Pb present will be volatilised and collected in the off-gas dust.
- Any presence of sulfur will be treated with the HIsarna off-gas treatment system.
- The presence of other elements (i.e. Ca, Si, Al, etc) does have an impact on the process but not related to the hot metal product. Excess Ca, Si or Al adds up to the processing costs: it will require more coal for melting and more slag is produced. This will impact the overall mass balance and the economics of using the treated BLP.
- The initial feed rate was fixed at 8263kgs/hr to produce 4923kg of hot metal. With the incorporation of the treated BLP, hot metal production will decrease to 4240kg/hr or potentially less. This will obviously impact the economics further to what was discussed in the previous point.
- Treated BLP feed rate was increased until the CEF value reached 0.2wt%

Figure 5.61 provides idea of the elemental compositions of any HIsarna input stream that would use treated BLP. It is meant to highlight any elemental changes and any corresponding effects. It is not intended to provide detailed modelling on the chemistry, energy, or costs that would result if the treated BLP is incorporated into HIsarna feed. Undoubtedly all these factors would play a role in deciding whether to incorporate the treated BLP into the HIsarna process.

6

Conclusions and Recommendations

6.1. Conclusion

This thesis has presented some approaches in addressing the research question: Can jarosite residue from the Zn industry be used for HIsarna steelmaking? Jarosite is an iron-rich residue that is produced by Zn refineries. Using conventional BF ironmaking, it was not possible to use jarosite due to high concentrations of Zn. HIsarna ironmaking has enabled the exploration of the research question because it is a revolutionary technology that allows for greater flexibility in its raw materials. There were limits, however, to certain impurities that would need to be removed from the jarosite, namely Cu, Sn, Ni, Cr, and Mo. These elements were classed as CEF metals and the sum of the augmented concentrations of all the elements could not exceed 0.2 wt% of the feed of HIsarna. More specifically, Cu + Ni + Cr + 5* Sn + 10*Mo ≤0.2 wt%. From the literature, Cu comprises a large fraction of the CEF metals and so a special focus was given to Cu removal. In addition, sulfur was an element that was also monitored for environmental reasons.

The jarosite source was received from Nyrstar, Budel, a local Zn refinery. Nyrstar labels their jarosite as BLP (Budel Leach Product). This thesis tackled the research question by first establishing the phases that existed in the BLP the concentrations of the CEF metals. The project then aimed to treat the residue using hydrometallurgical, pyrometallurgical, and a combination of hydro- and pyrometallurgical processes. The processes were selected based on how effective they were in removing Cu (and indirectly the remaining CEF metals). The CEF values were then established for the treated residue to determine if the treatment was effective. In addition, since multiple strategies were employed in treating BLP, treatment effectiveness ratios (Cu/Fe wt%) and (CEF/Fe wt%) for residues, and Cu/Fe (leaching efficiency%) and CEF/Fe (leaching efficiency%) for leach solutions were used to compare the different approaches. The treatment effectiveness is a unit-less ratio which the value (lower for for residues and higher for leach solutions) determined how effective the treatment was.

XRD analysis of the BLP showed that the BLP consisted of plumbojarosite, zinc ferrite and lead sulfate. XRF indicated that the CEF concentration equaled 1.76 wt%, close to 9 times what was considered acceptable for HIsarna feedstock. Cu was the largest constituent of the CEF metals with 0.7 wt% followed by Sn (0.17 wt%). SEM of BLP showed that Cu (and the remaining CEF metals) did not exist as a separate phase but existed within the structure of plumbojarosite. This meant that mineral specific beneficiation methods could not be employed to separate Cu. Plumbojarosite would need to be selectively broken down to release Cu (and other CEF metals) and keep Fe as a solid. Thermogravimetric analysis (TGA) was also carried out on the BLP from RT-1400 °C. The TGA revealed distinct mass changes at about 400°C and 650°C. From the literature, the mass change occurring at 400°C

was likely a dehydroxylation reaction (jarosite is converted to an iron sulphate with the loss of water). At 650°C, desulfurization occurred (iron sulfate is converted to hematite while releasing SO_2).

Three hydrometallurgical processes were followed: acid, alkaline and ammoniacal leaching. Acid leaching involved breaking down the jarosite into constituent ions with the selection of acids being tailored to selectivity of Cu (or CEF) over Fe. Four acids were used: sulfuric, oxalic, hydrochloric and acetic. Leaching efficiencies of all the acids were very low with the highest leaching efficiency of Cu achieved by oxalic acid (25%). Oxalic acid was the best performing lixiviant because it targeted Fe and was more effective in breaking down the jarosite. Selectivity of Cu (and CEF) over Fe was not established with any of the acids. Looking at treatment effectiveness, acetic acid had the highest treatment effectiveness with regard to leach solutions (14.44). Fe(III) Ac was insoluble so acetic acid was able to selectively dissolve Cu over Fe; however, acetic acid had the lowest overall Cu leaching efficiency (approximately 5%). For residues, HCl had the best Cu treatment effectiveness (0.024) and acetic acid had the best CEF treatment effectiveness (0.065). Overall CEF value far exceeded what was required for HIsarna steelmaking. Due to the low leaching efficiencies and no Fe selectivity, acid leaching was not deemed a viable path for treating BLP residues for acceptability into HIsarna ironmaking.

Alkaline leaching was selected as potential treatment strategy due to OH^- breaking down jarosite and immediately cause any released Fe to re- precipitate due to the high pH. Four approaches were attempted: 0.5M NaO, 1M NaOH, 1M NaOH + 0.1M EDTA, 3M NaOH. As was indicated by the results, in all four leach solutions, there was no appreciable amount of Cu detected in the leach solution. The high pH was likely the reason for the re-precipitation of Cu back into the residue. Sn was able to be leached into solution (l̃eaching efficiency 30%) with 3M NaOH. Leach with EDTA (a chelating agent) was attempted to see if Cu^{2+} could be held in solution. The sampling results show that, indeed Cu^{2+} was momentarily leaching into solution but as the leaching reaction progressed, the Cu leaching efficiency dropped to close to 0. This was likely due to the high pH and the presence of amorphous iron hydroxide which is an effective scavenger of impurity metals like Cu. The Cu treatment effectiveness of the residue indicated that all alkaline treatments were similarly ineffective (0.03). The best CEF treatment effectiveness was with 1M NaOH + 0.1M EDTA (0.060). Overall CEF value far exceeded what was required for HIsarna steelmaking. The extremely low leaching efficiencies and poor Fe selectivity also made the alkaline leaching approach unviable.

Deep Eutectic solvents were used to explore the how effectively Cu could be leached from BLP. Choline Chloride:Ethylene Glycol and Choline Chloride and Glycerol (at eutectic mixtures) were used to leach BLP. From the outset it became clear that these kind of lixiviants were hard to work with in the lab due to very high viscosity. Leaching results showed very low leach efficiency of Cu and the CEF metals (≤2%). Glycerol was a more effective hydrogen bond donor than ethylene glycol for leaching Cu. In addition, the solids could not be recovered with the setup used for this thesis. Consequently, no further experimentation was carried out with DES.

Ammoniacal leaching was selected due to metals like Cu being able to form complexes with ammonia whilst leaving Fe as a solid (this is due to the poor complexing ability of Fe with ammonia and the relatively high pH of ammonia that prevent Fe from existing in solution). Ammoniacal leaching was carried out with NH_4Cl: NH_4OH at varying ratios and concentrations. Cu was not leached into solution when the lixiviant was either NH_4Cl or NH_4OH only. Leaching efficiencies of Cu was low (10-15%) in the best case which was when there was a combination of NH_4Cl and NH_4OH. Cu was the only CEF metal that was leached during this method; however, selectivity was established with ammoniacal leaching as Fe was not leached into any of the solutions. Subsequently, a parametric study was carried out to see if the leaching efficiencies could be increased. The parametric study was based off 0.5M NH_4Cl: 0.5M NH_4OH. This involved carrying out the leaching at 25°and 75°C (as opposed to 50 °C), adding NaCl to the system, and using a sulfate based ammoniacal system. Overall, the highest Cu leaching efficiency was achieved with 0.5M NH_4Cl: 0.5M NH_4OH: 0.1M NaCl. It was unclear as

to why the presence of NaCl increased the leaching efficiency although it was determined that it was not purely because of the presence of Na^+. What was also clear was that the leaching efficiency of Cu was really dependent on the stability of the $[Cu(NH_3)_4]^{+2}$ ion in solution. Analysing the results showed that for a particular pH and $[NH_3]$ + $[NH_4^+]$ concentration, the $[Cu(NH_3)_4]^{+2}$ has a certain stability and a corresponding Cu leaching efficiency could be expected. The optimal pH range was determined to be 8.5-9. The optimal $[NH_3]$ + $[NH_4^+]$ concentration was harder to determine as higher concentrations did lead to higher Cu leaching efficiencies, however there was a limit. 3M NH_4Cl: 3M NH_4OH solution yielded one of the highest leaching efficiency of Cu (13.675%); however, as previously mentioned, the presence of NaCl to 0.5M NH_4Cl: 0.5M NH_4OH yielded the highest efficiency. The residue with the lowest Cu concentration was when BLP was leached with 0.3M NH_4Cl: 0.75M NH_4OH with 0.621 wt% Cu. The potentially higher pH was likely beneficial for $[Cu(NH_3)_4]^{+2}$] stability. Overall, 0.5M NH_4Cl: 0.5M NH_4OH: 0.1M NaCl achieved the best treatment effectiveness of Cu in the PLS (14380) and the residue (0.026). The CEF value for this solution was still in excess of what was required for HIsarna steelmaking (CEF = 1.65 wt%)

Two strictly pyrometallurgical treatments were attempted: (1) Thermal Decomposition and (2) Chloridisation. Thermal decomposition involved heating roughly 5g of solid in an horizontal furnace in a N_2 atmosphere. Results showed that as the temperature of the treatments increased, sulfur was the only element that was leaving the sample to a correspondingly higher degree. Analysis of the residue showed an increasing concentration of all metals present in the BLP as the treatment temperature increased. The decreasing mass change was attributed to the loss of water, oxygen and sulfur. At 1000°C approximately 77% of the sulfur is lost.

Chloridisation involved mixing BLP (76%) with $CaCl_2$(24%) and heating it at elevated temperatures. Chloridisation was effective in removing elements like Zn, Pb, Cu, and to some extent Sn. Elements like Zn and Pb left the sample to a substantial degree at temperatures of 600°C and higher. Cu only volatilised and left the sample at sufficient quantities at temperatures ≥1000°C (99%). Sn would be removed from the sample at 600 °C (57%) but would remain in the solid at higher temperatures (only 6% of Sn would be removed at 1000°C). This obviously has an impact on the CEF value so simply heating the mixture at 1000°C was insufficient. Some of the sulfur was fixed by the Ca when comparing sulfur loss to thermal decomposition. At 1000 °C, 49% of sulfur left when compared to 77% during thermal decomposition.

Consequently, a staging treatment was applied whereby the sample was initially subjected to 600°C treatment and then the temperature was increased to 1000°C. This achieved the the lowest CEF concentration (0.84 wt%). The Cu treatment effectiveness (0.0085) and CEF treatment effectiveness (0.035) was the lowest achieved out of all treatments.

The combined hydro- and pyrometallurgical treatment involved sulfur fixation with Na_2CO_3. BLP was mixed with Na_2CO_3 and subjected to thermal treatments at 700 and 800 °C. These residues were then subsequently washed and analysed. The initial understanding was that Na_2CO_3 fixed the sulfur in the BLP as a sulfate salt whilst also keep other metals like Cu as a sulfate salt as well. Fe would be converted to hematite and the subsequent wash would remove all the sulfate salts leaving behind a clean hematite. The results from the experiment show that this was not the case. Heating BLP with Na_2CO_3 resulted in the formation of Na_2SO_4 but may have potentially converted any other metal sulfate salts to oxides. The subsequent wash would have removed all the sodium an sulfur but concentrated the remain metals in the residue which is what was observed. The CEF values of the residues were higher than that of the original untreated BLP completely rendering this treatment ineffective. The best Cu treatment effectiveness (0.029) was achieved by calcining BLP and Na_2CO_3 (10g) at 700C for 15 minutes followed by at water wash at 50°C.

Overall, the chloridisation experiments were the most effective at lowering the CEF concentrations in the residue such that is could be used in HIsarna ironmaking. Chloridisation was also able to fix some of the sulfur present in the BLP. Out of all the chloriisation approaches, the temperature staging

treatment (600-1000°C) was the most effective in removing Cu and Sn. The CEF requirements for HIsarna feed were not achieved however, with the staging treatment only producing a CEF value of 0.84 wt%. Consequently, this could not be considered as feed for HIsarna by itself. It could be incorporated with the existing HIsarna feed such that the CEF value did not exceed 0.2 wt%. Simple elemental balances were carried out based on previously run pilot plant conditions to determine the maximum amount treated BLP that could be incorporated into the feed. The current hot metal production rate of 4923 kg/hr was based of an input of 8263 kgs/hr of iron ore. Based on this, up to 1970 kgs of treated BLP can be added to the HIsarna feed without the CEF exceeding 0.2wt%. If this were to be done issues such as lower hot metal production and the higher concentration of Ca, Si, and Al would increase coal consumption. Both of these issues would impact the economics of HIsarna steelmaking.

6.2. Recommendations

Chloridisation presents the most promising strategy for removing Cu and CEF from BLP. Almost all the Cu was removed when simply mixing BLP and $CaCl_2$ and calcining at 1000-1100°C. The presence of Sn and Mo became problematic at these temperatures. Staged treatment was the most effective at reducing the CEF value. The staged treatment resulted in 99.1% chlorine loss, 57% Sn loss, 20% Fe loss, 79% Cu loss, 71 % Zn loss, and 95% Pb loss. Further work should be directed at varying the $CaCl_2$ ratio in the mix to provide sufficient chlorine to enable all the Zn, Sn, Cu and Sn to leave the residue. The temperature variations in the treatment would be interesting to study especially to see if more Fe leaves the sample at lower temperatures. This was observed at 600°C when compared to 1000°C. It was also unclear what kind of chloride compounds were leaving the sample. Further work should be directed at analysing off-gases during volatilisation or collecting and analysing dusts. This would provide a clearer picture of the reactions taking place and subsequently the optimal reaction conditions. Finally, a wash step should be included after the chloridisation treatment. It was demonstrated that except for the staging treatment, chlorine was still present in the solid residue. Although XRD was unable to identify any chlorine containing compounds, it would be interesting to see if the chlorine is present as a water soluble metal chloride (particularly with respect to the CEF metals).

The hydrometallurgical approaches were unsuccessful. Only ammoniacal leaching showed the required selectivity of removing Cu and the CEF metals over Fe. Even then, leaching efficiencies were low ($\tilde{1}$5% for Cu). Because of this, there is limited scope for further work. A detailed study into the kinetics might provide some insight into the low leaching efficiencies.

Similarly to the hydrometallurgical treatments, the combined hydro- and pyrometallurgical treatment was also largely unsuccessful. There is limited scope for further work as the thermodynamics support the formation of CuO during the calcination step (rather than a water soluble sulfate salt). It would be interesting to see if the same results are seen when the reactions are carried out in air rather than in a N_2 environment. The wash method after the calcination step also has an impact on Cu removal. Varying the temperature of the treatments and the concentrations of Na_2CO_3 may yield greater insight into the effectiveness of the approach.

Bibliography

[1] N. Resources, "Zinc market overview," *Investor Relations*, 2018.

[2] "2020 world refined zinc supply and usage," *ILZSG*, 2020.

[3] M. A. Reuter, A. van Schaik, J. Gutzmer, N. Bartie, and A. Abadías-Llamas, "Challenges of the circular economy: a material, metallurgical, and product design perspective," *Annual Review of Materials Research*, vol. 49, pp. 253–274, 2019.

[4] "Zinc1960-2020 data: 2021-2022 forecast: Price: Quote: Chart: Historical: News."

[5] B. VANDERHEYDEN, "Reclaiming valuable metals from process residues through hisarna iron-making (reclamet) - focus on pre-processing," *Sixth PROMETIA Annual Seminar*, 2019.

[6] M. L. Free and M. Moats, "Chapter 2.7 - hydrometallurgical processing," in *Treatise on Process Metallurgy* (S. Seetharaman, ed.), pp. 949 – 982, Elsevier, 2014.

[7] Y. Yang, S. Song, H. Tang, L. Wang, W. Sun, and Y. Hu, "Purification and comprehensive recovery metal values from zinc hydrometallurgical solution," in *PbZn 2020: 9th International Symposium on Lead and Zinc Processing*, pp. 899–903, Springer, 2020.

[8] J. Babcan, "Die synthese von jarosit kfe 3 (so 4) 2 (oh) 6," *Geol Zbornik Geol Carpath*, vol. 22, pp. 299–304, 1971.

[9] D. Matsuura, Y. Usami, and K. Ichiya, "Recent operational improvements of hematite plant at akita zinc co., ltd.," in *PbZn 2020: 9th International Symposium on Lead and Zinc Processing*, pp. 865–876, Springer, 2020.

[10] A. Monhemius, "The iron elephant: A brief history of hydrometallurgists' struggles with element no. 26.," 2016.

[11] T. Chen and J. Dutrizac, "Jarofix: Addressing iron disposal in the zinc industry," *Jom*, vol. 53, no. 12, pp. 32–35, 2001.

[12] F. Schrama, E. M. Beunder, J. van Boggelen, R. Boom, and Y. Yang, "Desulphurisation of hisarna hot metal: a comparisson study based on plant data," in *3rd International Conference on Science and Technology of Ironmaking & Steelmaking (STIS 2017)*, 2017.

[13] A. Keys, M. van Hout, and B. Daniëls, "Decarbonisation options for the dutch steel industry," 2019.

[14] K. Nakajima, O. Takeda, T. Miki, K. Matsubae, and T. Nagasaka, "Thermodynamic analysis for the controllability of elements in the recycling process of metals," *Environmental science & technology*, vol. 45, no. 11, pp. 4929–4936, 2011.

[15] F. R. Carrillo-Pedroza, M. J. Soria-Aguilar, E. Salinas-Rodríguez, A. Martínez-Luevanos, T. E. Pecina-Treviño, and A. Dávalos-Sánchez, "Oxidative hydrometallurgy of sulphide minerals," in *Recent Researches in Metallurgical Engineering* (M. Nusheh, H. G. Ahuett, and A. Arrambide, eds.), ch. 2, Rijeka: IntechOpen, 2012.

[16] X. Meng and K. N. Han, "The principles and applications of ammonia leaching of metals—a review," *Mineral Processing and Extractive Metullargy Review*, vol. 16, no. 1, pp. 23–61, 1996.

[17] C. K. Gupta, *Hydrometallurgy in Extraction Processes, Volume II*. Routledge, 2017.

[18] G. K. Schweitzer and L. L. Pesterfield, *The aqueous chemistry of the elements*. OUP USA, 2010.

[19] "Zinc end uses," *ILZSG*, 2017.

[20] U. G. Survey, "Mineral commodities summary (zinc)," *Mineral Commodity Summaries*, 2019.

[21] R. J. Sinclair, "The extractive metallurgy of zinc," Australasian Institute of Mining and Metallurgy Victoria, 2005.

[22] J. Claassen, E. Meyer, J. Rennie, and R. Sandenbergh, "Iron precipitation from zinc-rich solutions: defining the zincor process," *Hydrometallurgy*, vol. 67, no. 1-3, pp. 87–108, 2002.

[23] P. Kangas, M. Nyström, I. Orko, P. Koukkari, P. Saikkonen, and J. Rastas, "The jarogain process for metals recovery from jarosite and electric arc furnace dust: Process design and economics," 2017.

[24] S. Spatari, M. Bertram, K. Fuse, T. Graedel, and E. Shelov, "The contemporary european zinc cycle: 1-year stocks and flows," *Resources, Conservation and Recycling*, vol. 39, no. 2, pp. 137–160, 2003.

[25] B. Schwab, "Zinc," *Ullmann's Encyclopedia of Industrial Chemistry*, pp. 1–25, 2015.

[26] V. Kuklík and J. Kudlacek, *Hot-dip galvanizing of steel structures*. Butterworth-Heinemann, 2016.

[27] C. J. Krauss, "Effects of minor elements on the production of electrolytic zinc from zinc sulphide concentrates.(retroactive coverage)," in *Zinc'85: Proceedings of the International Symposium on Extractive Metallurgy of Zinc*, pp. 467–481, 1985.

[28] C. Tuck, S. Xun, and S. Singerling, "Global iron ore production data; clarification of reporting from the usgs," *Mining Engineering Magazine February*, pp. 20–23, 2017.

[29] J.-P. Birat, "Society, materials, and the environment: The case of steel," *Metals*, vol. 10, no. 3, p. 331, 2020.

[30] C. Lanzerstorfer, B. Bamberger-Strassmayr, and K. Pilz, "Recycling of blast furnace dust in the iron ore sintering process: investigation of coke breeze substitution and the influence on off-gas emissions," *ISIJ International*, vol. 55, no. 4, pp. 758–764, 2015.

[31] A. Siegmund, "Pbzn 2010: Papers originally presented at lead-zinc 2010," *Lead-Zinc 2010*, 2010, publisher=Wiley.

[32] V. R. Sarma, K. Deo, and A. Biswas, "Dissolution of zinc ferrite samples in acids," *Hydrometallurgy*, vol. 2, no. 2, pp. 171–184, 1976.

[33] T. Chen and L. Cabri, "Mineralogical overview of iron control in hydrometallurgical processing," *Iron control in hydrometallurgy*, pp. 19–55, 1986.

[34] T. K. Dichmann and J. Finch, "The role of copper ions in sphalerite-pyrite flotation selectivity," *Minerals engineering*, vol. 14, no. 2, pp. 217–225, 2001.

[35] B. Yang, X. Tong, Z. Lan, Y. Cui, and X. Xie, "Influence of the interaction between sphalerite and pyrite on the copper activation of sphalerite," *Minerals*, vol. 8, no. 1, p. 16, 2018.

[36] M. J. Dias, A. D. de Souza, C. C. S. de Oliveira, D. D. Pereira, and M. F. L. Araújo, "Increase in zinc recovery from a silicate concentrate by pre-neutralization process," in *PbZn 2020: 9th International Symposium on Lead and Zinc Processing*, pp. 247–252, Springer, 2020.

[37] T. Yue, Z. Xu, Y. Hu, H. Han, and W. Sun, “Magnetic separation and recycling of goethite and calcium sulfate in zinc hydrometallurgy in the presence of maghemite fine particles,” *ACS Sustainable Chemistry & Engineering*, vol. 6, no. 2, pp. 1532–1538, 2018.

[38] A. A. Llamas, N. Bartie, M. Heibeck, M. Stelter, and M. Reuter, “Resource efficiency evaluation of pyrometallurgical solutions to minimize iron-rich residues in the roast-leach-electrowinning process,” in *PbZn 2020: 9th International Symposium on Lead and Zinc Processing*, pp. 351–364, Springer, 2020.

[39] A. Gordon and R. Pickering, “Improved leaching technologies in the electrolytic zinc industry,” *Metallurgical and Materials Transactions B*, vol. 6, no. 1, pp. 43–53, 1975.

[40] E. Salinas, A. Roca, M. Cruells, F. Patiño, and D. Córdoba, “Characterization and alkaline decomposition–cyanidation kinetics of industrial ammonium jarosite in naoh media,” *Hydrometallurgy*, vol. 60, no. 3, pp. 237–246, 2001.

[41] I. A. Reyes, I. Mireles, F. Patiño, T. Pandiyan, M. U. Flores, E. G. Palacios, E. J. Gutiérrez, and M. Reyes, “A study on the dissolution rates of k-cr (vi)-jarosites: kinetic analysis and implications,” *Geochemical transactions*, vol. 17, no. 1, p. 3, 2016.

[42] T. C.-M. Cheng, *Production of hematite in acidic zinc sulphate media*. PhD thesis, McGill University Libraries, 2002.

[43] S. Creedy, A. Glinin, R. Matusewicz, S. Hughes, and M. Reuter, “Outotec® ausmelt technology for treating zinc residues,” *World Metall Erzmetall*, vol. 66, no. 4, pp. 230–235, 2013.

[44] M. Pelino, C. Cantalini, C. Abbruzzese, and P. Plescia, “Treatment and recycling of goethite waste arising from the hydrometallurgy of zinc,” *Hydrometallurgy*, vol. 40, no. 1-2, pp. 25–35, 1996.

[45] D. Calla-Choque and G. Lapidus, “Acid decomposition and silver leaching with thiourea and oxalate from an industrial jarosite sample,” *Hydrometallurgy*, vol. 192, p. 105289, 2020.

[46] C. N. Alpers, D. Nordstrom, and J. W. Ball, “Solubility of jarosite solid solutions precipitated from acid mine waters, iron mountain, california, usa solubilité des solutions solides de jarosite précipitées à partir des eaux minières acides, iron mountain, californie, us a,” *Sciences Géologiques, bulletins et mémoires*, vol. 42, no. 4, pp. 281–298, 1989.

[47] I. A. Reyes, F. Patiño, M. U. Flores, T. Pandiyan, R. Cruz, E. J. Gutiérrez, M. Reyes, and V. H. Flores, “Dissolution rates of jarosite-type compounds in h2so4 medium: A kinetic analysis and its importance on the recovery of metal values from hydrometallurgical wastes,” *Hydrometallurgy*, vol. 167, pp. 16–29, 2017.

[48] W. Nheta and M. E. Makhatha, “Leaching of nickel from a jarosite precipitate with hydrochloric acid,” International Conference on Chemical and Environmental Engineering (ICCEE’2013), 2013.

[49] T. Palden, B. Onghena, M. Regadío, and K. Binnemans, “Methanesulfonic acid: a sustainable acidic solvent for recovering metals from the jarosite residue of the zinc industry,” *Green Chemistry*, vol. 21, no. 19, pp. 5394–5404, 2019.

[50] W. Kunda and H. Veltman, “Decomposition of jarosite,” *Metallurgical Transactions B*, vol. 10, no. 3, pp. 439–446, 1979.

[51] H. N. Vu, P. Dvorak, and T. Sita, “Study of conversion of waste jarosite precipitates to hematite,” *Inżynieria Mineralna*, vol. 15, 2014.

[52] Y.-m. CHEN, M.-t. TANG, S.-h. YANG, J. HE, C.-b. TANG, J.-g. YANG, and J.-y. LU, “Novel technique of decomposition of ammonium jarosite bearing indium in naoh medium,” *The Chinese Journal of Nonferrous Metals*, vol. 7, p. 028, 2009.

[53] E. N. Malenga, A. Mulaba-Bafubiandi, and W. Nheta, “Alkaline leaching of nickel bearing ammonium jarosite precipitate using koh, naoh and nh4oh in the presence of edta and na2s,” *Hydrometallurgy*, vol. 155, pp. 69–78, 2015.

[54] H. Rodríguez, *Ionic liquids for better separation processes*. Springer, 2015.

[55] T. Palden, M. Regadío, B. Onghena, and K. Binnemans, “Selective metal recovery from jarosite residue by leaching with acid-equilibrated ionic liquids and precipitation-stripping,” *ACS Sustainable Chemistry & Engineering*, vol. 7, no. 4, pp. 4239–4246, 2019.

[56] E. L. Smith, A. P. Abbott, and K. S. Ryder, “Deep eutectic solvents (dess) and their applications,” *Chemical reviews*, vol. 114, no. 21, pp. 11060–11082, 2014.

[57] A. P. Abbott, G. Capper, D. L. Davies, K. J. McKenzie, and S. U. Obi, “Solubility of metal oxides in deep eutectic solvents based on choline chloride,” *Journal of Chemical & Engineering Data*, vol. 51, no. 4, pp. 1280–1282, 2006.

[58] A. P. Abbott, J. Collins, I. Dalrymple, R. C. Harris, R. Mistry, F. Qiu, J. Scheirer, and W. R. Wise, “Processing of electric arc furnace dust using deep eutectic solvents,” *Australian journal of chemistry*, vol. 62, no. 4, pp. 341–347, 2009.

[59] N. R. Rodriguez, L. Machiels, B. Onghena, J. Spooren, and K. Binnemans, “Selective recovery of zinc from goethite residue in the zinc industry using deep-eutectic solvents,” *Rsc Advances*, vol. 10, no. 12, pp. 7328–7335, 2020.

[60] D. Kmetova, M. Stofko, and S. Kmet, “Ammoniacal leaching for extraction of non-ferrous metals from deep-sea nodules,” *International Journal of Mineral Processing*, vol. 15, no. 1-2, pp. 145–153, 1985.

[61] M. K. Jha, V. Kumar, and R. Singh, “Review of hydrometallurgical recovery of zinc from industrial wastes,” *Resources, conservation and recycling*, vol. 33, no. 1, pp. 1–22, 2001.

[62] M. Olper, “The ezinex process–a new and advanced method for electrowinning zinc from a chloride solution,” *World Zinc’93*, pp. 491–494, 1993.

[63] M. Kerolli-Mustafa, V. Mandić, L. Ćurković, and J. Šipušić, “Investigation of thermal decomposition of jarosite tailing waste,” *Journal of thermal analysis and calorimetry*, vol. 123, no. 1, pp. 421–430, 2016.

[64] H. Spratt, L. Rintoul, M. Avdeev, and W. Martens, “The thermal decomposition of hydronium jarosite and ammoniojarosite,” *Journal of Thermal Analysis and Calorimetry*, vol. 115, no. 1, pp. 101–109, 2014.

[65] S. Steinlechner and J. Antrekowitsch, “Extraction of zinc, silver and indium via vaporization from jarosite residue,” in *REWAS 2019*, pp. 189–195, Springer, 2019.

[66] V. Piskunov, A. Matveev, and A. Yaroslavtsev, “Utilizing iron residues from zinc production in the ussr,” *JOM*, vol. 40, no. 8, pp. 36–39, 1988.

[67] C. C. Chan and D. W. Kirk, “Behaviour of metals under the conditions of roasting msw incinerator fly ash with chlorinating agents,” *Journal of hazardous materials*, vol. 64, no. 1, pp. 75–89, 1999.

[68] H. NAGASUE, “Basic research for chloridization of copper and zinc in copper converter slag,” *Journal of the Mining and Metallurgical Institute of Japan*, vol. 94, no. 1090, pp. 865–870, 1978.

[69] H. Wang, C. Zheng, and S. Qin, “Study of a novel chloride volatilization process for the treatment of jarosite residue,” in *PbZn 2020: 9th International Symposium on Lead and Zinc Processing*, pp. 835–845, Springer, 2020.

[70] L. Tang, C. Tang, J. Xiao, P. Zeng, and M. Tang, “A cleaner process for valuable metals recovery from hydrometallurgical zinc residue,” *Journal of cleaner production*, vol. 201, pp. 764–773, 2018.

[71] D. Mombelli, C. Mapelli, S. Barella, A. Gruttadauria, and E. Spada, “Jarosite wastes reduction through blast furnace sludges for cast iron production,” *Journal of Environmental Chemical Engineering*, vol. 7, no. 2, p. 102966, 2019.

[72] D. Zhu, C. Yang, J. Pan, Z. Guo, and S. Li, “New pyrometallurgical route for separation and recovery of fe, zn, in, ga and s from jarosite residues,” *Journal of cleaner production*, vol. 205, pp. 781–788, 2018.

[73] A. Glinin, S. Creedy, R. Matusewicz, S. Hughes, and M. Reuter, “Outotec® ausmelt technology for treating zinc residues,” *Proceedings of the EMC, Weimar, Germany*, pp. 23–26, 2013.

[74] Y. Wang, H. Yang, X. Hou, W. Gao, H. Gui, and Q. Liu, “The effect of pellet technology on direct reduction of jarosite residues from zinc hydrometallurgy,” *Physicochem. Probl. Miner. Process*, vol. 55, no. 3, pp. 802–811, 2019.

[75] Y.-y. Wang, H.-f. Yang, B. Jiang, R.-l. Song, and W.-h. Zhang, “Comprehensive recovery of lead, zinc, and iron from hazardous jarosite residues using direct reduction followed by magnetic separation,” *International Journal of Minerals, Metallurgy, and Materials*, vol. 25, no. 2, pp. 123–130, 2018.

[76] M. Rämä, S. Nurmi, A. Jokilaakso, L. Klemettinen, P. Taskinen, and J. Salminen, “Thermal processing of jarosite leach residue for a safe disposable slag and valuable metals recovery,” *Metals*, vol. 8, no. 10, p. 744, 2018.

[77] S. Ju, Y. Zhang, Y. Zhang, P. Xue, and Y. Wang, “Clean hydrometallurgical route to recover zinc, silver, lead, copper, cadmium and iron from hazardous jarosite residues produced during zinc hydrometallurgy,” *Journal of hazardous materials*, vol. 192, no. 2, pp. 554–558, 2011.

[78] J. Van Boggelen, H. Meijer, C. Zeilstra, and Z. Li, “The use of hisarna hot metal in steelmaking,” *Scanmet V. Luleå (Sweden)*, 2016.

[79] J. E. Dutrizac and J. L. Jambor, “Jarosites and their application in hydrometallurgy,” *Reviews in Mineralogy and Geochemistry*, vol. 40, no. 1, pp. 405–452, 2000.

[80] S. Bell, B. Davis, A. Javaid, and E. Essadiqi, “Final report on effect of impurities in steel,” tech. rep., Report, 2006.

[81] N. Sano, H. Katayama, M. Sasabe, and S. Matsuoka, “Research activities on removal of residual elements from steel scrap in japan,” *Scandinavian journal of metallurgy*, vol. 27, no. 1, pp. 24–30, 1998.

[82] I. Les, “Effects of tramp elements in flat and long products,” *EC Report (EUR16672)*, pp. 9–15, 1995.

[83] P. BESTA, A. SIKOROVÁ, S. KUBICA, Š. VILAMOVÁ, and P. PROSICKÝ, “The impact of zinc compounds on blast furnace lining life,” 2015.

[84] H. Elomaa, S. Seisko, J. Lehtola, and M. Lundström, “A study on selective leaching of heavy metals vs. iron from fly ash,” *Journal of Material Cycles and Waste Management*, vol. 21, no. 4, pp. 1004–1013, 2019.

[85] S. O. Lee, T. Tran, Y. Y. Park, S. J. Kim, and M. J. Kim, “Study on the kinetics of iron oxide leaching by oxalic acid,” *International Journal of Mineral Processing*, vol. 80, no. 2-4, pp. 144–152, 2006.

[86] B. Beverskog and I. Puigdomenech, “Revised pourbaix diagrams for iron at 25–300 c,” *Corrosion Science*, vol. 38, no. 12, pp. 2121–2135, 1996.

[87] B. Beverskog and I. Puigdomenech, “Revised pourbaix diagrams for chromium at 25–300 c,” *Corrosion Science*, vol. 39, no. 1, pp. 43–57, 1997.

[88] H. Yildirim, M. Ateş, M. D. Turan, Z. A. Sarı, H. Nizamoğlu, and A. Cam, “Selective iron dissolution from zinc plant residue,” *JOURNAL OF MATERIALS AND ELECTRONIC DEVICES*, vol. 4, no. 1, pp. 8–10, 2020.

[89] J. Majzlan, A. Navrotsky, and U. Schwertmann, “Thermodynamics of iron oxides: Part iii. enthalpies of formation and stability of ferrihydrite (fe (oh) 3), schwertmannite (feo (oh) 3/4 (so4) 1/8), and ε-fe2o3,” *Geochimica et cosmochimica acta*, vol. 68, no. 5, pp. 1049–1059, 2004.

[90] Z. Youcai and R. Stanforth, “Extraction of zinc from zinc ferrites by fusion with caustic soda,” *Minerals Engineering*, vol. 13, no. 13, pp. 1417–1421, 2000.

[91] R. Grant, “Zinc production,” 2001.

[92] Y.-H. Chen and F.-A. Li, “Kinetic study on removal of copper (ii) using goethite and hematite nano-photocatalysts,” *Journal of colloid and interface science*, vol. 347, no. 2, pp. 277–281, 2010.

[93] A. Bekényiová, I. Štyriaková, and Z. Danková, “Sorption of copper and zinc by goethite and hematite,” *ARHIV ZA TEHNIČKE NAUKE/ARCHIVES FOR TECHNICAL SCIENCES*, vol. 1, no. 12, 2015.

[94] V. A. Grover, J. Hu, K. E. Engates, and H. J. Shipley, “Adsorption and desorption of bivalent metals to hematite nanoparticles,” *Environmental Toxicology and Chemistry*, vol. 31, no. 1, pp. 86–92, 2012.

[95] T. Varley, E. P. Barrett, C. Stevenson, R. H. Bradford, S. Croasdale, B. Howe, and W. A. Schmidt, *The Chloride Volatilization Process of Ore Treatment*. US Government Printing Office, 1923.

[96] K. Tamilselvan, *Metal Hydrazine Cinnamates: Synthesis and Characterization*. Anchor Academic Publishing, 2016.

[97] B. Charles and K. J. Fredeen, “Concepts, instrumentation and techniques in inductively coupled plasma optical emission spectrometry,” *Perkin Elmer Corp*, 1997.

[98] J. Fitzsimmons, D. Medvedev, and L. Mausner, “Specific activity and isotope abundances of strontium in purified strontium-82,” *Journal of Analytical Atomic Spectrometry*, vol. 31, no. 2, pp. 458–463, 2016.

Appendices

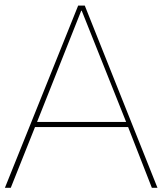

Hydrometallurgy

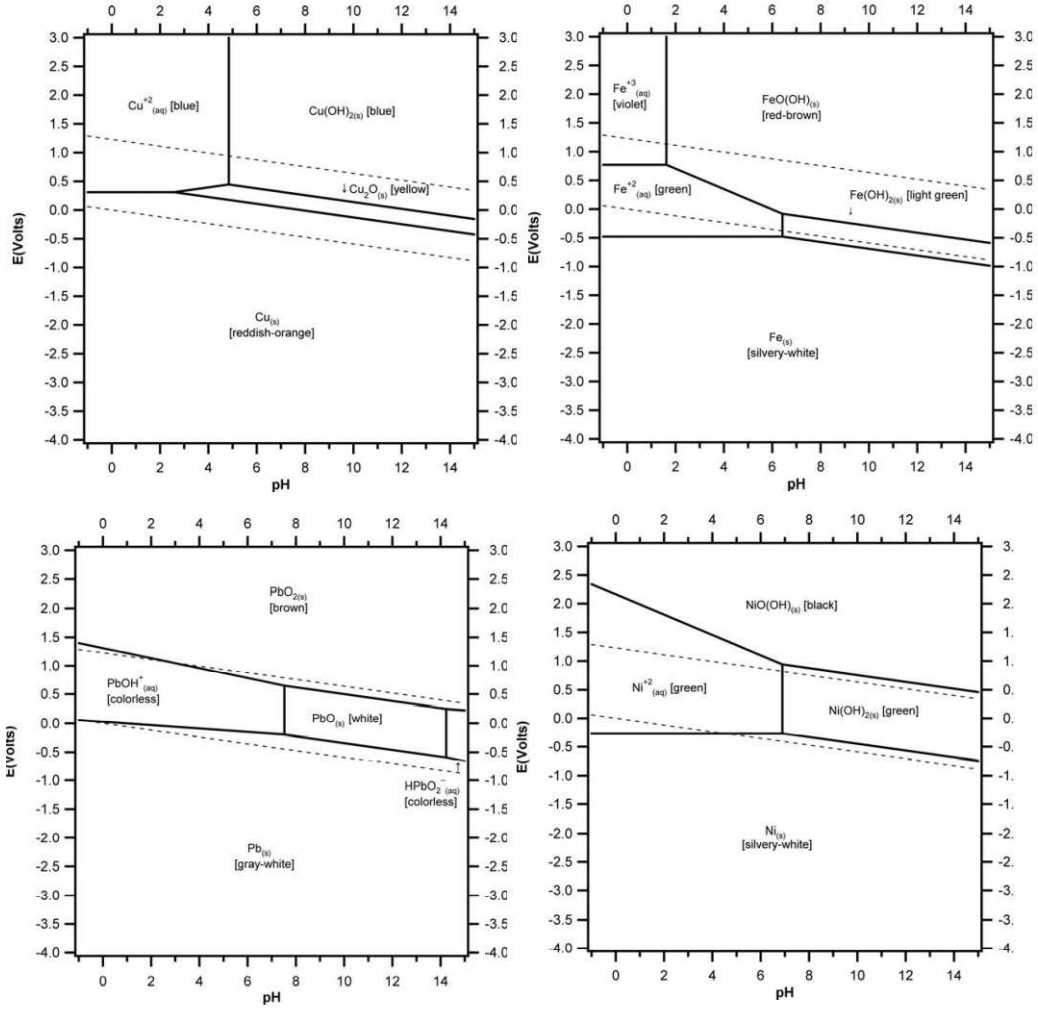

Figure A.1: Pourbaix diagrams of Me-H_2O at 25°C. Me = Cu, Fe, Pb, Ni. Metal concentration = 0.1M [18]

.

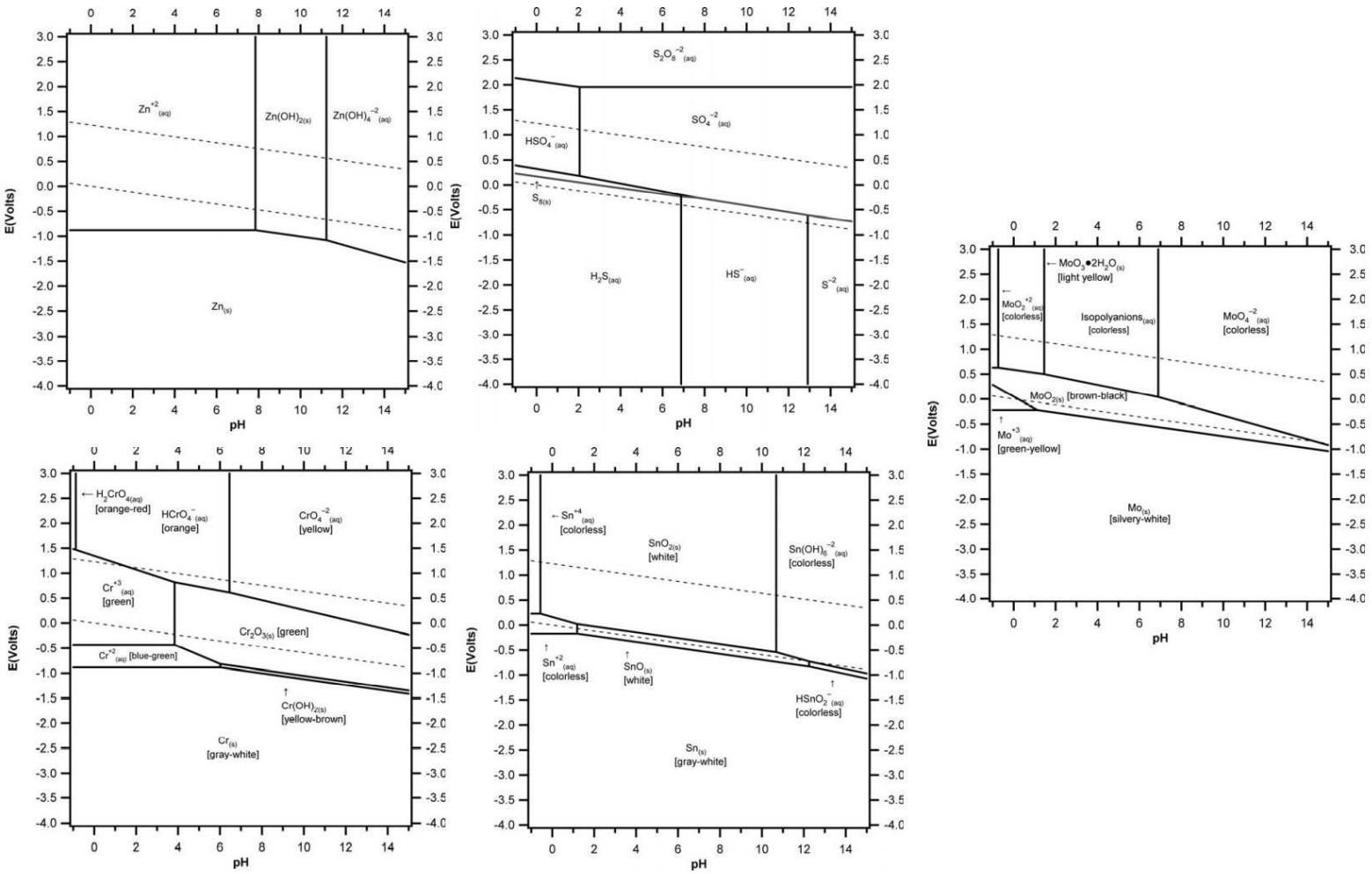

Figure A.2: Pourbaix diagrams of Me-H_2O at 25°C. Me = Zn, S, Cr, Sn, Mo. Metal concentration = 0.1M [18]

.

A.1. Acid Leaching

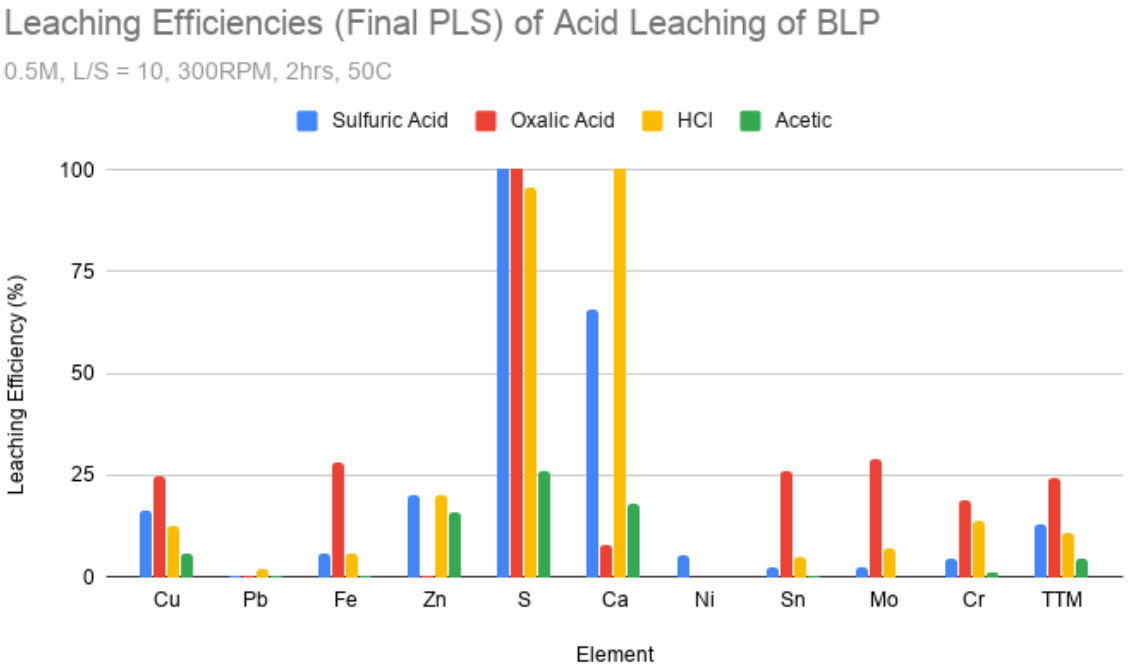

Figure A.3: Leaching efficiency of elements in final PLS from acid leaching of BLP (more detailed). L/S=10, Temp = 50°C, duration = 2hrs, conc = 0.5M, RPM = 300

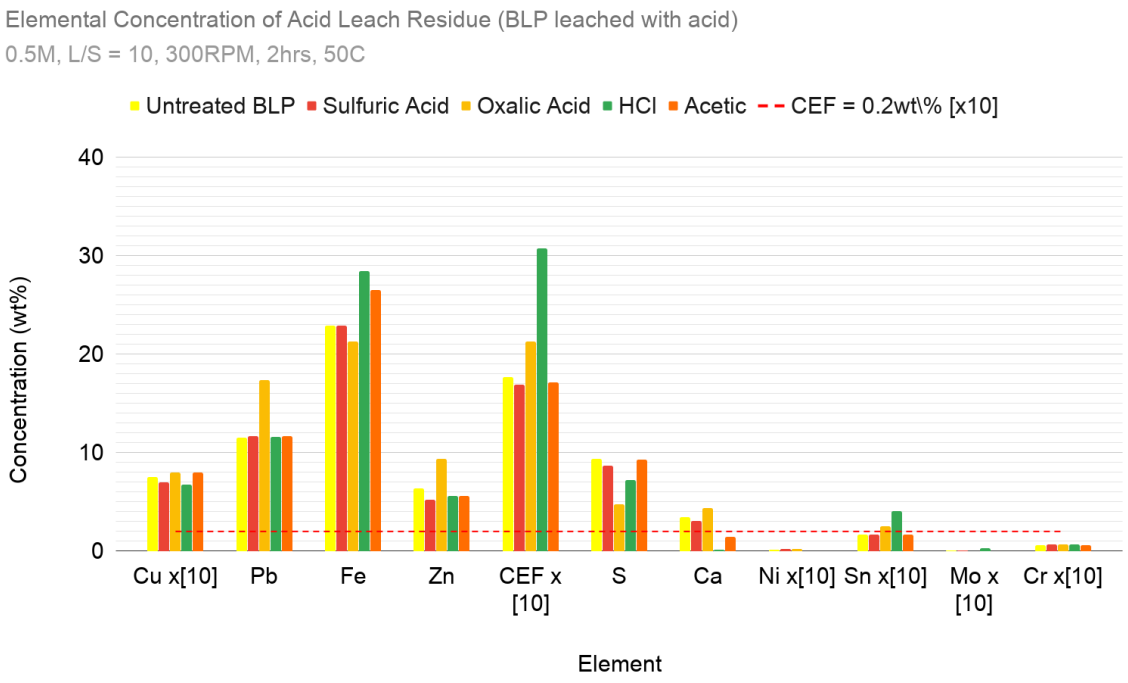

Figure A.4: Elemental composition of leach residue from acid leaching of BLP(more detailed). L/S=10, Temp = 50°C, duration = 2hrs, conc = 0.5M, RPM = 300

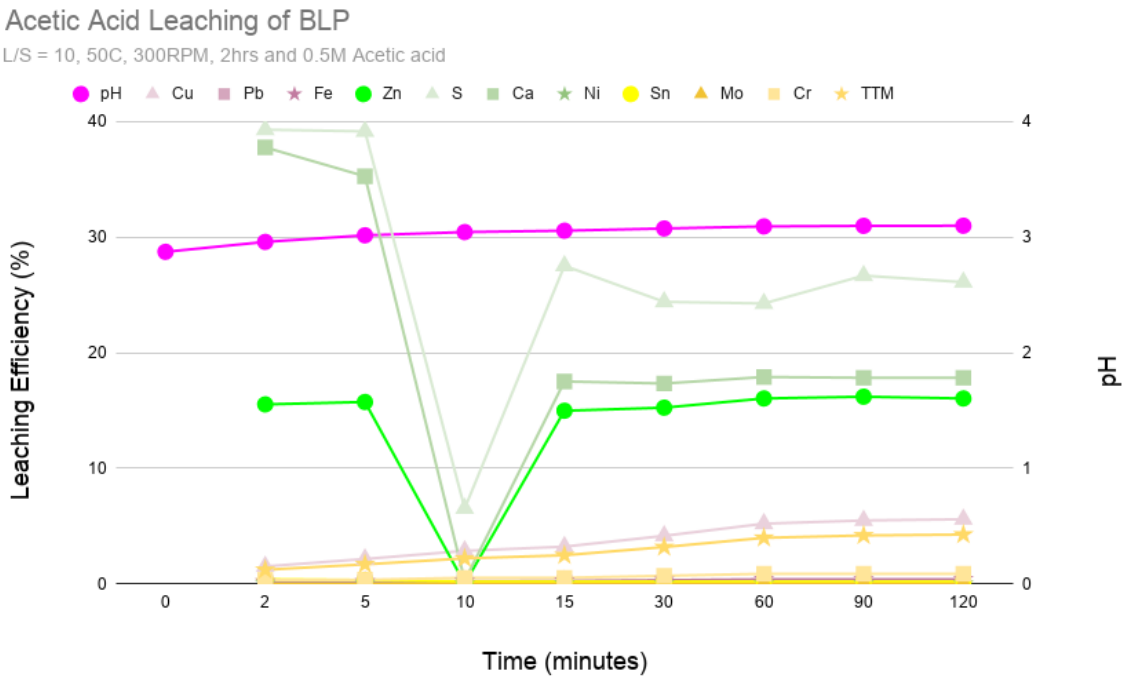

Figure A.5: Leaching efficiency of elements in BLP with acetic acid at various time intervals. L/S=10, Temp = 50°C, duration = 2hrs, conc = 0.5M, RPM = 300

A.1.1. XRD

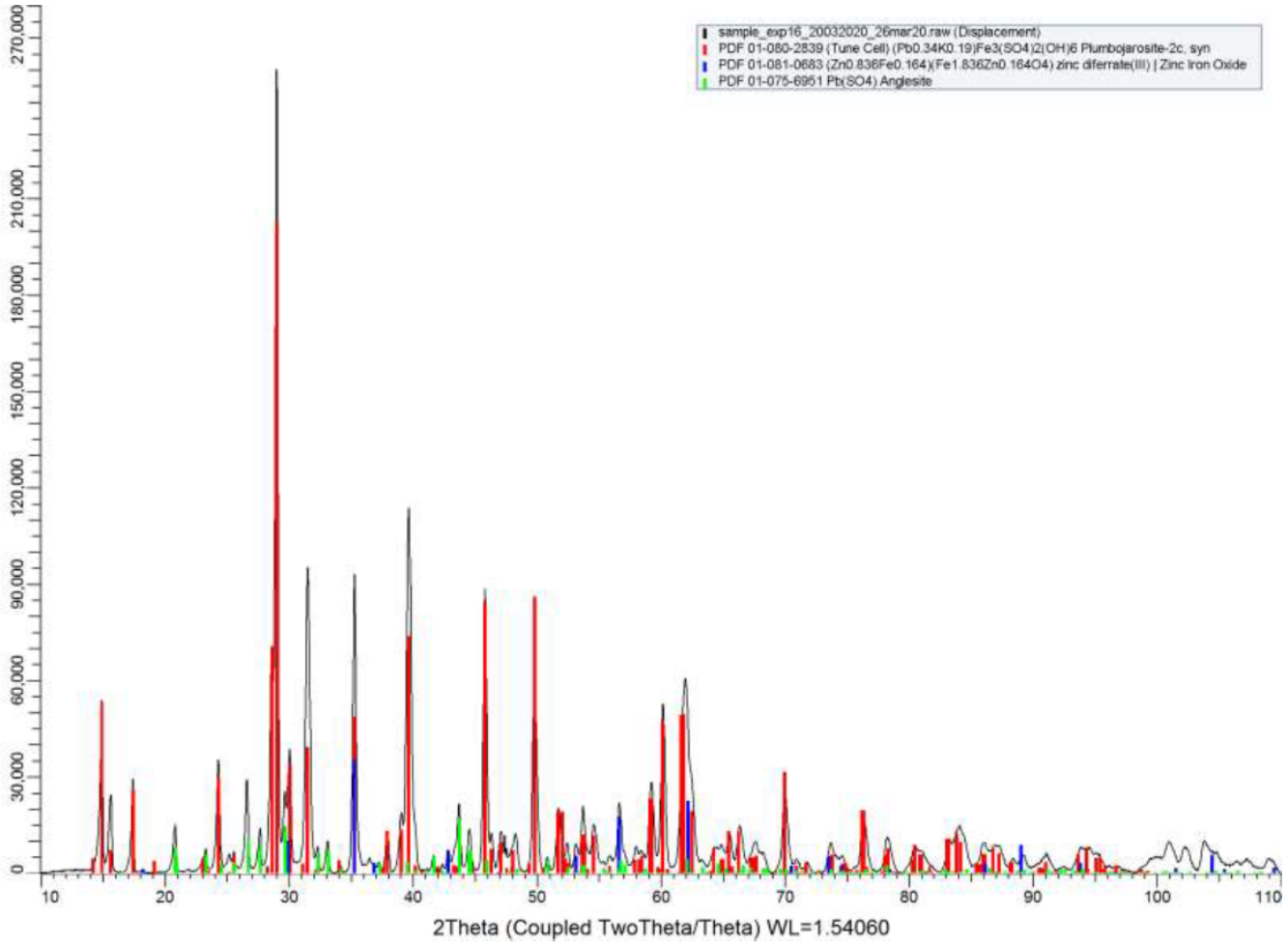

Figure A.6: XRD of residue BLP leached with 0.5M HCl, 50°C, 2hrs, 300 RPM

.

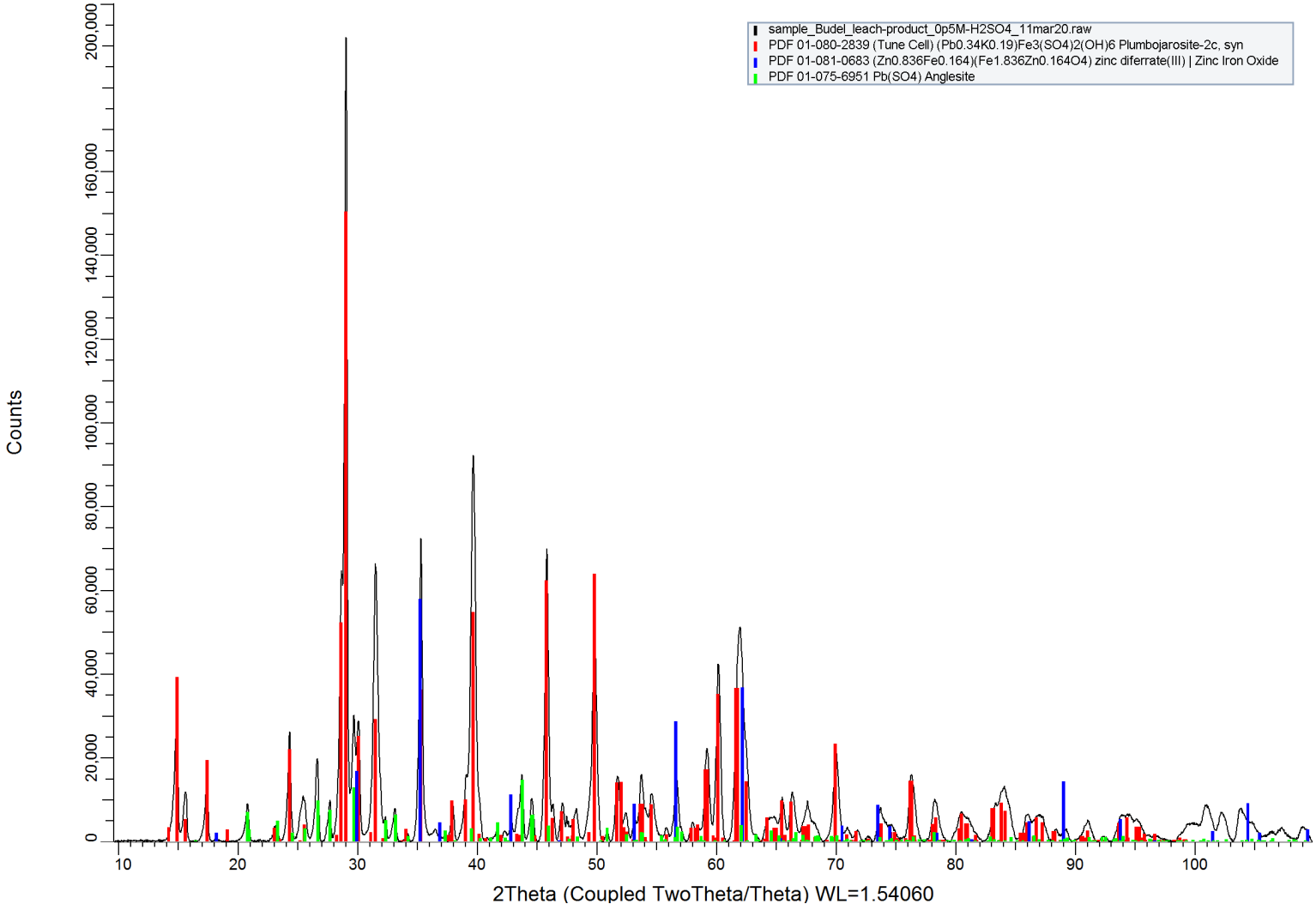

Figure A.7: XRD of residue BLP leached with 0.5M H_2SO_4, 50°C, 2hrs, 300 RPM

.

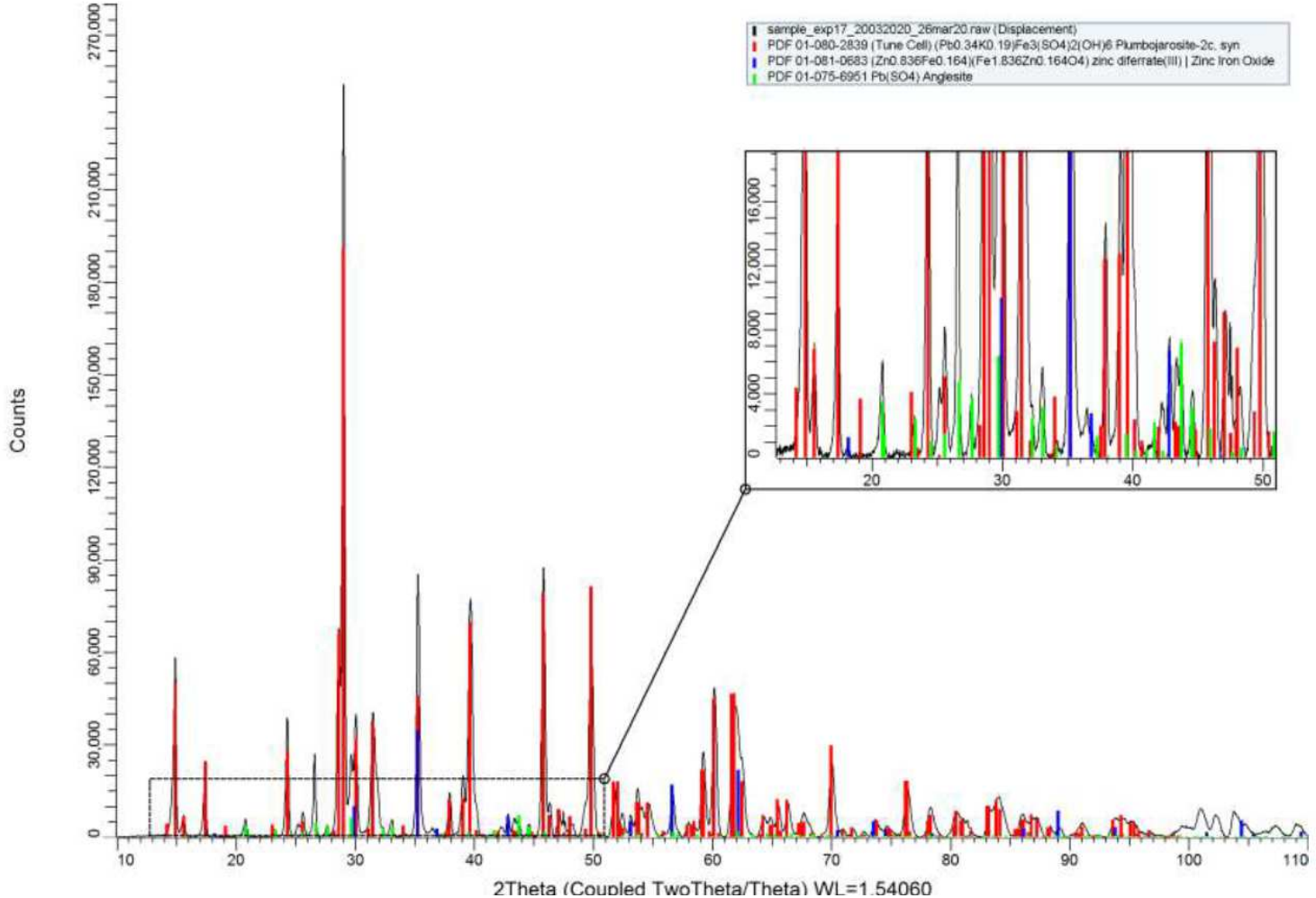

Figure A.8: XRD of residue BLP leached with 0.5M acetic acid, 50°C, 2hrs, 300 RPM

.

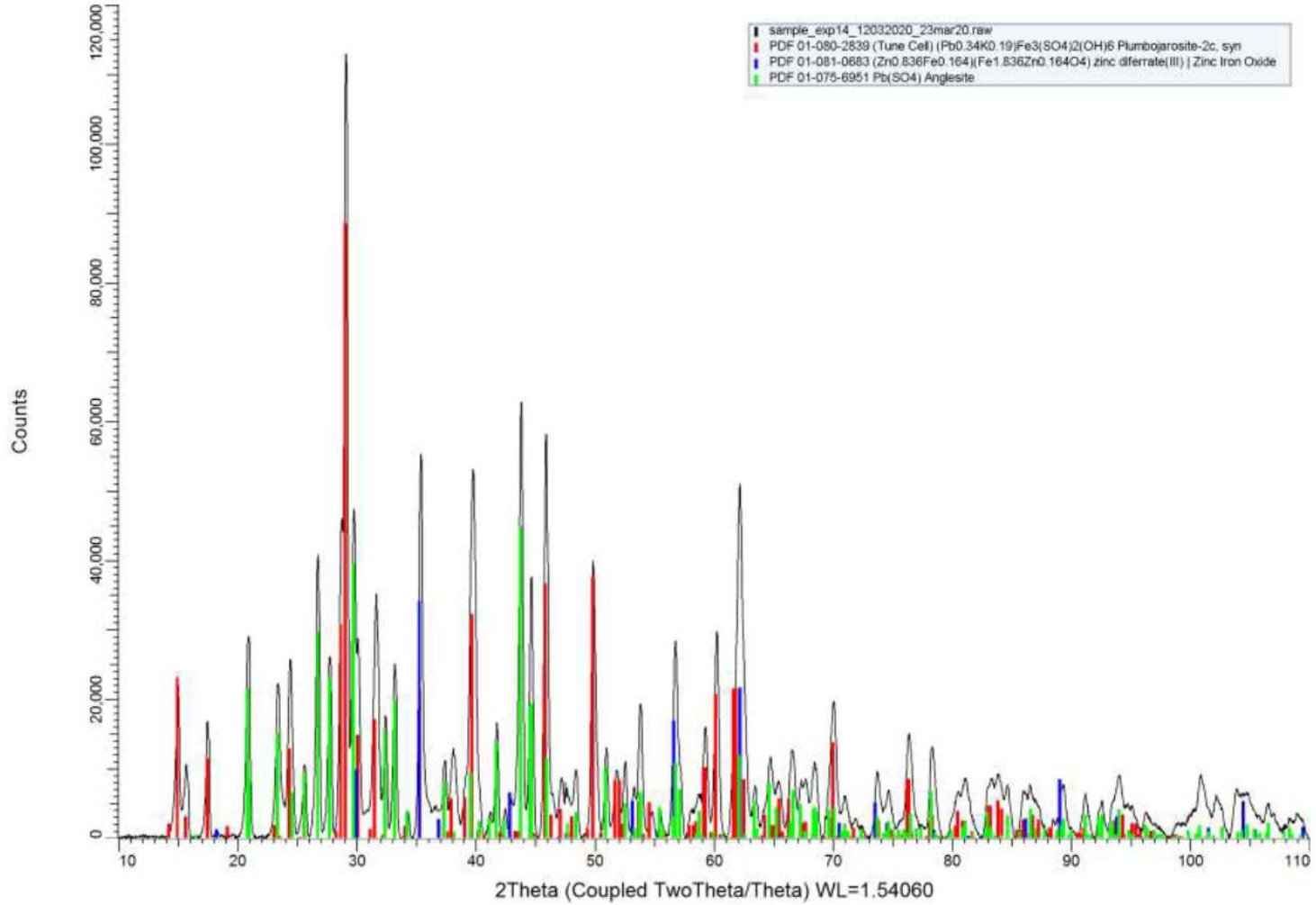

Figure A.9: XRD of residue BLP leached with 0.5M oxalic acid, 50°C, 2hrs, 300 RPM

.

A.2. Alkaline Leaching

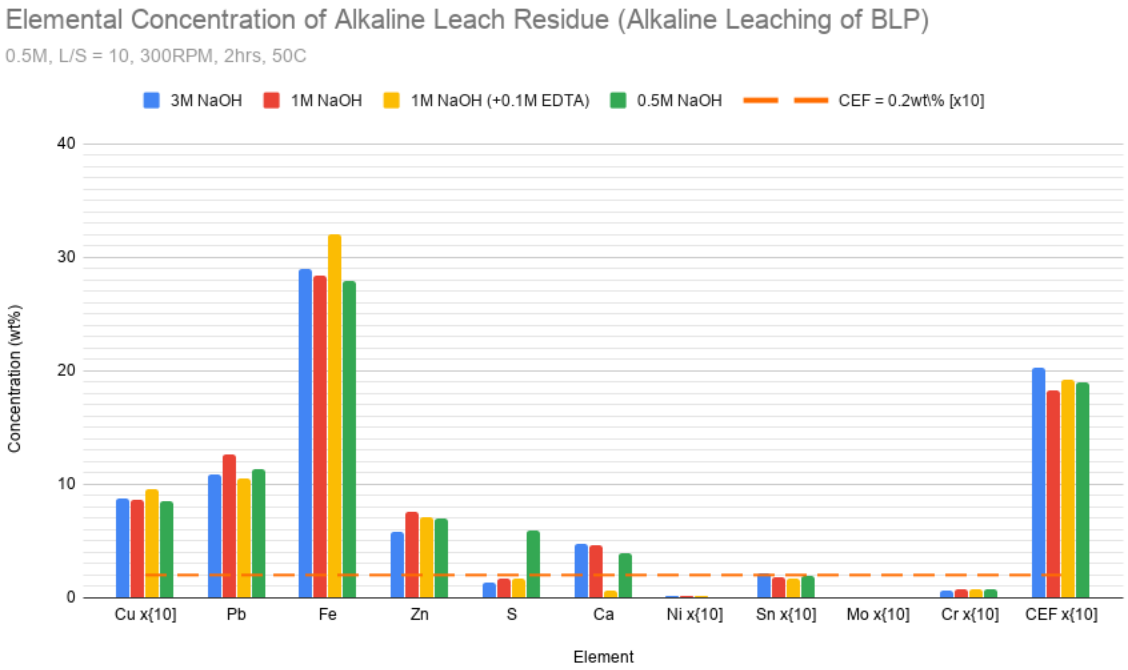

Figure A.10: Elemental composition of leach residue from alkaline leaching of BLP. L/S=10, Temp = 50°C, duration = 2hrs, conc = 0.5M, RPM = 300

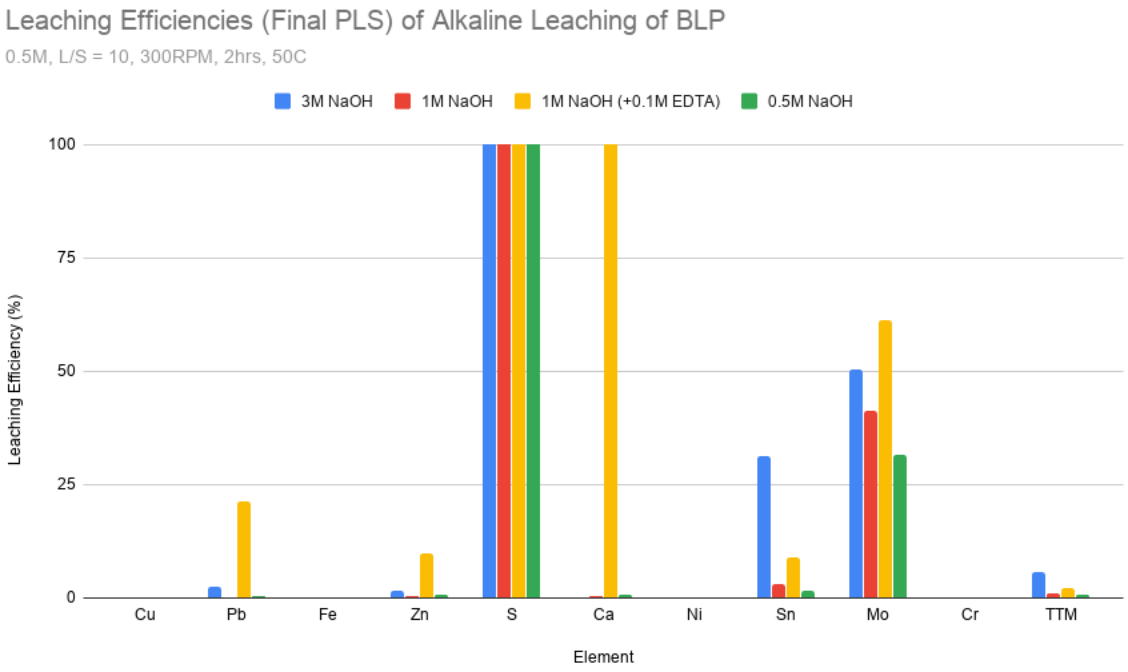

Figure A.11: Leaching efficiency of elements in final PLS from alkaline leaching of BLP. L/S=10, Temp = 50°C, duration = 2hrs, conc = 0.5M, RPM = 300

A.2.1. Leach Residue XRD

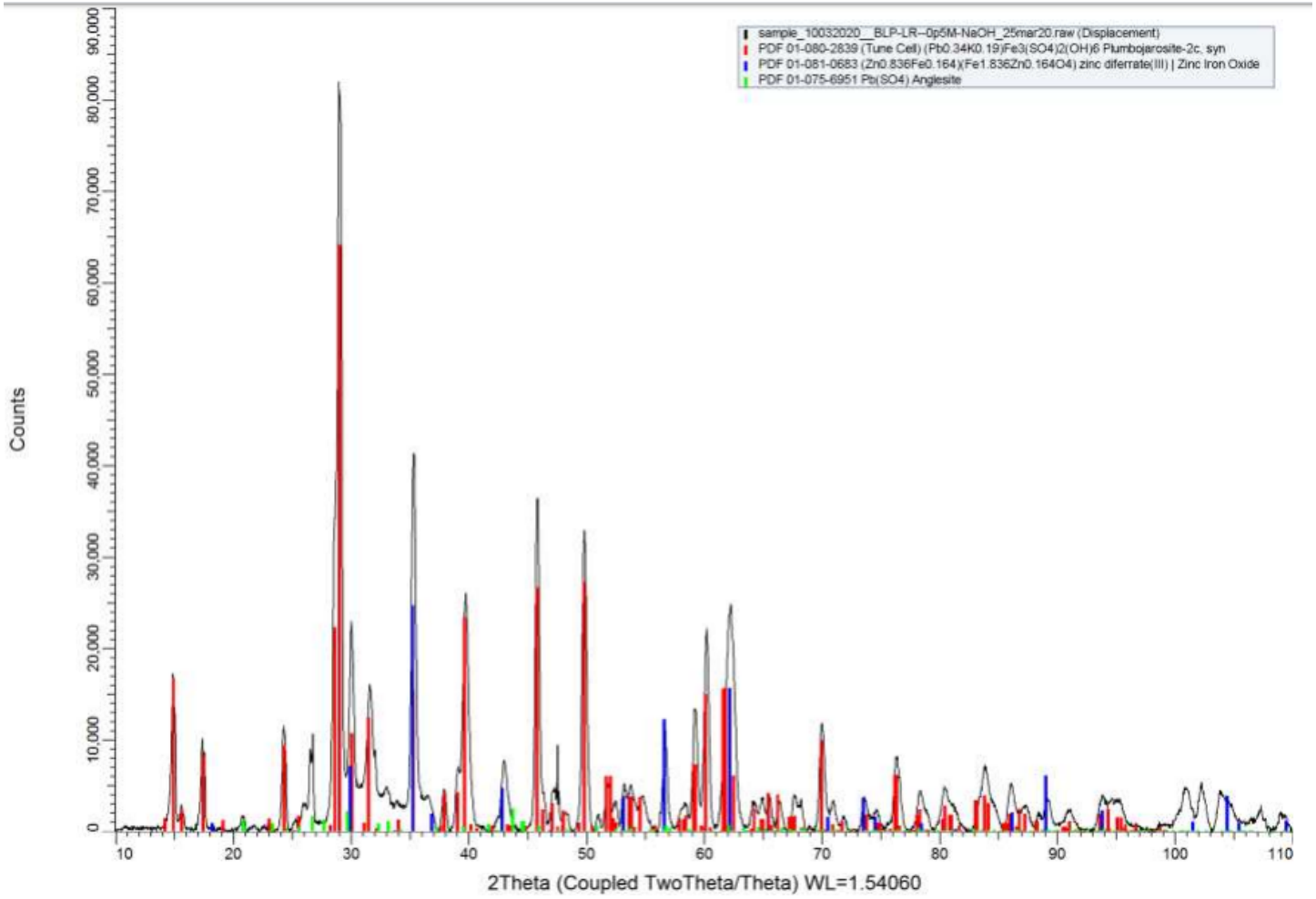

Figure A.12: XRD of BLP leach residue: 0.5M NaOH, Time = 2hrs, L/S=10, 300RPM, Temp = 50°C. Phases indicated include plumbojarosite, zinc iron oxide, lead sulfate

.

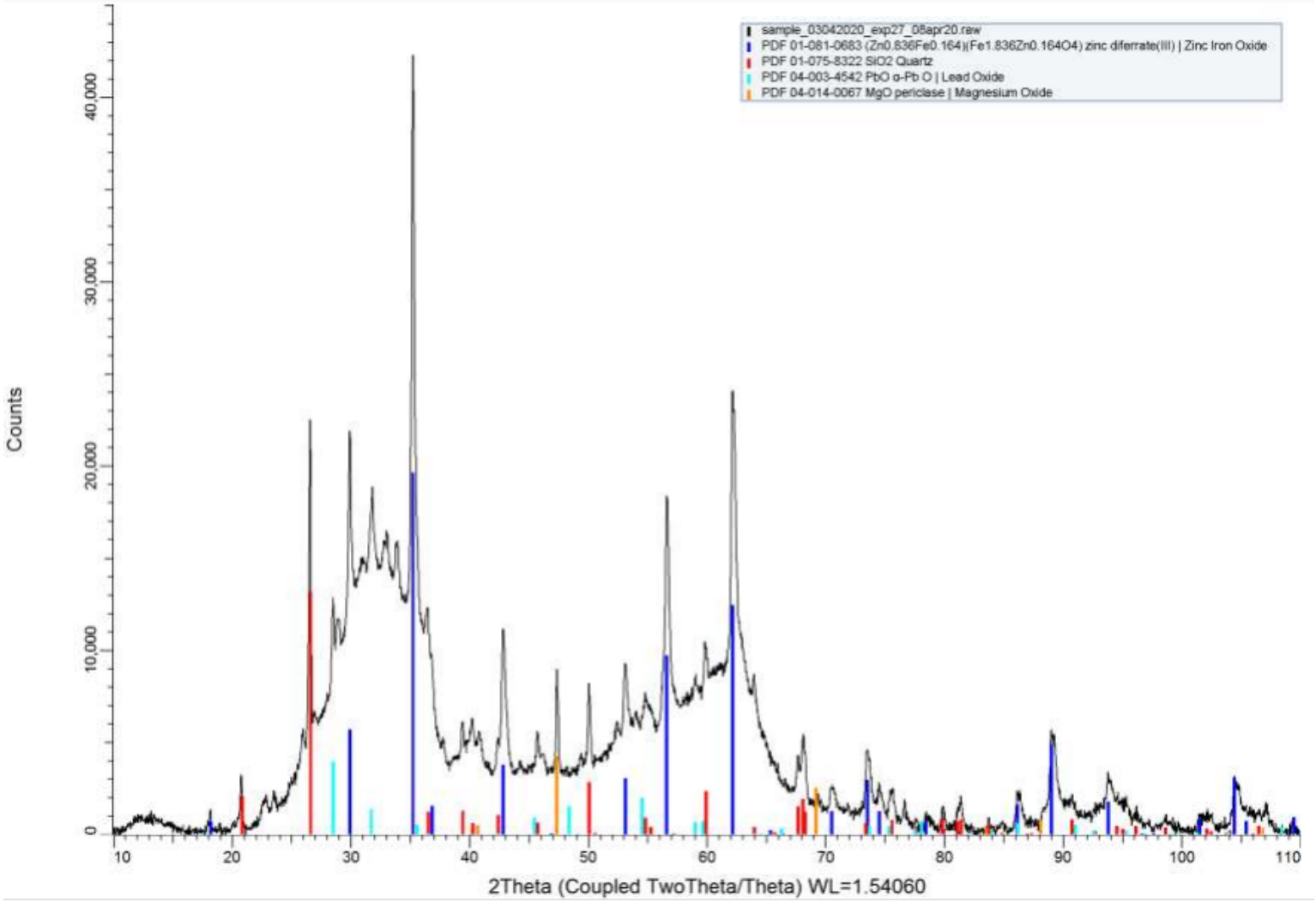

Figure A.13: XRD of BLP leach residue: 1M NaOH, Time = 2hrs, L/S=10, 300RPM, Temp = 50°C. Phases indicated include quartz, zinc iron oxide, lead oxide, magnesium oxide

.

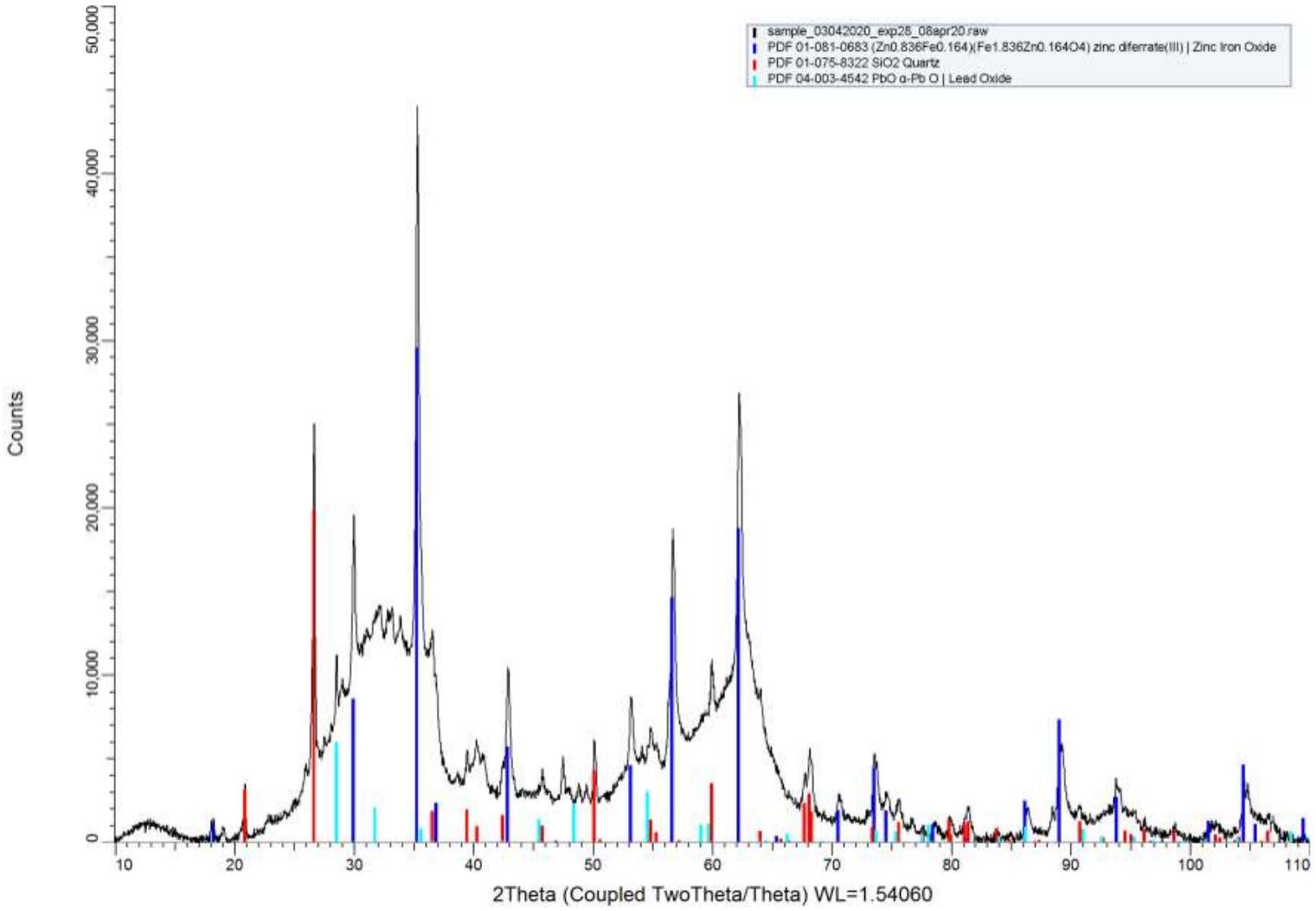

Figure A.14: XRD of BLP leach residue: 1M NaOH + 0.1M EDTA, Time = 2hrs, L/S=10, 300RPM, Temp = 50°C. Phases indicated include quartz, zinc iron oxide, lead oxide

.

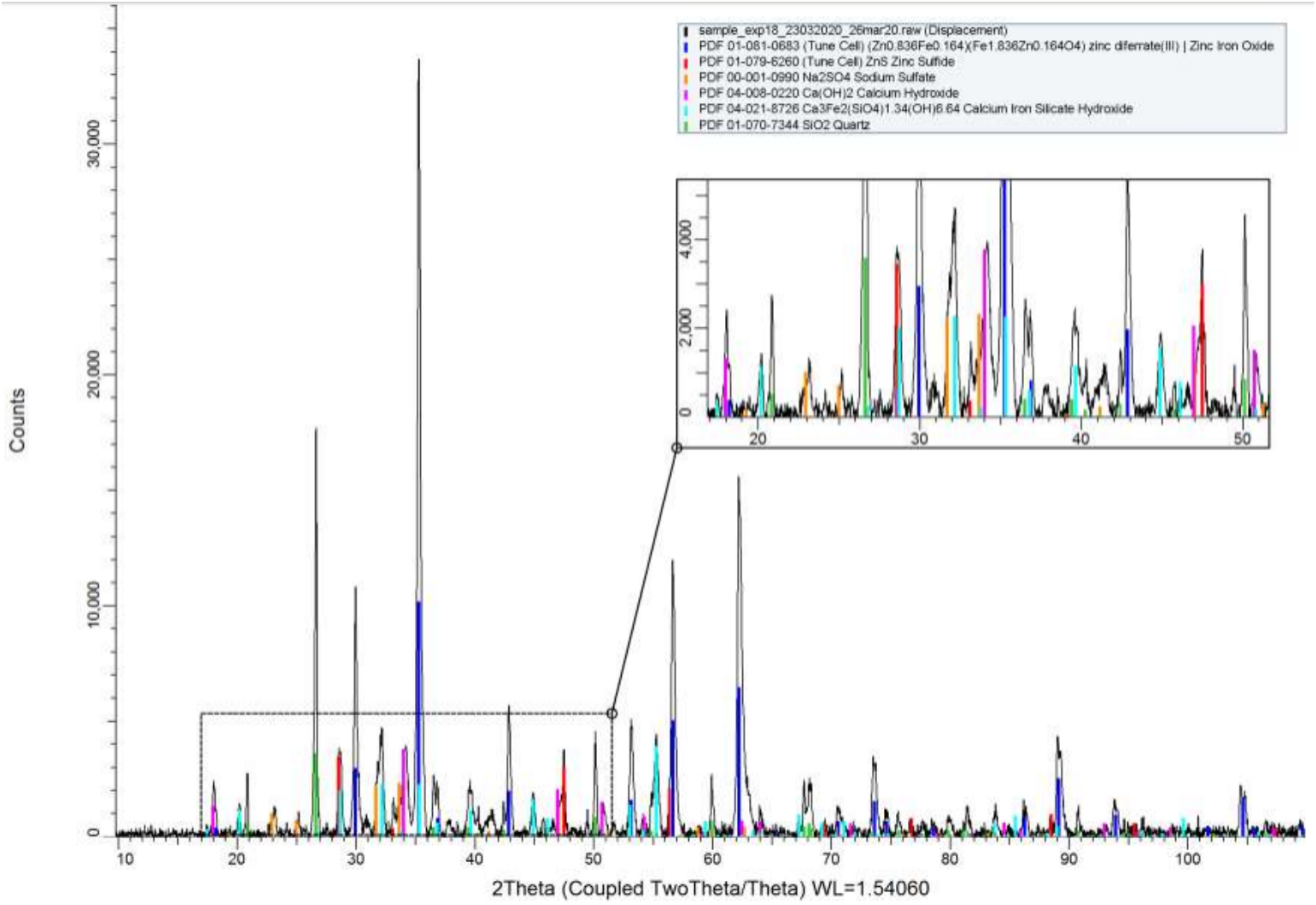

Figure A.15: XRD of BLP leach residue: 3M NaOH, Time = 2hrs, L/S=10, 300RPM, Temp = 50°C. Phases indicated include zinc sulfide, zinc iron oxide, sodium sulfate, calcium hydroxide, quartz, calcium iron silicate hydroxide

.

A.3. Ammoniacal Leaching

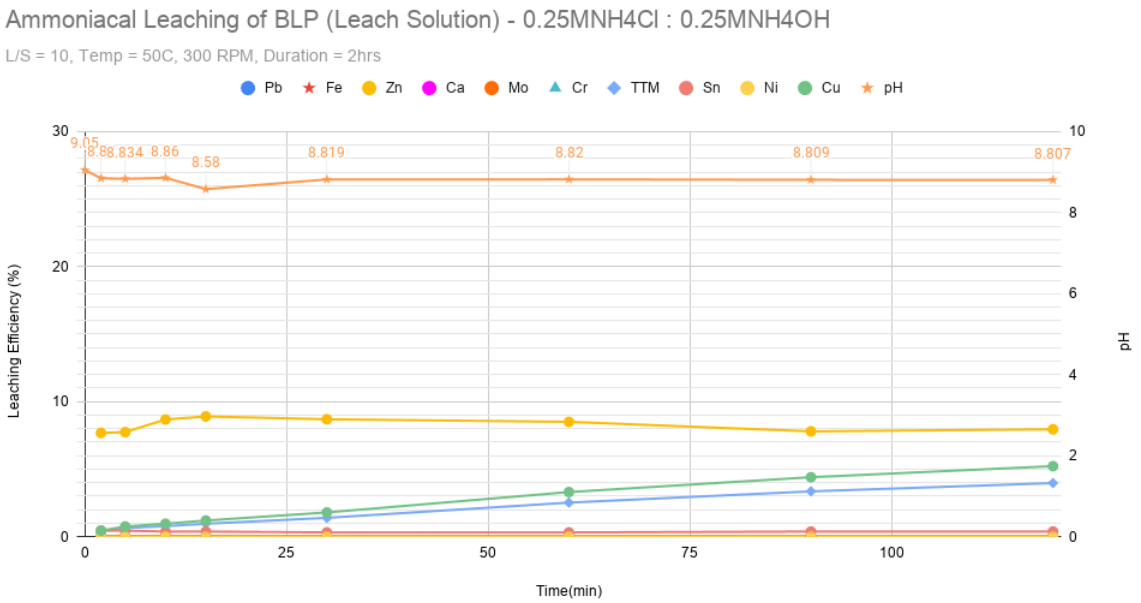

Figure A.16: Elemental leaching efficiencies of BLP leached with 0.25M NH_4Cl: 0.25M NH_4OH, 50°C, 300 RPM, Duration = 2hrs, L/S = 10

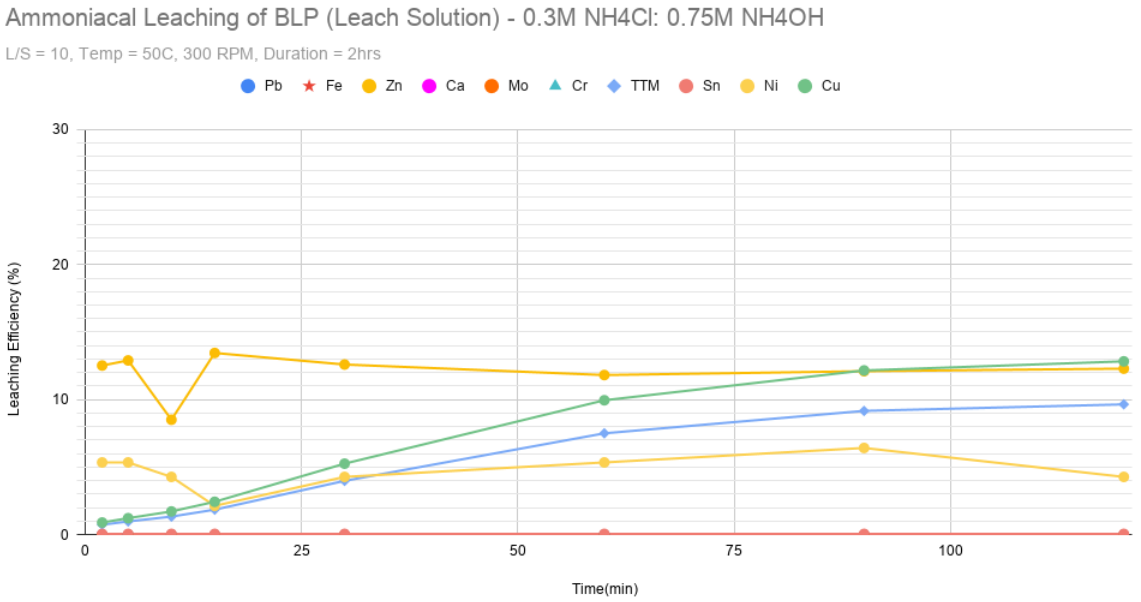

Figure A.17: Elemental leaching efficiencies of BLP leached with 0.30M NH_4Cl: 0.75M NH_4OH, 50°C, 300 RPM, Duration = 2hrs, L/S = 10

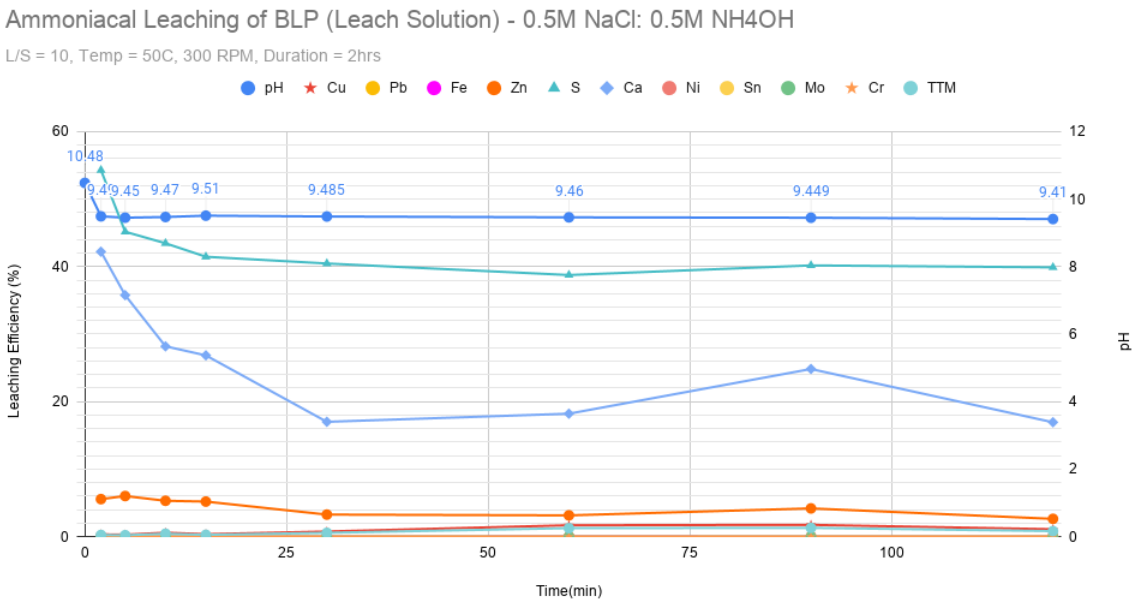

Figure A.18: Elemental leaching efficiencies of BLP leached with 0.5M NaCl: 0.50M NH_4OH, 50°C, 300 RPM, Duration = 2hrs, L/S = 10

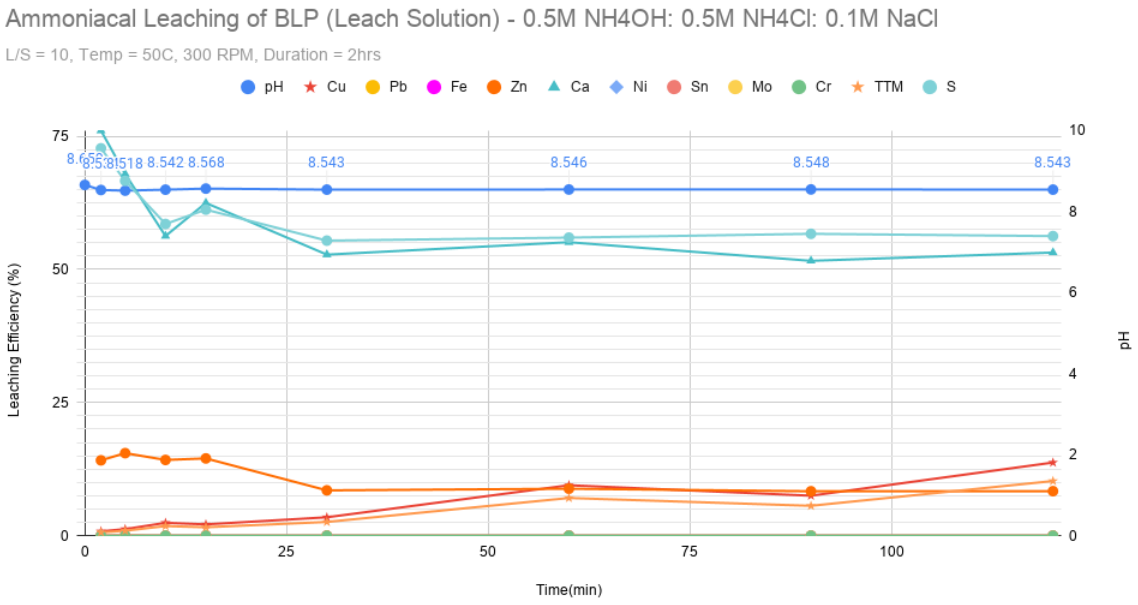

Figure A.19: Elemental leaching efficiencies of BLP leached with 0.5M NH_4Cl: 0.50M NH_4OH: 0.1M NaCl, 50°C, 300 RPM, Duration = 2hrs, L/S = 10

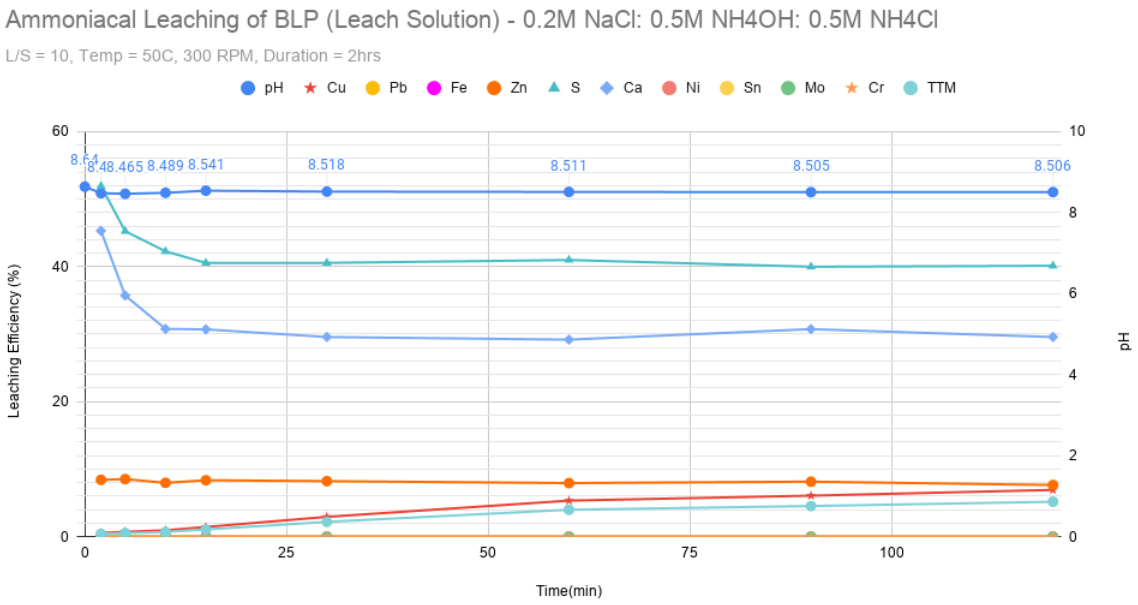

Figure A.20: Elemental leaching efficiencies of BLP leached with 0.5M NH_4Cl: 0.50M NH_4OH: 0.2M NaCl, 50°C, 300 RPM, Duration = 2hrs, L/S = 10

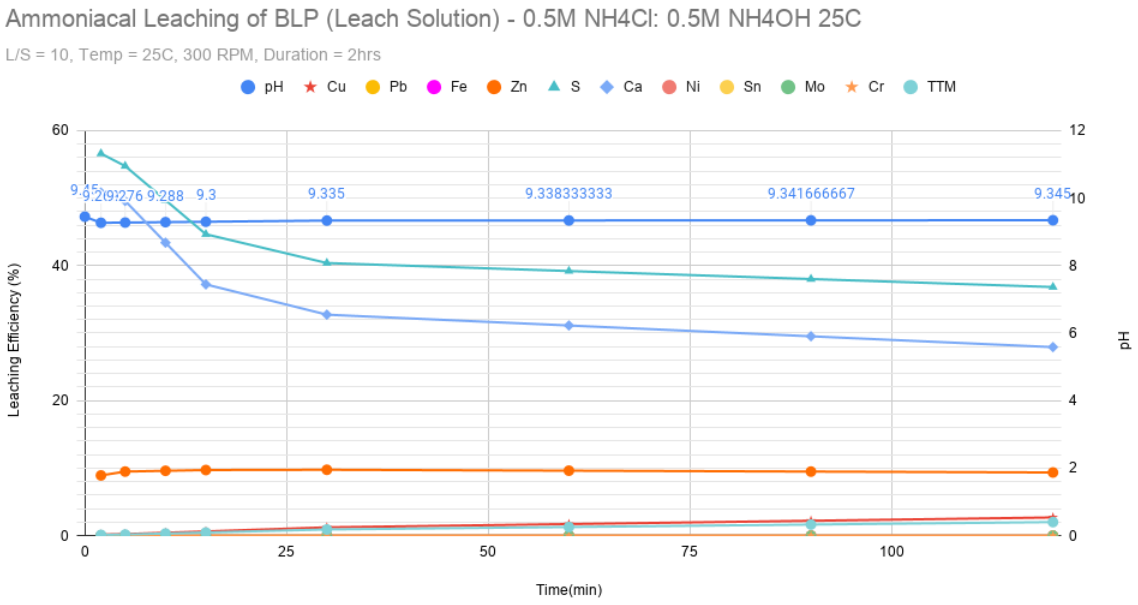

Figure A.21: Elemental leaching efficiencies of BLP leached with 0.5M NH_4Cl: 0.50M NH_4OH, 25°C, 300 RPM, Duration = 2hrs, L/S = 10

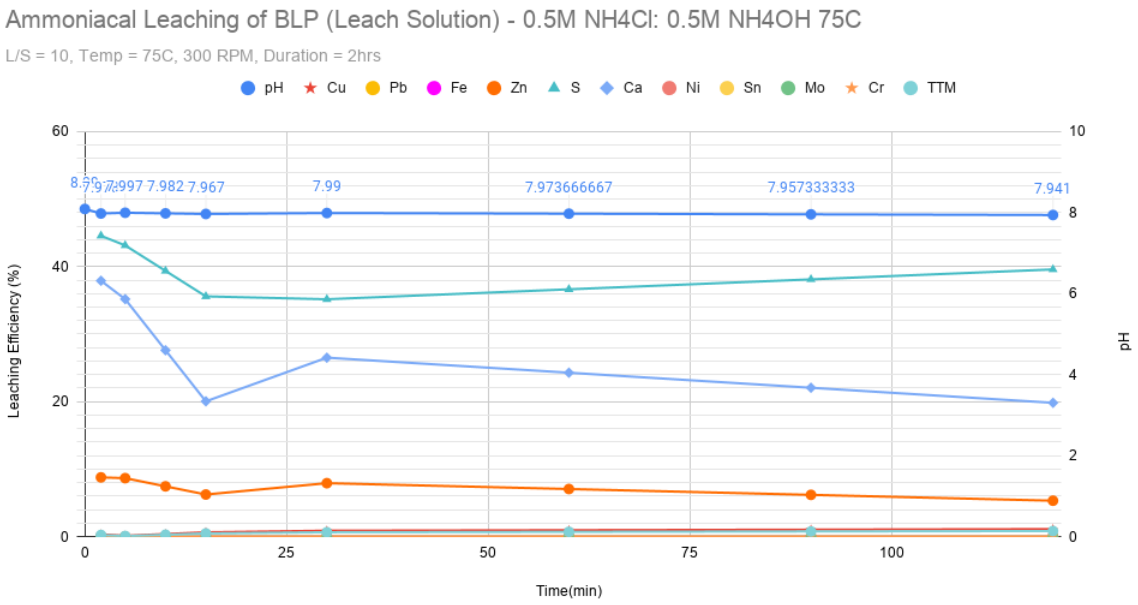

Figure A.22: Elemental leaching efficiencies of BLP leached with 0.5M NH_4Cl: 0.50M NH_4OH:, 75°C, 300 RPM, Duration = 2hrs, L/S = 10

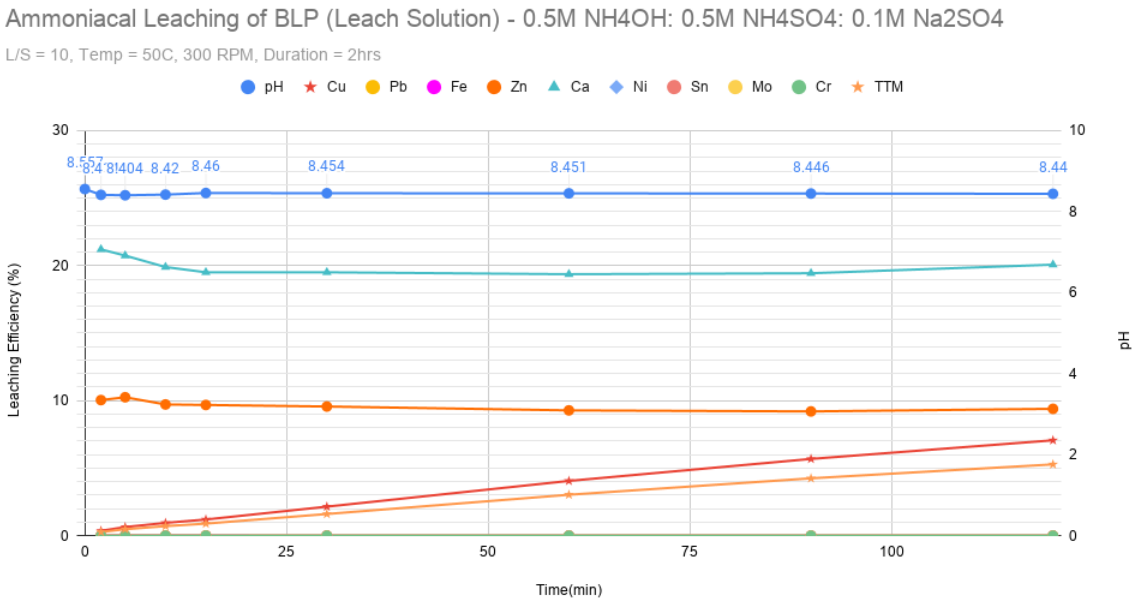

Figure A.23: Elemental leaching efficiencies of BLP leached with 0.5M NH_4SO_4: 0.50M NH_4OH: 0.1M Na_2SO_4, 50°C, 300 RPM, Duration = 2hrs, L/S = 10

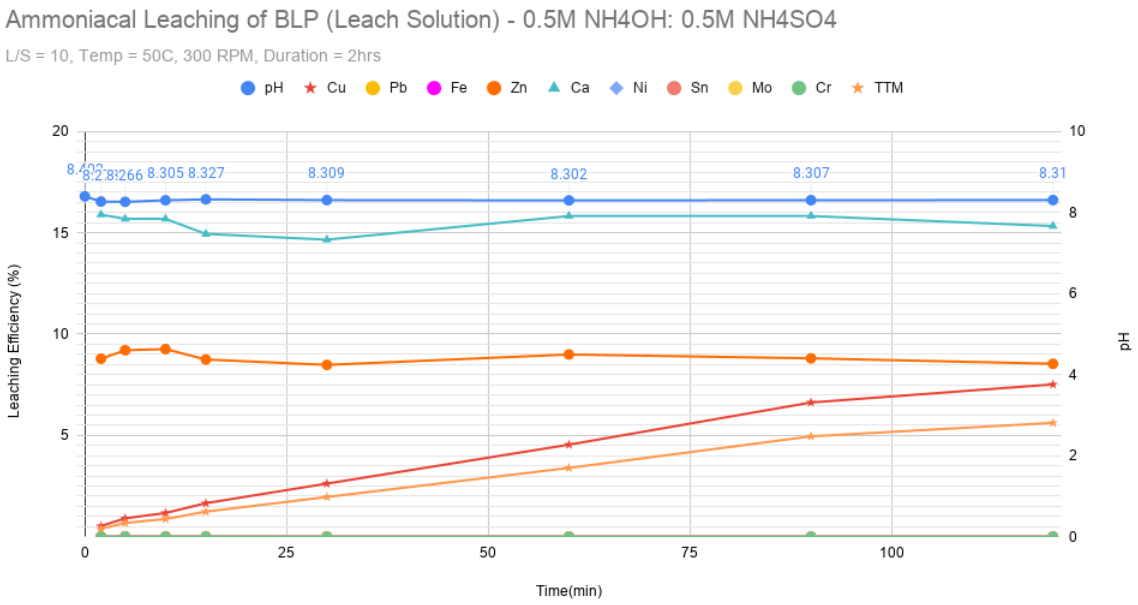

Figure A.24: Elemental leaching efficiencies of BLP leached with 0.5M NH_4SO_4: 0.50M NH_4OH, 50°C, 300 RPM, Duration = 2hrs, L/S = 10

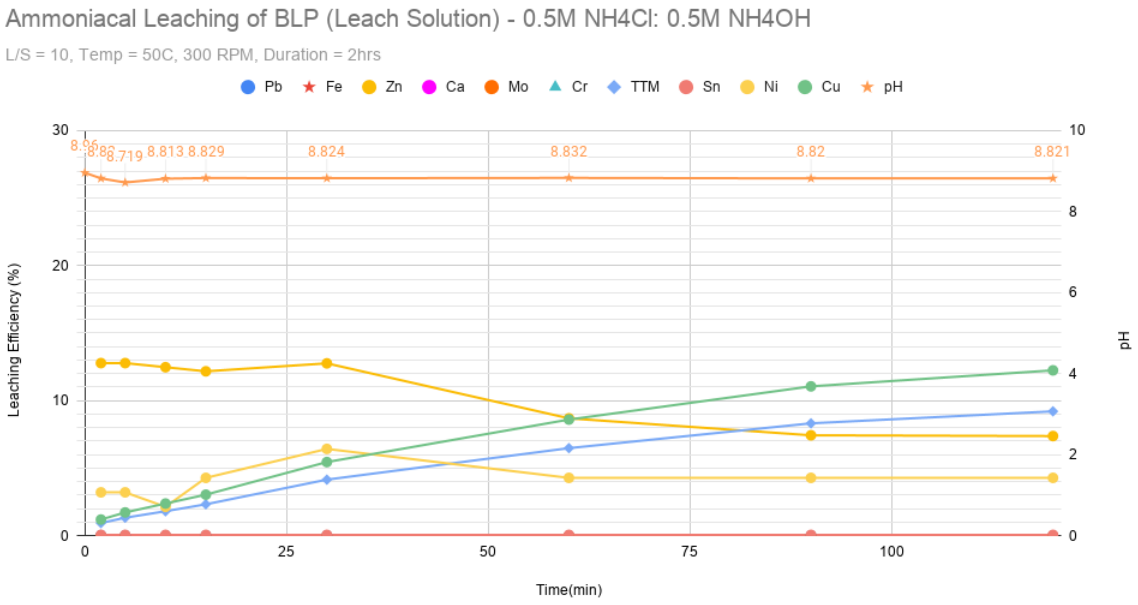

Figure A.25: Elemental leaching efficiencies of BLP leached with 0.5M NH_4Cl: 0.50M NH_4OH, 50°C, 300 RPM, Duration = 2hrs, L/S = 10

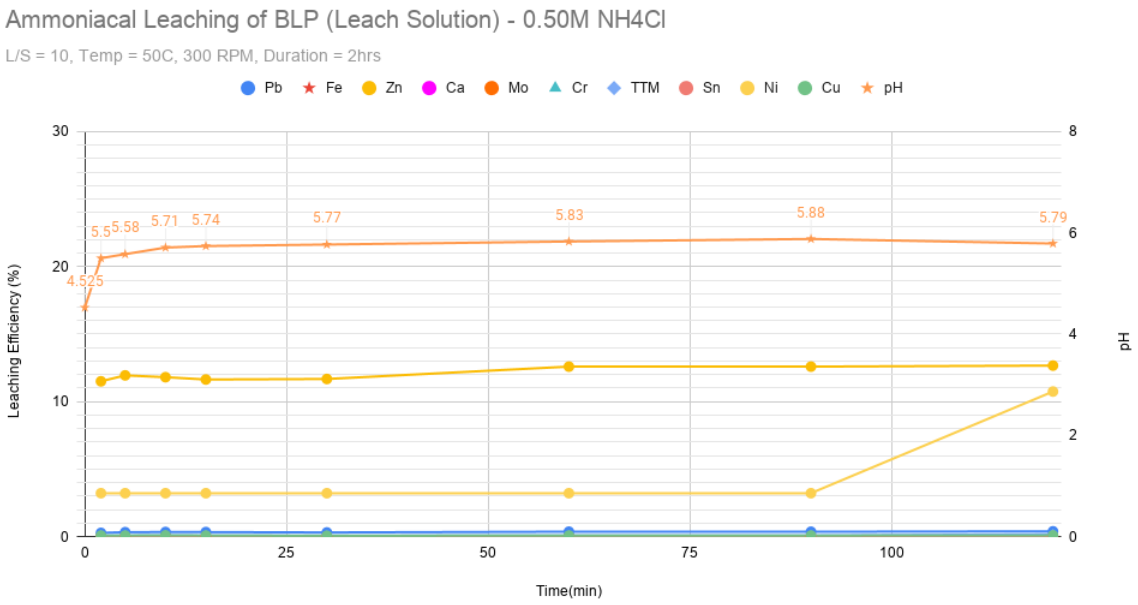

Figure A.26: Elemental leaching efficiencies of BLP leached with 0.5M NH_4Cl, 50°C, 300 RPM, Duration = 2hrs, L/S = 10

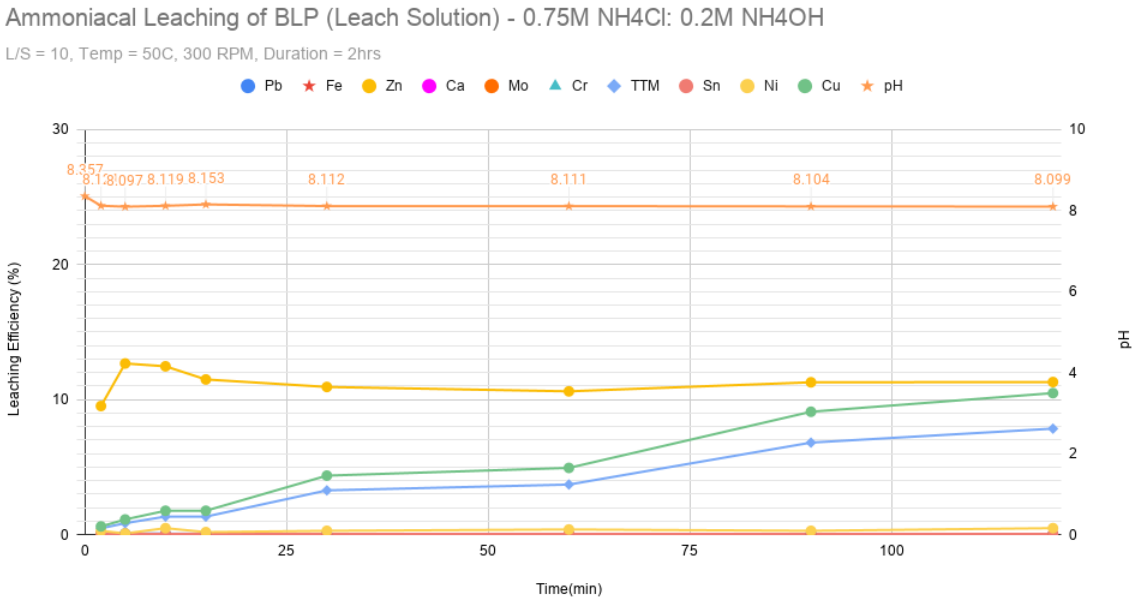

Figure A.27: Elemental leaching efficiencies of BLP leached with 0.75M NH_4Cl: 0.2M NH_4OH, 50°C, 300 RPM, Duration = 2hrs, L/S = 10

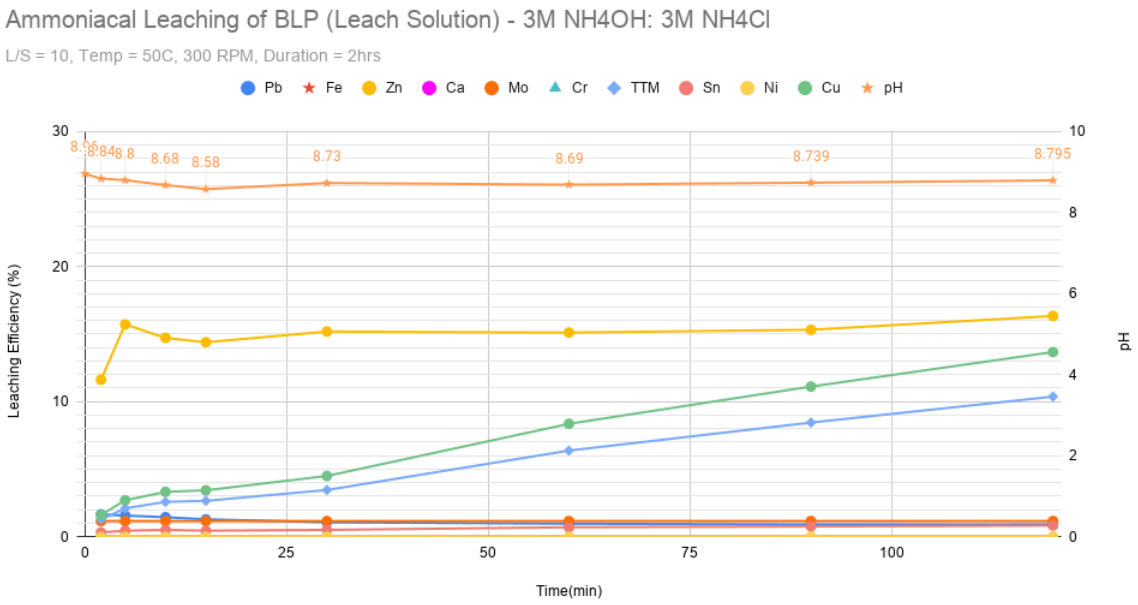

Figure A.28: Elemental leaching efficiencies of BLP leached with 3M NH_4Cl: 3M NH_4OH, 50°C, 300 RPM, Duration = 2hrs, L/S = 10

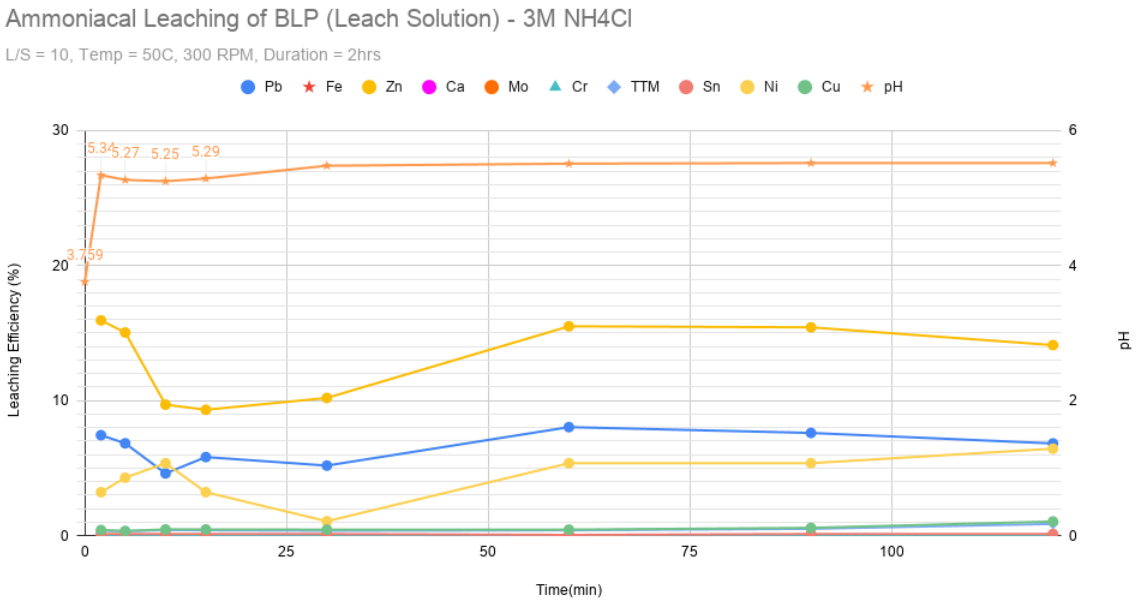

Figure A.29: Elemental leaching efficiencies of BLP leached with 3M NH_4Cl, 50°C, 300 RPM, Duration = 2hrs, L/S = 10

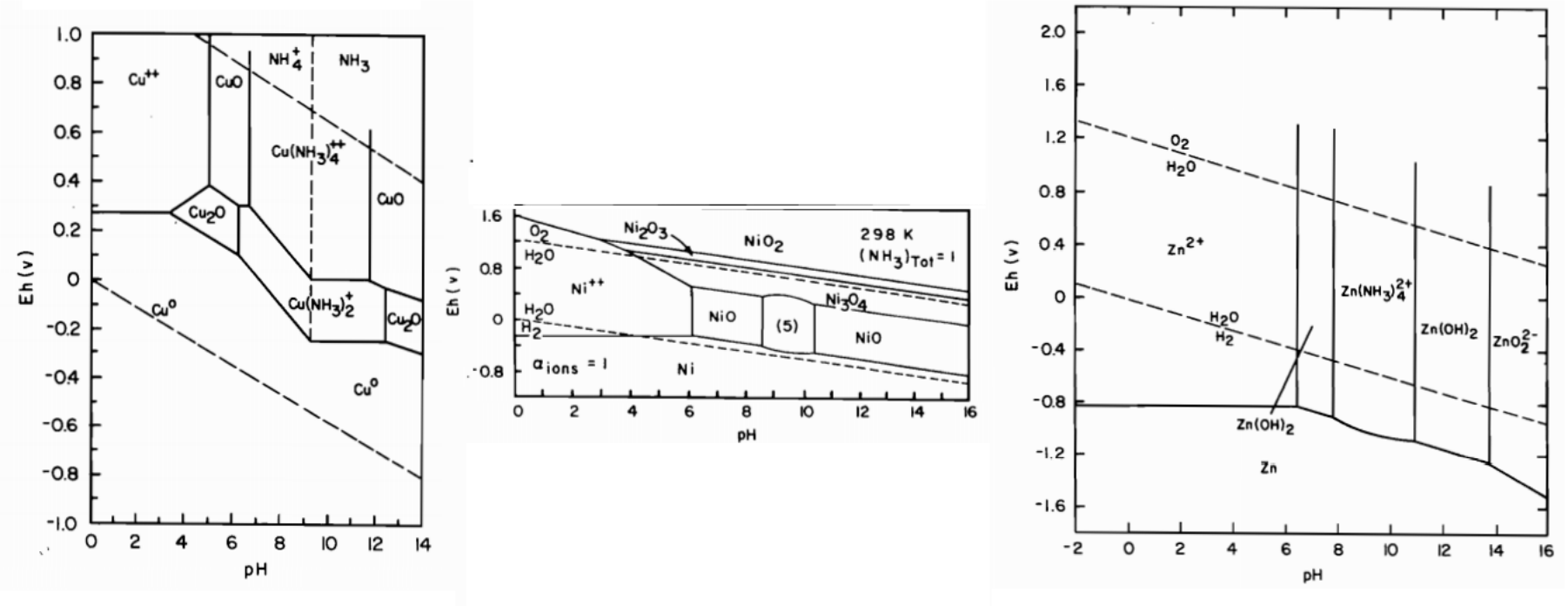

Figure A.30: Pourbaix diagrams for Me-NH_3-H_2O at 25°C. (Left) Cu (middle) Ni, 5 = $Ni(NH_3)_6^{2+}$ (right) Zn

.

B

Pyrometallurgy

B.1. Thermal Decomposition

B.1.1. XRD

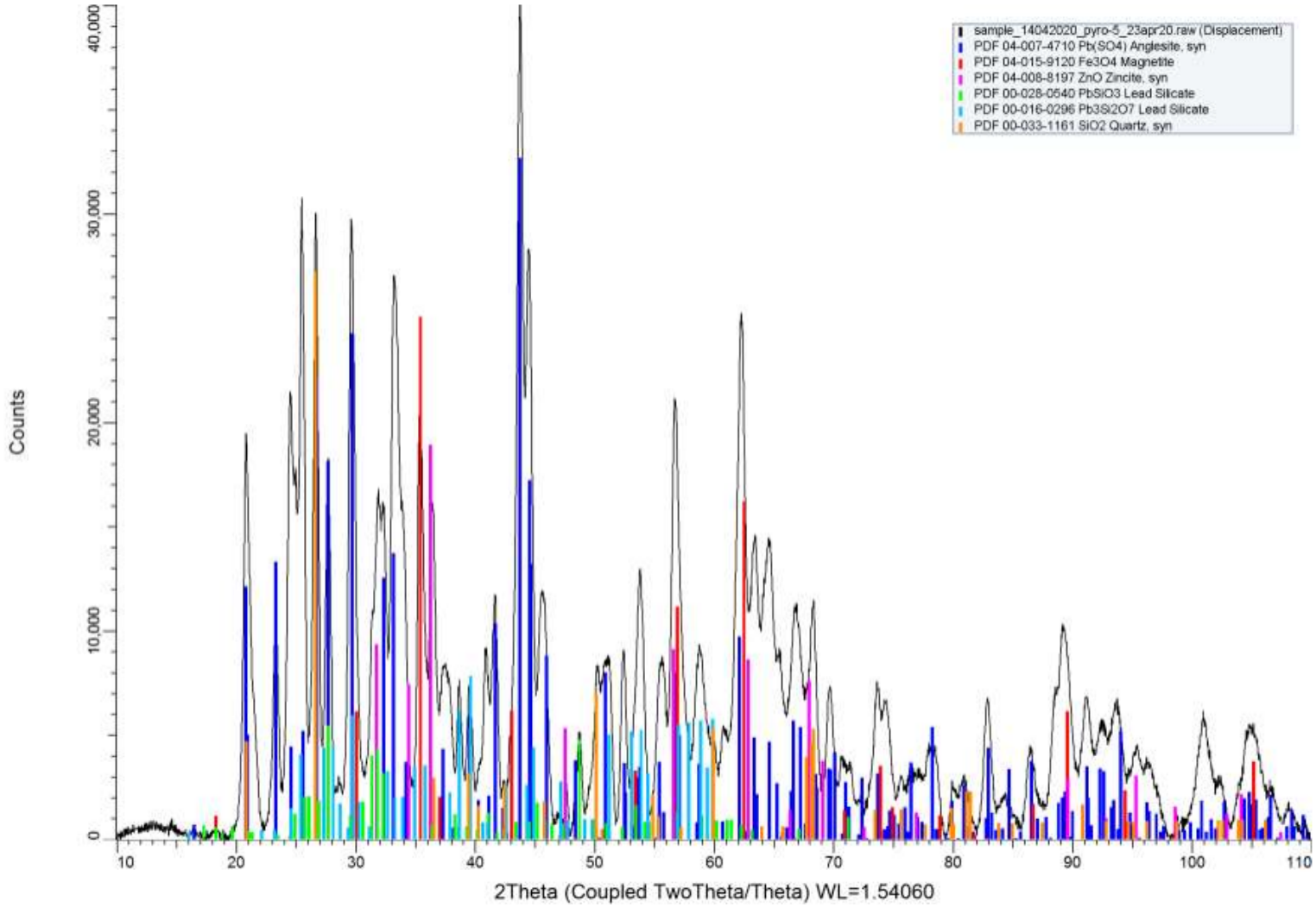

Figure B.1: XRD of decomposed BLP in horizontal furnace.Temperature = 500°C, mass approx 5g, duration = 15mins, inert atmosphere 0.5L/min N_2

.

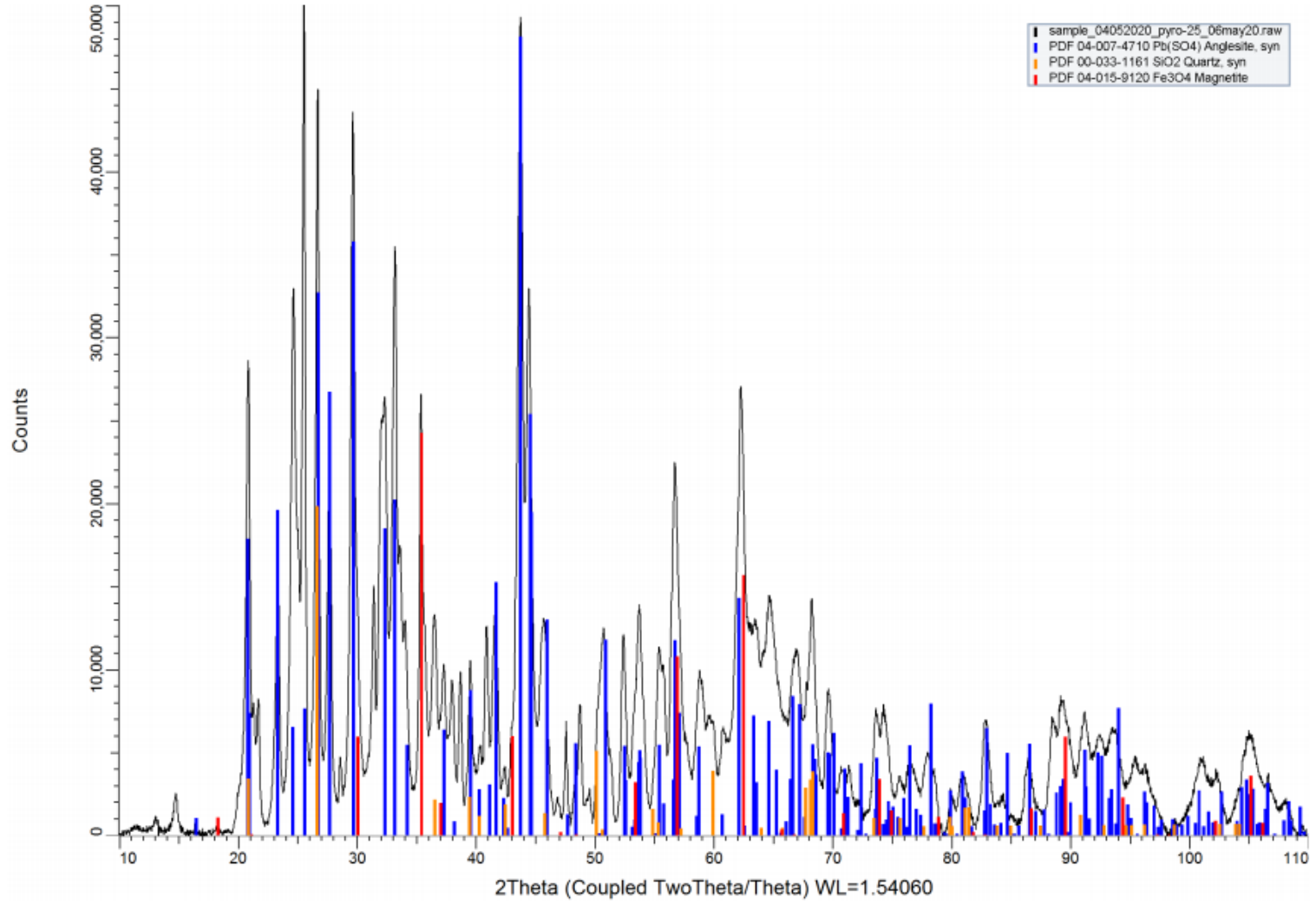

Figure B.2: XRD of decomposed BLP in horizontal furnace.Temperature = 500°C, mass approx 5g, duration = 30mins, inert atmosphere 0.5L/min N_2

.

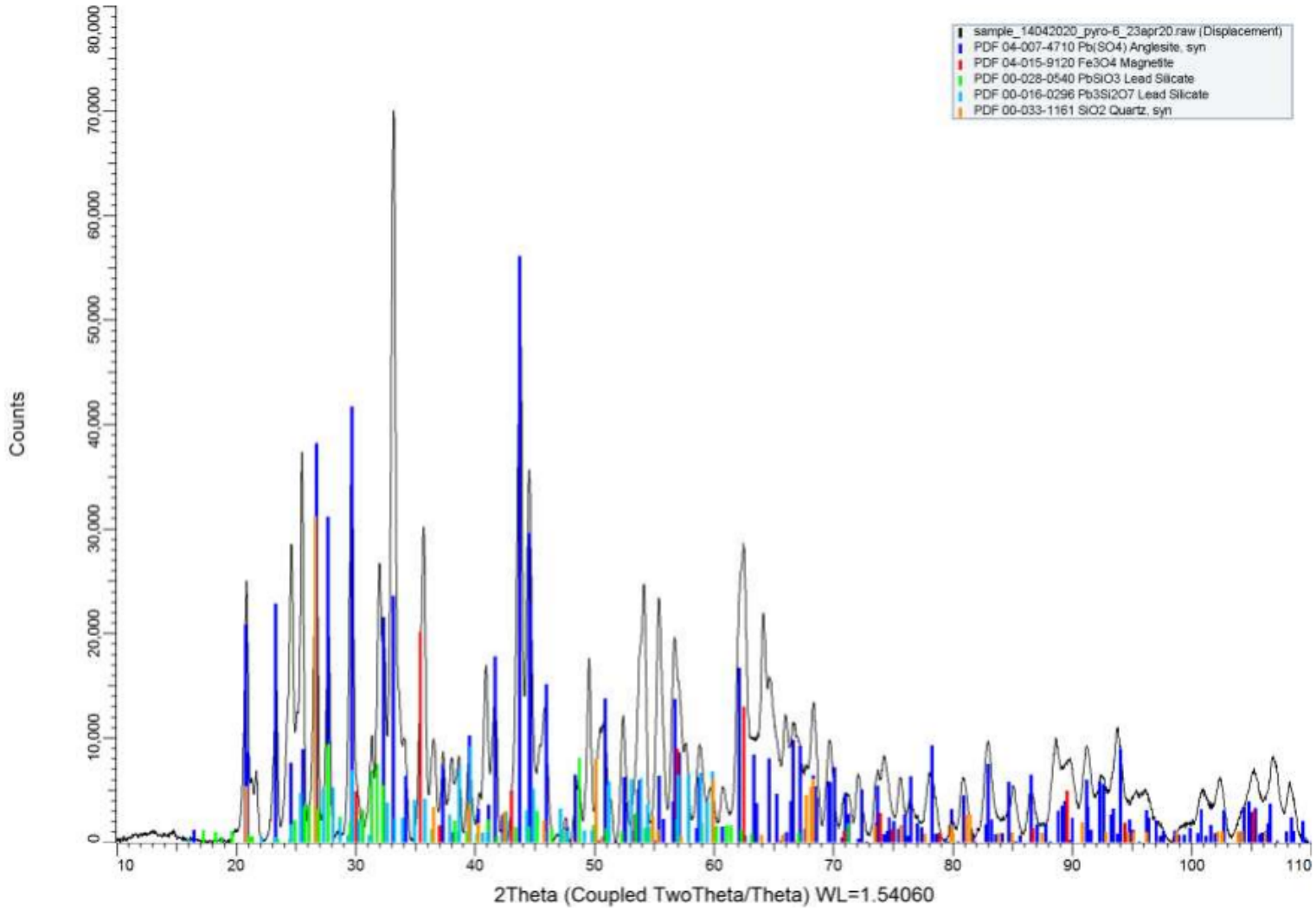

Figure B.3: XRD of decomposed BLP in horizontal furnace.Temperature = 600°C, mass approx 5g, duration = 15mins, inert atmosphere 0.5L/min N_2

.

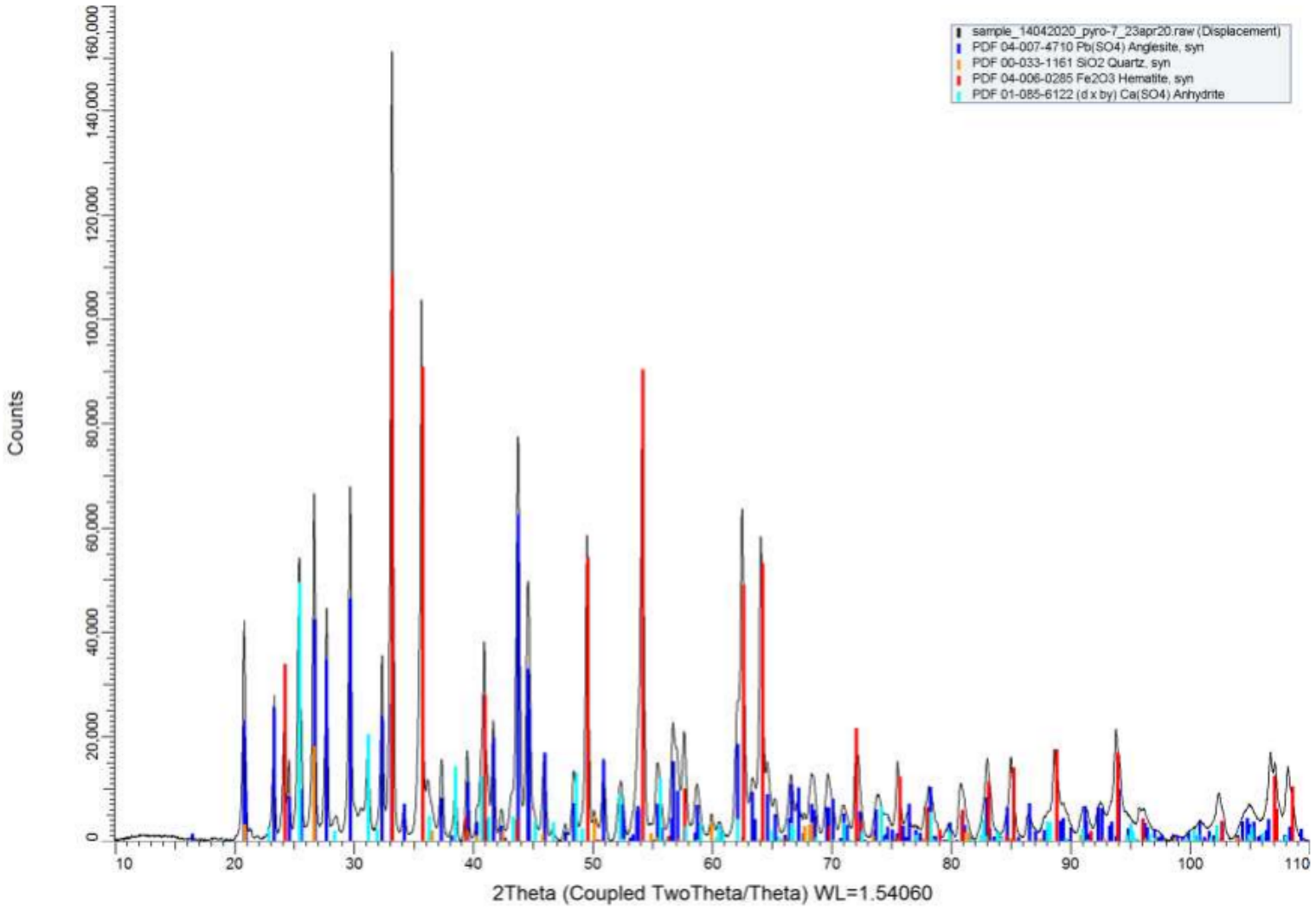

Figure B.4: XRD of decomposed BLP in horizontal furnace.Temperature = 700°C, mass approx 5g, duration = 15mins, inert atmosphere 0.5L/min N_2

.

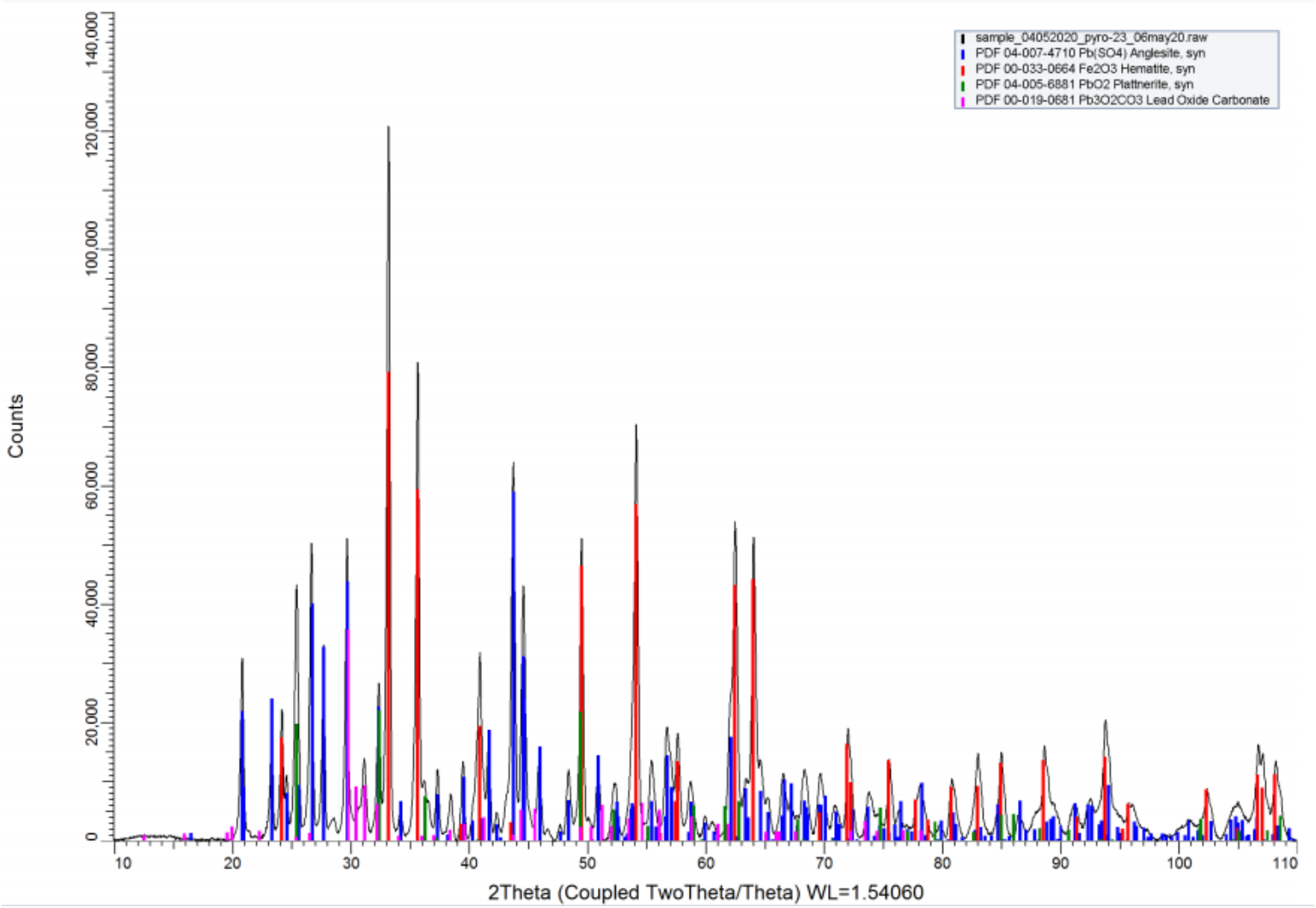

Figure B.5: XRD of decomposed BLP in horizontal furnace.Temperature = 700°C, mass approx 5g, duration = 30mins, inert atmosphere 0.5L/min N_2

.

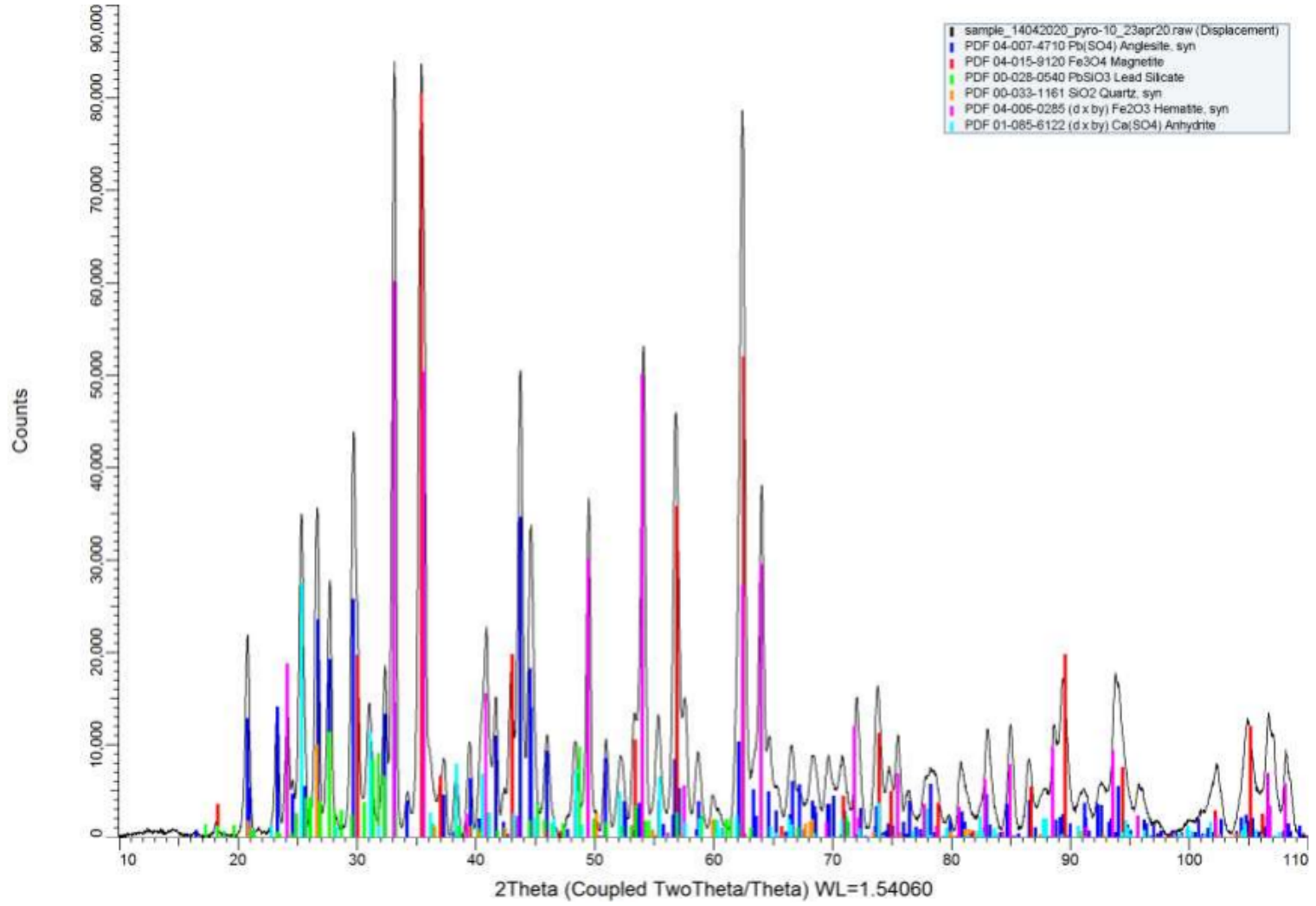

Figure B.6: XRD of decomposed BLP in horizontal furnace.Temperature = 800°C, mass approx 5g, duration = 15mins, inert atmosphere 0.5L/min N_2

.

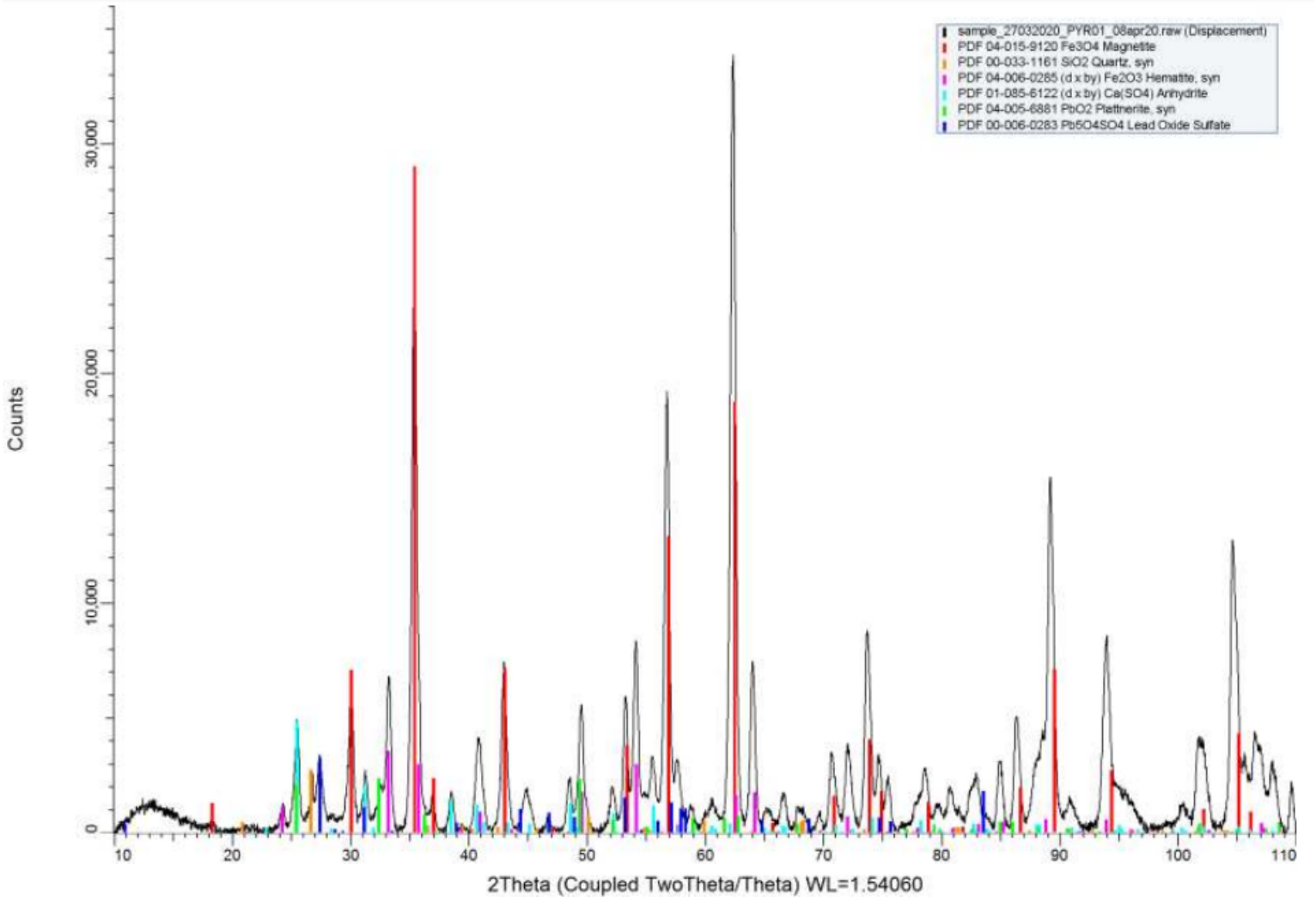

Figure B.7: XRD of decomposed BLP in horizontal furnace.Temperature = 1000°C (1), mass approx 5g, duration = 15mins, inert atmosphere 0.5L/min N_2

.

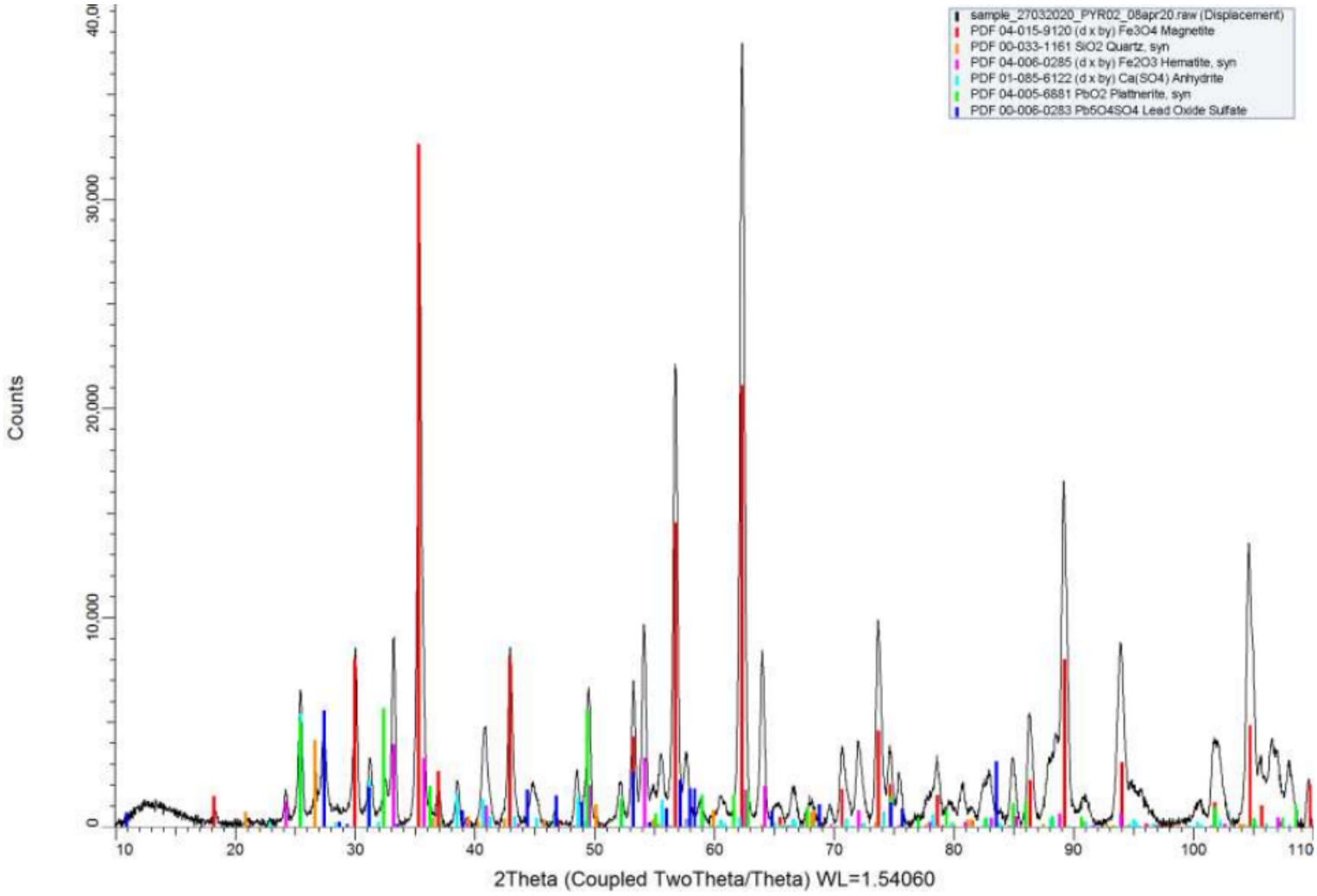

Figure B.8: XRD of decomposed BLP in horizontal furnace.Temperature = 1000°C (2), mass approx 5g, duration = 15mins, inert atmosphere 0.5L/min N_2

.

B.1.2. Mass Spec (Qualitative)

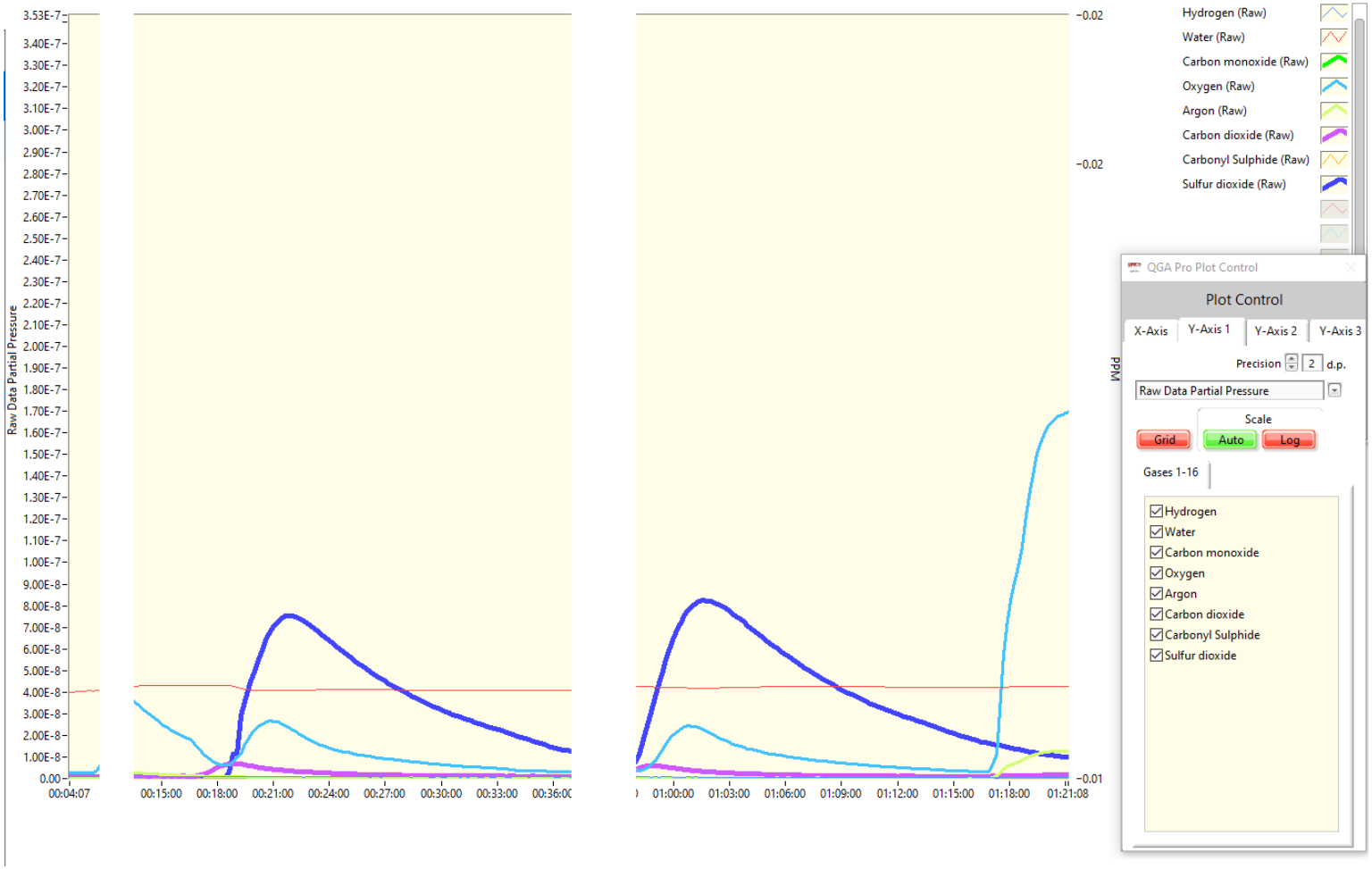

Figure B.9: Mass spec of BLP thermal decomposition reactions occurring at 1000°C (twice) showing evolution of SO_2 (dark blue line) and O_2(light blue)

.

B.2. Chloridisation

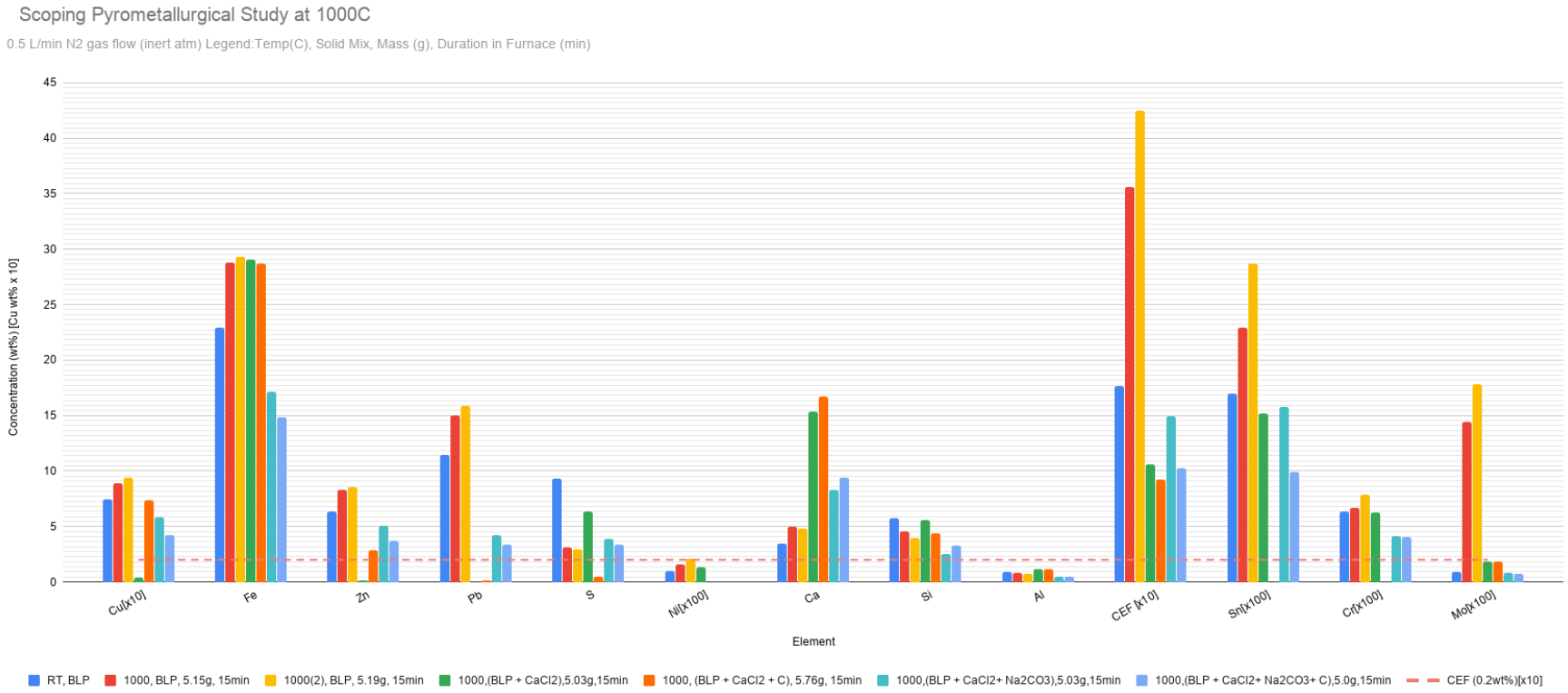

Figure B.10: Elemental composition of residual solid after BLP is mixed with $CaCl_2$, C, Na_2SO_4 heated at 1000 °C. This chart compares the sample directly to BLP and thermally decomposed BLP

.

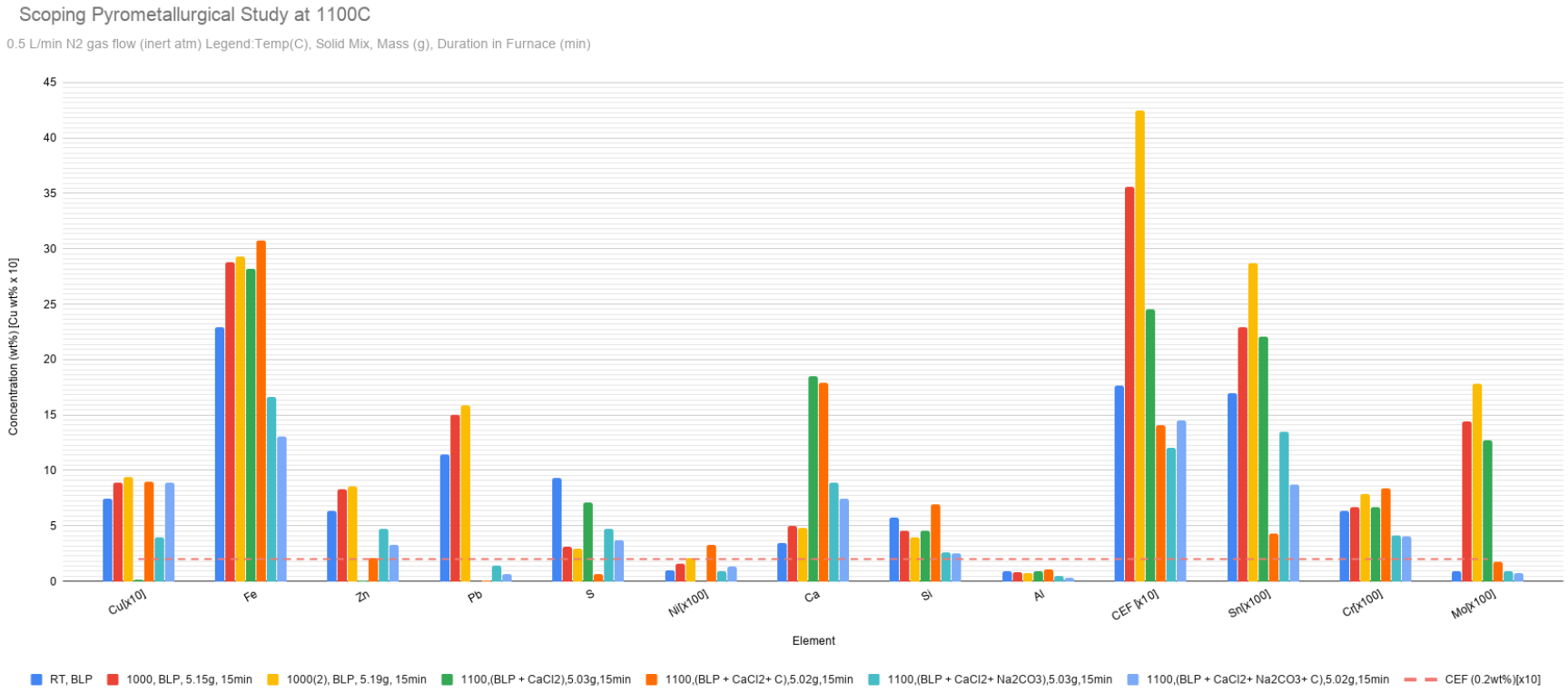

Figure B.11: Elemental composition of residual solid after BLP is mixed with $CaCl_2$, C, Na_2SO_4 heated at 1100 °C. This chart compares the sample directly to BLP and thermally decomposed BLP

.

B.2.1. XRD

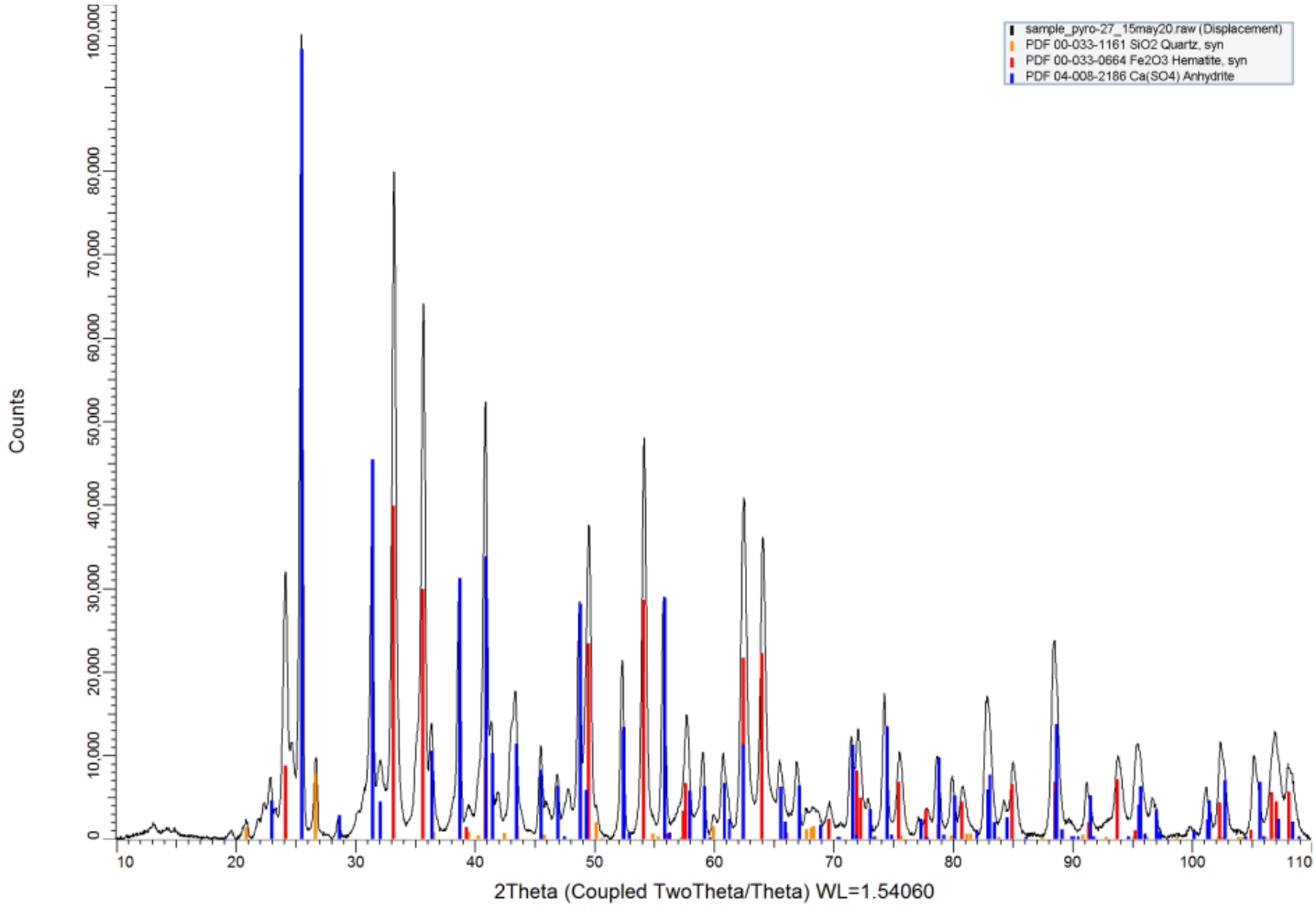

Figure B.12: XRD of BLP mixed with $CaCl_2$ heated at 700 °C for 15 mins in horizontal furnace (N_2 atmosphere 0.5 L/min)

.

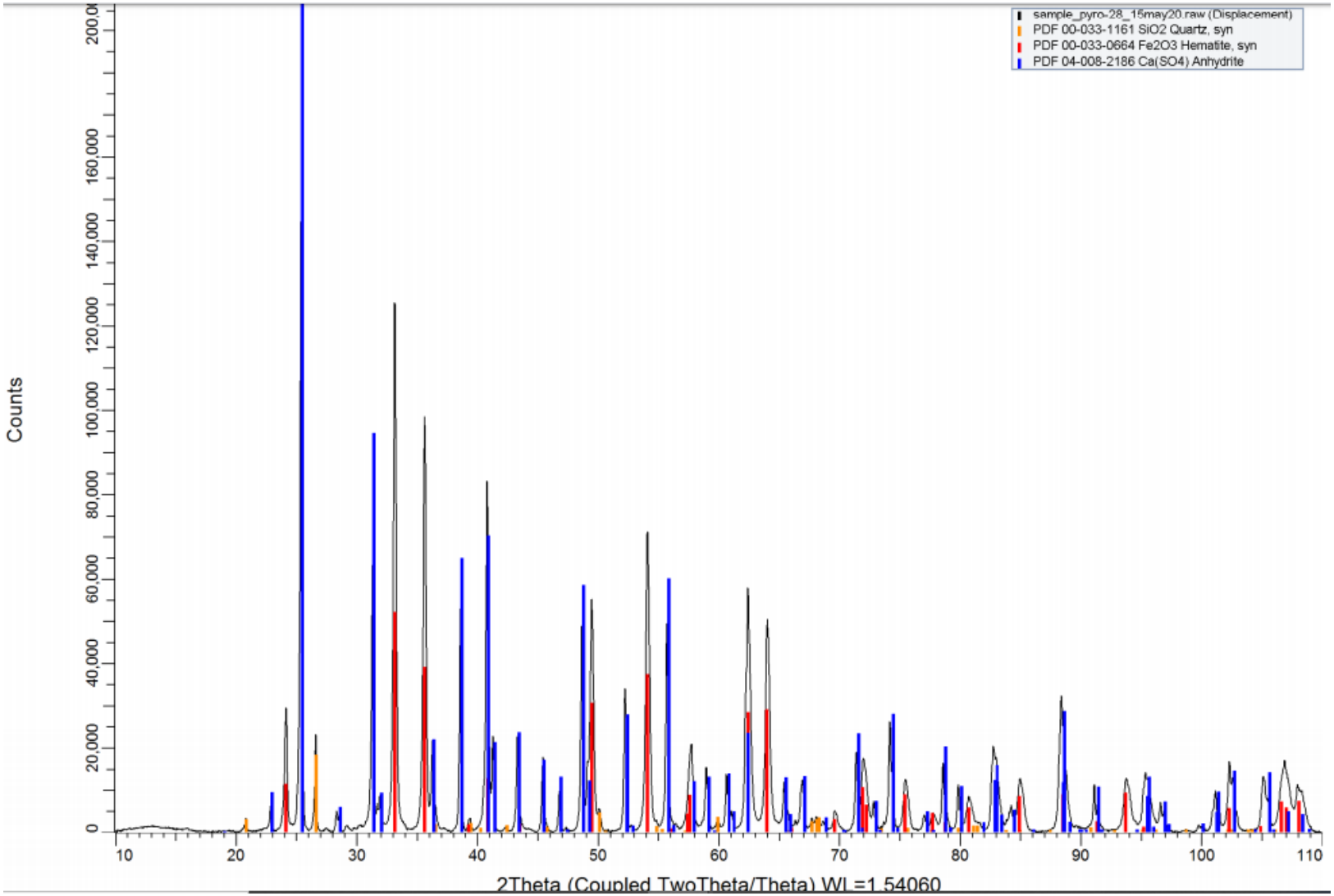

Figure B.13: XRD of BLP mixed with $CaCl_2$ heated at 800 °C for 15 mins in horizontal furnace (N_2 atmosphere 0.5 L/min)

.

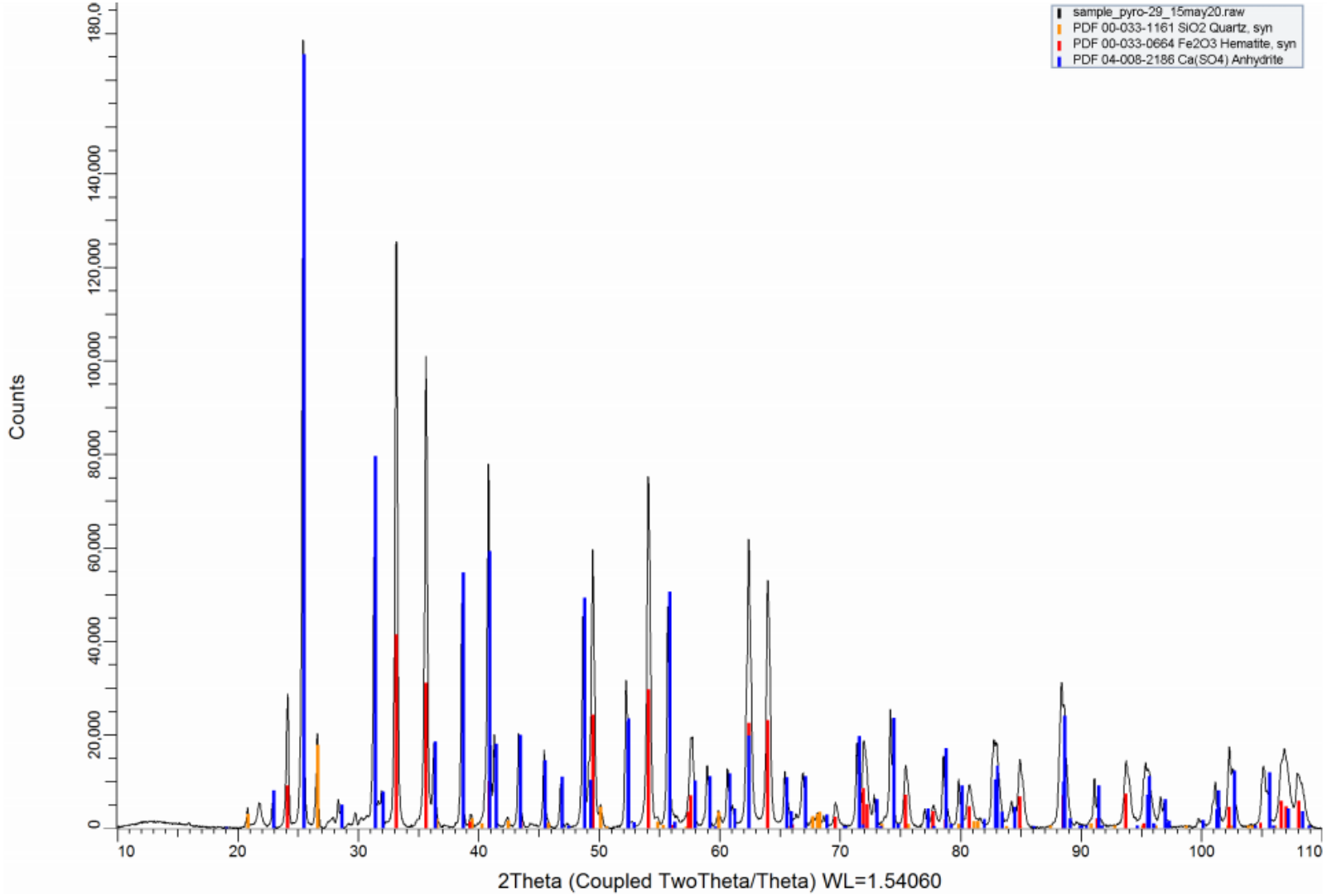

Figure B.14: XRD of BLP mixed with $CaCl_2$ heated at 900 °C for 15 mins in horizontal furnace (N_2 atmosphere 0.5 L/min)

.

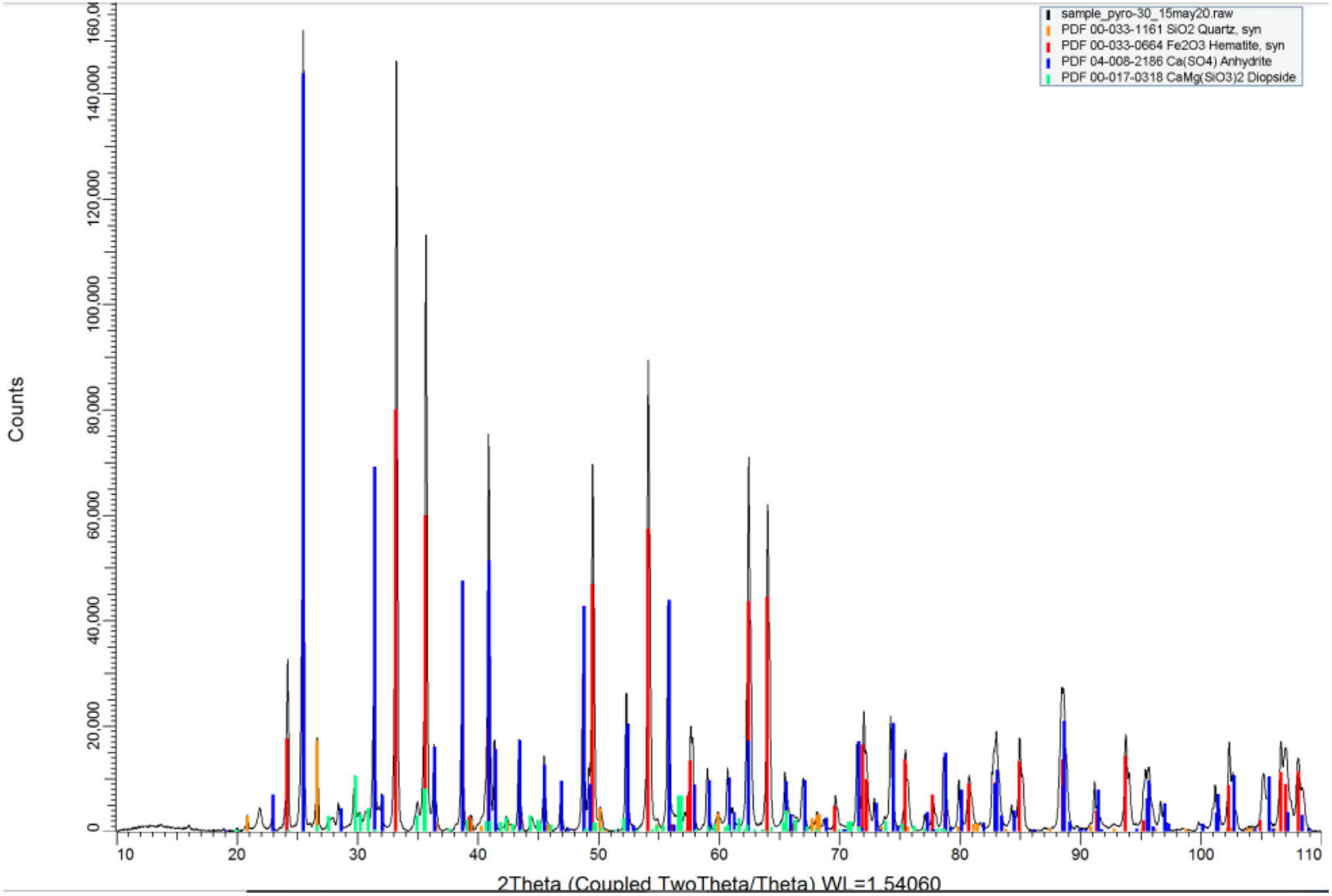

Figure B.15: XRD of BLP mixed with $CaCl_2$ heated at 1000 °C for 15 mins in horizontal furnace (N_2 atmosphere 0.5 L/min)

.

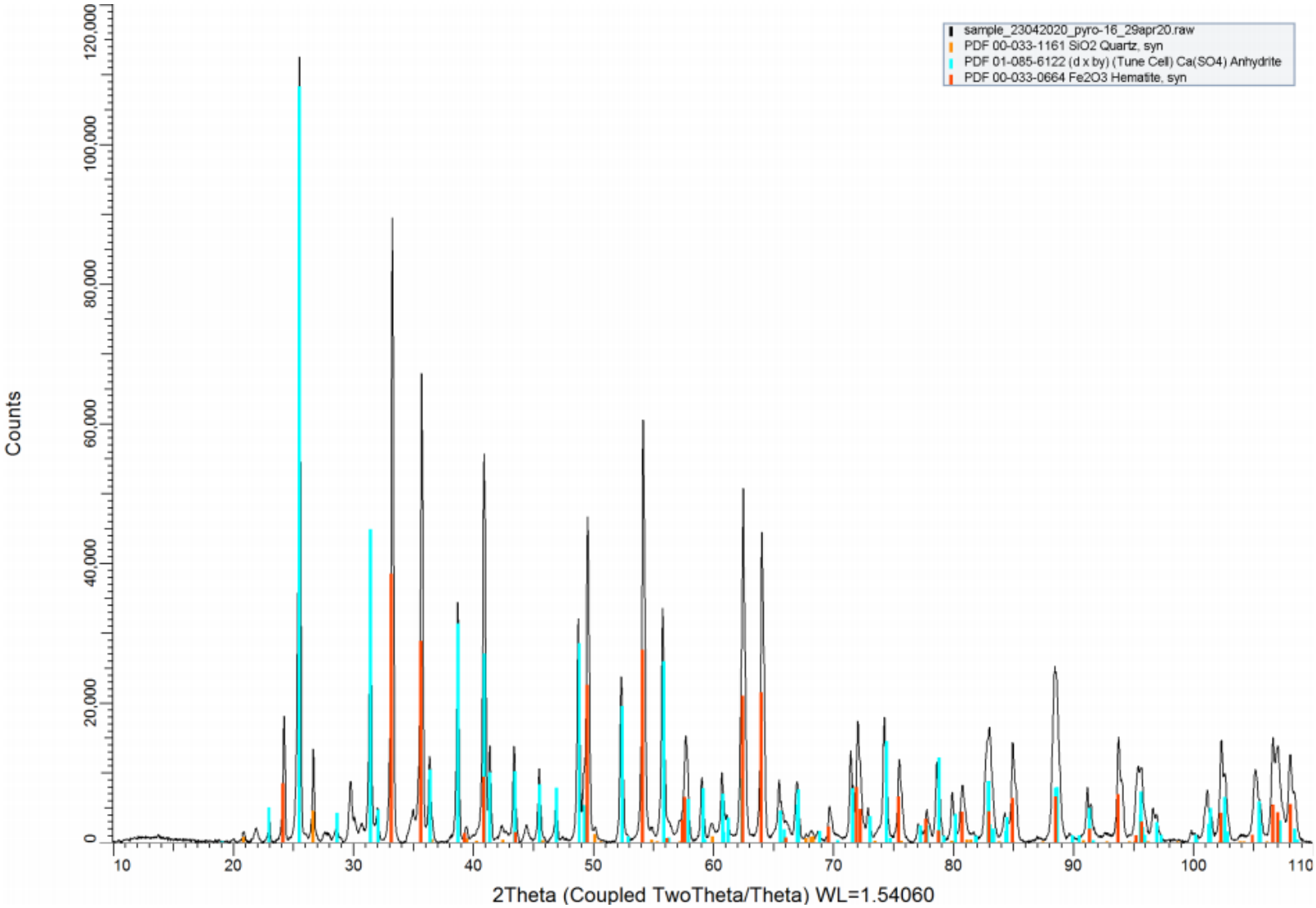

Figure B.16: XRD of BLP mixed with $CaCl_2$ (10g) heated at 1000 °C for 30 mins in horizontal furnace (N_2 atmosphere 0.5 L/min)

.

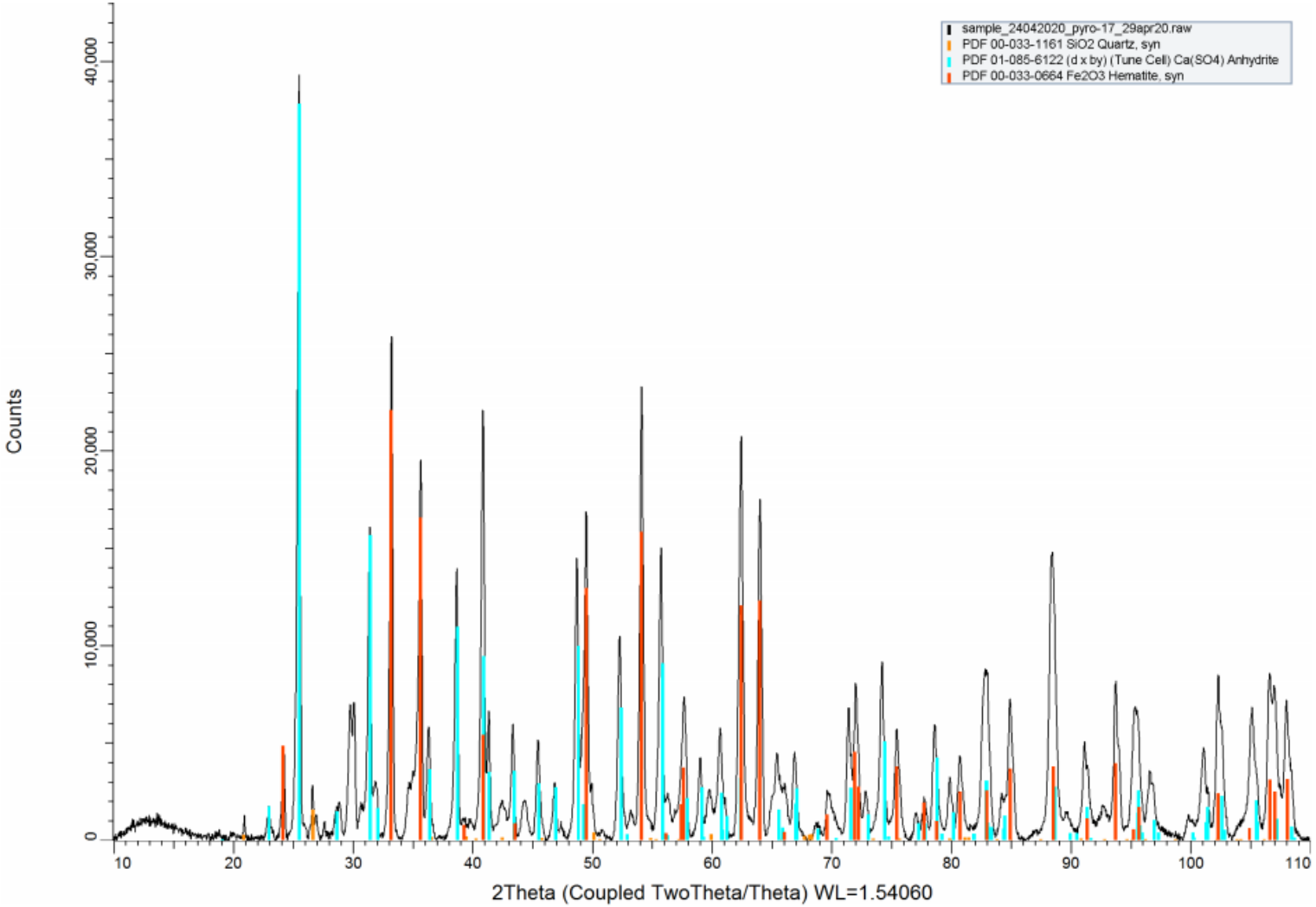

Figure B.17: XRD of BLP mixed with $CaCl_2$ heated at 1100 °C for 15 mins in horizontal furnace (N_2 atmosphere 0.5 L/min)

.

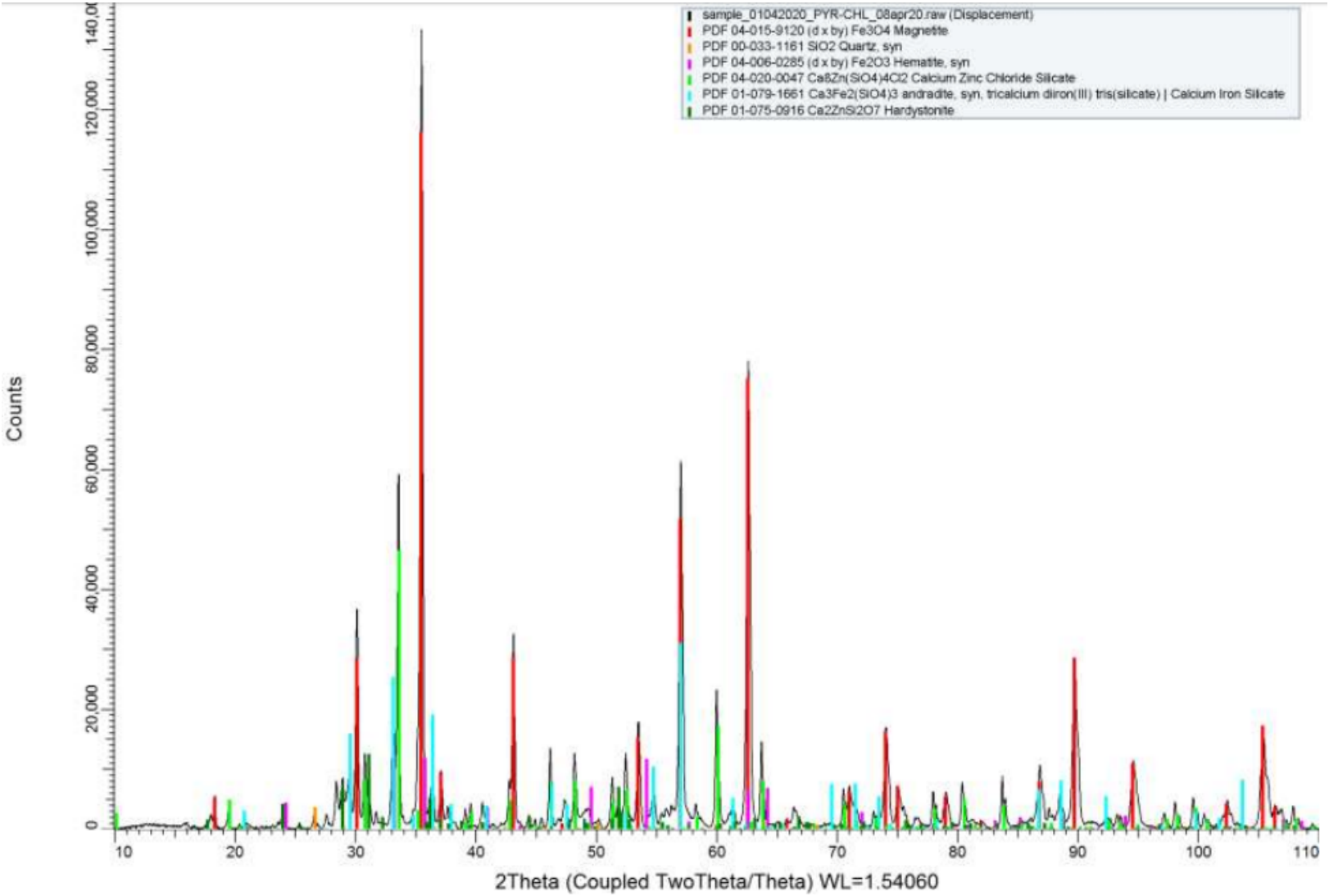

Figure B.18: XRD of BLP mixed with $CaCl_2$ and C heated at 1000 °C for 15 mins in horizontal furnace (N_2 atmosphere 0.5 L/min)

.

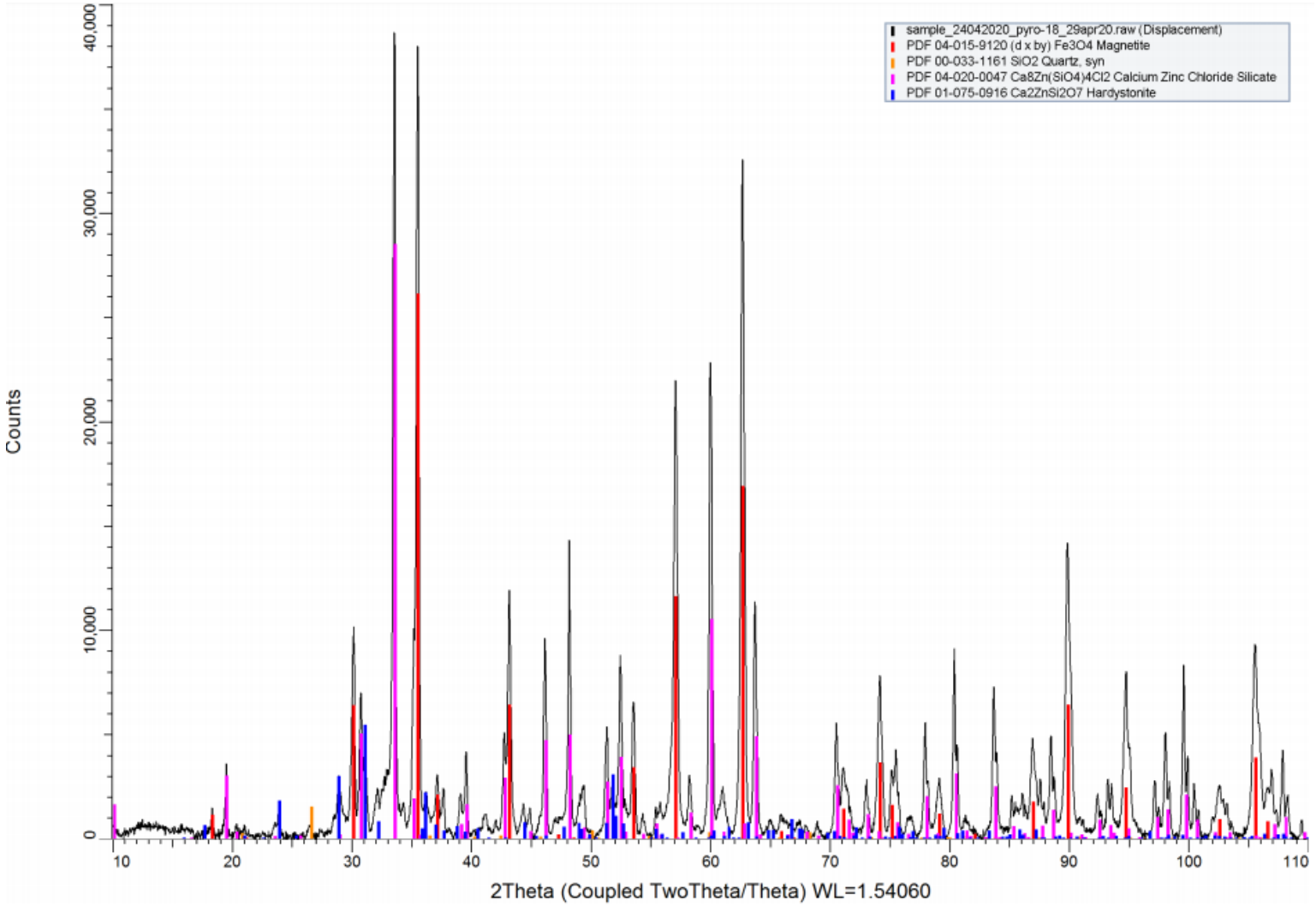

Figure B.19: XRD of BLP mixed with $CaCl_2$ and C heated at 1100 °C for 15 mins in horizontal furnace (N_2 atmosphere 0.5 L/min)

.

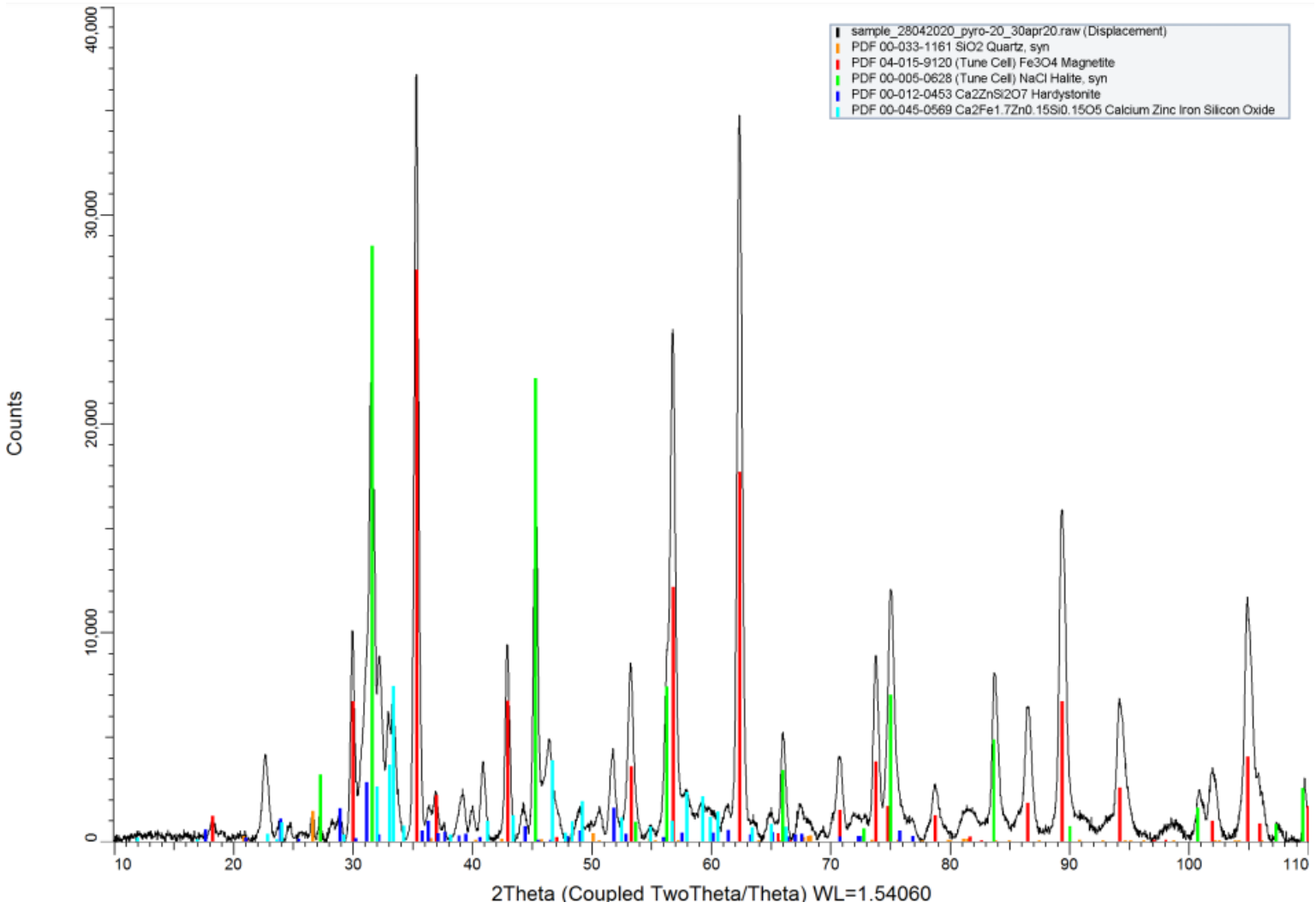

Figure B.20: XRD of BLP mixed with $CaCl_2$ and Na_2CO_3, heated at 1000°C for 15 mins in horizontal furnace (N_2 atmosphere 0.5 L/min)

.

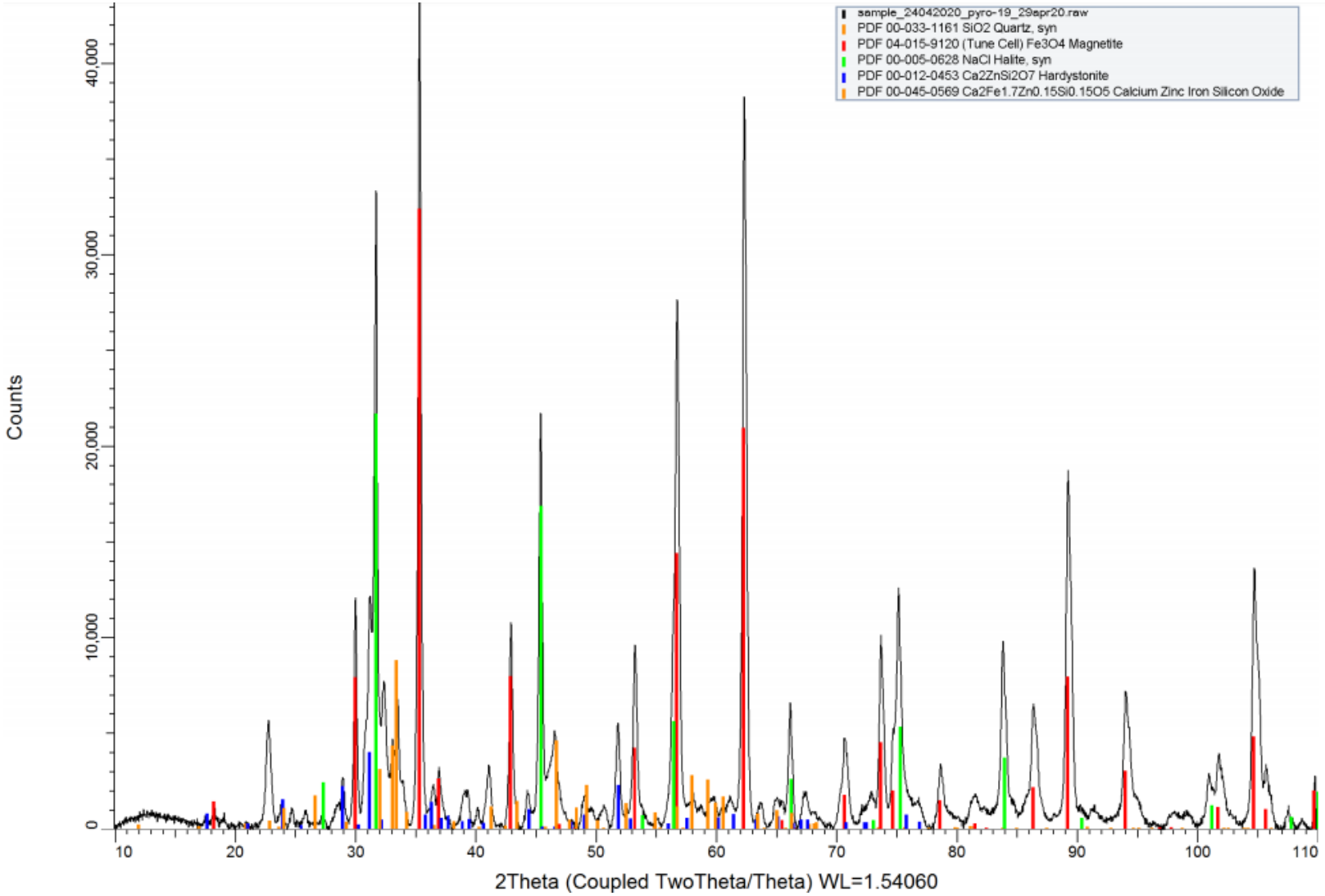

Figure B.21: XRD of BLP mixed with $CaCl_2$ and Na_2CO_3 heated at 1100 °C for 15 mins in horizontal furnace (N_2 atmosphere 0.5 L/min)

.

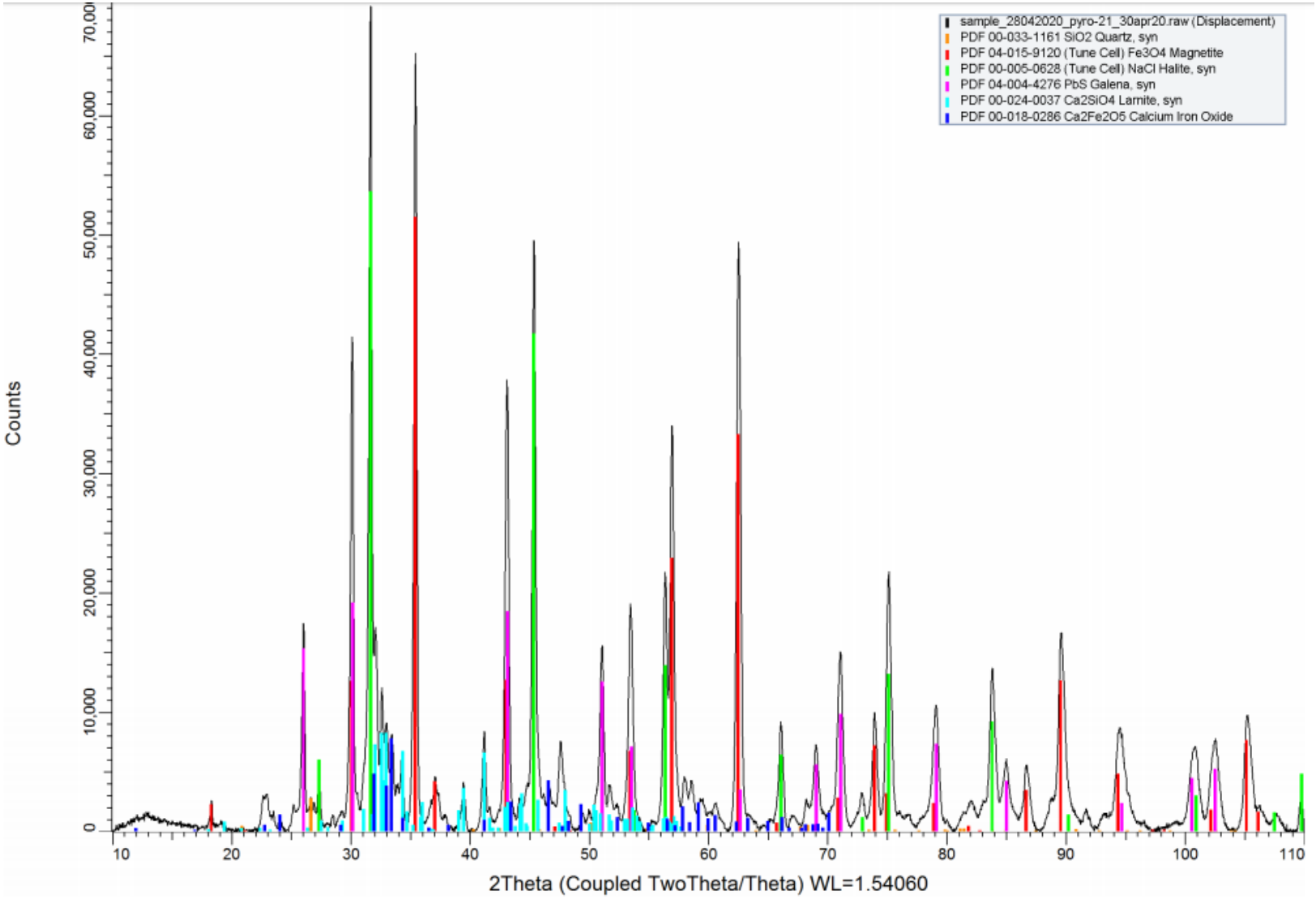

Figure B.22: XRD of BLP mixed with $CaCl_2$ and Na_2CO_3 and C heated at 1000 °C for 15 mins in horizontal furnace (N_2 atmosphere 0.5 L/min)

.

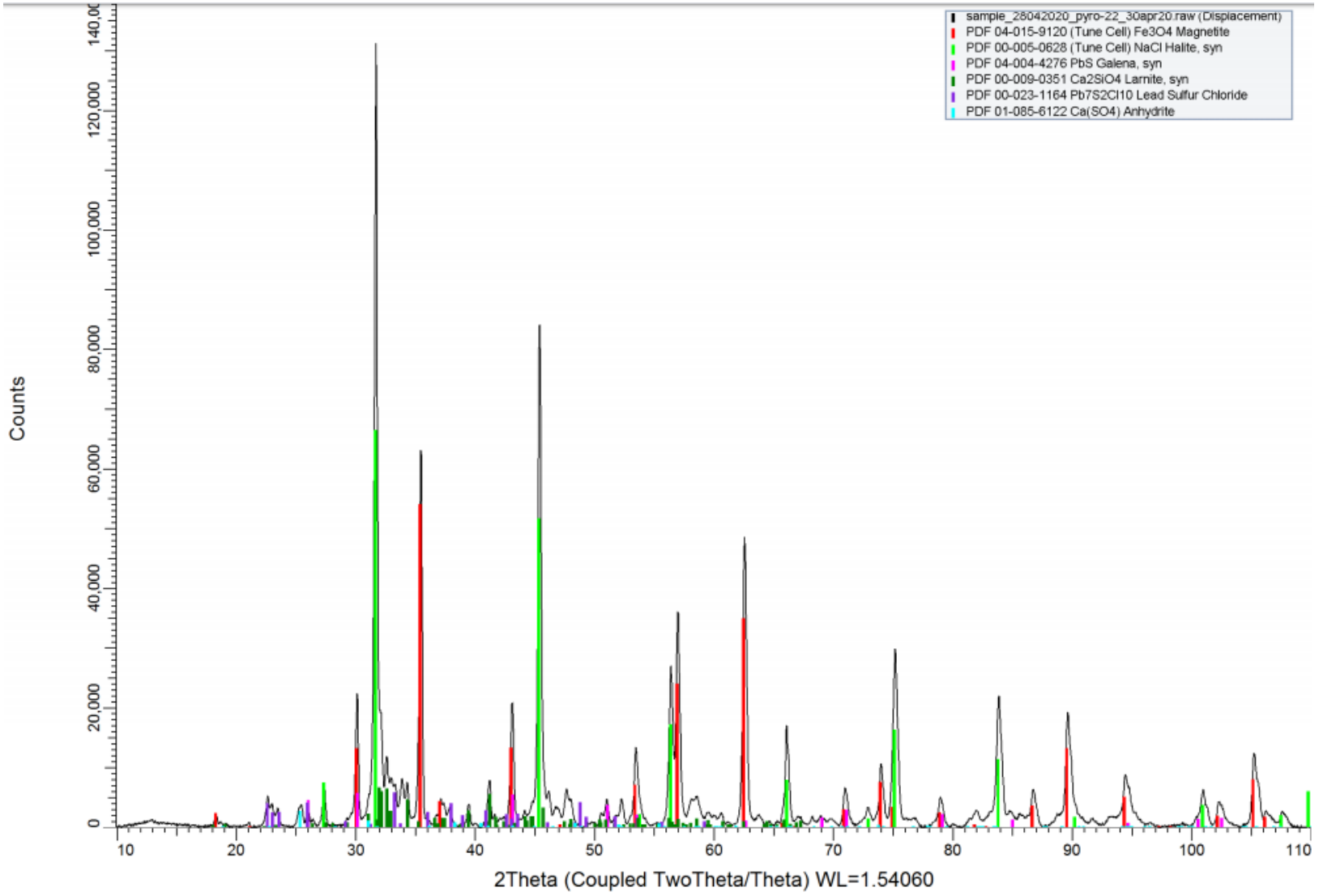

Figure B.23: XRD of BLP mixed with $CaCl_2$ and Na_2CO_3 and C heated at 1100 °C for 15 mins in horizontal furnace (N_2 atmosphere 0.5 L/min)

.

C

Combined Pyro- and Hydrometallurgy

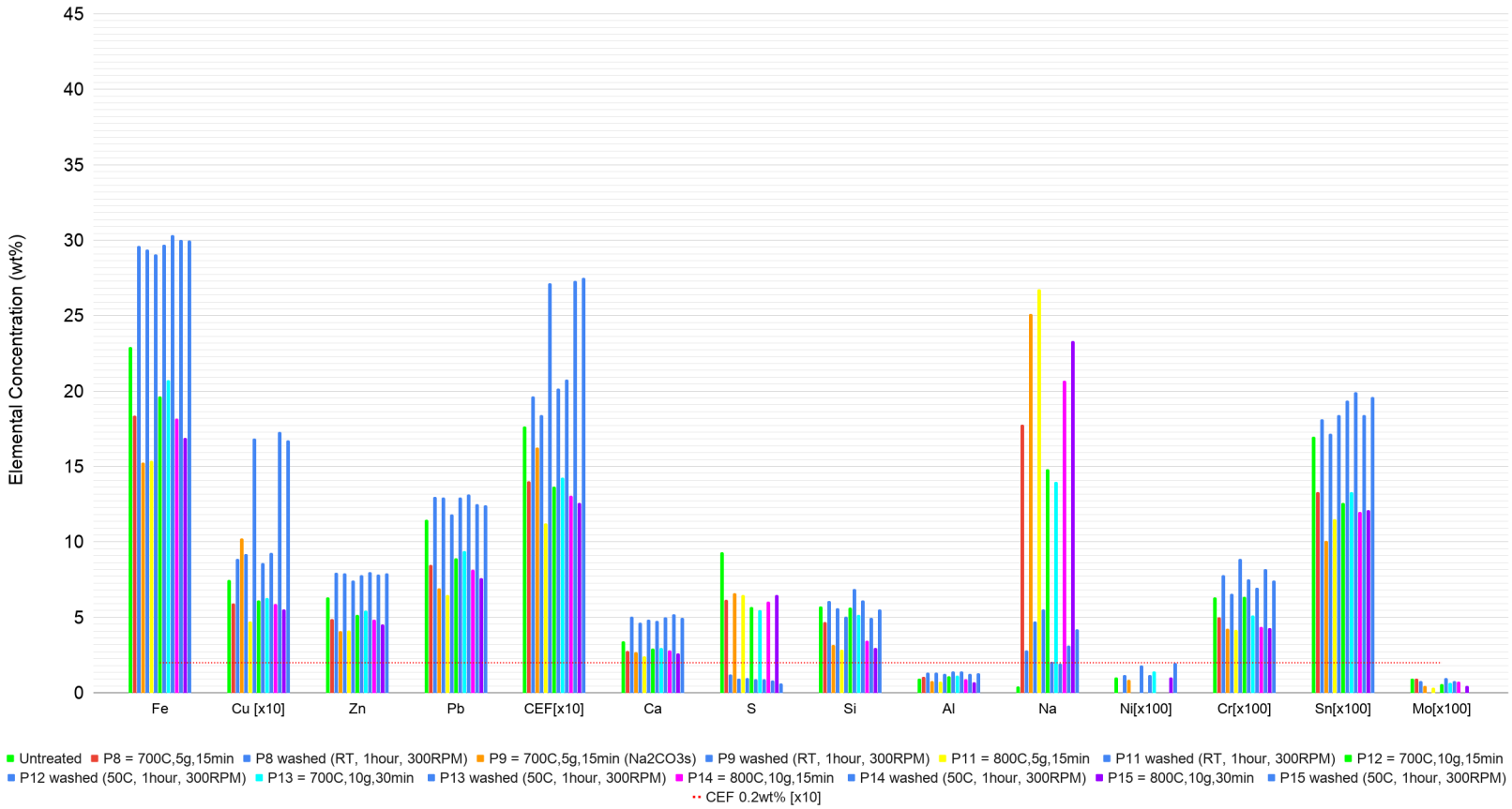

Figure C.1: Elemental composition of residual solids after sulfur fixation experiments with BLP. This chart compares directly to BLP (light green column). Blue columns immediately after a coloured colomn show residual concentrations in the washed solid (coloured column)

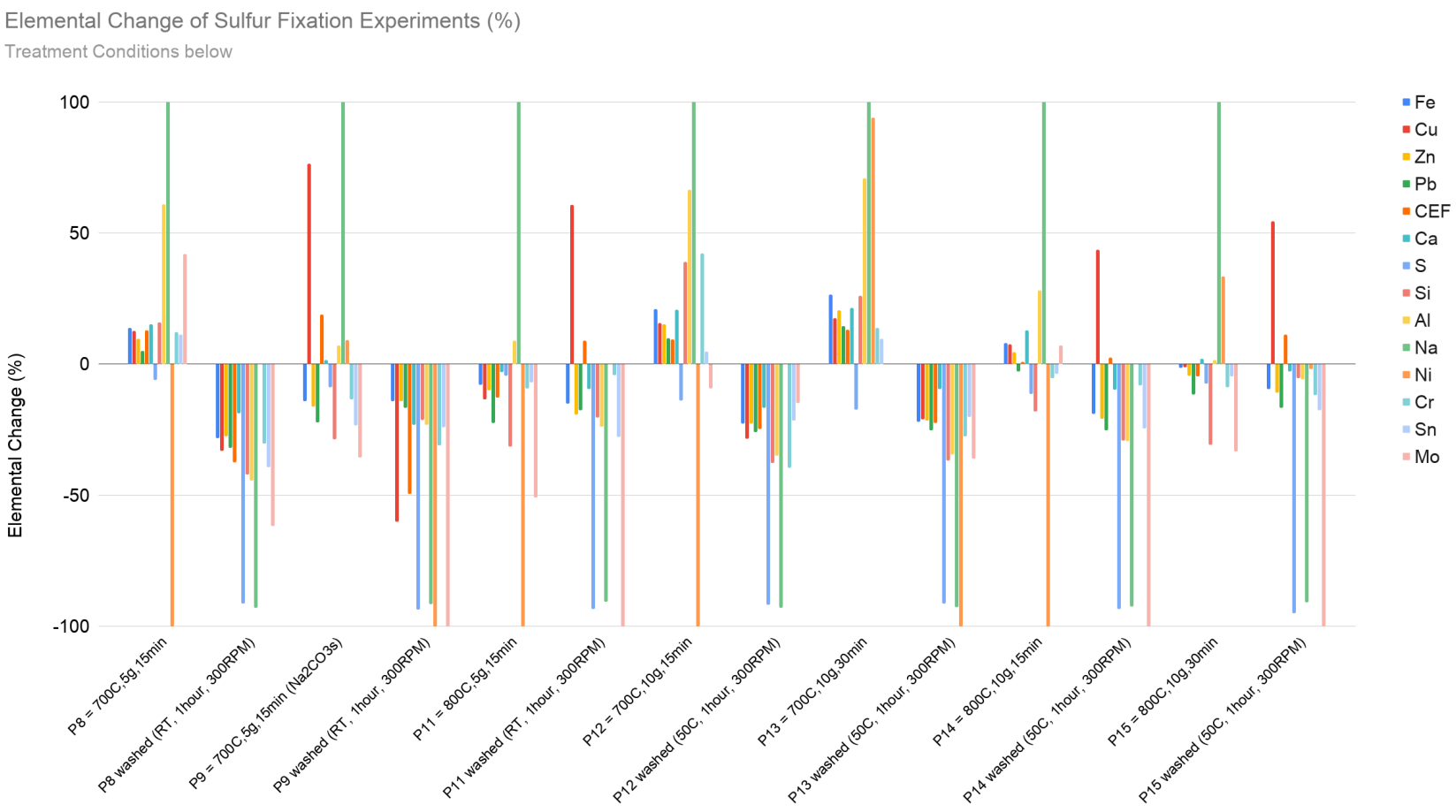

Figure C.2: Summary of the elemental change (%) leaving the sample for each treatment. Treatment on x-axis

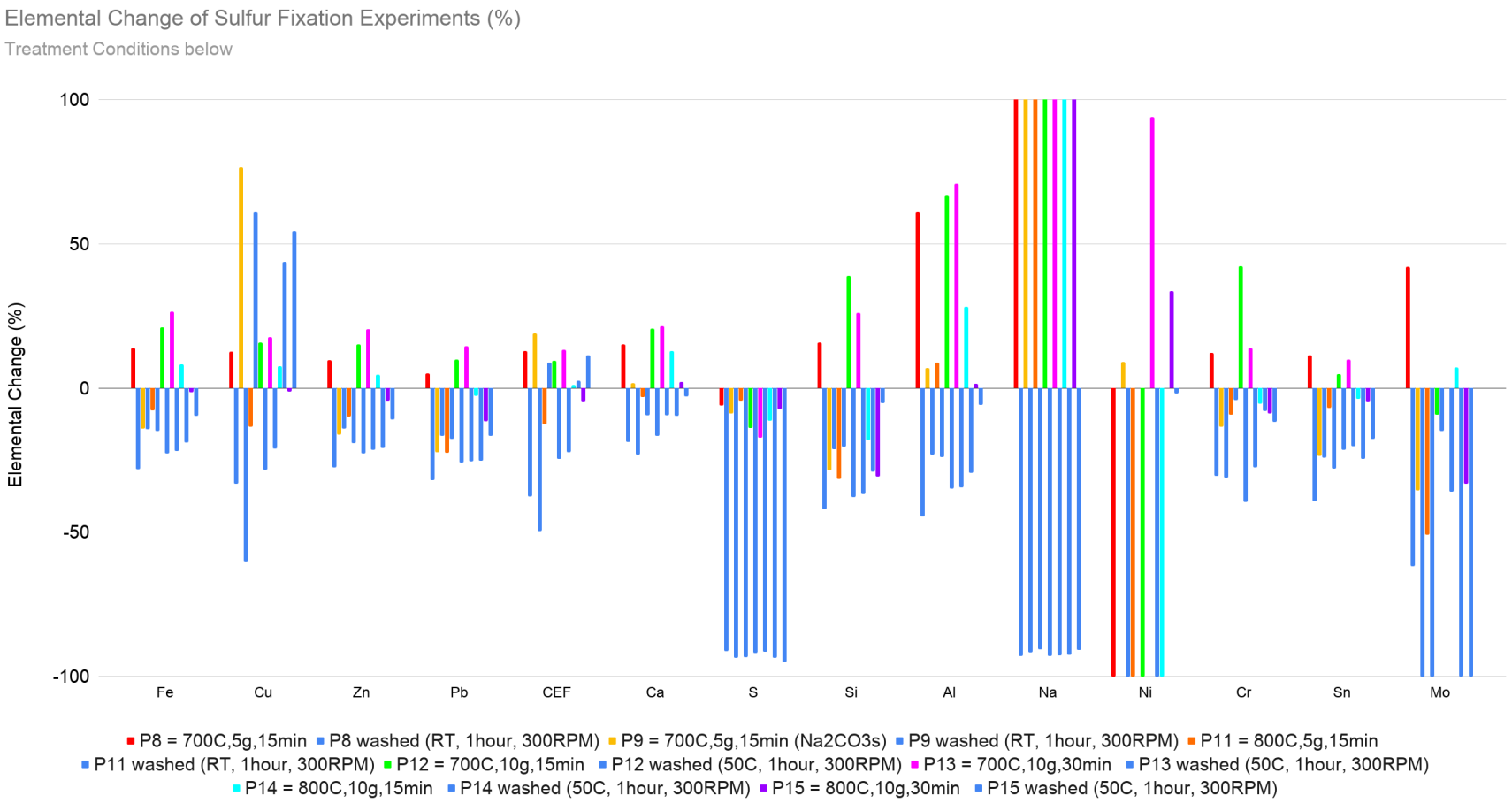

Figure C.3: Summary of the elemental change (%) leaving the sample for each treatment. Elements on x-axis.

C.1. Treatment Effectiveness

Treatment Effectiveness		P8	P9	P11	P12	P13	P14	P15
		Calcination						
		700, (BLP + Na2CO3p), 5g, 15min	700, (BLP + Na2CO3s), 5g, 15min	800, (BLP + Na2CO3p), 5g, 15min	700, (BLP + Na2CO3p), 10g,15min	700, (BLP + Na2CO3p), 10g,30min	800, (BLP + Na2CO3p), 10g,15min	800, (BLP + Na2CO3p), 10g,30min
Cu/Fe		0.0323	0.0671	0.0307	0.0312	0.0303	0.0325	0.0327
CEF/Fe		0.0764	0.1065	0.0730	0.0696	0.0688	0.0719	0.0745
	Washing							
		RT, 1hour, 300RPM	RT, 1hour, 300RPM	RT, 1hour, 300RPM	50C, 1hour, 300RPM	50C, 1hour, 300RPM	50C, 1hour, 300RPM	50C, 1hour, 300RPM
Residue	Cu/Fe	0.0300	0.0312	0.0580	0.0290	0.0306	0.0575	0.0559
	CEF/Fe	0.0664	0.0627	0.0934	0.0679	0.0684	0.0910	0.0917
PLS	Cu/Fe	0.0000	0.0000	0.0000	0.0000	0.0000	N/A (Fe = 0)	0.0000
	TTM/Fe	58.3964	18.3242	38.5407	145.6909	198.8355	N/A (Fe = 0)	484.8178

C.2. XRD

C.2.1. Calcined Residue

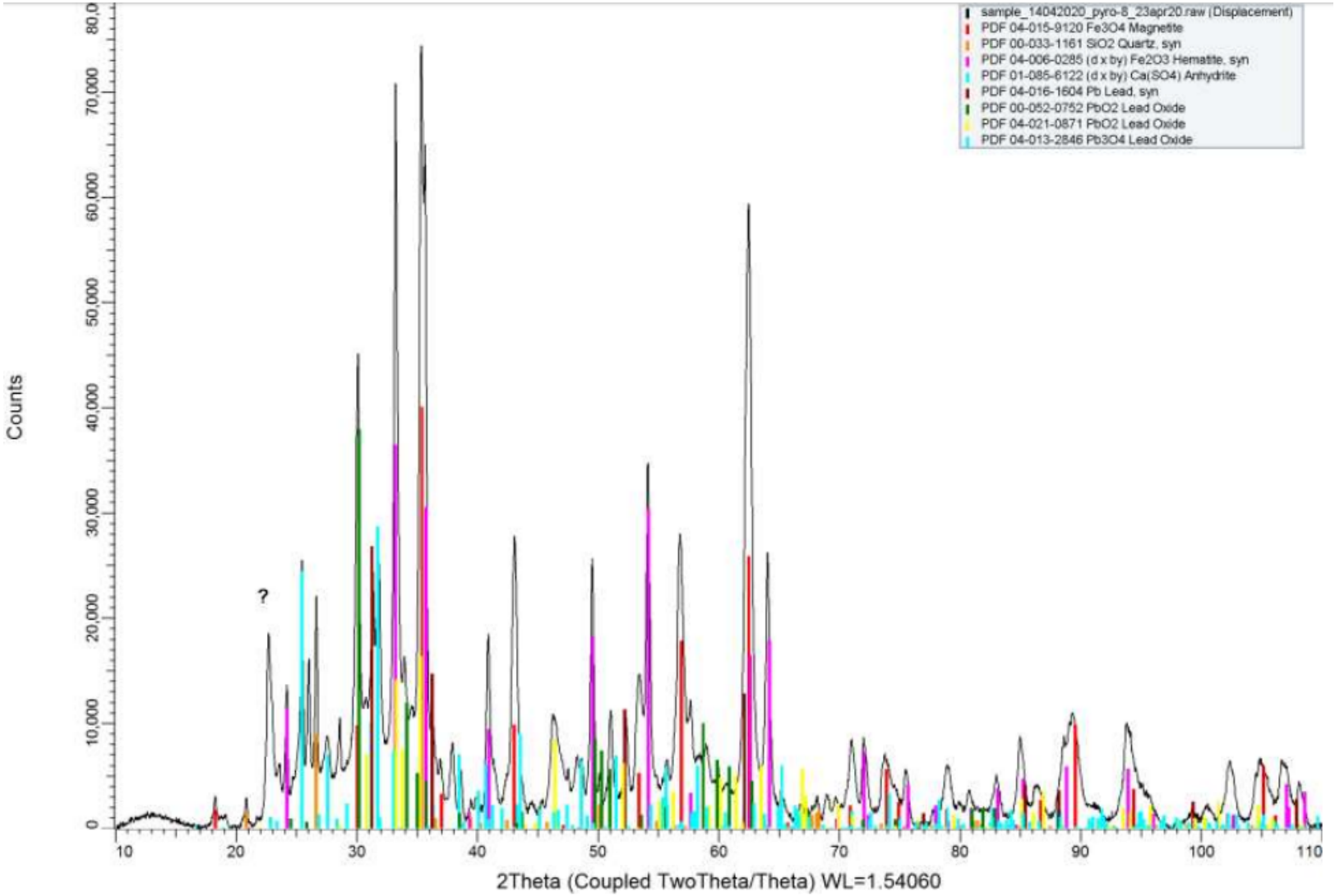

Figure C.4: XRD of BLP mixed with Na_2CO_3 (5g) and calcined at 700 °C for 15 mins in horizontal furnace (N_2 atmosphere 0.5 L/min). (P8)

.

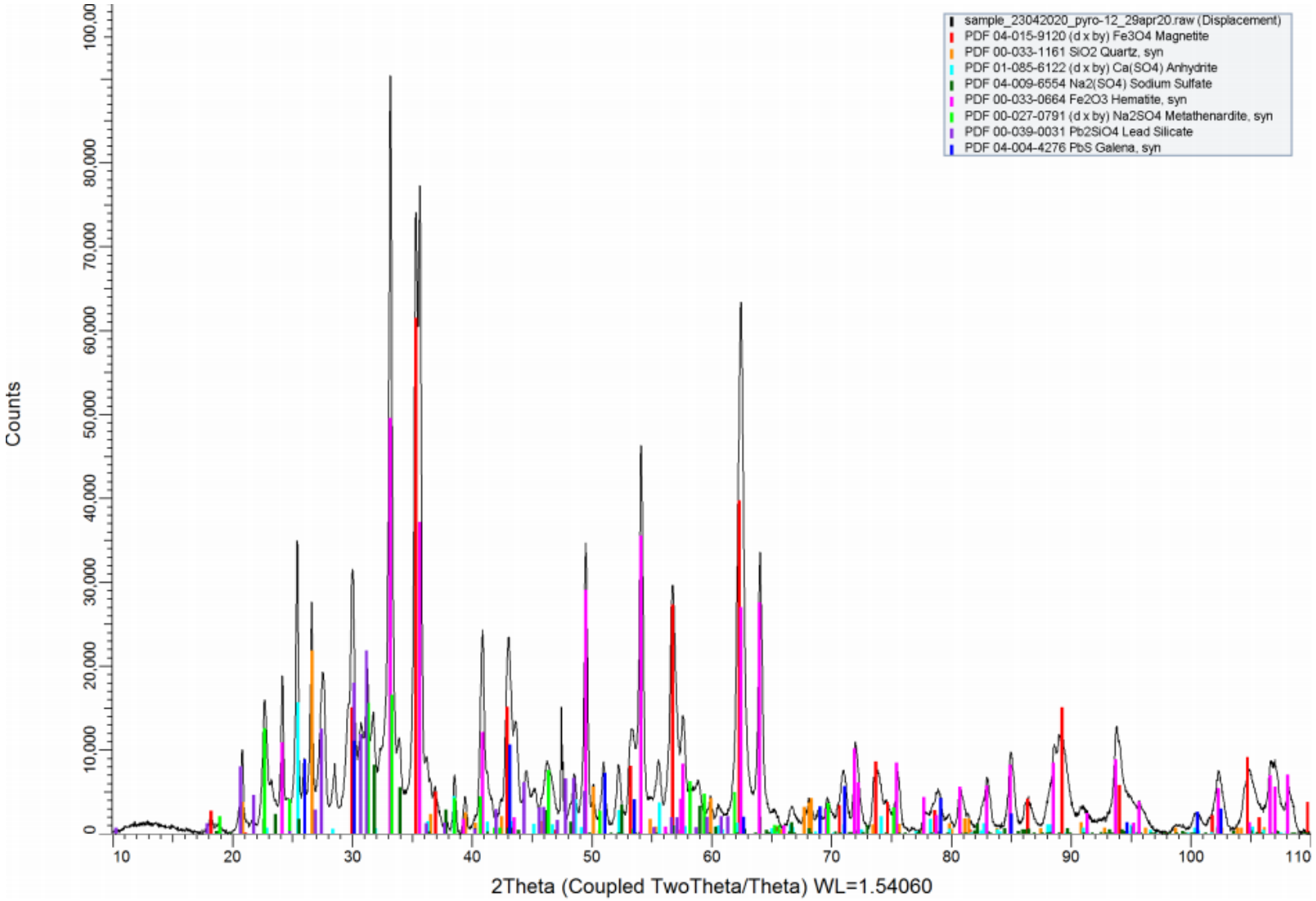

Figure C.5: XRD of BLP mixed with Na_2CO_3 (10g) and calcined at 700 °C for 15 mins in horizontal furnace (N_2 atmosphere 0.5 L/min)(P12)

.

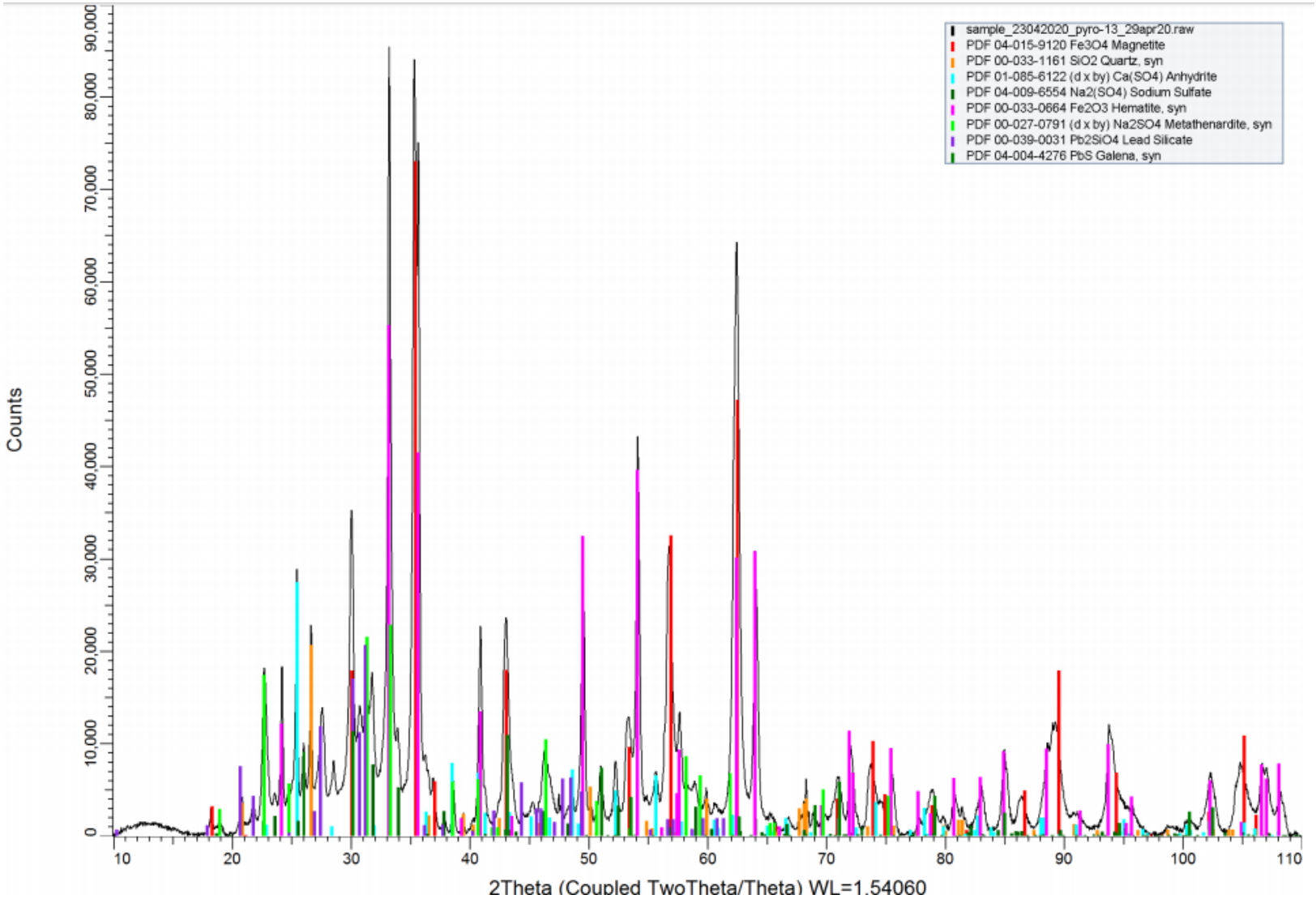

Figure C.6: XRD of BLP mixed with Na_2CO_3 (10g) and calcined at 700 °C for 30 mins in horizontal furnace (N_2 atmosphere 0.5 L/min)(P13)

.

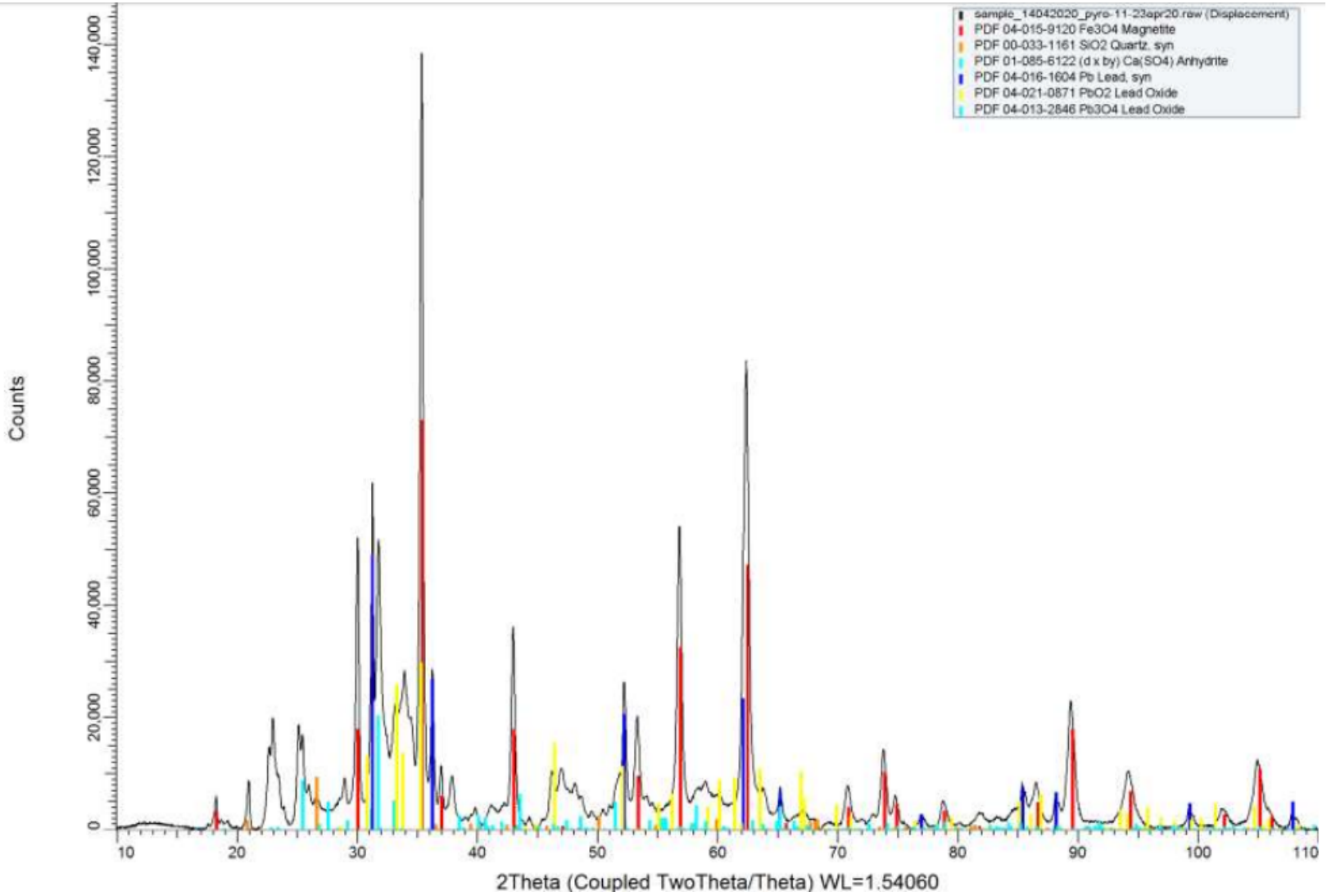

Figure C.7: XRD of BLP mixed with Na_2CO_3 (5g) and calcined at 800 °C for 15 mins in horizontal furnace (N_2 atmosphere 0.5 L/min). (P8)

.

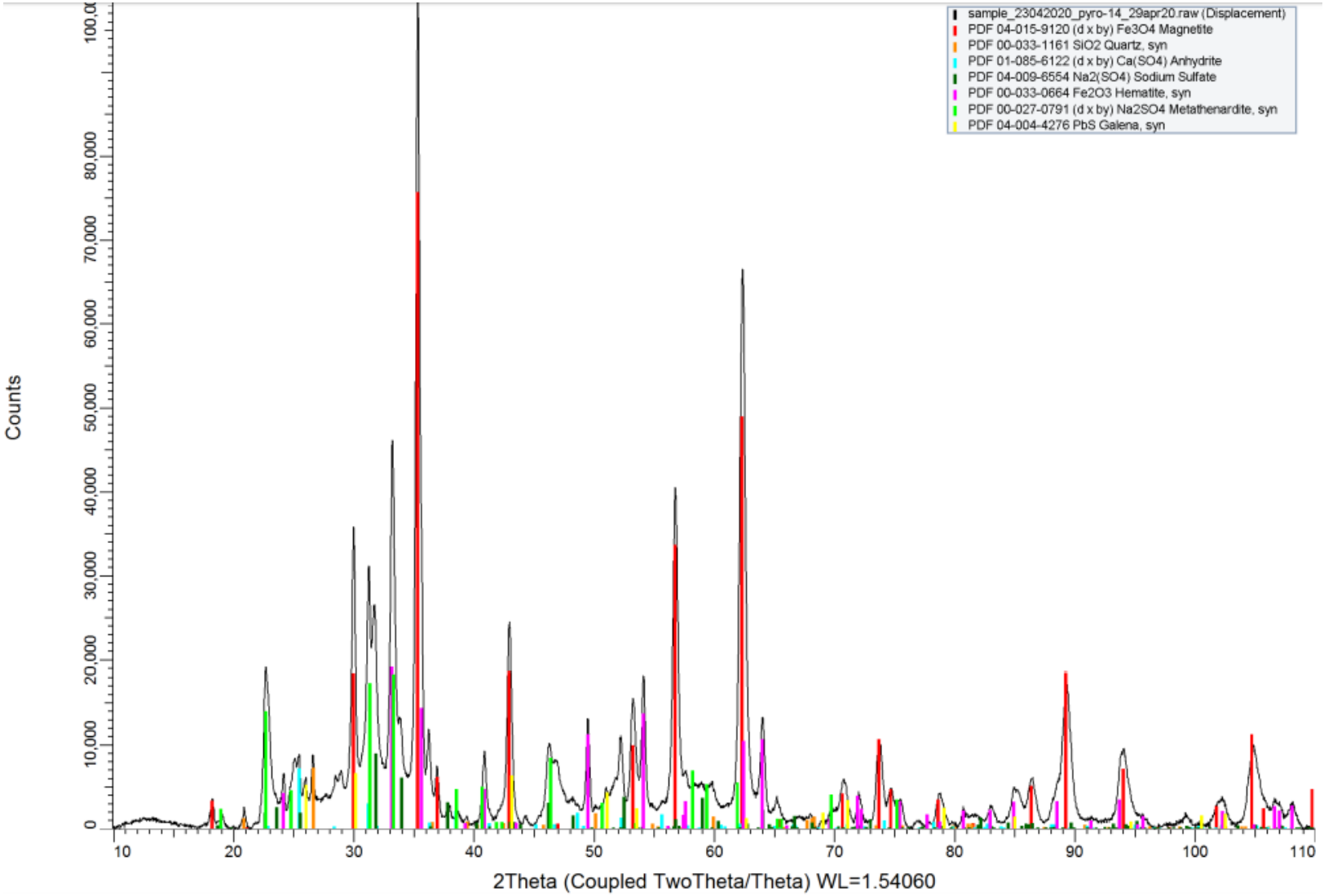

Figure C.8: XRD of BLP mixed with Na_2CO_3 (10g) and calcined at 800 °C for 15 mins in horizontal furnace (N_2 atmosphere 0.5 L/min)(P14)

.

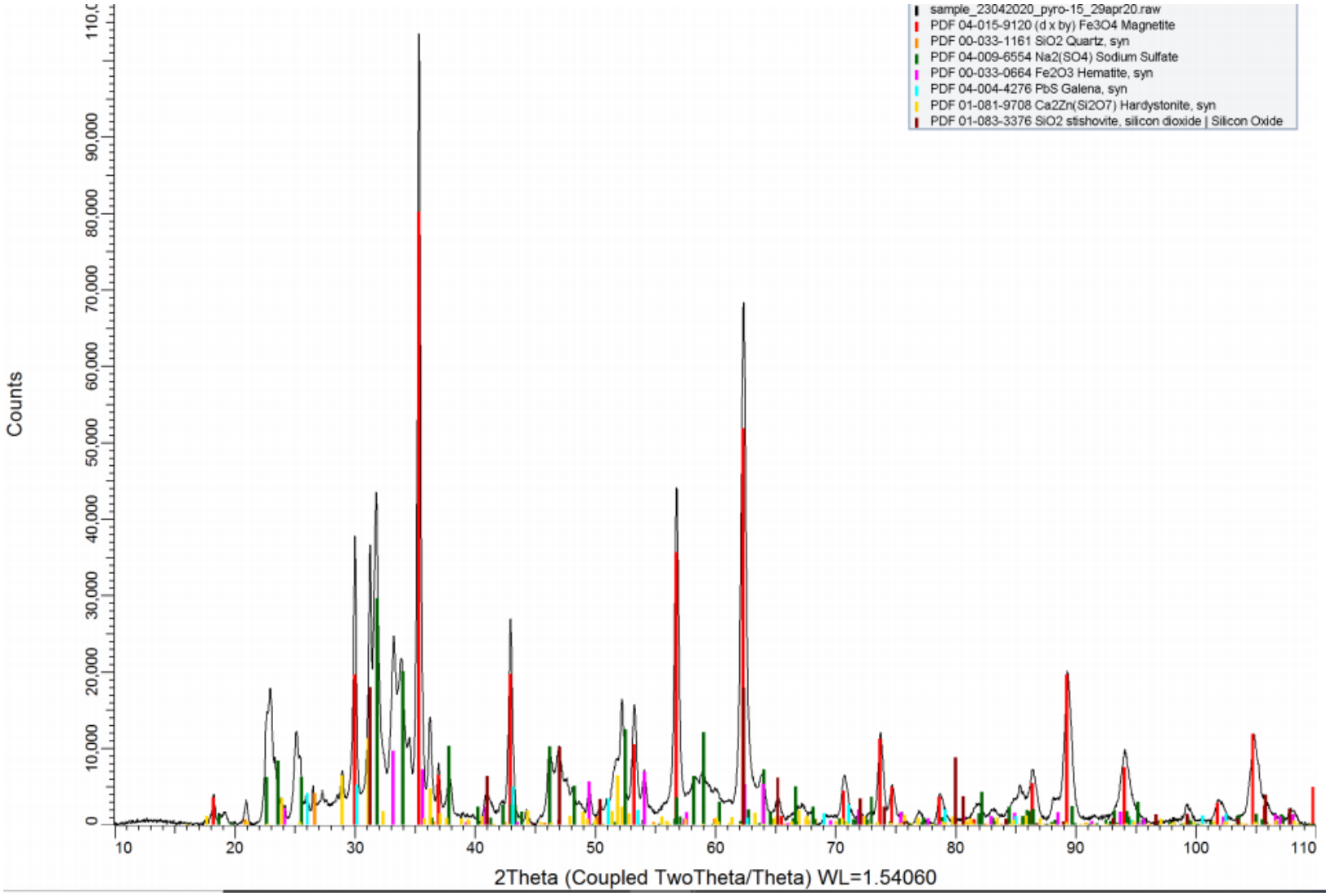

Figure C.9: XRD of BLP mixed with Na_2CO_3 (10g) and calcined at 800 °C for 30 mins in horizontal furnace (N_2 atmosphere 0.5 L/min)(P15)

.

C.2.2. Washed Residue

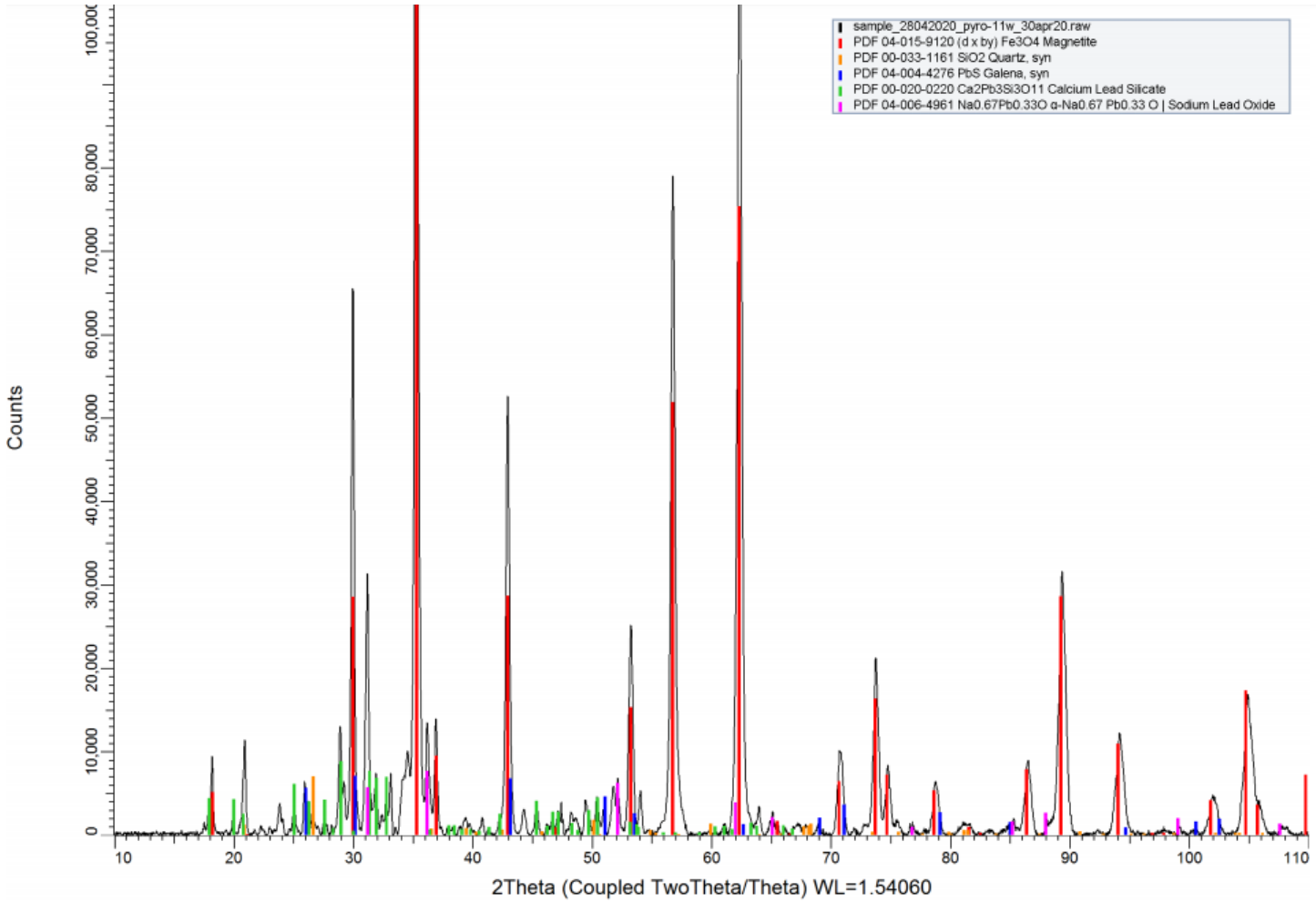

Figure C.10: P11 washed residue washed. Treatment conditions detailed in the body of text

.

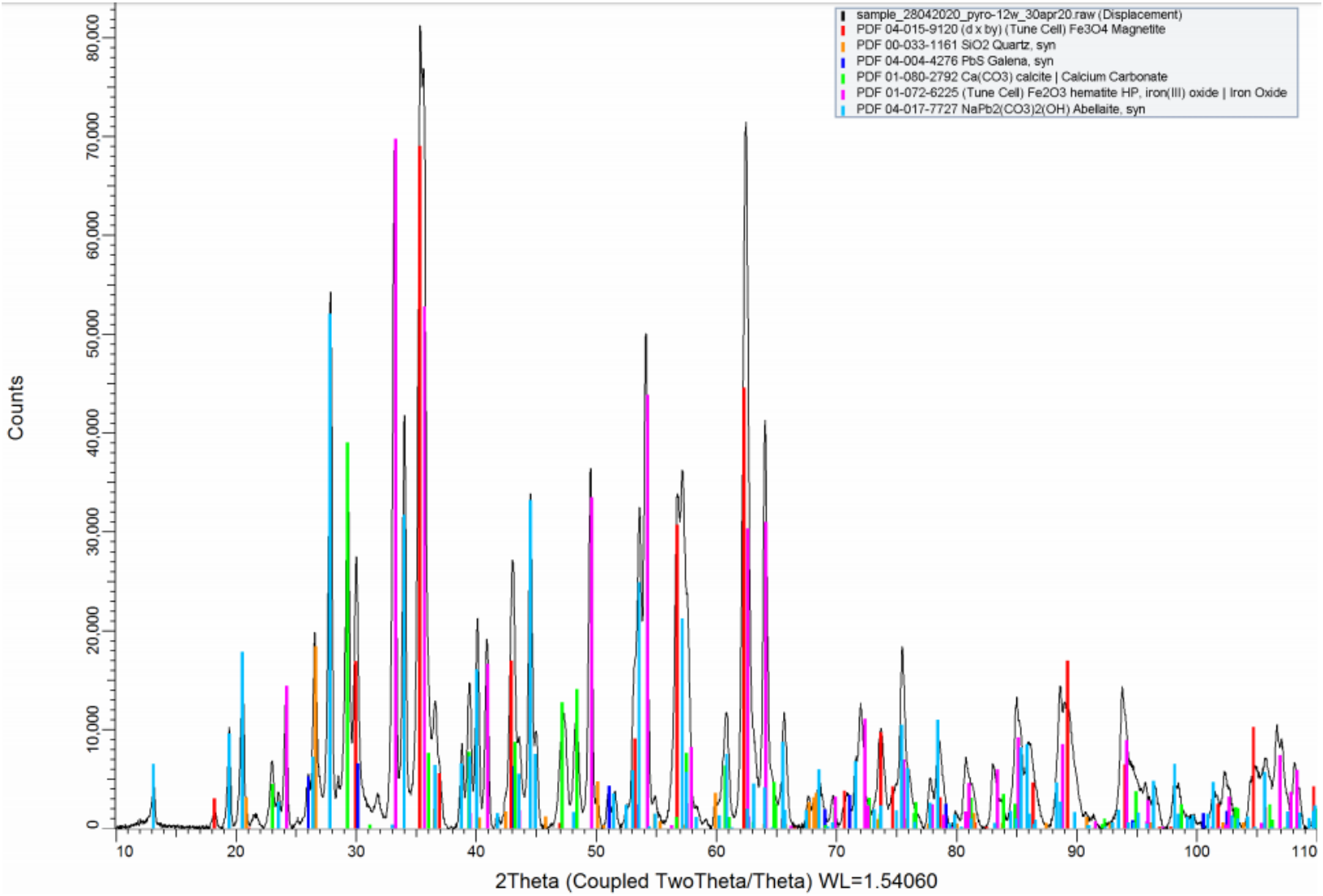

Figure C.11: P12 washed residue washed. Treatment conditions detailed in the body of text

.

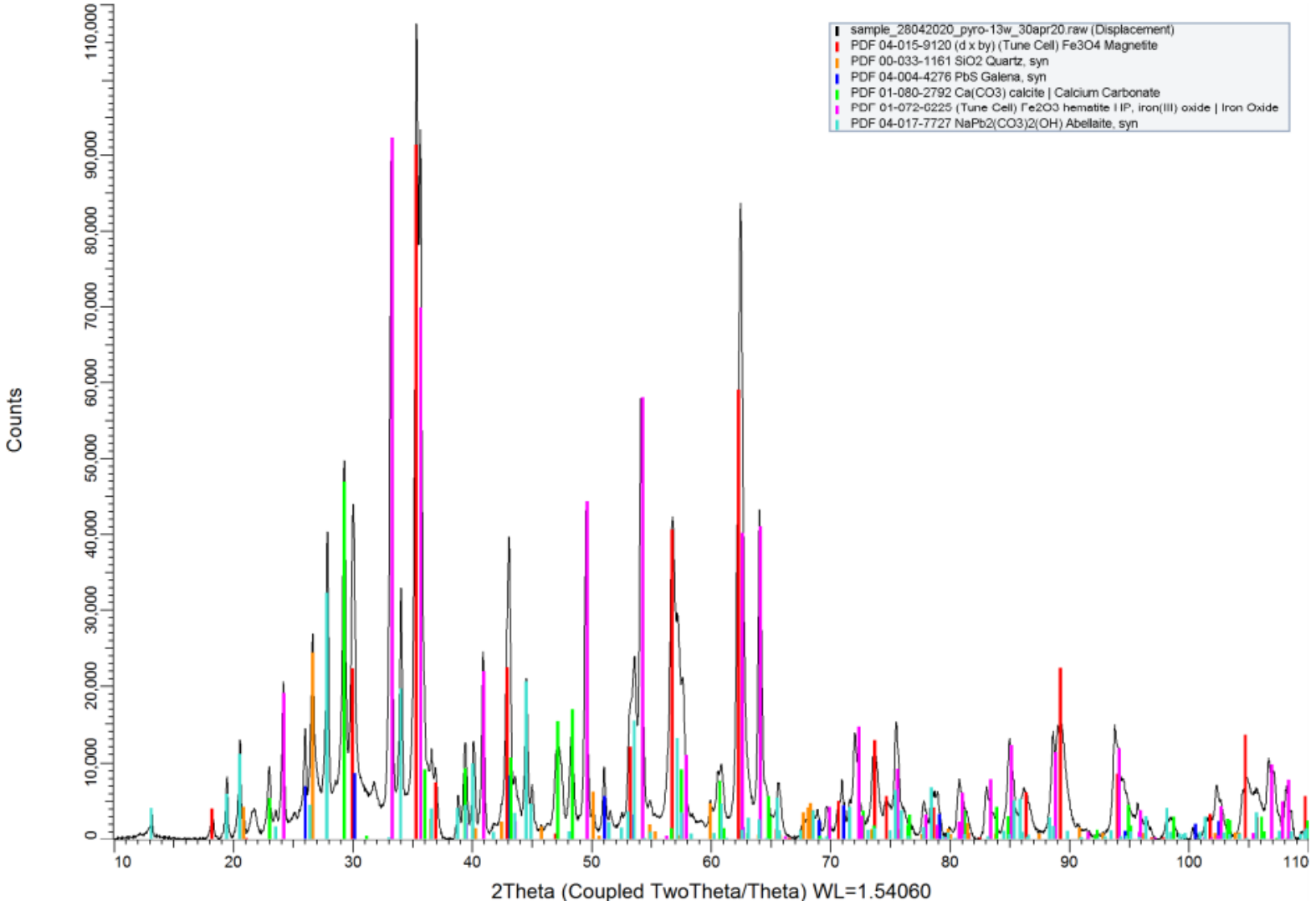

Figure C.12: P13 washed residue washed. Treatment conditions detailed in the body of text

.

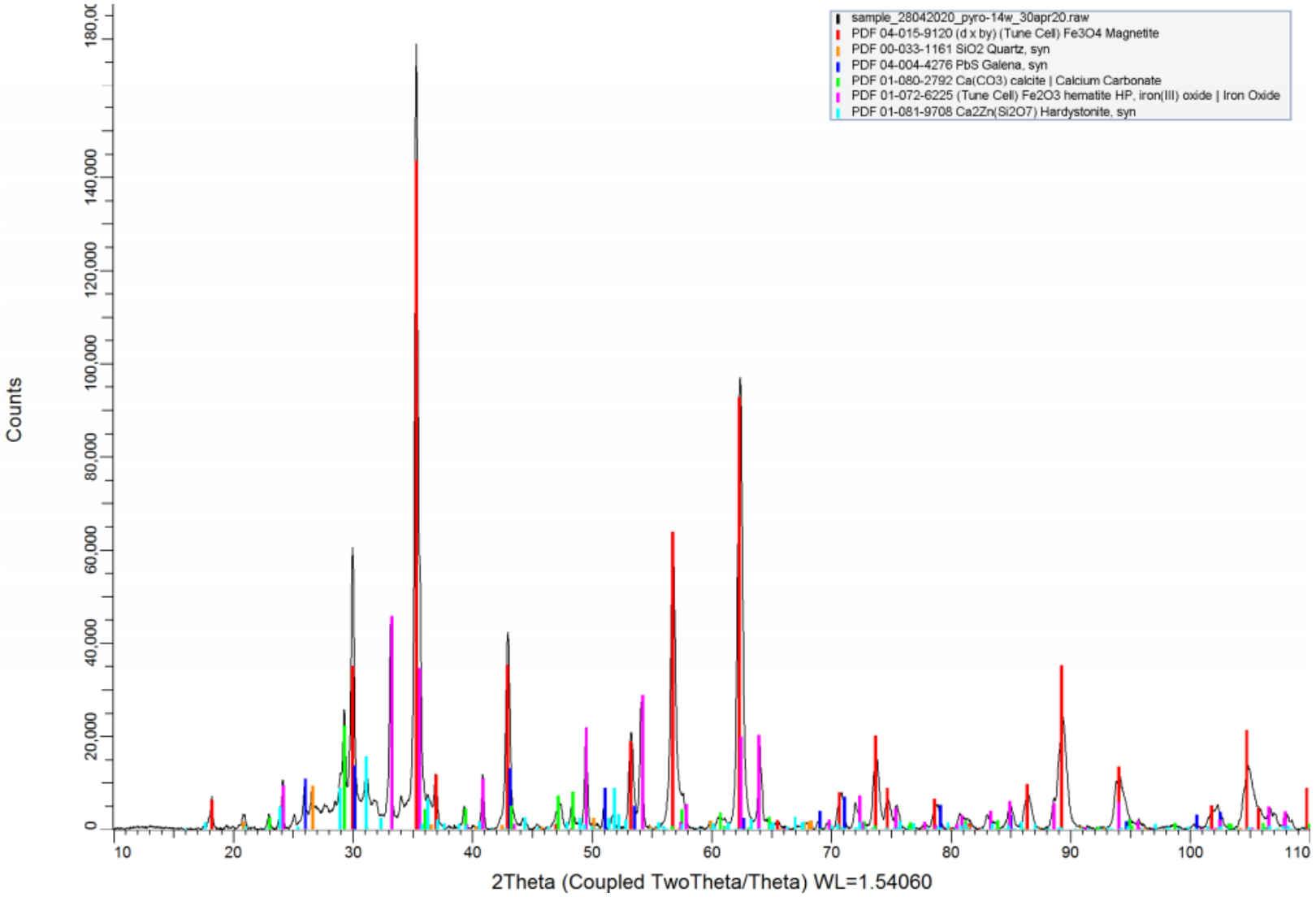

Figure C.13: P14 washed residue washed. Treatment conditions detailed in the body of text

.

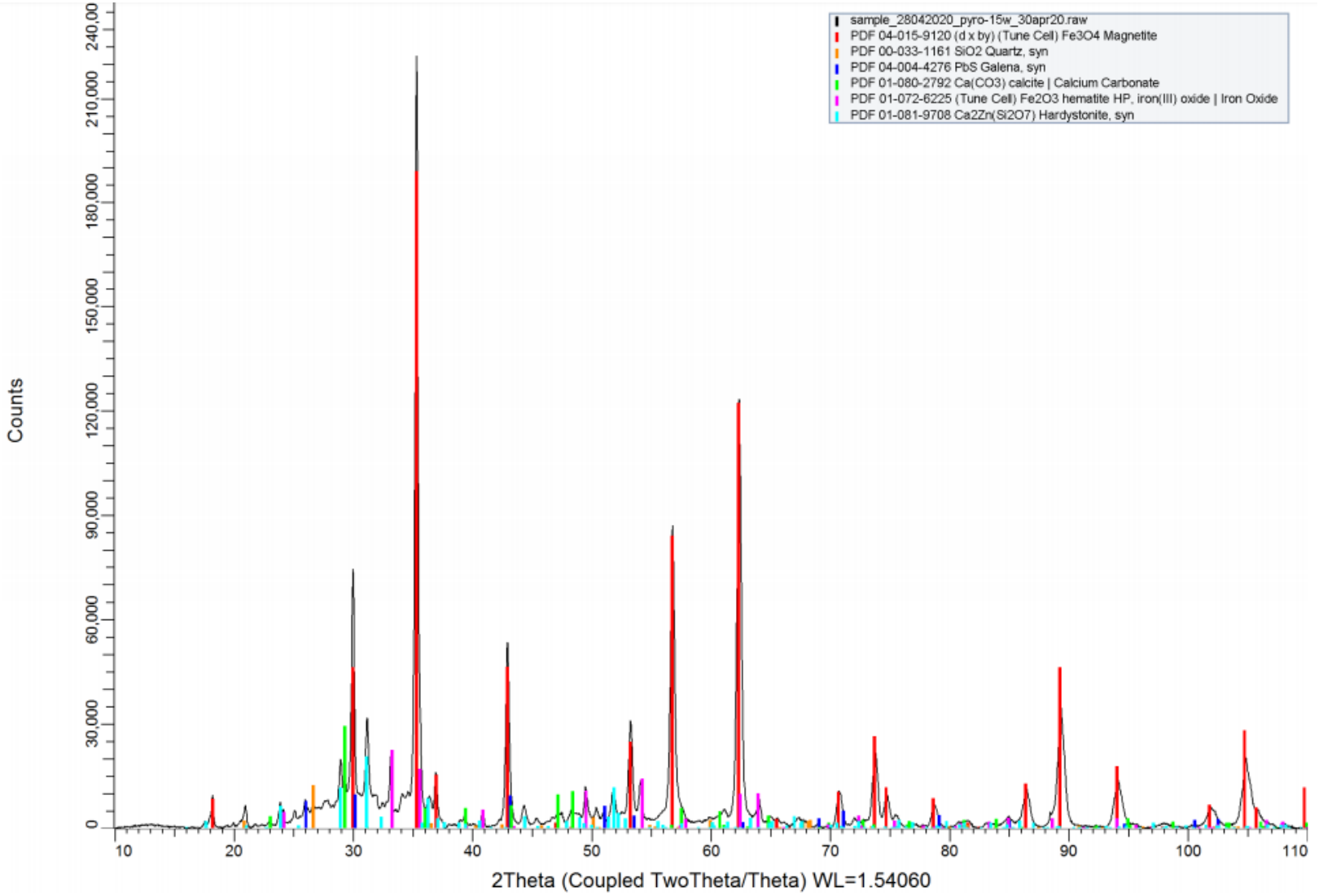

Figure C.14: P15 washed residue washed. Treatment conditions detailed in the body of text

.